Titre: Title:	Experimental Performance Characterization and Modeling of Photovoltaic-Thermal Systems for Integration in High Performance Residential Buildings
Auteur: Author:	Véronique Delisle
Date:	2016
Type:	Mémoire ou thèse / Dissertation or Thesis
Référence: Citation:	Delisle, V. (2016). Experimental Performance Characterization and Modeling of Photovoltaic-Thermal Systems for Integration in High Performance Residential Buildings [Ph.D. thesis, École Polytechnique de Montréal]. PolyPublie. https://publications.polymtl.ca/2231/

UNIVERSITÉ DE MONTRÉAL

EXPERIMENTAL PERFORMANCE CHARACTERIZATION AND MODELING OF PHOTOVOLTAIC-THERMAL SYSTEMS FOR INTEGRATION IN HIGH PERFORMANCE RESIDENTIAL BUILDINGS

VÉRONIQUE DELISLE

DÉPARTEMENT DE GÉNIE MÉCANIQUE

ÉCOLE POLYTECHNIQUE DE MONTRÉAL

THÈSE PRÉSENTÉE EN VUE DE L'OBTENTION

DU DIPLÔME DE PHILOSOPHIAE DOCTOR

(GÉNIE MÉCANIQUE)

AOÛT 2016

UNIVERSITÉ DE MONTRÉAL

ÉCOLE POLYTECHNIQUE DE MONTRÉAL

Cette thèse intitulée :

EXPERIMENTAL PERFORMANCE CHARACTERIZATION AND MODELING OF PHOTOVOLTAIC-THERMAL SYSTEMS FOR INTEGRATION IN HIGH PERFORMANCE RESIDENTIAL BUILDINGS

présentée par : DELISLE Véronique

en vue de l'obtention du diplôme de : Philosophiae Doctor

a été dûment accepté par le jury d'examen constitué de :

M. BERNIER Michel, Ph. D., président

M. KUMMERT Michaël, Doctorat, membre et directeur de recherche

Mme SANTATO Clara, Doctorat, membre

M. FUNG Alan S., Ph. D., membre externe

ACKNOWLEDGEMENTS

This doctoral degree was a great learning experience and it left me with a humbling life lesson: if you cannot explain it, you do not understand it and you need to read more. This project made me become a much better researcher and for that, I would like to take the opportunity to acknowledge a number of people for their assistance and guidance over the past five years.

I would like to thank my supervisor, Professor *Michaël Kummert*. His active listening was extremely useful at generating new ideas and solutions. His comments were greatly appreciated and helped me becoming much better at writing, presenting and disseminating results.

I would like to show my appreciation to my current and former colleagues at Natural Resources Canada. In particular, I would like to acknowledge *Sophie Pelland*, *Yves Poissant*, *Dave Turcotte* and *Josef Ayoub* who supported me by either reviewing my work or stimulating new ideas.

I have to mention the great understanding and flexibility provided by my director at Natural Resources Canada, *Lisa Dignard-Bailey*, during the course of this project. Lisa was very supportive from the beginning and I would probably not have started this degree if it had not been of her support and enthusiasm.

Thank you to *Martin Kegel* for his support throughout this process. His understanding was greatly appreciated.

I would like to give a special thank you to *Michel Bernier*, member of this jury. He gave me a first taste of research in building energy efficiency and renewable energy technologies by supervising my 4th year undergraduate studies project ten years ago. He encouraged me at pursuing a Master's degree at the University of Waterloo and more recently, convinced me of doing a Ph. D. He laid out the first stone of my professional career, a career that I truly enjoy and for this, I am very grateful.

Finally, I would like to thank Professors *Alan Fung* and *Clara Santato* for being members of the jury despite their busy schedule.

RÉSUMÉ

Les capteurs photovoltaïques intégrés aux bâtiments avec récupération de chaleur (BIPV-T) convertissent l'énergie solaire absorbée en énergie électrique et thermique simultanément à partir d'une seule et même superficie de toit ou de façade, tout en agissant comme une composante intégrale de l'enveloppe du bâtiment. Ainsi, les capteurs BIPV-T démontrent un grand potentiel d'intégration aux bâtiments ayant une superficie limitée de toit ou de façade avec une bonne exposition au soleil ou un objectif énergétique agressif comme par exemple, l'atteinte d'une consommation énergétique nette nulle.

Bien que le caractère esthétique et la double-fonctionnalité de cette technologie présente un certain intérêt, le nombre de produits BIPV-T ou de modules photovoltaïques avec récupération de chaleur (PV-T) sur le marché demeure limité. La faible adoption par le marché de cette technologie peut être expliquée par le manque d'information sur son coût-bénéfice, son coût élevé, l'absence d'outils pour estimer la production énergétique et le manque de solutions complètes incluant non seulement le capteur, mais également des stratégies d'utilisation de l'énergie thermique produite. L'objectif de cette thèse est de contribuer à l'élimination de certains obstacles freinant l'adoption des capteurs BIPV-T et PV-T utilisant l'air comme fluide pour récupérer la chaleur en améliorant les connaissances reliées à la caractérisation de la performance et à ses bénéfices réels.

La caractérisation de la performance de capteurs PV-T est un défi. Étant donné que les cellules photovoltaïques agissent en tant qu'absorbeur thermique, le rendement thermique est influencé par le rendement électrique et vice-versa. Afin de capturer cette interaction lors de la caractérisation de la performance, un lien doit être établi entre les rendements thermique et électrique. Le Chapitre 4 présente les résultats d'essais expérimentaux effectués en conditions intérieures et extérieures sur deux capteurs PV-T non-vitrés pour valider une méthode qui consiste à utiliser la température équivalente des cellules pour relier la production d'électricité à la production d'énergie thermique dans un capteur PV-T. Cette température peut être estimée à partir de la tension en circuit ouverte sans avoir à mesurer la température des cellules photovoltaïques. Son utilisation évite donc les problèmes associés à la non-uniformité de la température de l'absorbeur et à l'accès à la surface arrière des cellules pour l'installation de senseurs. En récupération de chaleur, il a été démontré que la température équivalente des

cellules pouvait être estimée à partir de l'ensoleillement et des températures de l'air à l'entrée et à la sortie du capteur. Puisque ces variables font partie intrinsèque de la caractérisation thermique du capteur, la température équivalente des cellules peut être utilisée pour relier le rendement électrique au rendement thermique. La validation de cette relation a été démontrée en développant une méthode graphique présentant à la fois la performance thermique et la performance électrique du capteur. Le système de graphiques développé peut être utilisé à des fins de conception pour estimer la production thermique et électrique à partir des conditions environnementales et d'opération.

Les données obtenues durant les essais expérimentaux ont été utilisées pour valider un modèle d'un capteur PV-T à air applicable pour des installations intégrées ou non au bâtiment et opérant dans des configurations en boucle ouverte ou fermée. Ce modèle est présenté au Chapitre 5 et a été implémenté dans un outil de simulation énergétique pour permettre d'étudier les interactions entre la production thermique et électrique du capteur et les charges électriques, de ventilation et de chauffage de l'air et de l'eau chaude domestique d'un bâtiment.

Le modèle validé a été utilisé pour expérimenter une nouvelle méthode développée dans le but d'identifier le coût-bénéfice réel d'intégration des capteurs BIPV-T à air dans des bâtiments résidentiels à haute performance en comparaison à des technologies d'énergie solaire standards. Ce type de comparaison n'est pas simple à effectuer puisque deux types d'énergies de différentes valeurs sont produits. De plus, le coût de capteurs BIPV-T est difficile à évaluer parce que cette technologie est relativement nouvelle sur le marché et les produits sont souvent développés pour un bâtiment spécifique et une application particulière.

Les Chapitres 5 et 6 proposent une nouvelle approche pour analyser le coût-bénéfice. Cette approche utilise le concept du coût du seuil de rentabilité définit comme le coût incrémental maximal pour récupérer la chaleur d'une installation BIPV pour que le coût du BIPV-T (en dollars par unité d'énergie produite utile) soit égal à celui de la technologie solaire à laquelle il est comparé. Pour demeurer compétitif, le coût incrémental doit être inférieur à celui du coût du seuil de rentabilité. Ainsi, plus ce coût est élevé, plus il est facile pour un système BIPV-T d'être compétitif avec d'autres technologies.

Le coût-bénéfice d'un système BIPV-T utilisant le concept du coût du seuil de rentabilité est évalué au Chapitre 6 en comparaison avec (i) un système BIPV et (ii) un système de même

superficie composé de modules PV et de capteurs solaires thermiques utilisés pour le chauffage de l'eau domestique. Pour obtenir ce coût, la production d'énergie utile équivalente des différents systèmes a été obtenue pour six maisons à haute efficacité énergétique fonctionnant entièrement à l'électricité situées dans diverses villes à travers le Canada. Quatre différentes stratégies de l'utilisation de l'énergie thermique ont été considérées : (1) préchauffage de l'air neuf, (2) préchauffage de l'eau chaude domestique à travers un échangeur de chaleur air-eau, (3) chauffage de l'eau et de l'air avec une pompe à chaleur air-eau et (4) chauffage de l'eau domestique avec un chauffe-eau pompe à chaleur. En comparaison avec un système BIPV, les systèmes BIPV-T produisent toujours plus d'énergie utile. Par conséquent, le coût du seuil de rentabilité d'un système BIPV-T par rapport à un système BIPV est toujours positif. En considérant le coût d'installations BIPV égal à celui de modules PV, le coût du seuil de rentabilité peut s'élever à 2,700 CAD pour une maison de deux étages de taille moyenne située à Montréal en comparaison à une installation BIPV. Ce coût peut être aussi élevé que 4,200 CAD en comparaison avec un toit d'une même superficie ayant des modules PV et des capteurs solaires thermiques côte-à-côte. Si le coût d'installations BIPV diminuait de 10% par rapport à celui de modules PV, le coût du seuil de rentabilité pourrait augmenter jusqu'à 6,400 CAD.

Cette information présente une certaine valeur d'un point de vue de conception parce qu'elle donne un estimé du coût incrémental maximal qui devrait être associé à la conversion d'un toit BIPV en un système BIPV-T pour demeurer compétitif avec d'autres types de technologies d'énergie solaire.

ABSTRACT

Building-integrated photovoltaics with thermal energy recovery (BIPV-T) convert the absorbed solar energy into both thermal and electrical energy simultaneously using the same roof or façade area while acting as a standard building envelope material. Thus, BIPV-T show great potential to be integrated in buildings with limited roof or façade area with good solar exposure or in buildings with aggressive energy performance targets such as net-zero.

Despite the aesthetic and dual-functionality attractiveness of this technology, the number of BIPV-T products and stand-alone photovoltaic with thermal energy recovery (PV-T) collectors remains limited. The slow market uptake of PV-T technology can be explained by the absence of performance characterization standards and product certification, the lack of information on their cost-benefit, the high cost, the absence of tools to estimate their yield and the lack of whole system solution sets. This thesis aims at contributing to removing some of the barriers to the market uptake of PV-T technology by increasing the knowledge on both its performance characterization and its true benefit focusing on systems using air as the heat recovery fluid.

Performance characterization is a challenge for PV-T collectors because PV cells act as the thermal absorber and as a result, the thermal performance is affected by the electrical performance and vice-versa. To capture this interaction during performance characterization, a link between the thermal and electrical yield needs to be established. Chapter 4 presents the results of indoor and outdoor experimental tests performed on two unglazed PV-T modules to validate a method that consists of using the equivalent cell temperature to estimate the PV cells' temperature in a PV-T collector and relate the thermal yield to the electrical yield. This temperature gives a good representation of the actual temperature of the solar cells and can be estimated from the open-circuit voltage without having to actually measure the solar cells' temperature. The equivalent cell temperature solves the problems associated with temperature gradient and PV cells' accessibility for sensor mounting. Under heat recovery conditions, it was found that the equivalent cell temperature could be predicted with the irradiance level and the inlet and outlet fluid temperatures. Since these variables are intrinsically part of the thermal performance characterization, the equivalent cell temperature can be used to link the collector electrical and thermal yield. This relation was further demonstrated by presenting a graphical method that encapsulates both the electrical and thermal performance of the collector. The system

of plots that was developed can be used to estimate the collector thermal and electrical yield from the environmental and operating conditions, which is useful for design purposes.

The data collected during this experiment was used to validate a model of an air-based PV-T collector applicable to both stand-alone and building-integrated products operating in either a closed-loop or an open-loop configuration. This model is presented in Chapter 5 and was implemented in an energy simulation tool to allow interactions between the collector thermal and electrical energy production and a building electrical, ventilation and domestic hot water and space heating loads.

The validated model was used to test a new methodology developed to identify the true cost-benefit of integrating BIPV-T air collectors in high performance residential buildings compared to standard solar technologies such as BIPV or side-by-side PV modules and solar thermal collectors. Such comparison is not straightforward to perform because two types of energy of different values are being produced. In addition, the actual cost of BIPV-T is difficult to evaluate because the technology is relatively new on the market and often consists of a custom product developed for a specific building and application.

To address this issue, Chapter 5 and Chapter 6 propose a new approach to the classic cost-benefit analysis. This approach uses the concept of break-even cost defined as the maximum incremental cost to recover the heat from a BIPV system to break-even with the cost (in dollars per unit of useful energy produced) of the solar energy technology that it is being compared with. To remain competitive, the actual incremental cost must be lower than the break-even cost. Thus, the higher the break-even cost, the easier it is for a BIPV-T system to be competitive with other technologies.

The cost-benefit of BIPV-T systems using the concept of break-even cost is evaluated in Chapter 6 in comparison with (i) a BIPV system and (ii) side-by-side PV modules and solar thermal collectors used for domestic hot water heating. To obtain this cost, the useful equivalent energy production of the different systems was first obtained for six all-electric energy-efficient homes located in various cities across Canada. Four different heat management scenarios were considered for the BIPV-T system: (1) fresh air preheating, (2) domestic hot water preheating through an air-to-water heat exchanger, (3) domestic hot water and space heating with an air-to-water heat pump and (4) domestic hot water heating (DHW) with a heat pump water

heater. Compared to BIPV systems, BIPV-T systems always produce more useful energy. As a result, the break-even cost compared to a BIPV system considering the price of BIPV equal to that of standard roof-mounted PV modules was found to be always positive and up to 2,700 CAD for a medium 2-storey home located in Montreal. For that same house, the break-even cost of a BIPV-T system compared to an installation of side-by-side PV modules and solar thermal collectors was estimated at 4,200 CAD. If the price of BIPV were to get 10% lower than PV, however, this break-even cost could increase to 6,400 CAD.

This information is valuable from a design perspective because it indicates the maximum incremental cost that should be associated with converting a BIPV roof into a BIPV-T system to remain cost-competitive with other solar technology options.

TABLE OF CONTENTS

LIST OF TABLES

LIST OF FIGURES

LIST OF SYMBOLS AND ABBREVIATIONS

The list of symbols and abbreviations presented in this section is applicable to Chapters 1, 2, 3, 7 and 8. The articles presented in Chapters 4 to 6 have their own nomenclature. The symbols and abbreviations used in the articles presented in Chapters 4 to 6 are described in these specific chapters.

Abbreviation

a-Si	Amorphous silicon
ANSI	American National Standards Institute
ASHRAE	American Society of Heating, Refrigerating and Air-Conditioning Engineers
BIPV	Building-integrated photovoltaics
BIPV-T	Building-integrated photovoltaics with thermal energy recovery
CdTE	Cadmium telluride
CIGS	Copper indium gallium selenide
CMHC	Canada Mortgage and Housing Corporation
CSA	Canadian Standards Association
DHW	Domestic Hot Water
EN	European Normalization
ERS	EnerGuide Rating System
HVAC	Heating, Ventilation and Air-Conditioning
HWB	Hottel-Whillier Bliss
IEC	International Electrotechnical Commission
ISO	International Standards Organization
I-V	Current-Voltage
LIC	Low Irradiance Condition

NOCT	Normal Operating Cell Temperature
pc-Si	Polycrystalline silicon
PV	Photovoltaic
PV-T	Photovoltaic with thermal energy recovery
STC	Standard Testing Condition
TESS	Thermal Energy System Specialists
TRNSYS	Transient System Simulation Program

Symbols

A_a	Aperture area [m²]
A_g	Gross area [m²]
a	Empirically determined coefficient establishing the upper limit for module temperature at low wind speeds in the calculation of the cell temperature [-]
a_1	Coefficient in thermal efficiency equation [W/(m²·K)]
a_2	Coefficient in thermal efficiency equation [W/(m²·K²)]
AM_a	Air mass [-]
b	Empirically determined coefficient establishing the upper limit for module temperature at high irradiance in the calculation of the cell temperature [-]
b_u	Coefficient in thermal efficiency equation [s/m]
b_1	Coefficient in thermal efficiency equation [W/(m²·K)]
b_2	Coefficient in thermal efficiency equation [W·s/(m^3·K)]
C_0	Empirically-determined coefficient in the calculation of the maximum power point current [-]
C_1	Empirically-determined coefficient in the calculation of the maximum power point current [-]

C_2	Empirically-determined coefficient in the calculation of the maximum power point voltage [-]
C_3	Empirically-determined coefficient in the calculation of the maximum power point voltage [-]
c_p	Specific heat capacity [kJ/(kg·K)]
COP_{HP}	Heat pump coefficient of performance [-]
E_0	Reference irradiance [W/m²]
E_b	Beam component of incident solar radiation [W/m²]
E_d	Diffuse component of incident solar radiation [W/m²]
E_e	Effective irradiance [-]
E_L	Long-wave in-plane radiation [W/m²]
F_R^*	Solar thermal collector heat removal factor [-]
$f_1(AM_a)$	PV module spectrum dependency function [-]
$f_2(\theta)$	PV module incidence angle dependency function [-]
f_d	Fraction of diffuse irradiance used by the module [-]
G	In-plane solar irradiance [W/m²]
G''	Net in-plane solar irradiance [W/m²]
I_{mp}	Current at maximum power point [A]
I_{mp0}	Current at maximum power point at reference conditions[A]
I_{sc}	Short-circuit current [A]
I_{sc0}	Short-circuit current at reference conditions [A]
I_{scr}	Reference cell short-circuit current [A]
I_{scr0}	Reference cell short-circuit current at reference conditions [A]
k	Ross coefficient [K·m²/W]

$\dot{m}$	Mass flow rate [kg/h]
$\dot{m}_i$	Air inlet mass flow rate [kg/h]
$\dot{m}_o$	Air outlet mass flow rate [kg/h]
N_s	Number of cells in series [cells]
P_{flow}	Pumping power [W]
P_{mp}	Maximum power point [W]
$P_{PV,DC}$	DC PV system power [W]
Q_{el}	Electrical energy [kWh]
Q_{th}	Thermal energy [kWh]
$Q_{T,P}$	Primary energy [kWh]
SF	Soiling factor [-]
T^*	Characteristic temperature [°C] or [K]
T_0	Reference cell temperature [°C]
T_a	Ambient temperature [°C] or [K]
T_i	Fluid inlet temperature [°C] or [K]
T_m	Mean fluid inlet temperature [°C] or [K]
T_o	Fluid outlet temperature [°C] or [K]
T_{PV}	Temperature of solar cells [°C]
T_{PVr}	Temperature of the reference solar cell [°C]
U_L^*	Solar thermal collector heat loss coefficient [W/(m²·K)]
V_f	Free stream wind speed in the windward side of the PV array [m/s]
V_{mp}	Voltage at maximum power point [V]
V_{mp0}	Voltage at maximum power point at reference conditions [V]
V_{oc}	Open-circuit voltage [V]

V_{oc0}	Open-circuit voltage at reference conditions [V]
V_w	Wind velocity [m/s]

Greek Symbols

α	Absorptance [-]
α_{Imp}	Maximum power point current temperature coefficient [A/°C]
α_{Isc}	Short-circuit current temperature coefficient [A/°C]
α_{Iscr}	Reference cell short-circuit current temperature coefficient [A/°C]
β_{Vmp}	Maximum power point voltage temperature coefficient [V/°C]
β_{Voc}	Open-circuit voltage temperature coefficient [V/°C]
ε	Emissivity [-]
$\gamma_{Pmp,rel}$	Maximum power point relative temperature coefficient [1/°C]
η_0	Maximum thermal efficiency [-]
η_{el}	Electrical efficiency [-]
$\eta_{el,net}$	Net electrical efficiency [-]
η_{fan}	Fan efficiency [-]
$\eta_{gen,grid}$	Grid efficiency [-]
η_{motor}	Motor efficiency [-]
$\eta_{p\rightarrow th}$	Efficiency for converting primary energy to thermal energy [-]
$\eta_{PV,system}$	PV system efficiency [-]
η_{th}	Thermal efficiency [-]
$\eta_{th,eq}$	Equivalent thermal efficiency [-]
$\eta_{T,net}$	Net combined efficiency [-]
$\eta_{T,P}$	Combined primary energy saving efficiency [-]

σ	Stefan-Boltmann constant [$W/(m^2 \cdot K^4)$]
θ	Incidence angle [°]
$(\tau\alpha)_e$	Effective transmittance-absorptance product [-]
ω	Ratio of Ross coefficients [-]

CHAPTER 1 INTRODUCTION

In 2014, photovoltaic (PV) technology provided 1.1% of the total electricity consumption worldwide (IEA PVPS, 2015) with an installed capacity of 177 GW. In Canada, it is 0.4% of the total electricity that was supplied by solar PV during that same year. Despite this modest penetration, the PV market is growing fast. In 2014, the total installed PV capacity in Canada was 1.84 GW (Poissant & Bateman, 2014) corresponding to 1.5 times the capacity installed in 2013 and 2.4 times that recorded in 2012. This market growth can be explained by the attractive incentives programmes that were launched in recent years (e.g., the Ontario feed-in tariff) combined with the drop in PV module prices, from 5.5 CAD/Wp in 2004 to 0.85 CAD/Wp in 2014 (Poissant & Bateman, 2014). For grid-connected distributed systems which mainly consist of PV systems mounted on the roof or façade of residential and commercial buildings, additional factors have contributed to this increased interest: the levelised cost of electricity for PV that has reached or is about to reach grid parity in some locations in Canada and the need or will of building owners to comply to specific energy consumption targets. Achieving low levels of energy consumption, especially aggressive ones such as net-zero, cannot be possible with only energy conservation and energy efficiency measures. It also requires the optimal integration of renewable energy technologies such as solar thermal and solar PV.

Standard (non-concentrated) PV modules typically convert between 7% (amorphous-silicon) to 16% (cadmium telluride) of the incident solar energy into electricity. The rest of the energy is either reflected or converted into heat if the photons have an energy level not within the band gap of the solar cells. This heat is generally lost to the surroundings and is unwanted since it contributes to increasing the temperature of the cells and reducing their efficiency. In a photovoltaic module with thermal energy recovery (PV-T), the heat generated by the solar cells is recovered either actively or passively by a heat recovery fluid that can be a liquid or air instead of being lost to the environment. Thus, compared to stand-alone PV modules, PV-T collectors produce both thermal and electrical energy simultaneously using the same surface area. Considering that buildings only have a limited amount of available façade or roof surface area with solar energy potential, PV-T is a promising technology when targeting a high energy performance building.

Similar to solar thermal collectors, PV-T collectors can use either liquid or air as the heat recovery fluid, can be glazed or unglazed and work either in a closed-loop or open-loop configuration. PV-T collectors can also be integrated to the building envelope. These are called building-integrated photovoltaics with thermal energy recovery (BIPV-T). BIPV-T collectors replace a component of the building envelope by acting as the roof, façade, window or curtainwall and thus, generally provide a greater aesthetic than PV-T collectors.

In Canada, a number of recent projects have demonstrated that BIPV-T collectors can fulfill part of the energy requirements of buildings. As part of Canada's Mortgage and Housing Corporation (CMHC) Equilibrium competition, the EcoTerra Home (Noguchi et al., 2008) and the Alstonvale Home (Pogharian et al., 2008) have showed the potential of BIPV-T in energy-efficient single-family homes. The BIPV-T transpired collector integrated to the façade of the John Molson School of Business Building in Montreal (Athienitis et al., 2011) has proven that BIPV-T can be beneficial for preheating fresh air in commercial buildings. These projects all use air as the heat recovery fluid. Compared to liquids such as a water and glycol mixture, air has several disadvantages for use in solar thermal technologies. It has a lower thermal conductivity, which generally leads to a reduced thermal efficiency compared to liquid collectors. It also has a lower thermal capacity which makes it more difficult to store the thermal energy collected for a later use. In a BIPV-T application, however, the choice of air instead of liquid ensures greater safety and simplicity. Even though air leakage or infiltration might affect the thermal performance of a BIPV-T air collector, it will not create safety issues if the solar cells get in contact with the fluid as it would be the case in a liquid-based collector. In addition, when the fluid is air, it can be directly drawn from outdoors and work in open-loop avoiding the complexity of a closed-loop system.

Despite their great potential, PV-T and BIPV-T technologies remain niche markets. Several barriers to their market uptake have been identified in the last 10 years including the absence of performance characterization standards and product certification, the lack of information on their cost-benefit, the high cost, the absence of tools to estimate their yield and the lack of whole system solution sets (Goetzler et al., 2014; Zondag, 2008).

The work presented in this document aims at removing some of these barriers to the market uptake of BIPV-T technology by increasing the knowledge on both its performance

characterization and its true benefit. Understanding the actual value of BIPV-T compared to standard solar technologies such as PV modules or solar thermal collectors will advance the science on its current worth. In addition, it will identify future research required for its integration into efficient buildings to become common practice.

The work performed for this thesis has three main objectives. The first objective consists of developing and validating experimentally a model that can apply to BIPV-T and PV-T air collectors. The aim is to understand how its performance is affected by certain design characteristics as well as environmental and operating conditions. Ultimately, the goal is to implement it in an energy simulation tool to study the interactions with a building and its ventilation, space heating and domestic hot water heating systems. Several models of BIPV-T or PV-T air collectors have been developed and even validated experimentally, but the results obtained are difficult to compare. The main reason is that there are no standardized methods to characterize the thermal and electrical performance of PV-T collectors.

This leads to the second objective of the study which is to address some of the issues related to the thermal and electrical performance characterization of PV-T collectors. In a PV-T collector, PV cells act as the thermal absorber or as part of the thermal absorber and as a result, the thermal performance is affected by the electrical performance and vice-versa. Therefore, the application of separate PV and solar thermal collector standard performance test procedures are not sufficient to characterize the performance of PV-T collectors.

The validated model is used to fulfill the third objective of this study, which is to develop a methodology to identify the true benefit of integrating BIPV-T air collectors in high performance residential buildings compared to standard solar technologies such as PV modules and solar thermal collectors. Performing such comparison is not straightforward for BIPV-T air collectors because two types of energy having different values are generated and several performance indicators can be used. In fact, studies that have looked at quantifying the benefits of PV-T or BIPV-T air collectors show a very large spectrum of results.

CHAPTER 2 LITERATURE REVIEW

This literature review presents an overview of the research conducted on different topics related to PV-T or BIPV-T technology. More specifically, it addresses the three objectives described in Chapter 1. It is divided in two main sections. Section 2.1 discusses the different methods to characterize the performance of solar technologies and the models currently available in simulation tools. Section 2.2 focuses on a review of the approaches taken to quantify the benefit of photovoltaics with heat recovery and how it compares with more common solar energy technologies.

2.1 Performance Characterization of Solar Technologies

Standardized methods to measure and present the performance of a product are of great importance for any technology. Universal performance testing methods ensure that two products can be directly compared because both the metrics employed and the experimental procedures followed to obtain these metrics are the same. The added benefit is that the parameters and performance indicators measured during performance characterization can often be used in simplified models to predict the technology yield under specific conditions. This section presents an overview of the methods typically used to characterize the performance of solar thermal and PV technologies and discusses the additional challenges with combined photovoltaic and thermal technologies. It also includes a review of PV-T and BIPV-T models available in common whole-building simulation tools.

2.1.1 Solar Thermal Collectors

There are many different types of solar thermal collectors: liquid-based, air-based, glazed, unglazed, concentrators, open-loop and closed-loop. The variables influencing the performance of a solar thermal collector will depend on the heat transfer fluid, the presence of glazing, the design (e.g., concentrator, flat-plate, sheet-and-tube, etc.), the type of inlet (multiple entries or one single entry) and the collector operating mode (open-loop vs closed-loop).

The simplest representation of the thermal efficiency, η_{th}, of a non-concentrating solar thermal collector operated under steady-state conditions is given by the Hottel-Whillier Bliss (HWB) equation (Hottel & Whillier, 1958):

$$\eta_{th} = F_R^*(\tau\alpha)_e - F_R^* U_L^* \left(\frac{T^* - T_a}{G}\right) \tag{2-1}$$

In Equation (2-1), U_L^* is the collector heat loss coefficient, F_R^* is the heat removal factor and $(\tau\alpha)_e$ is the collector effective transmittance-absorptance product. The term $(T^* - T_a)/G$ is known as the reduced temperature where T_a is the ambient temperature, G is in the in-plane solar irradiance and T^* is a characteristic temperature. In North America, this characteristic temperature is generally the fluid inlet temperature, T_i. In European and international standards, however, it is more common to use the fluid mean temperature, T_m. This mean fluid temperature is calculated as the arithmetic average of the fluid inlet (T_i) and outlet (T_o) temperatures. The heat loss coefficient, U_L^*, is not always constant and for some flat-plate collectors, can be a function of $T^* - T_a$ as shown by Gordon (1981). In that case, the term $F_R^* U_L^*$ in Equation (2-1) becomes

$$F_R^* U_L^* = a_1 + a_2(T^* - T_a) \tag{2-2}$$

where a_1 and a_2 are constants. By substituting Equation (2-2) in the thermal efficiency relation shown in Equation (2-1), η_{th} can be expressed as

$$\eta_{th} = F_R^*(\tau\alpha)_e - a_1\left(\frac{T^* - T_a}{G}\right) - a_2\frac{(T^* - T_a)^2}{G} \tag{2-3}$$

or

$$\eta_{th} = \eta_0 - a_1\left(\frac{T^* - T_a}{G}\right) - a_2\frac{(T^* - T_a)^2}{G} \tag{2-4}$$

In Equation (2-4), η_0 is the collector maximum efficiency obtained when $T^* = T_a$. Equations (2-1) and (2-4) are generally only valid for glazed collectors. The steady-state efficiency for unglazed collectors or for collectors with the heat recovery fluid in direct contact with the cover is slightly different. In these particular products, the heat recovery fluid temperature is much more influenced by the collector convective and radiative heat losses to the surroundings. As a result, the wind speed and long-wave radiation have a greater effect on the performance and they need to be taken into account in the efficiency equation. The long-wave radiation, E_L, is

accounted for by using the net incident solar radiation, $G"$, as opposed to the in-plane solar irradiance in the calculation of the thermal efficiency. $G"$ is defined as:

$$G" = G + \frac{\varepsilon}{\alpha}(E_L - \sigma T_a^4) \tag{2-5}$$

In Equation (2-5), ε/α is the collector emissivity over absorptance ratio, σ is the Stefan-Boltzmann constant and T_a is the ambient temperature in Kelvins. As for the wind effect, it is accounted for by expressing $F_R^*(\tau\alpha)_e$ and $F_R^*U_L^*$ as linear functions of wind velocity, V_w, as shown in Harrison et al. (1989):

$$F_R^*(\tau\alpha)_e = \eta_0(1 - b_u V_w) \tag{2-6}$$

$$F_R^*U_L^* = (b_1 + b_2 V_w) \tag{2-7}$$

In Equations (2-6) and (2-7), b_u, b_1 and b_2 are constants. Hence, the thermal efficiency of unglazed collectors (or collectors where the fluid is in direct contact with the glazing) is given by:

$$\eta_{th} = \eta_0(1 - b_u V_w) - (b_1 + b_2 V_w)\left(\frac{T^* - T_a}{G"}\right) \tag{2-8}$$

The efficiency relations given in Equations (2-1), (2-4) and (2-8) are applicable to both liquid or air collectors, but are only valid for a specific flowrate in the case of air collectors. As explained by Kramer (2013), the main difference between air and liquid collectors is that the heat transfer coefficient between the absorber and the fluid is much lower in an air collector and much more dependent on flowrate. In an air collector, the lower the flowrate, the higher is the temperature of the absorber and the higher are the collector convective and radiative losses to the surroundings.

Another difference between liquid and air collectors is that air collectors are never perfectly sealed and the amount of air leaking from or infiltrating the collector affects its performance (Bernier & Plett, 1988). In a liquid-based collector, the thermal efficiency is given by

$$\eta_{th} = \frac{\dot{m}c_p(T_o - T_i)}{GA_a} \tag{2-9}$$

where A_a is the collector aperture area and $c_p$and $\dot{m}$ represent the fluid heat specific heat and flowrate, respectively. In an air collector, however, air leakage is related to its operating gauge pressure. If the collector operates under negative pressure relative to the ambient, ambient air will be infiltrating the collector. On the opposite, if the collector operates under positive pressure, air will be leaking from the collector. As a result, the thermal efficiency of an air-based solar thermal collector is calculated using:

$$\eta_{th} = \frac{\dot{m}_o c_p (T_o - T_i) + (\dot{m}_o - \dot{m}_i) c_p (T_i - T_a)}{G A_a} \tag{2-10}$$

In Equation (2-10), the subscripts i and o refer to the collector inlet and outlet, respectively. For unglazed solar thermal collectors, Equations (2-9) and (2-10) can still be used, but G is replaced by G". Note that G (or G") must be multiplied by a conversion factor corresponding to 3.6 kJ/(h·W) if the units in the nomenclature are used.

Several standards provide performance and reliability test methods for solar thermal collectors. The most common ones applicable to air collectors are:

- ANSI/ASHRAE 93-2010 "Methods of Testing to Determine the Thermal Performance of Solar Collectors" (ASHRAE, 2010)
- CAN/CSA-F378 Series-11 "Solar Collectors" (CSA, 2012)
- ISO 9806 "Solar thermal collectors – Test methods" (ISO, 2013)

The standard ANSI/ASHRAE 93-2010 mostly focuses on performance testing with test procedures to obtain air leakage rate, steady-state thermal efficiency, time constants and incidence angle dependence. In addition to performance tests, CAN/CSA-F378 Series-11 and ISO 9806 also contain reliability tests including, but not limited to, external thermal shock, exposure, high-temperature resistance and mechanical load. All three standards contain indoor and outdoor testing procedures. The standard ANSI/ASHRAE 93-2010 applies only to glazed collectors, but CAN/CSA-F378 Series-11 and ISO 9806 are applicable to both glazed and unglazed products. In the case of ISO 9806, it can even be used for glazed and unglazed PV-T collectors, referred to as hybrid collectors. In this standard, a PV-T collector is considered unglazed when the absorber "is close connected to the electricity generation and if there is no extra glazing in front" (ISO, 2013). For PV-T collectors, it is specified that testing can be done

with the PV operating at maximum power point, in open-circuit or even in short-circuit conditions as long as the PV operating mode is mentioned in the test report.

The test loops, instruments and measurements recommended in the different standards are similar. In ANSI/ASHRAE 93-2010, a test loop having both upstream and downstream sections is required. Each section has airflow, temperature and pressure measuring stations to account for air leakage or infiltration. A pre-conditioning apparatus is located at the collector inlet to allow regulating the fluid inlet temperature. A similar testing loop is recommended in CAN/CSA-F378 Series-11, but only one flowrate measurement is mandatory. In ISO 9806, distinct testing loops are required depending on whether the collector is typically used in a closed-loop or open-loop configuration. The closed-loop is similar to that proposed in ANSI/ASHRAE 93-2010.

A comparison of the measurements required by the three standards during the steady-state thermal efficiency test is shown in Table 2-1. The main differences are that the CAN/CSA F378 Series-11 standard requires only one flowrate measurement and ISO 9806 for open-loop collectors requires fewer measurements since the test loop only has a downstream section. In addition, ISO 9806 does not require that the wind direction be measured. In all standards, it is recommended to use a pyranometer for short-wave irradiance measurement and a pyrheliometer for direct normal irradiance.

Table 2-1: Steady-state thermal efficiency test required measurements

	ANSI/ASHRAE 93-2010	CAN/CSA F378 Series-11	ISO 9806	
			Closed-loop	Open-loop
Ambient pressure	X	X	X	
Ambient air temperature	X	X	X	X
Humidity ratio	X	X	X	X
Inlet gauge pressure	X	X	X	
Outlet gauge pressure	X	X	X	X
Differential pressure	X	X	X	
Inlet fluid temperature	X	X	X	
Outlet fluid temperature	X	X	X	X
Fluid temperature rise	X	X	X	X
Inlet flowrate	X		X	
Outlet flowrate	X	X[1]	X	X
In-plane short-wave irradiance	X	X	X	X
Direct normal irradiance (outdoor testing)	X	X	X	X
In-plane long-wave irradiance	X[2]	X[2]	X[3]	X[3]
Surrounding air speed	X	X	X	X
Surrounding air direction	X	X		

The inlet temperature, flowrate and wind speed conditions under which the steady-state thermal efficiency of air collectors should be measured vary between standards. These are summarized in Table 2-2.

[1] Only one air flowrate is required, either at the inlet or outlet

[2] Only necessary for indoor testing

[3] The in-plane long-wave irradiance can also be calculated if it cannot be measured. Procedures are given in the standard for both indoor and outdoor testing conditions.

Table 2-2: Conditions for air collectors steady-state thermal efficiency measurements

	ANSI/ASHRAE 93-2010	CAN/CSA F378 Series-11	ISO 9806
Inlet temperature	4 values of $(T_i - T_a)$: 0%, 30%, 60% and 90% of the value of $(T_i - T_a)$ at a given temperature		**Open-loop:** $T_i = T_a$ **Closed-loop:** 4 values of T_m with one value such that $T_m = T_a + 3$ K
Flowrate	0.01 $m^3/(s \cdot m^2)$[4] 0.03 $m^3/(s \cdot m^2)$	2 values: min and max values recommended by the manufacturer	3 values: between 30 to 300 $kg/(h \cdot m^2)$[4] or as recommended by the manufacturer
Wind speed	**Glazed – indoor**: 3 to 4 m/s **Glazed – outdoor**: 2 to 4 m/s	**Glazed – indoor**: 3 to 4 m/s **Glazed – outdoor**: 2 to 4 m/s **Unglazed – indoor**: 0.75 to 1 m/s, 1.5 to 2 m/s and >2.5 m/s **Unglazed – outdoor**: 2 to 4.5 m/s	**Glazed:** 2 to 4 m/s **Unglazed:** <1 m/s, 1 to 2 m/s and 2.5 to 3.5 m/s

2.1.2 PV Modules

The performance of a PV Module can be characterized by its current-voltage (I-V) curve. On this curve, three points can be identified: the short-circuit current (I_{sc}), the open-circuit voltage (V_{oc}) and the maximum power point (P_{mp}). This maximum power point is the point at which the current and voltage are such that the power produced by the PV module is maximized. The current and voltage at maximum power point are known as I_{mp} and V_{mp}. These five key parameters of an I-V curve depend mainly on the incident solar radiation and cell temperature and to a secondary order, on the air mass and incidence angle as demonstrated in the model of King et al. (2004):

$$I_{sc} = I_{sc0} E_e [1 + \alpha_{Isc}(T_{PV} - T_0)] \quad (2\text{-}11)$$

[4] Per gross collector area

$$I_{mp} = I_{mp0}[C_0 E_e + C_1 E_e^2]\left[1 + \alpha_{Imp}(T_{PV} - T_0)\right] \quad (2\text{-}12)$$

$$V_{oc} = V_{oc0} + N_s \delta(T_{PV}) \ln(E_e) + \beta_{Voc}(E_e)(T_{PV} - T_0) \quad (2\text{-}13)$$

$$V_{mp} = V_{mp0} + C_2 N_s \delta(T_{PV}) \ln(E_e) + C_3 N_s [\delta(T_{PV}) \ln(E_e)]^2 + \beta_{Vmp}(E_e)(T_{PV} - T_0) \quad (2\text{-}14)$$

$$P_{mp} = I_{mp} V_{mp} \quad (2\text{-}15)$$

In Equations (2-11) to (2-15), I_{sc0}, I_{mp0}, $V_{oc0}$and V_{mp0} are the short-circuit current, current at maximum power point, open-circuit voltage and voltage at maximum power point at a reference irradiance level E_0 (typically 1000 W/m^2) and cell temperature T_0 (typically 25 °C) for an air mass, AM_a, of 1.5 and an incidence angle, θ, of 0°. α_{Isc}, α_{Imp}, β_{Voc} and β_{Vmp} are the temperature coefficients for short-circuit current, current at maximum power point, open-circuit voltage and voltage at maximum power point. C_0, C_1, C_2 and C_3 are empirically-determined coefficients. T_{PV} is the solar cells temperature. N_s is the number of cells in series. E_e is the effective irradiance defined as the PV module in-plane solar irradiance taking into account the solar spectral variation, the optical losses due to solar angle-of-incidence and module soiling.

The most common method to obtain the effective irradiance is by measuring the short-circuit current of a calibrated reference cell (I_{scr}) that uses the same solar cell technology than the module under test and that is positioned at the same slope and orientation. The reference cell has identical solar spectral and incidence angle dependence as the module and the level of irradiance as seen by the PV module is calculated with:

$$E_e = \frac{I_{scr}}{I_{sc0r}\left(1 + \alpha_{Iscr}(T_{PVr} - T_0)\right)} SF \quad (2\text{-}16)$$

In Equation (2-16), SF is the module soiling factor and the subscript *r* refers to the reference cell. If instead of a reference cell, thermopile-based instruments (e.g., pyranometers or pyheliometers) are used to measure the irradiance level, the effective irradiance can still be calculated, but corrections are required to take into account the fact that the irradiance sensor(s) and module spectrum and incidence angle effect differ. In this case, E_e is calculated with the following relation:

$$E_e = f_1(AM_a)\left(\frac{E_b f_2(\theta) + f_d E_d}{E_0}\right) SF \tag{2-17}$$

In Equation (2-17), E_b and E_d are the beam and diffuse components of incident solar radiation and $f_1(AM_a)$ and $f_2(\theta)$ are the module spectrum and incidence angle dependency functions. f_d is the fraction of diffuse irradiance used by the module. In the worst case scenario, these effects can be neglected and E_e can simply be calculated with

$$E_e = \left(\frac{E}{E_0}\right) SF \tag{2-18}$$

where E is the in-plane solar irradiance measured by a pyranometer. In Marion (2012), the effect of correcting for temperature, incidence angle and spectrum for estimating daily efficiencies of four PV modules of different technologies is studied. Two different spectrum correction methods are tested: a complex model that accounts for the spectral irradiance and spectral response of both the modules and irradiance sensor for each wavelength and a simpler model that uses the air mass correction factor developed by Sandia National Laboratory (King et al., 2004) corresponding to $f_1(AM_a)$ in Equation (2-17). It was found that the daily efficiency standard deviation was the lowest when correcting for temperature, incidence angle and spectrum with the complex method. Using the air mass correction factor, however, the results were improved only for the mono-crystalline module and only slightly for the CIGS module. They were worst for the CdTe and a-Si/a-Si/a-Si:Ge PV modules. This was explained by the fact that these two modules are much more sensitive to water vapor that is not taken into account in the simple air mass correction $f_1(AM_a)$.

Simpler models than that developed by King et al. can be used to predict the maximum power point of PV modules. One of the simplest models is that used in the software PVFORM (Menicucci & Fernandez, 1988) and is given as:

For E_e>125 W/m^2:

$$P_{mp} = E_e P_{mp0}\left[1 + \gamma_{Pmp,rel}(T_{PV} - T_0)\right] \tag{2-19}$$

For E_e≤125 W/m^2:

$$P_{mp} = \frac{0.008(E_e E_0)^2}{E_0}\left[1 + \gamma_{Pmp,rel}(T_{PV} - T_0)\right] \quad (2\text{-}20)$$

In Equations (2-19) and (2-20), $\gamma_{Pmp,rel}$ is the relative maximum power point temperature coefficient. As it can be observed in the models presented, the cell temperature is a key input to the prediction of the performance of PV modules. This temperature is generally determined from the ambient temperature, irradiance level, wind speed, solar cell technology and mounting configuration. Several models have been developed for predicting the temperature of PV cells. The simplest equation for steady-state operating temperature of a PV module under no wind conditions is

$$T_{PV} = T_a + kG \quad (2\text{-}21)$$

where k is the Ross coefficient (Ross, 1976). This coefficient expresses the temperature rise above ambient with increasing solar flux:

$$k = \frac{\Delta(T_{PV} - T_a)}{\Delta G} \quad (2\text{-}22)$$

A summary of typical Ross coefficients for different mounting configurations is given in Table 2-3.

Table 2-3: Values of Ross coefficient (Skoplaki et al., 2008)

Mounting type	k (K·m^2/W)
Free standing	0.021
Flat roof	0.026
Sloped roof: well cooled	0.020
Sloped roof: not so well cooled	0.034
Sloped roof: highly integrated, poorly ventilated	0.056
Façade integrated: transparent PV	0.046
Façade integrated: opaque PV, narrow gap	0.054

In Skoplaki et al. (2008), the effect of wind on the cell temperature is introduced with a modified version of Equation (2-21) that takes into account the free stream wind speed in the windward side of the PV array, V_f:

$$T_{PV} = T_a + \omega\left(\frac{0.32}{8.91 + 2V_f}\right)G \tag{2-23}$$

In Equation (2-23), ω is the ratio of the Ross coefficient for the specific mounting configuration to the Ross coefficient on the free-standing case:

$$\omega = \frac{k_{free\ standing}}{k_{mounting\ type}} \tag{2-24}$$

In King et al. (2004), the back surface module temperature is estimated with the following relation

$$T_{PV} = T_a + G\left(e^{a+bV_f}\right) \tag{2-25}$$

In Equation (2-25), a and b are empirically determined coefficients establishing the upper limit for module temperature at low wind speeds and high irradiance and the rate at which the module temperature drops as wind speed increases, respectively. Table 2-4 provides examples of values for these coefficients obtained for different modules and mounting types.

Table 2-4: Values of *a* and *b* for different modules and mounting types (King et al., 2004)

Module	Mounting	*a*	*b*
Glass/cell/glass	Open rack	-3.47	-0.0594
Glass/cell/glass	Close roof mount	-2.98	-0.0471
Glass/cell/polymer sheet	Open rack	-3.56	-0.0750
Glass/cell/polymer sheet	Insulated back	-2.81	-0.0455
Polymer/thin-film/steel	Open rack	-3.58	-0.113
22X Linear concentrator	Tracker	-3.23	-0.130

The methodology required to obtain the different electrical parameters characterizing a PV module is described in the two international standards IEC 61215 (IEC, 2005) and IEC 61646 (IEC, 1998) focusing on the design qualification and type approval of crystalline silicon and thin-film terrestrial PV modules, respectively. In these standards, indoor and outdoor procedures are given to obtain the PV module power, efficiency, current and voltage at maximum power point along with the short-circuit current and open-circuit voltage at Standard Testing Condition

(STC), Normal Operating Cell Temperature (NOCT) and Low Irradiance Condition (LIC). These conditions are as follows:

- STC: Irradiance level of 1000 W/m^2, module temperature of 25 °C and a solar spectrum of air mass 1.5
- NOCT: Irradiance level of 800 W/m^2, ambient temperature of 20 °C, wind speed of 1 m/s, module tilted at 45° and a solar spectrum of air mass 1.5
- LIC: Irradiance level of 200 W/m^2, module temperature of 25 °C and a solar spectrum of air mass 1.5

Procedures are also given to obtain the temperature coefficients for current, voltage and peak power. In order to perform these different tests, the following measurements must be made:

- Irradiance with a calibrated reference cell
- Current and voltage of the PV reference device and PV module under test
- Temperature of the module cells and PV reference device
- Wind speed and direction
- Ambient temperature

2.1.3 PV-T Technology

Sections 2.1.1 and 2.1.2 showed that the electrical yield of PV modules and the thermal yield of solar thermal collectors are influenced by different variables. The thermal efficiency of air solar thermal collectors is mainly influenced by the reduced temperature, the flowrate, the incidence angle and for unglazed collectors, by the wind speed. As for the amount of electricity produced by PV modules, it essentially depends on the irradiance level and cell temperature and to a second degree order, on the solar spectrum and incidence angle.

The thermal yield of PV-T collectors is influenced by the same variables than solar thermal collectors, but it is also affected by the amount of electricity produced by the PV cells. As for the electrical yield, it depends on the irradiance level, cell temperature, solar spectrum and incidence angle as in a PV module, but in PV-T collectors, the temperature of the cells does not depend only on ambient conditions and mounting configuration. It is also affected by the heat recovery

fluid temperature. The relation between the cell and the heat recovery fluid temperatures cannot be encapsulated solely with the reduced temperature. As shown in Tripanagnostopoulos et al. (2002), the electrical efficiency of a PV-T collector would depend only on the reduced temperature if the ambient temperature and incident solar radiation were kept constant during the experiment.

This interaction between the thermal and electrical yield of a PV-T collector is one of the issues with their performance characterization. Additional challenges were identified by the European initiative PV Catapult (2005) which produced a guide to highlight the main issues with PV-T collector performance testing and suggest elements to incorporate into the standards IEC 61215 (IEC, 2005) and EN 12975-2 (ECS, 2005) (the European standard for solar thermal collector testing) to address these issues. The guideline focused on non-concentrating liquid PV-T collectors using c-Si PV cells. One of the main issues discussed in this document is whether or not thermal and electrical measurements should be done separately or simultaneously in a PV-T collector since the thermal performance influences the electrical performance and vice-versa. Taking thermal measurements with the PV short-circuited or in open-circuit would later require the introduction of a thermal performance correction factor to account for the fact that in reality, the collector also produces electricity. PV Catapult concluded that since this factor was probably not straightforward to obtain, the collector should be producing electricity when taking thermal measurements and that it should be operating at its maximum power point. I-V curves should still be taken at regular time intervals, however, to simultaneously collect data for the electrical performance characterization. This is in contradiction with the standard ISO 9806 (ISO, 2013) that leaves it up to the manufacturer or testing facility to decide if the PV module during PV-T collector thermal testing should operate at maximum power point, in open-circuit or in short-circuit conditions.

Table 2-5: Indoor solar simulator minimum requirements

	ANSI/ASHRAE 93-2010	ISO 9806	IEC 61215 and 61646
Non-uniformity of irradiance	±10%[5]	±15%[5]	≤ ±5%[6]
Solar spectrum optical air mass	1.5	1.5	1.5
Maximum thermal irradiance	<50 W/m^2	≤ 5% of hemispherical irradiance	-
Minimum fraction of incident irradiance with θ<60°	-	80%	-
Minimum fraction of incident irradiance with θ<20°	90%	-	-
Spectral match[7]	-	-	0.6-1.4
Temporal instability	≤ ±3%	-	≤ ±5%

Another issue discussed in the guideline is the feasibility of performing PV-T collector measurements indoors. In IEC 61215, a radiant source Class B or better in accordance with the standard IEC 60904-9 "Solar simulator performance requirements" (IEC, 1995) is recommended. As shown in Table 2-5, the non-uniformity required for indoor solar simulators for solar thermal collector testing is not as strict as that found in IEC 61215. Also, even though the indoor testing of solar thermal collectors requires the level of irradiance per wavelength to be quantified, it does not have specific requirements with regards to spectral distribution. As a result, it is possible that most indoor simulators used for solar thermal collector testing cannot be utilized for PV-T collectors since these do not usually have the spatial uniformity and spectral distribution required for PV testing. Similarly, the lamps used in PV testing installations are not appropriate for solar thermal collectors because these only provide a flash of light and thus, do not allow for

[5] The spatial deviation is defined here as the deviation of the irradiance at a point on the collector gross area from the mean irradiance over the gross area

[6] The non-uniformity of irradiance is defined as [max irradiance – min irradiance] / [max irradiance + min irradiance]*100 where the max and min irradiance are measured over the module gross area

[7] The spectral match is the ratio of the actual percentage of total irradiance to the required percentage specified for each wavelength interval

steady-state thermal testing. As a result, PV Catapult recommended performing outdoor measurements even though the control of wind speed and irradiance is more difficult.

For glazed collectors, PV Catapult suggests taking four measurements of thermal efficiencies and reduced temperature in steady-state conditions for four different average fluid temperatures, T_m, in order to obtain 16 measurement points. For unglazed collectors, three temperature values T_m at three different wind speeds are recommended for a total of 9 measurement points. For the electrical measurements, PV Catapult suggests obtaining instantaneous maximum power point measurements through current-voltage (I-V) tracing in order to fill out a matrix with 100 W/m^2 irradiance bins and 5 °C temperature bins in a minimum span of 30 °C. In a PV-T collector, it can be difficult to estimate the temperature of solar cells because the absorber has a temperature gradient in the direction of the flow. Also, the cells are not always accessible for sensor mounting. To avoid this issue, the draft states that the temperature used in the thermal bins should have a direct relation with the actual PV temperature so that the latter can be calculated during the data analysis from the measured temperature, weather and collector thermal performance.

The other main issue mentioned by PV Catapult is the fact that for PV modules, reference cells are required to measure solar irradiance, but for solar thermal collectors, pyranometers are recommended. On this aspect, it was suggested using a pyranometer since the spectral response of c-Si modules does not vary too much. If other cell technologies were to be used such as CdTe or a-Si, for example, the irradiance measurement would need to be corrected for spectral response since the response of these technologies differ much more from the AM 1.5 spectrum as shown by Marion (2012) and Magare et al. (2016).

2.1.4 PV-T Models in Building or Energy Simulation Tools

Models for PV-T or BIPV-T collectors can be found in commonly used energy simulation tools. For example, the EnergyPlus program (US DOE, 2013) has a simple PV-T model that can be applied to both air-based and water-based collectors (NREL, 2015). It requires the thermal efficiency as a parameter and calculates the amount of thermal energy recovered, Q_{th}, and the outlet temperature with the following relations:

$$Q_{th} = A_{surf} f_{act} G \eta_{th} \tag{2-26}$$

$$T_o = T_i + \frac{Q_{th}}{mc_p} \tag{2-27}$$

In Equations (2-26) and (2-27), A_{surf} is the net area of the surface and f_{act} is the fraction of surface area with active PV-T collector. For air collectors, the model includes a bypass damper that can be controlled based on a user-defined setpoint to determine how much air is drawn through the PV-T collector.

BIPV-T models have also been implemented in the multi-platform building energy software tool ESP-r (University of Strathclyde, 2002). Lomanowski (2010) developed an integrated BIPV-T heat pump model in ESP-r. Chow et al. (2003) completed a numerical analysis of a BIPV-T façade on a large hotel complex in China using that same tool.

The TRNSYS (Klein et al., 2009) simulation tool has embedded PV-T and BIPV-T models and has often been used for modeling of both stand-alone collectors and complete systems (Kalogirou, 2001; Mei et al., 2003; Bakker et al., 2005). It offers two different categories of models. The first category is based on the Hottel-Whillier bliss model modified by Florschuetz (1979) for PV-T collectors. It is available in the standard library under Type 50 (50a, 50b, 50c and 50d for flat-plate collectors). The drawback of this model is that it requires both the modified collector efficiency factor and the loss coefficients as parameters which are often unknown. The second category of models is available under the non-standard TESS (Thermal Energy System Specialists) electrical library (Thornton et al., 2012) and includes Types 560, 563, 566, 568 and 569. These models have been developed by performing a series of energy balance equations on the different layers of a collector control volume. They are two-dimensional models that consider a temperature gradient in the direction of the fluid flow. The heat transfer coefficients in the channel are assumed to be the same at the top and bottom surfaces. These models require more information than Type 50 regarding the collector actual design such as the thickness and resistance of the different collector layers. In addition, some Types of the 560 series can interact with the building on which they are mounted. In this case, the collector back surface radiative and convective heat losses to the building are calculated which can be useful to evaluate the impact of a BIPV-T roof or façade on a building space heating and cooling loads. A summary and comparison of the currently available TRNSYS types is given in Table 2-6. Using these models require that information on the collector design be known. The main drawbacks are that they do not take air leakage (or infiltration) into account, the top and bottom surfaces heat transfer

coefficients in the cavity are assumed be the same which is not the case in reality (Candanedo et al., 2011) and some useful outputs are not given such as the temperature distribution across the collector.

Table 2-6 : TRNSYS PV-T and BIPV-T models comparison

		Type #						
Category	Characteristic	50	560	563	566	567	568	569
Collector type applicability	Liquid-based	X	X	X				
	Air-based	X			X	X	X	X
	Glazed	X			X	X		
	Unglazed	X	X	X			X	X
	Flat-plate	X			X	X	X	X
	Sheet-and-tube		X	X				
Top convective heat loss coefficient	Constant	X						
	Input		X	X	X	X	X	X
	Calculated from T_a, V_w and geometry	X						
Transmittance-absorptance product	Constant	X					X	X
	Calculated from incidence angle	X						
	Calculated from user-specified parameter (1st order IAM)		X	X	X	X		
	Calculated from cover properties				X	X		
Building interaction	None	X						
	With zone air temperature		X		X			X
	With detailed building model			X		X	X	
PV efficiency	Provided as an input				X	X	X	X
	Provided in a file as a function of temperature and irradiance				X	X	X	X
	Calculated from T_{PV} with provided reference efficiency and temperature coefficient	X						
	Calculated from G and T_{PV} with provided reference efficiency and temperature and irradiance coefficients		X	X	X	X	X	X

2.1.5 Conclusion

This section showed that characterizing the performance of PV-T technology is not as straightforward as following the procedures recommended in performance standards for PV modules and solar thermal collectors. One of the reasons is that in a PV-T collector, there is an

interaction between the electrical and thermal yield. It might be possible to encapsulate this relation through the solar cells temperature, but it is not clear how this temperature relates to the thermal yield and to the ambient and operating conditions. In addition, it is not straightforward to actually measure the temperature of the solar cells in a PV-T collector because of the absorber non-uniform temperature and the fact that the back of the cells is not always accessible for sensor mounting. Obtaining a relation between the electrical and thermal performance could be useful because it can lead to the development of simple performance prediction models suitable for design purposes.

Section 2.1 also showed that there are PV-T and BIPV-T models available in common building or energy simulation tools. Some of these models are very simple, but require parameters that can only be obtained from experimental testing. Other models are more complex and are based on energy balance equations performed on the different collector layers. These models have some drawbacks, however. For example, it is not clear if they have been validated experimentally and identical relations are used to estimate the top and bottom surfaces heat transfer coefficients in the cavity.

2.2 Benefits of PV-T and BIPV-T Technology

Section 2.1 focused on the performance characterization of solar technologies, including PV-T collectors, and the different variables that affect the amount of energy produced. In this section, the emphasis is on the various methods used

- To optimize the performance of PV-T or BIPV-T collectors and systems; and
- To quantify the benefits compared to other solar technologies.

2.2.1 Collector

PV-T collectors produce both thermal and electrical energy. Depending on the application, a PV-T collector can be designed to maximize either the electricity or the thermal energy production. Most of the time, however, the search is for a good balance between the two types of energy. Several methods have been used to encapsulate the thermal and electrical performance into one single metric and find the optimal collector design.

The concept of combined efficiency defined as the sum of the electrical and thermal efficiencies is often used for comparing different designs (Garg & Adhikari, 2000; Othman et al., 2007; Sopian et al., 2000):

$$\eta_T = \eta_{th} + \eta_{el} \tag{2-28}$$

The combined efficiency was used by Garg & Adhikari (2000) to compare single glazed and double glazed PV-T air collectors. They concluded that the reduced heat losses of the double glazed collector were not worth the transmission losses, and thus, that a single glazed collector was more appropriate. Chow et al. (2009) compared the performance of glazed and unglazed thermosyphon PV-T collectors. They found that the thermal efficiency of the glazed collector was higher than that of the unglazed collector (50.4% vs 40.8%), but that the electrical efficiency was lower for the glazed than for the unglazed collector (9.3% compared to 12.1%). When considering the combined efficiency as defined in Equation (2-28), they concluded that the glazed collector generally had a better performance regardless of the collector rated electrical efficiency, irradiance level, ambient temperature and wind speed.

One of the issues with the combined efficiency as a performance indicator is that it does not take into account the fan power required to circulate the heat recovery fluid in the collector. If heat transfer enhancement strategies such as fins or double pass flow paths are added to the collector to increase the thermal energy production, the combined efficiency does not consider the incremental fan power associated with the added pressure drop of such design feature. This aspect was taken into account by Hegazy (2000) who used the net combined efficiency, $\eta_{T,net}$, as a performance indicator to compare different PV-T collector designs:

$$\eta_{T,net} = \eta_{th} + \eta_{el,net} \tag{2-29}$$

In Equation (2-29), $\eta_{el,net}$ is the net electrical efficiency defined as:

$$\eta_{el,net} = \frac{\eta_{PV,system} P_{PV,DC} - P_{flow}/\eta_{fan}\eta_{motor}}{A_g G} \tag{2-30}$$

In Equation (2-30), A_g is the collector gross area, $P_{PV,DC}$ is the DC PV system power, P_{flow} is the flow pumping power and η_{fan} and η_{motor} are the fan and electrical motor efficiencies,

respectively. The PV system efficiency, $\eta_{PV,system}$, accounts for balance of system (BOS) losses (batteries, cables, inverter, etc.) and was estimated at 56% by Hegazy. This performance indicator was used to compare different designs of glazed PV-T air collectors with monocrystalline solar cells on a daily basis. These four designs were considered:

1. Air flowing over the absorber
2. Air flowing below the absorber
3. Air flowing on both sides of the absorber in a single pass configuration
4. Air flowing on both sides of the absorber in a double pass configuration

The best net combined efficiency was obtained with the air flowing on both sides of the absorber in a single pass configuration regardless of flowrate. Daily combined efficiencies for the Egyptian climate ranging from 32% to 54% were obtained for flowrates between 18 kg/(h·m^2) and 144 kg/(h·m^2).

The studies mentioned previously all assume that both thermal and electrical energy have the same value. This is not necessarily the case, however, as the relative value between the electricity and thermal energy depends on what the two types of energy are offsetting. To take this aspect into account, some researchers (Huan et al., 2001; Jiang et al., 2008; Tiwari & Sodha, 2007) have used a combined primary energy saving efficiency, $\eta_{T,P}$, as a performance indicator to compare different PV-T collector designs. In this case, the electrical efficiency is divided by the grid efficiency at generating electricity, $\eta_{gen,grid}$, to convert it into primary energy as shown in Equation (2-31):

$$\eta_{T,P} = \eta_{th} + \frac{\eta_{el}}{\eta_{gen,grid}} \tag{2-31}$$

Huang et al. (2001) used this definition to study the performance of an unglazed sheet-and-tube PV-T water collector with polycrystalline silicon cells (pc-Si). Using a grid efficiency of 38% corresponding to a typical thermal power plant, they obtained a daily combined primary energy saving efficiency of 38%. Jiang et al. (2008) evaluated the influence of PV coverage on the performance of a PV-T Trombe wall also using the combined primary energy saving efficiency and a grid efficiency of 38%. They obtained that the combined primary energy saving efficiency

of a PV-T Trombe wall improved from 15% to 37.5% when increasing the PV coverage ratio from 0.2 to 0.9 even though the thermal efficiency decreased from 7.5% to 2.5%. Tiwari & Sodha (2007) also used this performance indicator to study the effect of glazing and Tedlar films on PV-T air collector designs. As expected, they found that glazed collectors had a greater thermal efficiency, but lower electrical efficiency than unglazed collectors. Using a grid efficiency of 40%, the benefit of a Tedlar film was established as being dependent on flowrate and collector length.

To take the different value between electrical and thermal energy into account, Garg & Adhikari (2000) used the concept of combined exergetic efficiency. Using that concept, they concluded that an unglazed PV-T air collector usually performed better than a double glazed PV-T collector, except at high levels of radiation and ambient temperature. With that same objective of accounting for a relative value between thermal and electrical energy, a concept similar to primary energy called the equivalent thermal energy has also been used. Athienitis et al. (2011) used the equivalent thermal efficiency, $\eta_{th,eq}$, to evaluate the performance of a BIPV-T transpired air collector. In this case, the electrical energy is converted into thermal energy assuming it is being used to run a heat pump. Thus, the electrical energy is multiplied by a heat pump coefficient of performance (COP_{HP}) and $\eta_{th,eq}$ is given by:

$$\eta_{th,eq} = \eta_{th} + COP_{HP} * \eta_{el} \tag{2-32}$$

Coventry & Lovegrove (2003) considered different methodologies to convert electrical energy into thermal energy for a liquid PV-T collector used for domestic hot water heating: based on exergy, greenhouse gas emissions, life cycle emissions and a market analysis. For this last approach, they considered both a free market energy cost and a renewable energy market energy cost where incentives and subsidies are available for renewable energy technologies. They obtained relative values of electrical energy over thermal energy varying between 1.33 (open market energy cost) and 16.8 (exergy analysis). A critical review of the different methods led the authors to conclude that the best approach was a market analysis based on renewable energy technologies. With this methodology, a relative value of electricity compared to thermal energy of 4.24 was obtained. A comparison of PV-T liquid systems using either c-Si or a-Si modules as the absorber showed that a-Si cells would be better only up to a relative value of 4.5.

2.2.2 System

When considering PV-T systems as opposed to collectors only, several methods can also be used to evaluate the performance.

One method to quantify the performance of a PV-T system is to compare the building space heating, domestic hot water heating or space cooling load with and without the presence of a PV-T collector. This strategy was used in Mei et al. (2003) where a study of the Mataro library near Barcelona, Spain, is presented. This building has a BIPV-T façade that preheats outdoor air for direct space heating usage. Compared to a brick façade, it is stated that this system reduces the heating load by nearly 12%. Ben Nejma et al. (2013) simulated and validated experimentally a 70 m^2 PV-T air collector operated at 1,500 m^3/h (~25 $kg/(h \cdot m^2)$) in a net-zero energy house (NZEH) in Chambéry, France. In this case, the PV-T collector was coupled with a water-to-water heat pump and a 1000 L storage tank supplying fan coils for space heating purposes. This system reduced the space heating electrical consumption by approximately 150 kWh/y (or 10%) compared to the same system without a PV-T collector. Cartmell et al. (2004) examined the solar system of the Brocks Hill Environment Centre in the UK. This building has a 37 m^2 PV-T air collector coupled with a 12.5 m^2 solar air collector booster. The thermal energy recovered was either used directly to supply an air-handling unit or indirectly, to preheat water entering the main storage tank through an air-to-water heat exchanger. Monitored data showed that this system was able to contribute to 64.4% and 35% of the annual hot water and thermal loads, respectively.

Another approach consists of focusing on the added value of having a specific technology assisted by a PV-T collector. Kamel & Fung (2014) completed simulations to evaluate the performance of a 46 m^2 BIPV-T air collector combined with an air source heat pump (ASHP) in different Canadian locations for a semi-detached prototype home. The solar assisted ASHP system was operated at 0.4 kg/s (~30 $kg/(h \cdot m^2)$). Compared to a stand-alone ASHP, this system reduced the energy consumption (compressor and outdoor fan) by 1,111 kWh/y (or 10.8%) for Edmonton and 1,188 kWh/y (or 18%) for Toronto. Pantic et al. (2010) considered a BIPV-T air collector for both space and water heating coupled with a rockbed storage unit. During winter, the preheated fresh air was directly fed to the house air handling unit whenever space heating was required. It was stored in a rockbed storage unit for later use otherwise. In the summer, the air was used to heat water through an air-to-water heat exchanger. For a winter day, the heat load

was found to be reduced by nearly 49% after supplying heat from the rockbed storage. Chen et al. (2010a) considered using a BIPV-T collector for space heating through a ventilated concrete slab (VCS) located in the basement of a house by operating the collector at 250 L/s (~15 kg/(h·m^2)). They showed that between 9 and 12 kWh of thermal energy could be stored in the ventilated concreted slab during a clear sunny day with an outdoor temperature of 0 °C.

In Filliard et al. (2009), the influence of a PV-T collector on both the building energy consumption and the air-source heat pump performance is presented. In this study, the effect of coupling a 4 kW ASHP with a 30 m^2 PV-T air collector in a 135 m^2 single family house in Trappes, France, is investigated. It was found that at a flowrate of 2,000 m^3/h (~75 kg/(h·m^2)), the PV-T air collector could increase the heat pump COP from 3.06 to 3.67. It reduced the building heating energy consumption by only 2%, however, because of the additional fan required to recover the heat from the PV modules.

2.2.3 Comparison with other technologies

Sections 2.2.1 and 2.2.2 presented different strategies to present the performance and benefit of PV-T or BIPV-T collectors or systems. In this section, the focus is on studies that have looked at quantifying the benefit of PV-T or BIPV-T collectors or systems with respect to other solar energy technologies.

Santbergen & van Zolingen (2008) compared a PV-T system used for domestic hot water to side-by-side PV modules and solar thermal systems using the concept of primary energy. In this case, the primary energy savings were defined as:

$$Q_{T,P} = \frac{Q_{th}}{\eta_{p\rightarrow th}} + \frac{Q_{el}}{\eta_{gen,grid}} \tag{2-33}$$

In Equation (2-33), $\eta_{p\rightarrow th}$ is the efficiency for converting primary energy to thermal energy. Using $\eta_{gen,grid} = 0.40$ and $\eta_{p\rightarrow th} = 0.65$ for the thermal efficiency of a conventional gas fired domestic hot water system, the primary energy savings of the PV-T system were estimated at around 700 kWh/(m^2·y) compared to 300 kWh/(m^2·y) for a PV system and 500 kWh/(m^2·y) for a solar thermal system.

Bakker et al. (2005) compared a PV-T water heating system combined with a geothermal heat pump to side-by-side PV modules and solar thermal collectors producing the same amount of thermal and electrical energy. They found that the initial cost of the PV-T system was similar to that of the PV module and solar thermal collector side-by-side, but that the side-by-side system required 32% additional roof surface area. Da Silva & Fernandes (2010) also used the concept of equivalent area to compare a glazed sheet-and-tube PV-T liquid collector with pc-Si modules to side-by-side PV and solar thermal collectors producing the same amount of energy. They obtained annual thermal and electrical efficiencies of 15% and 9%, respectively for a four-person household in Lisbon. Side-by-side PV and thermal systems producing the same amount of thermal and electrical energy would have required an additional area of 60% compared to the PV-T collector.

In Tiwari et al. (2009), the concept of embodied energy is used to analyze the performance of PV-T air collectors for the New Delhi climatic conditions in comparison with stand-alone PV modules: the energy payback time (EPBT) defined as the ratio of embodied energy over annual energy generated and the life cycle conversion efficiency (LCCE) corresponding to the energy production of the system with respect to irradiance over the system lifetime. In this study, the total energy generated by a PV-T system is converted into equivalent thermal energy by dividing the electrical energy by a grid efficiency of 38%. For a PV-T collector with BOS operating during 15 years, they obtained the following performance indicators: EPBT=3.22 and LCCE=0.063. For a PV module, the following values were obtained: EPBT=4.15 and LCCE=0.0579. Thus, it was concluded that a PV-T collector was a better technology from an embodied energy perspective.

In order to compare simple PV modules to PV-T water collectors, Erdil et al. (2008) used the incremental simple payback defined as the incremental cost of a PV-T collector compared to a PV module divided by the incremental annual energy savings. They found that the incremental simple payback period of a PV-T collector compared to a PV module was 1.7 year using the thermal energy for domestic hot water heating.

2.2.4 Conclusion

This section presented different methodologies used in the literature to quantify the performance of PV-T collectors and systems and to show the actual benefit in comparison with other solar

energy technologies. The results of the different studies mentioned in Sections 2.2.1 to 2.2.3 are summarized in Table 2-7 and Table 2-8. Table 2-7 provides an overview of the variety of results obtained using different performance indicators including both liquid and air PV-T collectors and systems. This table shows that a large number of performance indicators can be used for PV-T collectors. They can be based on instantaneous, daily, monthly or annual calculations and can be developed from either economic, energy or exergy analysis. Table 2-8 gives an overview of the performance of different air-based PV-T or BIPV-T collectors when coupled with various heat management strategies. It shows that the performance of a PV-T collector varies significantly depending on the relative value given to electricity in comparison with thermal energy.

Table 2-7: Review of performance indicators used for PV-T and BIPV-T collectors and systems

Performance indicator	Results	Ref.
Total energy	Single glazed is better than double-glazed	Garg & Adhikari (2000)
	Glazed thermosiphon collector is better than unglazed	Chow et al. (2009)
Net energy	On a daily basis, a glazed mono c-Si PV-T air collector with air flowing on both sides of the absorber in a single pass configuration performs the best with $\eta_{T,net}$=32% at 18 kg/(h·m^2)	Hegazy (2000)
Primary energy	Daily combined primary energy saving efficiency of 38% for a pc-Si unglazed sheet-and-tube PV-T water collector	Huang et al. (2001)
	Combined primary energy saving efficiency of a PV-T Trombe wall improves from 15% to 37.5% when increasing the PV coverage ratio from 0.2 to 0.9	Jiang et al. (2008)
	The benefit of a Tedlar film is dependent on flowrate and collector length	Tiwari & Sodha (2007)
	A PV-T system used for DHW has primary energy savings of 700 kWh/(m^2·y) compared to 300 kWh/(m^2·y) for a PV system and 500 kWh/(m^2·y) for a solar thermal system	Santbergen & van Zolingen (2008)
Exergy	The combined exergetic efficiency of an unglazed PV-T air collector is better than that of a double glazed PV-T collector except at high irradiance and ambient temperature	Garg & Adhikari (2000)
Equivalent thermal energy	The BIPV-T air transpired collector has an equivalent thermal efficiency 17% and 7% higher than an unglazed transpired solar collector at low and high flowrates, respectively	Athienitis et al. (2011)
Market analysis	An a-Si PV-T liquid collector is better than one using c-Si only up to a relative value of 4.5	Coventry & Lovegrove (2003)
Economic	The incremental simple payback period of a water-based PV-T collector for DHW compared to a PV module is 1.7 year	Erdil et al. (2008)
Embodied energy	The energy payback time of a PV-T collector is 3.22 for a PV-T collector compared to 4.15 for a PV module	Tiwari et al. (2009)
Equivalent area	When used in combination with a geothermal heat pump, PV module and solar thermal collector side-by-side require 32% more roof surface area than a PV-T water heating system	Bakker et al. (2005)
	To produce the same amount of energy with side-by-side PV and solar thermal collectors than with a glazed sheet-and-tube pc-Si PV-T liquid collector, 60% more surface area would be required	Da Silva & Fernandes (2010)

Table 2-8: Review of the performance of BIPV-T and PV-T air systems

Strategy	City (Country)	Thermal Performance	Ref.
Fresh air preheating (commercial)	Montreal (Canada)	55 MWh/y of useful thermal energy production	Bambara (2012)
	Barcelona (Spain)	Heating load reduction of 11.6%	Mei et al. (2003)
Assisting ASHP (residential)	Edmonton (Canada)	1,111 kWh/y (10.8%) ASHP energy consumption reduction	Kamel & Fung (2014)
	Toronto (Canada)	1,188 kWh/y (18%) ASHP energy consumption reduction	(Kamel & Fung, 2014)
	Trappes (France)	2% building heating energy consumption reduction	Filliard et al. (2009)
Assisting WSHP for space heating with storage tank and fan coils (residential)	Chambéry (France)	150 kWh (10%) space heating electrical consumption reduction	Ben Nejma et al. (2013)
Assisting WSHP for space heating with storage tank and radiant floor (residential)	Montreal (Canada)	WSHP electrical consumption reduction by an additional 195 kWh/y (23.5%) with control strategy optimization	Candanedo & Athienitis (2009)
Supply of air handling unit for space heating and DHW preheating with air-to-water HX (commercial)	Leicester (UK)	Contribution to 64.4% of DHW load and 35% of space heating load	Cartmell et al. (2004)
Space heating through a VCS	Montreal (Canada)	Storage potential of 9-12 kWh during a sunny day at 0 °C	Chen et al. (2010a; 2010b)

This review shows that several methods can be used to compare the performance of PV-T collectors with other solar technologies to determine whether or not this technology is competitive. In addition, it demonstrates that when selecting the boundaries and control volumes of a study, several approaches can be taken. One of these approaches is to limit the control volume to the collector and to compare the area required by the PV-T system and the side-by-side PV modules and solar thermal collectors to produce the same amount of thermal and electrical energy. Another approach consists of expanding the control volume to the overall building space heating, ventilating or domestic hot water heating system.

CHAPTER 3 OBJECTIVES AND THESIS ORGANISATION

The work presented in this document aims at removing some of the barriers that currently limit the integration of PV-T or BIPV-T air collectors in high performance buildings. Its purpose is to address some of the issues related to the performance characterization of PV-T technology and to identify the actual cost-benefit of integrating BIPV-T air collectors in high performance residential buildings compared to more traditional solar energy technologies such as PV modules and liquid solar thermal collectors.

To achieve this objective, a model is developed and validated using experimental data. The experimental procedure followed to collect the data is based on existing PV modules and solar thermal collectors' performance characterization standards. Additional measurements are performed, however, to address some of the issues related to the thermal and electrical performance characterization of combined solar photovoltaic and thermal technologies. Finally, the validated model is used to quantify the benefits of integrating BIPV-T air collectors in high performance residential buildings and to compare the savings to those obtained with standard PV, BIPV and solar thermal collectors.

3.1 Thesis Objectives

This thesis has three main objectives that can be divided in sub-objectives:

- To develop and validate experimentally a model applicable to PV-T and BIPV-T air collectors and to implement this model in a commonly used energy simulation tool
    - Develop a 2-D steady-state model of a BIPV-T air collector;
    - Develop an experimental procedure to characterize the electrical and thermal performance of a BIPV-T air collector based on existing PV modules and solar thermal collectors standards;
    - Collect data on a prototype collector;
    - Compare the results obtained with the collector to that obtained with the model for a similar design under the same operating and environmental conditions;

  - Modify the model to improve its accuracy at predicting the thermal and electrical yield; and
  - Implement it in a commonly used energy simulation tool

- To address some of the issues related to the thermal and electrical performance characterization of PV-T air collectors
  - Using the data collected to validate the model, obtain the parameters generally required to characterize the performance of PV modules and solar thermal collectors;
  - Validate the potential of using the equivalent cell temperature method to determine the PV cells' operating temperature in a PV-T air collector
  - Identify the interaction between the collector thermal and electrical yield; and
  - Develop a system to simultaneously present the thermal and electrical performance.
- To identify the benefit of integrating BIPV-T air collectors in high performance buildings compared to standard solar technologies such as PV modules and solar thermal collectors
  - Using the validated model, develop a methodology to compare the cost-benefit of a BIPV-T air system to that of stand-alone PV modules and solar thermal systems;
  - Apply this methodology to a generic case where the useful part of the thermal energy produced by the collector is unknown;
  - Develop housing archetypes of energy-efficient Canadian residential homes;
  - Quantify the amount of electricity and useful thermal energy that can be produced by integrating BIPV-T air collectors in these housing archetypes considering various heat management strategies; and
  - Compare this benefit to that obtained with stand-alone PV module and solar thermal collectors.

3.2 Thesis Organization

This thesis is divided in eight chapters and follows the format of an article-based thesis. Chapter 1 introduces this thesis by providing some background information on the relevance and potential scientific contribution of the work proposed. In Chapter 2, a literature review is presented. This chapter covers the main issues related to the performance characterization of PV-T air collectors and the challenges in quantifying the benefits of this technology. Chapter 3 details the three main objectives of this thesis and provides a brief description of the content of each chapter.

Chapter 4 presents the first article entitled "Experimental Study to Characterize the Performance of Combined Photovoltaic-Thermal Air Collectors" published in the Journal of Solar Energy Engineering. This article provides a description of a procedure developed to characterize the performance of a PV-T air collector. An analysis of the data collected is presented as well as the different methods tested to obtain the electrical parameters and the thermal efficiency model coefficients. The application of the equivalent cell method to determine the PV cells' temperature in a PV-T air collector is validated. A correlation is developed to predict the solar cells temperature based on the in-plane irradiance and the air inlet and outlet temperatures. This correlation provides a relation between the collector thermal and electrical yield and allows the development of a 5-plot system to fully encapsulate the performance of solar collectors producing both thermal and electrical energy simultaneously.

Chapter 5 presents the second article entitled "A novel approach to compare building-integrated photovoltaics/thermal air collectors to side-by-side PV modules and solar thermal collectors" published in the journal Solar Energy. The first part of this article provides a detailed description of the BIPV-T air collector 2D steady-state model developed and implemented in TRNSYS, an energy simulation tool. The validation against experimental data is also presented. This validation helped selecting proper convective heat transfer correlations at the absorber surface and in the collector air cavity. The second part of this article focuses on the cost-benefit comparison of a BIPV-T air collector with side-by-side stand-alone PV modules and solar thermal collectors. This cost-benefit analysis is done using an innovative methodology that allows dealing with two types of energy without linking the collectors to specific heat management strategies.

Chapter 6 presents the third article entitled "Cost-Benefit Analysis of Integrating BIPV-T Air Systems into Energy-Efficient Homes" published in the journal Solar Energy. In this article, the

development of all-electric energy-efficient Canadian housing archetype models is presented. These homes are simulated with three different solar energy technologies: a BIPV system, side-by-side PV modules and solar thermal collectors (PV+T) and a BIPV-T system. For the BIPV-T system, four different heat management scenarios are considered. The cost-benefit of the BIPV-T system compared to the BIPV and PV+T systems is evaluated using a variation of the methodology developed in article 2 and the concept of break-even cost.

A general discussion and the conclusion and recommendations of the present study are given in Chapter 7 and Chapter 8, respectively.

CHAPTER 4 ARTICLE 1: EXPERIMENTAL STUDY TO CHARACTERIZE THE PERFORMANCE OF COMBINED PHOTOVOLTAIC/THERMAL AIR COLLECTORS

Delisle, V., Kummert, M., (2012). *Journal of Solar Energy Engineering*, *134*(3).

Note: The article in its original version used the abbreviation PV/T for combined photovoltaics with thermal energy recovery. It was modified to PV-T in this chapter to provide consistency throughout the document. Also, modifications were made to Section 4.4.4 and 4.5.1 to better explain the location of the cell temperature measurement and the concept of equivalent cell temperature.

4.1 Abstract

Background: Combined photovoltaic-thermal (PV-T) collectors show great potential for reaching the objective of net-zero energy consumption in buildings, but the number of products on the market is still very limited. One of the reasons for the slow market uptake of PV-T collectors is the absence of standardized methods to characterize their performance. Performance characterization is a challenge for PV-T collectors because of the interaction between the thermal and electrical yield. This study addresses this particular issue for PV-T air collectors used in either closed-loop or open-loop configurations. In particular, it presents the potential of the equivalent cell temperature method to determine the temperature of the PV cells in a PV-T air collector and validates models to predict the thermal performance and cell temperature for this particular type of solar collector. **Method of Approach**: Indoor and outdoor experimental tests were performed on two c-Si unglazed PV-T modules. The indoor part of this procedure provided the thermal diode voltage factor and the open-circuit voltage temperature coefficient, two parameters that are essential in the calculation of the equivalent cell temperature. The outdoor procedure consisted of acquiring simultaneous electrical and thermal measurements at various inlet temperatures and flowrates. **Results**: For the collector used in a closed-loop configuration, thermal efficiency models using the fluid inlet, outlet or average temperature in the calculation of the reduced temperature provided similar results. For an open-loop configuration, a thermal efficiency model as a function of the fluid outlet flowrate was found to be more appropriate. Using selection of variable methods, it was found that a multiple linear regression model using

the fluid inlet temperature, the irradiance and the fluid outlet temperature as predictive variables could be used to estimate both the PV module back surface average temperature and the equivalent cell temperature. When using the PV temperature predicted by these models in the electrical efficiency model, both PV temperatures showed similar performance. **Conclusions:** In collectors where the PV back surface temperature is not accessible for temperature sensors mounting, the equivalent cell temperature provides a valuable alternative to be used as the PV temperature. The PV-T collector thermal and electrical performance in either closed-loop or open-loop configurations was found to be encapsulated with a series of 5 plots.

4.2 Keywords

Characterization; equivalent cell temperature; performance; PV-T collector; testing

4.3 Introduction

Buildings account for almost a third of the worldwide energy consumption and greenhouse gas emissions. If current trends are maintained, the International Energy Agency (IEA) estimates that the building sector energy consumption could increase by 60% from 2007 to 2050 (IEA, 2010). This has resulted in an increased interest for net-zero energy buildings (NZEB) in recent years, and a number of research projects were launched on the technologies required to reach net-zero energy consumption. Combined photovoltaic-thermal (PV-T) collectors are among the technologies that are of great interest for NZEB both in residential and in commercial sectors. These collectors use PV cells as a thermal absorber and recover the heat losses from the PV to produce electricity and thermal energy simultaneously (PV Catapult, 2006). This can be done actively or passively, by a heat transfer fluid that can be either air or a liquid. Recovered heat can then be used directly in commercial buildings as pre-heated fresh air or in the case of a house, coupled with other technologies to provide domestic hot water heating or space heating.

A number of recent projects have demonstrated the potential of PV-T collectors to fulfill part of the energy requirements of buildings (Noguchi et al., 2008; Pogharian et al., 2008; Athienitis et al., 2011). The number of products available on the market is still, however, very limited. A study conducted on the barriers of the PV-T collector market penetration (Zondag, 2008) has shown that the absence of certification, the lack of information on their cost-benefit ratio compared to side-by-side PV and solar thermal collectors and the absence of tools to get a quick estimate of

the yield of these collectors were among the reasons for the slow interest of architects and manufacturers towards this technology. In fact, even though there are standardized testing methods to characterize the performance of solar thermal collectors and PV modules, separately, there are currently no standards adapted to PV-T collectors. Manufacturers can choose the procedure used to test their products and they are not required to present their performance in any particular way. As a result, it is difficult to compare different systems and to get a quick estimate of their performance.

This study addresses some of the issues related to the thermal and electrical performance characterization of PV-T collectors. In particular, the objectives are:

- To validate the potential of the application of the equivalent cell temperature method to determine the PV cell's temperature in PV-T air collectors,
- To validate models to predict the thermal performance of PV-T air collectors, and;
- To present a graphical method to encapsulate the performance of PV-T air collectors for system design purposes.

The focus is on collectors using air as the heat transfer fluid, since experience with this technology in Canada has mainly been obtained with air collectors (Noguchi et al., 2008; Pogharian et al., 2008; Athienitis et al., 2011). Both closed-loop systems (with recirculated air) and open-loop configurations (for fresh air preheating) are considered. To achieve these objectives, an experimental procedure with indoor and outdoor components was developed as presented in Section 4.5. During these indoor and outdoor experiments, data were collected to obtain the parameters required to calculate the PV equivalent cell temperature as well as the collector thermal and electrical efficiencies under a wide range of conditions. The potential of using the equivalent cell temperature as the PV operating temperature in a PV-T collector was evaluated. This was achieved by developing the electrical models in Section 4.6 using either the equivalent cell temperature or the PV back surface average temperature as the PV operating temperature and comparing their performance at predicting the PV efficiency. Then, models were developed to predict the collector thermal efficiency under quasi-stationary conditions for the collector operating in both closed-loop and open-loop conditions. Using statistical methods, the important variables in the prediction of the equivalent cell temperature and PV back surface average temperature were investigated and empirical models were developed to predict these

temperatures. These models provided a link between the electrical and thermal performance of the collector which was used to develop the graphical method encapsulating the collector thermal and electrical performances.

4.4 Literature Review

This section presents a literature review on PV modules and solar thermal collector performance characterization standards. It also provides an overview of the work related to PV-T collector performance characterization, highlighting the main issues with the testing of this technology.

4.4.1 PV Modules Standards

There are two international standards available on design qualification and type approval of PV modules: IEC 61215 for terrestrial c-Si PV modules (IEC, 2005) and IEC 61646 for thin film PV modules (IEC, 1998). In both documents, procedures are described for module characterization and durability testing. Tests associated with the performance characterization can be performed indoors or outdoors and include the determination of the maximum power point, the temperature coefficients, the normal operating cell temperature (NOCT) and the module performance at standard testing conditions (STC), NOCT and low irradiance.

4.4.2 Air Solar Thermal Collector Standards

In North America, the ANSI/ASHRAE standard 93-2010 (ASHRAE, 2010) is typically used for characterizing the performance of air and liquid solar thermal collectors. For air collectors, this standard contains procedures to obtain the collector's time constant, incidence angle modifier, infiltration (or leakage) rate as a function of collector pressure and thermal performance in quasi-stationary conditions. The collector's thermal efficiency, η_{th}, is represented with the following variation of the Hottel-Whillier Bliss (HWB) equation (Hottel & Whillier, 1958):

$$\eta_{th} = \left(\frac{A_a}{A_g}\right) F_R^* \left[(\tau\alpha)_e - U_L^* \left(\frac{T^* - T_a}{G}\right)\right] \tag{4-1}$$

In Equation (4-1), A_a/A_g is the ratio of collector aperture area over the collector gross area, U_L^* is the collector heat loss coefficient, $(\tau\alpha)_e$ is the effective transmittance-absorptance product and $(T^* - T_a)/G$ is the reduced temperature. In ANSI/ASHRAE 93-2010, the fluid inlet temperature,

T_i, is used as the characteristic temperature T^* in the calculation of the reduced temperature and thus, the heat removal factor F_R^* corresponds to the classical F_R coefficient of the HWB equation (Hottel & Whillier, 1958). This is different from what is typically used in Europe for solar thermal collectors. In the European standard EN 12975-2 (ECS, 2005) addressing the performance characterization of liquid solar thermal collectors, the arithmetic average fluid temperature, T_{fm}, is used as T^* along with the heat removal factor F_{av}.

In Europe, there are no official standards to characterize the performance of solar air collectors, but a draft has been developed for non-concentrating collectors where the fluid enters and leaves the collector by only one inlet and one outlet (Buchinger, 2006). According to this document, one of the main challenges for air solar collector characterization is that the heat transfer rate between the absorber and the heat transfer fluid is lower than in liquid collectors. As a result, the influence of flowrate on the collector's performance is greater and it is difficult to apply results obtained on a collector sample to one of greater surface area. This document has some similarities with the ANSI/ASHRAE standard 93-2010, but one main difference is the choice of T^*. Buchinger (2006) recommends using the fluid outlet temperature, T_o, as T^* as opposed to T_i or T_{fm}. In air collectors, T_o is close to the average collector temperature, hence it is a more logical choice for a temperature used in calculating the average loss coefficient.

4.4.3 PV-T Collector Characterization

There are currently no standards for characterizing or reporting on the performance of PV-T collectors. In the literature, the thermal performance of liquid PV-T collectors is often presented as a function of the reduced temperature $(T_i - T_a)/G$ (Sandnes and Rekstad, 2002; Zondag et al., 2002; Tonui & Tripanagnostopoulos, 2007). As for the electrical performance, its dependence on irradiance and temperature cannot be captured using only the reduced temperature. In order to encapsulate the electrical performance of an open-loop air PV-T collector, Othman et al. (2007) presented I-V curves for different irradiance levels at fixed flowrate and ambient temperature and the electrical efficiency for different flowrates as a function of the fluid average arithmetic temperature.

In 2003, the European initiative PV Catapult produced a guide to highlight the main issues with PV-T collector performance testing and to suggest elements to incorporate into the standards IEC

61215 (2005) and EN 12975-2 (ECS, 2005) to address these issues. The guide from PV Catapult (2005) focuses on non-concentrating liquid PV-T collectors using c-Si PV cells. One of the main issues discussed in this document is the fact that in a PV-T collector, the thermal performance influences the electrical performance and vice-versa. Thus, taking thermal measurements with the PV short-circuited or in open-circuit would later require the introduction of a thermal performance correction factor to account for the fact that in reality, the collector also produces electricity. PV Catapult concludes that since this factor is probably not straightforward to obtain, the PV-T collector should be producing electricity when taking thermal measurements and that it should be operating at its maximum power point. In order to save on testing time, it is further suggested that both electrical and thermal measurements be taken simultaneously by maintaining the PV at its maximum power point during thermal measurements and performing I-V curves at regular time intervals. Another issue discussed in the PV Catapult guide (2005) is the feasibility of performing PV-T collector measurements indoors. Most indoor simulators used for solar thermal collector testing cannot be utilized for PV-T collectors since these usually don't have the spatial uniformity and spectral distribution required for PV testing. Similarly, the lamps used in PV testing installations are not appropriate for solar thermal collectors because these only provide a flash of light and thus, do not allow for steady-state thermal testing. As a result, PV Catapult recommends performing outdoor measurements. For glazed collectors, PV Catapult suggests taking four measurements of thermal efficiencies and reduced temperature in steady-state conditions for four different average fluid temperatures, T_{fm}, in order to obtain 16 measurement points. For unglazed collectors, three temperature values T_{fm} at three different wind speeds are recommended for a total of 9 measurement points. The models suggested to characterize the performance are those of EN 12975-2 for liquid solar thermal collectors. These models have a higher level of complexity than the HWB model since for glazed collectors, a second order term is added to take the non-linearity of thermal losses into account and in the case of unglazed collectors, wind dependency terms are incorporated. For the electrical measurements, PV Catapult suggests obtaining instantaneous maximum power point measurements through current-voltage (I-V) tracing in order to fill out a matrix with 100 W/m^2 irradiance bins and 5 °C temperature bins in a minimum span of 30 °C. Considering that the PV temperature cannot necessarily be measured, the draft states that the temperature used in the thermal bins should have

a direct relation with the actual PV temperature so that the latter can be calculated during the data analysis from the measured temperature, weather and collector thermal performance.

As part of the International Energy Agency Solar Heating and Cooling Program (IEA SHC) Task 35 "PV-Thermal Solar Systems", a report was produced to suggest three types of characterization schemes for PV-T collectors with different levels of detail for design, rating and marketing purposes (Collins, 2008). The PV-T collector design scheme concept developed consists of a 3-plot system with a 1st plot presenting the thermal performance as a function of the reduced temperature, a 2nd plot showing the link between the reduced temperature and $(T_{PV} - T_a)/G$ and finally, a 3rd plot expressing $(T_{PV} - T_a)/G$ as a function of the electrical efficiency for various ambient temperatures. This scheme has great potential to be used for design purposes or for performance comparison between different collectors since both the thermal and electrical efficiencies can be obtained by navigating from one plot to another without having to perform any calculations. It has some limitations, however, because it only applies to a particular flowrate and wind speed and additionally, in the case of the 3rd graph, to a single inlet temperature.

4.4.4 Summary

This review shows that the variables affecting the thermal and electrical performance of solar thermal collectors and PV modules operating separately are known, but that it is not clear how the interaction between the electrical and thermal yields can be encapsulated in the performance characterization of combined PV-T collectors. As mentioned by PV Catapult (2005), one way to relate both aspects could be to link the PV temperature to the collector thermal performance. Finding a relation between the two is a challenge, however, because the PV temperature in a PV-T collector is difficult to measure. In a PV module, the PV cell temperature is usually measured by placing a temperature sensor at the back surface of one of the solar cells. In a PV-T collector, the back surfaces of the cells are not at a uniform temperature because air is circulating behind the cells to recover the heat losses. In addition, the back of the cells is not always accessible for sensor mounting because the air cavity is generally narrow. Thus, since it is not clear how this temperature can be measured, it is also not straightforward to determine how it can be predicted from the weather and collector operating conditions, an essential piece of information to link the electrical and thermal performance and obtain simple performance prediction models that can be used for design purposes.

4.5 Methodology

The experimental procedure developed consists of two parts: an indoor procedure to obtain particular electrical parameters and an outdoor procedure to acquire measurements to fully characterize the collector thermal and electrical performance. The experiment was carried out on two unglazed PV-T collector modules having a total gross area of 3.513 m^2 with an absorber consisting of monocrystalline-silicone (c-Si) cells.

4.5.1 Indoor Testing Procedure

The indoor test aimed at obtaining the thermal diode voltage factor, D, and the open-circuit voltage temperature coefficient, $\beta_{Voc,}$ two parameters that are essential in the calculation of the equivalent cell temperature, ECT. In a PV module, the ECT is the average temperature at the electronic junctions of the module corresponding to the temperature at which the PV module would operate if it were operating uniformly at this temperature. According to the standard IEC 60904-5 (2011) containing the detailed procedure on how to obtain this temperature, the ECT can be calculated with Equation (4-2) assuming the open-circuit voltage and irradiance are known variables.

$$ECT = T_{PV,1} + \frac{1}{\beta_{Voc}}\left[V_{oc} - V_{oc,1} + DNs\ln\left(\frac{G_1}{G}\right)\right] \tag{4-2}$$

In Equation (4-2), V_{oc} is the open-circuit voltage, and Ns is the total number of cells in series in the PV array. The subscript *1* refers to the reference observation for which the PV temperature is known. The coefficient β_{Voc} is evaluated with open-circuit measurements obtained at different temperatures, but constant irradiance levels. As for the parameter D, it is calculated with two open-circuit voltages measured at the same PV temperature, but different irradiance conditions, G_3 and G_4, using Equation (4-3).

$$D = \frac{1}{Ns}\frac{V_{oc4} - V_{oc3}}{\ln(G_4/G_3)} \tag{4-3}$$

The tests required for the calculation of the parameters D and β_{Voc} are performed indoors, because these require that the PV temperature be kept uniform, and varied within a 30 °C temperature range. In theory, this uniform temperature could be achieved outdoors with a PV-T

collector under stagnation conditions, i.e., with no flow in the collector. In outdoor and stagnation conditions, however, the temperature inside the collector cannot be controlled. Thus, obtaining measurements in a large PV temperature range is difficult in a limited time frame.

This indoor test was performed with a Class B large area pulsed solar simulator located in an environmental chamber. Only one of the two PV-T modules was used because of space limitations. The irradiance was measured with a monocrystalline reference cell and the PV temperature was obtained with 6 thermocouples mounted at different locations at the back surface of the cells. The temperature coefficients were determined with sets of measurements taken at 7 different average back surface temperatures ranging from 10 to 36 °C at an irradiance of 1000 W/m^2. As for the thermal diode voltage, it was determined from I-V curves taken with the PV back surface average temperature constant at 25 °C at 5 irradiance levels varying from 200 W/m^2 to 1000 W/m^2. For each measurement, the room was heated or cooled until all PV back surface measurements were stable. Then, the irradiance was set to the desired level using crystalline sheets having the capability of varying the irradiance without affecting the spectrum. Finally, an I-V curve was traced while the collector was flashed with the lamp, and both the back surface PV module temperatures and reference cell short-circuit current were recorded. A total of three I-V curves were obtained for each set of conditions.

4.5.2 Outdoor Testing Procedure

The objective of the outdoor test was to gather sufficient data to characterize the collector thermal and electrical performance in open-loop and closed-loop configurations at normal incidence angle. To obtain these measurements, the two collectors were mounted in series on a zenith-azimuth tracking testing rig. Two collectors were used so that the area would be greater than 3 m^2 as recommended in the draft standard for solar air heaters (Buchinger, 2006). The two collectors were mounted in a building-integrated configuration, a typical mounting configuration for residential buildings. This was done by adding 25.4 mm of Styrofoam board insulation with a corresponding thermal resistance of 0.88 m^2·K/W to the collector rear and side surfaces. The collector was instrumented according to the recommendations of the ANSI/ASHRAE standard 93-2010 as shown in Figure 4-1. Blowers were mounted at both collector inlet and outlet to regulate the pressure inside the collector.

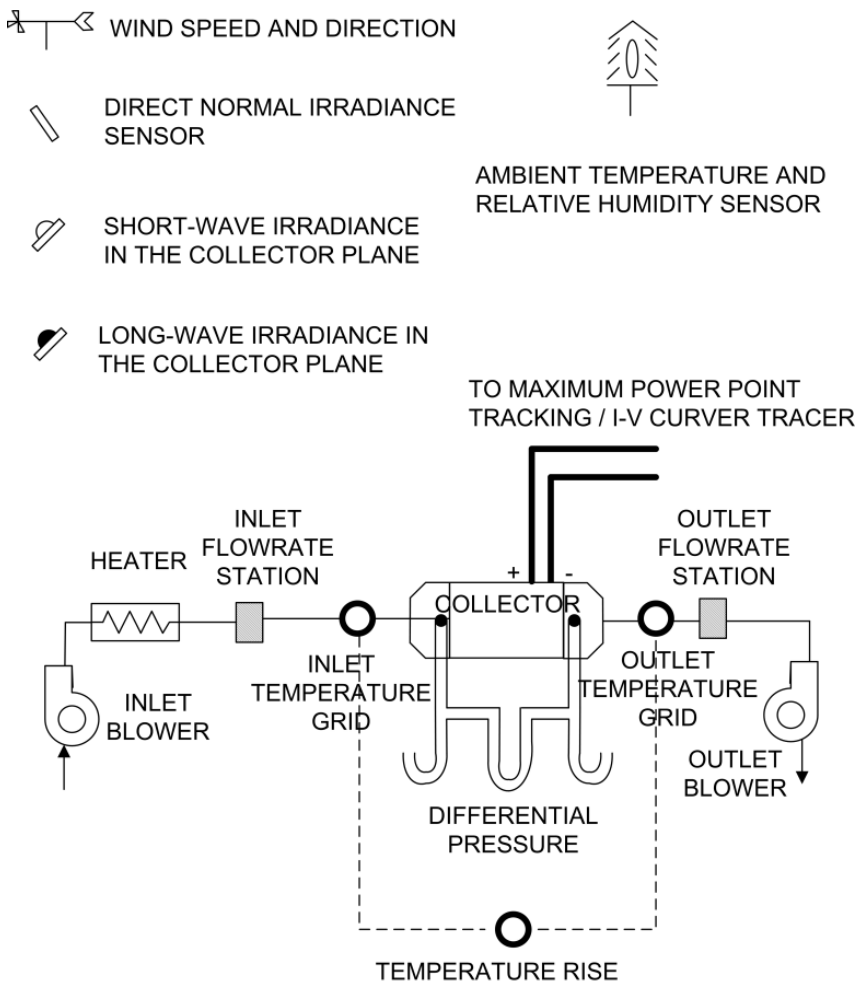

Figure 4-1: BIPV-T collector testing loop schematic

The inlet temperature and temperature rise measurements were done with type-T thermocouple grids located at the collector inlet and outlet. Each thermocouple grid consisted of a total of 12 thermocouples located in the middle of concentric circles of equal cross sectional areas as recommended in the ANSI/ASHRAE standard 93-2010 (ASHRAE, 2010). The pressure measurements were obtained with pressure taps located in the collector transition elements and a pressure transducer with digital output. Inlet and outlet flowrates were measured with differential pressure flow sensors. The in-plane short-wave and long-wave irradiance as well as the direct normal irradiance were measured with a pyranometer, pyrgeometer and pyrheliometer, respectively. The outdoor temperature and relative humidity were obtained with a humidity and temperature transmitter and the 10 m wind speed and direction were measured with a

propeller-type anemometer. The data measured by the sensors located on the testing rig were recorded at a 5 second time interval with a data acquisition system. As for the output signals of the wind, direct normal irradiance, ambient temperature and relative humidity sensors, these were recorded at a 1 minute time interval.

The collector was connected to a device that allowed continuous operation at maximum power point through a charge controller with a quick manual bypass to an I-V curve tracer. The PV back surface temperature was measured with 6 equidistant type-T thermocouples located at the back of the cells and was recorded at a 10 second time interval. The collector mounted on the testing rig for the combined electrical and thermal testing is shown in Figure 4-2.

Figure 4-2: PV-T collector mounted on the outdoor combined PV and thermal testing rig

Measurements were obtained for 9 different conditions consisting of the combinations of 3 fluid inlet temperatures (T_a, 40 °C and 44 °C) and three inlet flowrates (40, 55, 75 kg/(h·m^2)). During

measurements, normal incidence angle was maintained by varying the slope and azimuth angle of the collector. I-V curves were traced at 2 to 4 minute time intervals. For a measurement to be considered valid, quasi-stationary conditions had to be maintained for at least 45 minutes. The first 30 minutes consisted of the preconditioning phase and every subsequent 15 minute period was considered as a measurement phase. This 15 minute period was then sub-divided in three measurements of 5 minute. During this whole period (preconditioning and measurement), the fraction of diffuse radiation had to be less than 30% of the irradiance. Moreover, the in-plane irradiance had to be greater than 700 W/m^2, with a maximum deviation of ±50 W/m^2. The other maximum deviations allowed were set at ±20 W/m^2 for the long-wave irradiance, ±5% for both the inlet and outlet flowrates and ±1 K for the inlet and ambient temperatures. In addition to the combined electrical and thermal measurements, data under stagnation conditions were also collected. During stagnation, normal incidence angle was still maintained, but the air heating apparatus and inlet and outlet blowers were turned off.

4.6 Results

4.6.1 Electrical Model Validation

The parameter β_{Voc} was obtained with the data collected during the indoor test by performing a linear regression on V_{oc} as a function of $T_{PV\_back,AVG}$ at 1000 W/m^2. The slope of this linear regression corresponds to β_{Voc} and was found to be -(0.118 ± 0.001) V/°C with a correlation coefficient, R^2, of 0.99 where R^2 is defined in Appendix A in Section 4.11.1. Using Equation (4-3), a thermal diode voltage of (0.0320 ± 0.0007) V was calculated.

The coefficients of the electrical models to predict the electrical performance were obtained using either the ECT or $T_{PV\_back,AVG}$ as the PV temperature, where $T_{PV\_back,AVG}$ is the average of the temperature measurements taken at the back surface of the PV cells. The ECT was calculated for the outdoor measurements collected during the combined electrical and thermal testing using Equation (4-2). The reference observation in Equation (4-2) was selected from the dataset collected during the outdoor testing. In order to ensure that the average of the temperature measurements taken at the back of the PV cells was representative of the equivalent operating cell temperature, this observation was taken when the collector was under stagnation and quasi-stationary conditions and all T_{PV_back} measurements were within 3 °C.

The PV maximum power point as a function of $T_{PV\_back,AVG}$ and ECT for the outdoor observations is presented in Figure 4-3 (a) and (b), respectively. These graphs contain the information to identify the PV efficiency at the reference temperature for a number of irradiance levels, $\eta_{mpp}(G, T_{PV,ref})$, as well as the relative maximum power point temperature coefficient as a function of irradiance, $\gamma_{mpp,rel}(G)$. With this information, the PV efficiency at any given temperature and irradiance level, $\eta_{mpp}(G, T_{PV})$, can be computed by using:

$$\eta_{mpp}(G, T_{PV}) = \eta_{mpp}(G, T_{PV,ref}) * \left(1 + \gamma_{mpp,rel}(G) * \left(T_{PV} - T_{PV,ref}\right)\right) \quad (4\text{-}4)$$

Usually, $T_{PV,ref}$ in Equation) is 25 °C, but in this case, the ambient temperature did not allow PV measurements below 30 °C. As a result, $T_{PV,ref}$ was set at 55 °C. The performance of the model shown in Equation) using either $T_{PV\_back,AVG}$ or ECT as T_{PV} was tested against electrical measurements obtained under both stagnation and heat recovery conditions. As model performance indicators, the following statistical indices defined in Appendix A in Section 4.11.1 were used: mean bias error (MBE), root mean square error (RMSE) and correlation coefficient (R^2). The comparison of the model performance at predicting η_{mpp} using ECT and $T_{PV\_back,AVG}$ is shown in . The errors are small in both cases since the MBE and RMSE are under 0.3% and 1.6% for both temperatures and the R^2 is above 0.93.

Table 4-1: Comparison of the electrical efficiency model performance using T_{PV}=$T_{PV\_back,AVG}$ and T_{PV}=ECT

T_{PV}	MBE	MBE (%)	RMSE	RMSE (%)	R^2
$T_{PV\_back,AVG}$	-0.0003	-0.28	0.0017	1.59	0.93
ECT	0.0002	0.18	0.0012	1.07	0.97

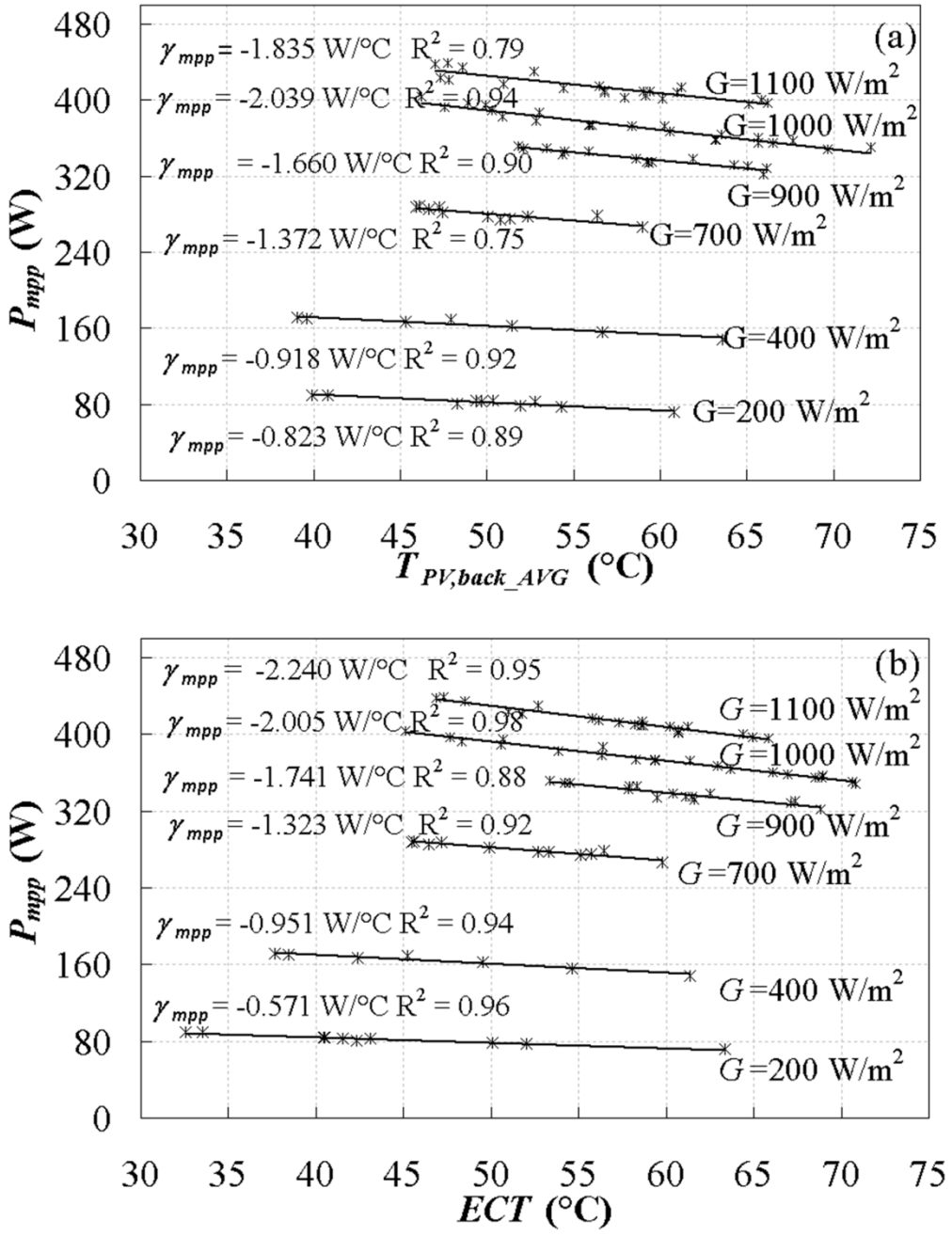

Figure 4-3: PV maximum power point for various irradiance levels as a function of (a) $T_{PV\_back,AVG}$ (b) ECT

4.6.2 Thermal Performance Model Validation for Closed-Loop Collectors

With the data collected during the outdoor experiment, the thermal efficiency of this air PV-T collector was computed using Equation (4-5).

$$\eta_{th} = \frac{c_p(m_o T_o - m_i T_i - m_L T_a)}{G A_g} \tag{4-5}$$

In Equation (4-5), the effect of temperature on air properties is neglected and as a result, the air thermal capacity, c_p, is assumed to be constant. A_g is the collector gross area, m_o and m_i are the outlet and inlet air flowrates and m_L is the air leakage rate taken as a positive value for infiltration and a negative value when leakage occurs.

The thermal efficiency as a function of the reduced temperatures$(T_i - T_a)/G$, $(T_o - T_a)/G$ and $(T_{fm} - T_a)/G$ is shown in Figure 4-4 where each point represents one of the three 5 minute averages of the 15 minute measurement period. These graphs include data taken at two flowrates, three inlet temperatures and an average wind speed of (0.9 ± 0.3) m/s. The uncertainty bars on this plot and on all subsequent plots represent the expanded uncertainty for a confidence level of 95%. The method employed for the calculation of the uncertainties is presented in Appendix B in Section 4.11.2. Figure 4-4 shows that the thermal efficiency decreases with the increase of reduced temperature, but increases with the increase of flowrate.

By performing a simple linear fit for each flowrate of Figure 4-4, the coefficients of the model shown in Equation) can be obtained.

$$\eta_{th} = \overline{F_R^*(\tau\alpha)_e} - \overline{F_R^* U_L^*}\left(\frac{T^* - T_a}{G}\right) \tag{4-6}$$

In Equation), $\overline{F_R^*}$ is the PV-T collector heat removal factor, $\overline{(\tau\alpha)_e}$ is the PV-T collector effective transmittance-absorptance product, and $\overline{U_L^*}$ is the overall PV-T collector heat loss coefficient. When $T^* = T_i$, this model corresponds to the Hottel and Whillier equation modified by Florschuetz (1979) for PV-T collectors. The difference between the solar thermal and PV-T collector models resides in the bars added above F_R^*, $(\tau\alpha)_e$ and U_L^* indicating that these variables

are affected by the electrical performance. Table 4-2 presents the model coefficients for the three T^* considered. The high R^2 values obtained for each temperature show that this model not only represents well the thermal performance of this PV-T collector, but also that all three temperatures can be used as T^* without any significant effect on the model performance.

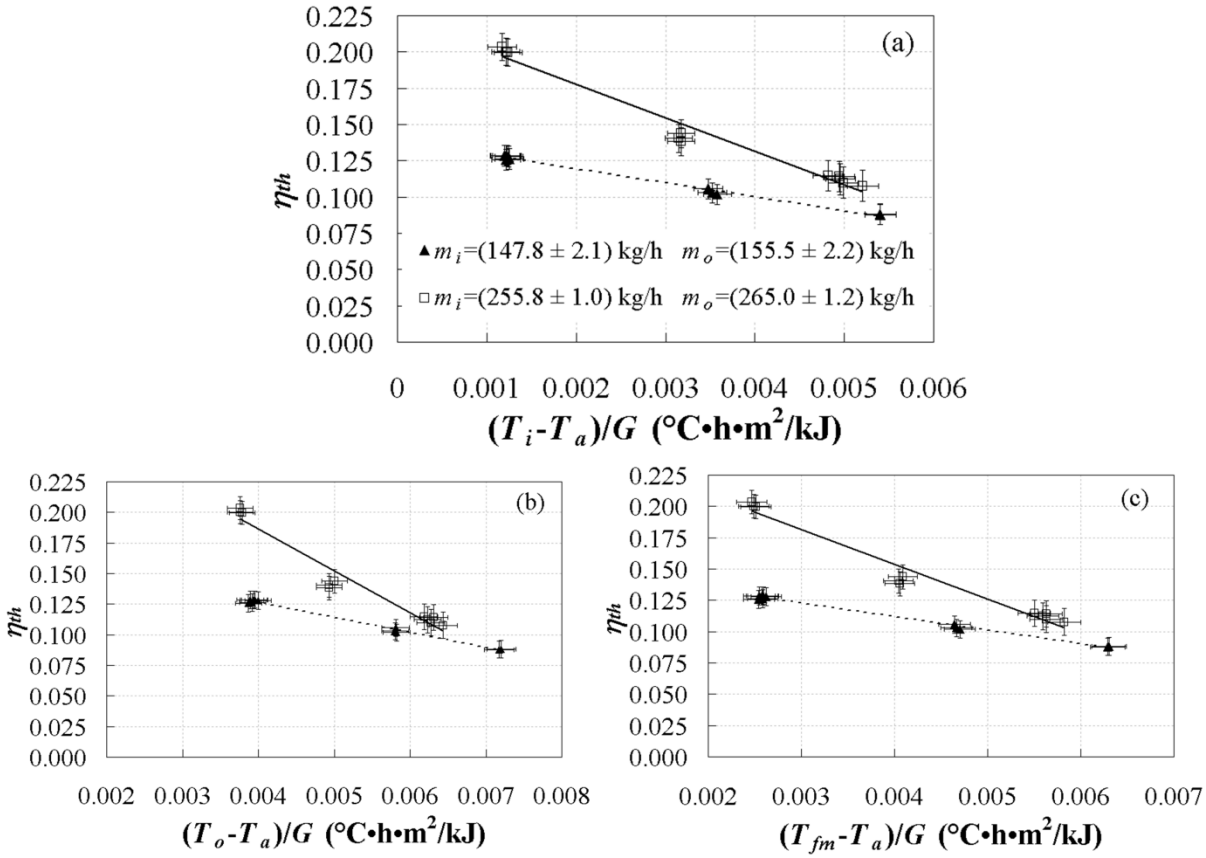

Figure 4-4: Thermal efficiency in closed-loop as a function of (a) $(T_i-T_a)/G$ (b) $(T_o-T_a)/G$ (c) $(T_{fm}-T_a)/G$

Table 4-2 : Thermal efficiency model coefficients

	$m_i = 147.8 \pm 2.1$ kg/h $m_o = 155.5 \pm 2.2$ kg/h			$m_i = 255.8 \pm 1.0$ kg/h $m_o = 265.0 \pm 1.2$ kg/h		
	$T^* = T_i$	$T^* = T_o$	$T^* = T_{fm}$	$T^* = T_i$	$T^* = T_o$	$T^* = T_{fm}$
$\overline{F_R^*(\tau\alpha)_e}$	0.139	0.176	0.155	0.233	0.323	0.264
$\overline{F_R^*U_L^*}$	9.713	12.318	10.865	23.442	34.194	27.675
R^2	0.99	0.99	0.99	0.97	0.95	0.96

4.6.3 Thermal Performance Validation for Open-Loop Collectors

With the collected data in open-loop configuration, i.e., drawing air directly from ambient without using the air heating unit, the range of reduced temperature is too small to detect any relation between η_{th} and $(T*-T_a)/G$. As a result, a model of the thermal efficiency as a function of a reduced temperature does not make sense for open-loop collectors. As shown in Figure 4-5, a representation of the thermal efficiency as a function of the outlet flowrate is more appropriate. These observations can be fit with a 2nd degree polynomial.

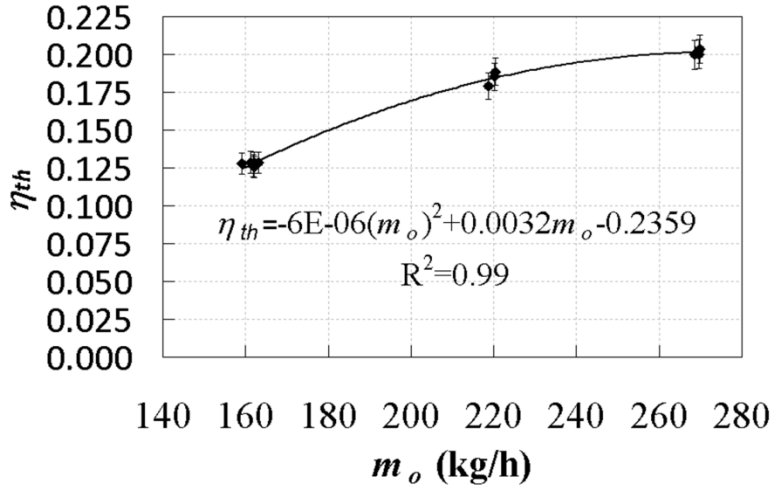

Figure 4-5: Thermal efficiency in open-loop as a function of outlet flowrate

4.6.4 PV Cells Temperature Prediction Model Validation

The Pareto diagrams in Figure 4-6 present the *t-value* of the different variables potentially influencing $T_{PV\_back,AVG}$ and ECT when air is circulating in the collector. The fluid average temperature, T_{fm}, is not included in these plots since it can be calculated from T_i and T_o. From this figure, it can be observed that the main variable influencing both ECT and $T_{PV\_back,AVG}$ is the fluid outlet temperature, T_o. The second and third most important variables are G and T_i for the ECT and T_i and G for the case of $T_{PV\_back,AVG}$. Considering a *p-value* of 0.05 as the threshold chosen for statistical significance, the fluid inlet and outlet flowrates can be considered as not

statistically significant variables in this case. The wind speed, V_w, and the ambient temperature, T_a, are statistically significant variables, but are not as important as T_o, G and T_i.

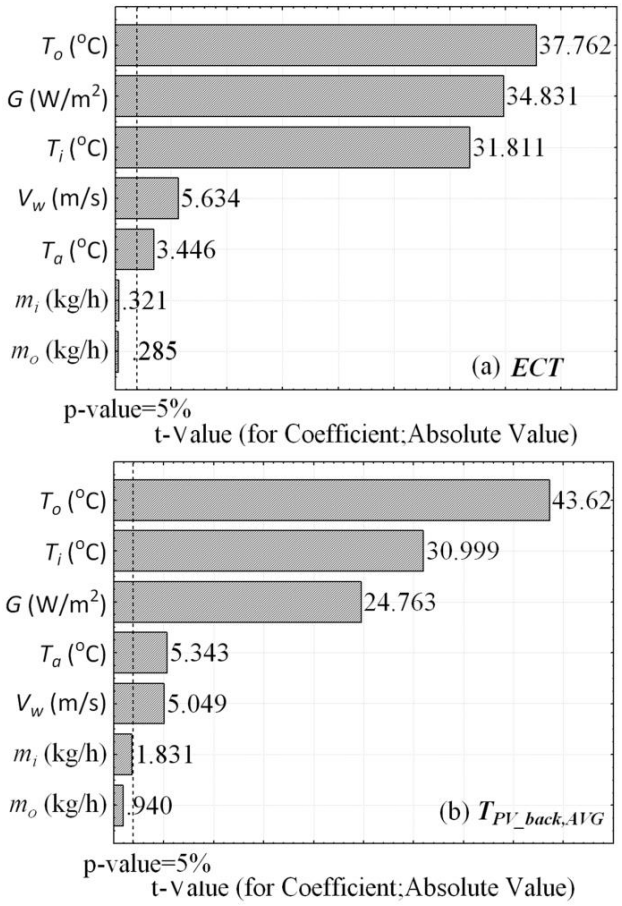

Figure 4-6: Pareto diagrams identifying the most important variables in the prediction of (a) *ECT* and (b) $T_{PV\_back,AVG}$

The electrical measurement dataset obtained under heat recovery conditions was randomly split into train and test datasets to first develop the model and then evaluate its performance. A comparison of the performance of some of the models investigated using selection of variables methods is shown in Table 4-3. This table only presents first order multiple linear regression models, but higher order models were also investigated as well as exponential models. A 3-variable multiple linear regression model was found to be sufficient using the variables T_i, T_o, and G. A residual analysis of this model conducted with both $T_{PV\_back,AVG}$ and ECT confirmed

the validity of the model with the residuals following a normal distribution and not showing any trend with the model variables.

Table 4-3: Model performance comparison at predicting T_{PV}

	ECT			$T_{PV\_back,AVG}$		
Variables in multiple linear regression	MBE (%)	RMSE (%)	R^2	MBE (%)	RMSE (%)	R^2
G, T_i, V_w, T_{fm}	-0.21	4.52	0.92			
G, T_i, T_{fm}	-0.27	4.60	0.91	-0.08	3.77	0.92
G, T_o, T_i	-0.27	4.60	0.91	-0.09	3.77	0.92
G, T_o, T_{fm}	-0.27	4.60	0.91	-0.08	3.77	0.92
T_o, T_i	0.69	8.30	0.72			
G, T_o, m_i, T_{fm}				-0.22	3.56	0.93
T_i, T_{fm}				0.45	5.60	0.82
$G, T_o, T_i, \ln(T_a)$				-0.12	3.75	0.92

Table 4-4: Multiple linear regression model performance at predicting T_{PV}

Coefficients	$T_{PV\_back,AVG}$	ECT
Intercept	4.426	-
T_o(1/°C)	1.867	2.127
T_i (1/°C)	-0.937	-1.234
G (m^2/W)	0.008	0.015
Performance Indicator		
MBE	-0.063	-0.158
MBE (%)	-0.109	-0.269
RMSE	1.855	2.178
RMSE (%)	3.225	3.715
R^2	0.937	0.941

The final models and their performance at predicting T_{PV} after this residual analysis and the removal of outliers are shown in Table 4-4. In the case of the ECT, this model does not have any intercept, because it was not found to be statistically significant. From this table, it can be concluded that both models have very similar performance at predicting T_{PV} with a R^2 of 0.937 in the case of $T_{PV\_back,AVG}$ and 0.941 for the ECT.

Table 4-5 presents the performance of the model shown in Equation) at predicting η_{mpp} when T_{PV} is calculated using the 3-variable multiple linear regression model coefficients of Table 4-4. According to these results, using ECT as T_{PV} in the case of this PV-T collector is comparable to using the average PV back surface temperature over the whole PV electrical efficiency range. As shown in Figure 4-7, the predictions using $T_{PV\_back,AVG}$ are better at low efficiency levels, while those using the ECT perform better at high efficiency levels.

Table 4-5: Comparison of the PV electrical efficiency models performance using T_{PV} calculated with the 3-variable multiple linear regression models of Table 4-4

T_{PV}	MBE	MBE (%)	RMSE	RMSE (%)	R^2
$T_{PV\_back,AVG}$	0.000	-0.247	0.002	1.766	0.903
ECT	0.000	0.146	0.002	1.598	0.920

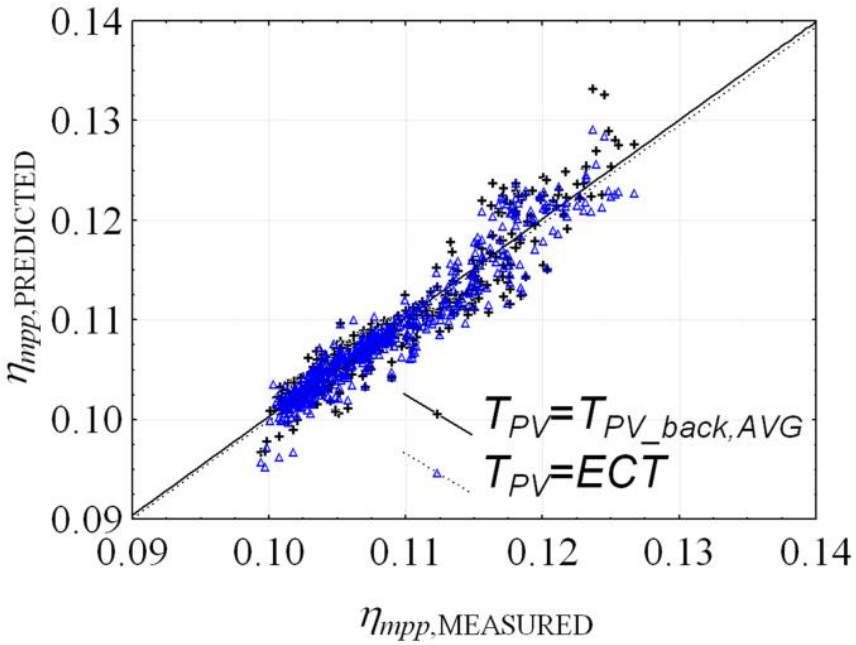

Figure 4-7: Comparison of the measured and predicted electrical efficiencies using T_{PV} calculated with the 3-variable multiple linear regression model

4.6.5 PV-T Model Development for Design Purposes

The models obtained for closed-loop collectors allow the computation of the PV-T collector thermal efficiency from the reduced temperature $(T^* - T_a)/G$ and flowrate. The electrical model expresses the electrical efficiency as a function of the irradiance and PV cell's temperature. This temperature can be estimated with models using the irradiance and fluid inlet and outlet temperatures as independent variables. These models can be presented in a 5-plot system that captures the collector performance. These 5-plot systems are applicable at the collector gauge pressure and wind speed range under which they were developed. They are also only valid for the building-integrated configuration considered here since the thermal efficiency and PV temperature models would not necessarily remain identical if the collector back and edges were poorly insulated.

The 5-plot system for the open-loop configuration is presented in Figure 4-8. The 1st plot presents the thermal efficiency as a function of the outlet flowrate obtained from experimental data. This first graph represents actual experimental data and extrapolation of the thermal efficiency curve should be avoided. In the 2nd graph, the temperature rise is plotted as a function of the outlet flowrate and irradiance. The curves on the 2nd plot are obtained using the measured thermal efficiency and outlet flowrate for irradiance levels varying from 200 W/m^2 to 1000 W/m^2 with steps of 200 W/m^2 using the following equation:

$$\frac{\eta_{th} G A_g}{m_o c_p} = T_o - T_i = T_{rise} \tag{4-7}$$

This temperature rise can be used in the 3rd plot to obtain the fluid outlet temperature for various ambient temperatures. This plot is not specific to this collector, but is simply used here to simplify going from one plot to another. The ambient temperature curves are selected to be representative of the ambient temperature range under which the collector is meant to operate even though interpolation is allowed. In the 4th plot, the PV temperature can be estimated since it is presented as a function of the fluid outlet temperature for various irradiance levels. The influence of the fluid inlet temperature is neglected because this last variable was found to be the least significant in the model to predict T_{PV}. This PV temperature can be used in the 5th plot to estimate the PV maximum power point. Plots 4 and 5 are produced from the models developed to

predict the PV temperature and the PV power production. The ranges used for the fluid outlet temperature, PV temperature and electrical power production should correspond to those typical of collector operation.

The method for using these plots can be illustrated with the following example represented with dotted lines in Figure 4-8. Assuming an outlet flowrate of 200 kg/h, an irradiance of 1000 W/m^2 and an ambient temperature of 20 °C, the 1st and 2nd plots indicate that the thermal efficiency is 0.164 and the temperature rise is 10 °C. Using this temperature rise in the 3rd plot, we get that T_o is 30 °C. With T_o, an estimate of 54 °C for T_{PV} is obtained in the 4th plot. This leads to a maximum power point of 385 W in the 5th plot. The estimates for T_{PV} and P_{mpp} with the 5-plot system are closed to the actual values calculated by the models when the fluid inlet temperature effect on the temperature of the PV cells is included. Using the actual models instead of plots 4 and 5, values of 54.1 °C and 384.3 W are obtained for T_{PV} and P_{mpp}, respectively.

The 5-plot system for the closed-loop collector presented in Figure 4-9 takes into account the fact that the air infiltrating the collector or leaking from the collector is not always at the same temperature than the air entering the collector through the actual inlet. In this case, the collector thermal efficiency can be expressed as a function of an effective inlet temperature, $T_{i,eff}$, with the following relation:

$$\eta_{th} = \frac{m_o c_p \left(T_o - T_{i,eff}\right)}{G A_g} \tag{4-8}$$

In Equation (4-8), $\left(T_o - T_{i,eff}\right)$ is the effective air temperature rise $T_{rise,eff}$ where the effective inlet temperature, $T_{i,eff}$, is defined as:

$$T_{i,eff} = \frac{m_i T_i + m_L T_a}{m_o} \tag{4-9}$$

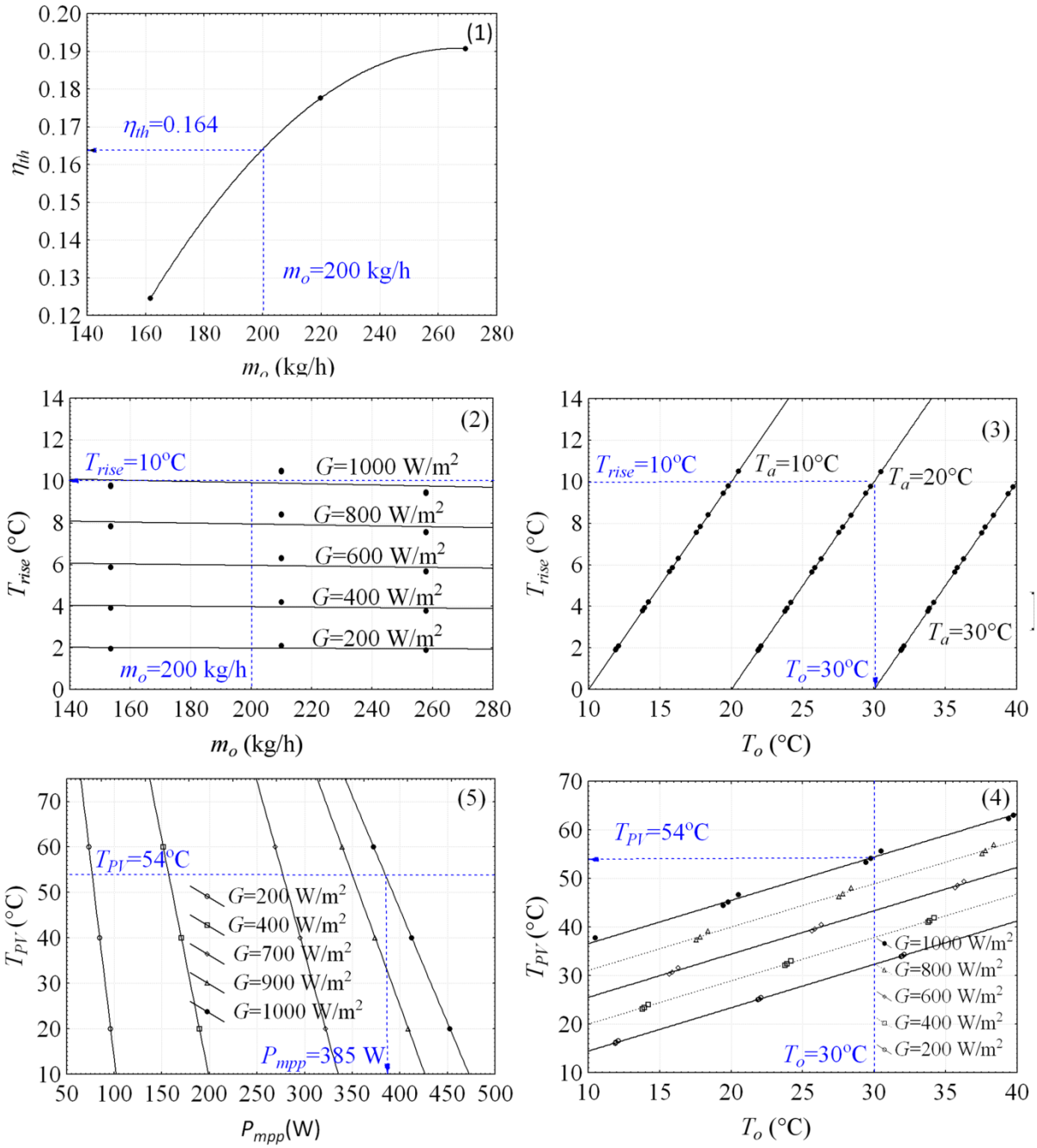

Figure 4-8: 5-plot system representing the PV-T collector performance in open-loop configuration

In Figure 4-9, the 1st plot presents the thermal efficiency as a function of the reduced temperature. In this case, T_i is the preferred characteristic temperature T^* since T_i is the only known variable at the design stage considering that T_o and T_{fm} are both obtained from the actual collector

performance. Similar to the 1st plot of the open-loop configuration, this graph is produced from experimental data. Thus, neither interpolation between curves nor extrapolation should be performed. The 2nd graph presents the effective air temperature rise, $T_{rise,eff}$, as a function of $m_o c_p/(GA_g)$. It is produced using Equation (4-8) with measured minimum and maximum thermal efficiencies, a single inlet and ambient temperature and irradiance levels varying from 200 to 1000 W/m^2. Interpolation between the curves should not occur because the variation of the effective temperature rise is not linear with $m_o c_p/(GA_g)$. The 3rd plot is obtained with the data used for the 2nd plot, but in addition, calculations are made for the full inlet temperature range. The last two graphs are identical to those of the open-loop configuration.

An example is shown on this graph for a collector having the following operating conditions: $m_i = 147.8$ kg/h, $T_i = 30$ °C, $T_a = 20$ °C and $G = 1000$ W/m^2. For a collector operating under the same gauge pressure as during testing, the fluid outlet flowrate is 155.5 kg/h and $T_{i,eff}$is estimated at 29.5 °C. With calculated values for $(T_i - T_a)/G$ and $m_o c_p/(GA_g)$ of 0.0028 (°C·h·m^2)/kJ and 0.0123 °C $^{-1}$, respectively, the first plot indicates that the thermal efficiency is 0.11. Using η_{th} in the second plot, $T_{rise,eff}$ is found to corresponds to 9 °C. From this 2nd plot, moving to the 3rd, 4th and 5th plots allows the estimation of T_o (38.5 °C), T_{PV} (62 °C), and P_{mpp} (367.5 W). Using the actual models instead of plots 4 and 5, values of 59.9 °C and 373 W are obtained for T_{PV} and P_{mpp}, respectively.

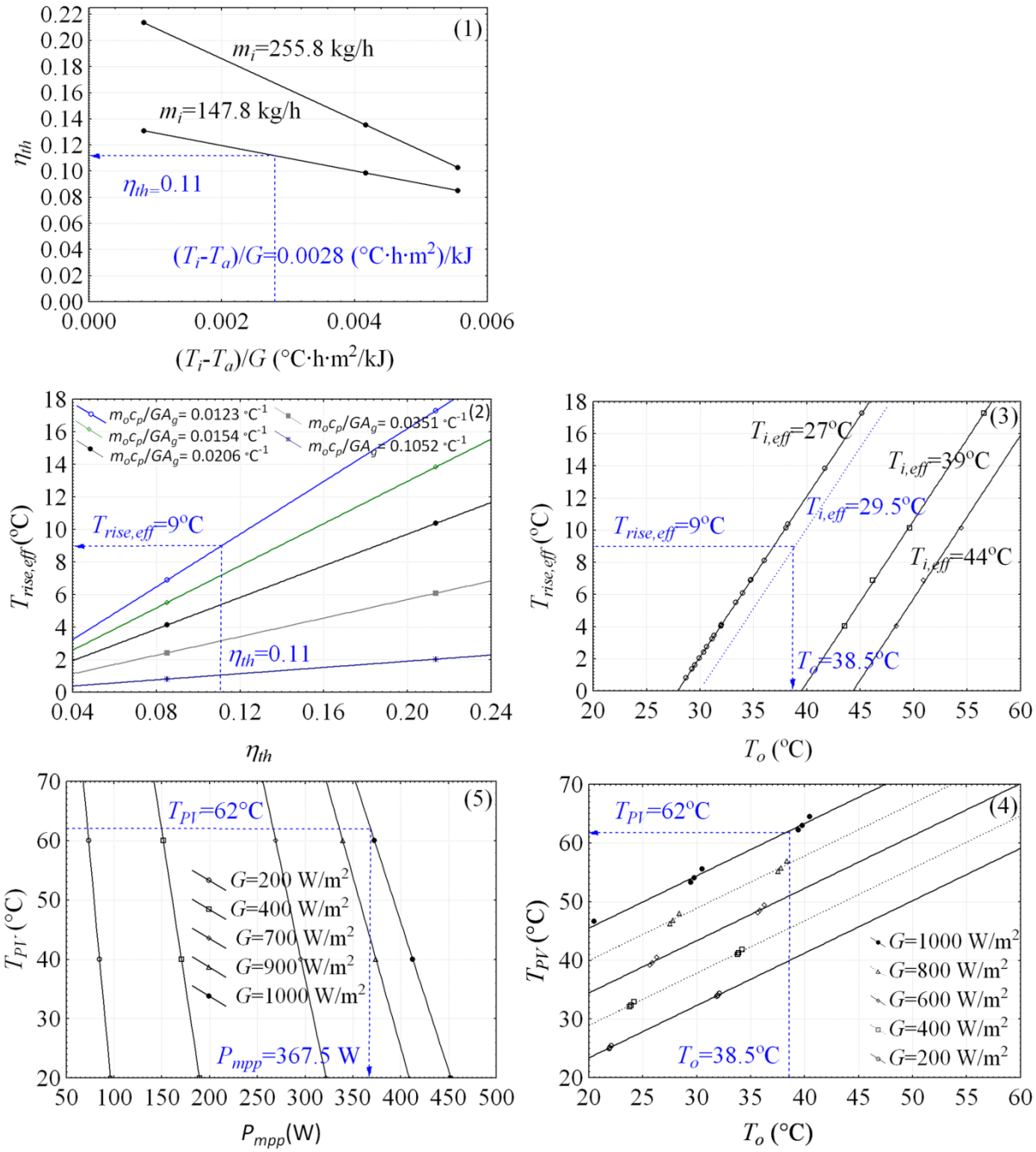

Figure 4-9: 5-plot system representing the PV-T collector in closed-loop

4.7 Discussion

In a PV-T collector, the channels or tubes behind the PV cause the electrical performance characterization to be somewhat of a challenge. One of the reasons is that the heat transfer fluid harvesting the heat from the PV causes the cells to be at a non-uniform temperature. For cells

mounted in series, the PV will operate at the average cell temperature. Thus, the measurement of the true average PV cell's temperature requires the mounting of multiple temperature sensors. This is feasible in theory, but in reality, in most PV-T collectors, it is difficult to access the back-surface of the PV cells. The equivalent cell temperature method has great potential for modeling the PV operating temperature, since it does not require any temperature measurements and only the short-circuit current needs to be recorded. It has the only disadvantage of requiring indoor testing to obtain the thermal diode voltage factor and open-circuit voltage. In theory, these two variables can be obtained outdoors, but obtaining a uniform temperature for the PV cells outdoors in a PV-T collector is a challenge and might be time consuming.

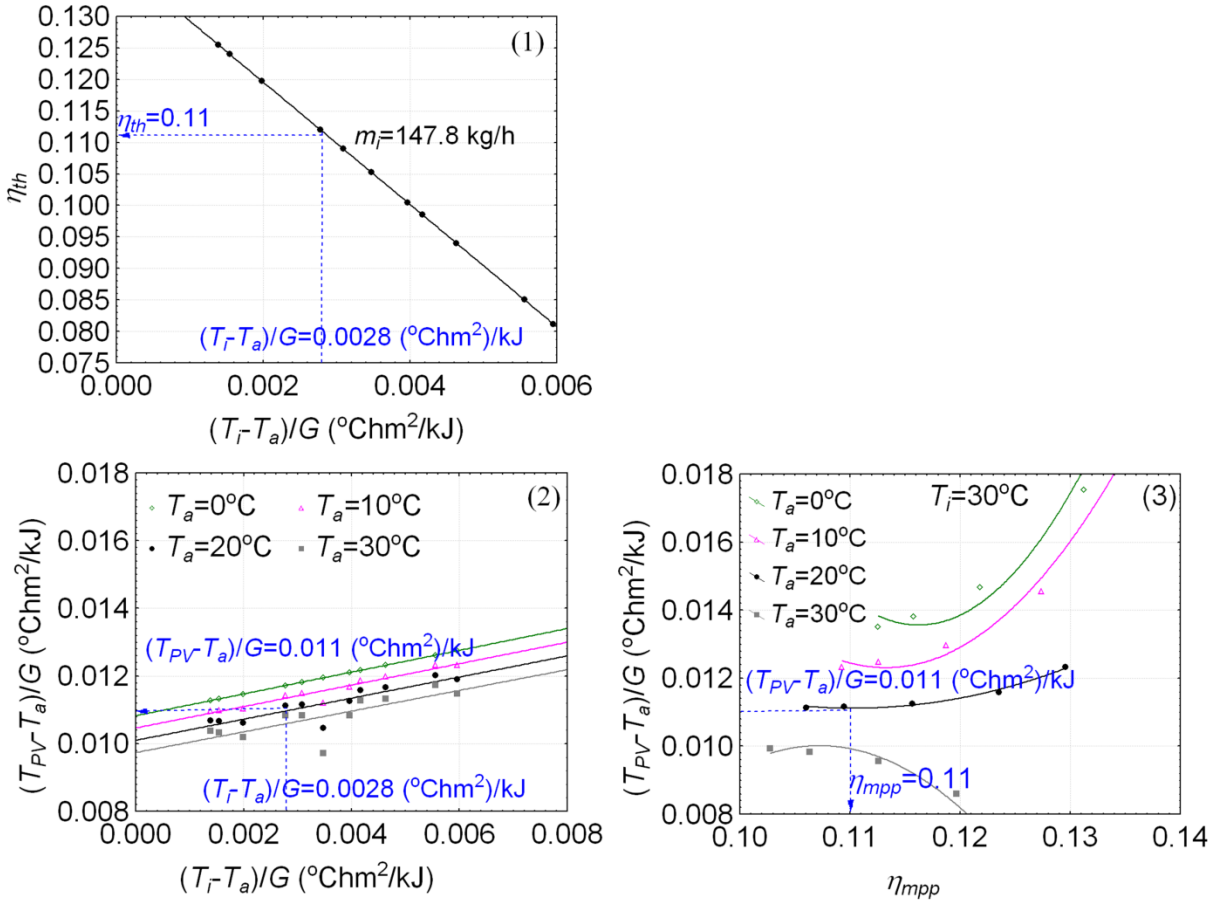

Figure 4-10: 3-plot system adapted from the IEA to represent the PV-T collector in a closed-loop configuration

Figure 4-10 presents the collector performance in closed-loop configuration according to the 3-plot design scheme concept developed by the IEA (Collins, 2008). This 3-plot system differs slightly from the original design scheme developed by the IEA, however, because the 2nd plot includes a categorization with regards to the ambient temperature. Using the same example than in section 4, we find in the 2nd plot that $(T_{PV} - T_a)/G$ corresponds to 0.011 (°C·h·m^2)/kJ for a reduced temperature of 0.0028 (°C·h·m^2)/kJ. In the 3rd plot, $(T_{PV} - T_a)/G$ is used to obtain a PV efficiency of 0.11. Thus, according to this design scheme, the maximum power point is estimated at 386 W which is acceptable since it is within 3.5% of the value obtained with the actual models. This error is slightly greater than the 1.5% obtained with the 5-plot system in section 4. Thus, in this case, the 5-plot offers a limited improvement in accuracy and is also restricted to one wind speed and operating pressure. The 5-plot system is valid at multiple flowrates, however, and it can be applied to both open-loop and closed-loop configurations. These are two significant advantages compared to the 3-plot system.

Some aspects of PV-T air collector performance are still unknown, however, such as the effect of slope on the collector performance and the validity of these schemes for collectors of different areas and module configurations (series vs parallel). Another important aspect of PV-T collectors is that these often operate under stagnation conditions. Models to predict the PV temperature using either the ECT or the back surface average temperature must also be developed for such operating conditions.

The collector studied here was found to have a relatively low thermal efficiency. The focus of this study, however, is not on the actual PV-T collector performance and coefficients obtained in the different models, but on the method used to fully characterize the thermal and electrical yield of this technology. This method could be applied to different types of PV-T air collectors to simplify the comparison of different designs.

4.8 Conclusions

Standardized methods to test, characterize and present the performance are important for every technology since these enable comparisons between different products and the development of simplified models to predict their yield. This study presented a characterization method and a

5-plot system applicable for design calculations of open-loop and closed-loop air PV-T collectors in a building-integrated configuration.

An important finding of this study is related to the PV temperature measurement and to its linkage with the collector thermal yield which has been an issue for the characterization of PV-T collectors. It was found that the use of the equivalent cell temperature as the PV operating temperature provided comparable results to the use of the average PV back surface temperature for predicting the collector electrical efficiency. An investigation of the important variables in the prediction of the PV temperature showed that a multiple linear regression model using the fluid inlet temperature, the irradiance and the fluid outlet temperature as independent variables could be used successfully to estimate both the PV back surface average temperature and equivalent cell temperature. When using the ECT and the PV back surface average temperature calculated with these models to compute the electrical efficiency, similar results were obtained. Nevertheless, the use of the ECT as opposed to $T_{PV\_back,AVG}$ provides a valuable alternative for PV-T collector characterization, for example in collectors where the PV back surface temperature is difficult to access for temperature sensor mounting or where measurement could affect the air flow in the channel. It does require the open-circuit voltage to be known, but I-V curves need to be traced for the electrical characterization. The thermal efficiency models using the inlet, outlet or average fluid temperature in the calculation of the reduced temperature had similar performance. Considering that the fluid inlet temperature is the only known temperature at the design stage, it was concluded that the use of this temperature made more sense for closed-loop collectors. For the collector tested in an open-loop configuration, the reduced temperature variation was found to be too small to detect any relation with the thermal efficiency. Thus, a model of the thermal efficiency as a function of the fluid outlet flowrate was found to be more appropriate.

From these models characterizing thermal and electrical performance, and the relation between the thermal and electrical yields, two series of graphs were developed for both closed-loop and open-loop configurations to encapsulate all the collector performance characteristics. These series consist of 5-plot systems that can be used for design purposes to estimate the thermal efficiency, the air temperature rise, the PV temperature and the PV electrical production from the weather and collector operating conditions.

4.9 Acknowledgements

Financial support for this project was provided by the ecoENERGY Technology Initiative (ecoETI), a federal program led by Natural Resources Canada aiming towards greenhouse gas emissions reduction and clean air. The authors would like to acknowledge Yves Poissant and Dave Turcotte for their contribution on the development of the experimental procedure. The outdoor experimental measurements were performed at Canada's National Solar Testing Facility (Alfred Brunger).

4.10 Nomenclature

Symbols

A	Area (m^2)
c_p	Air specific heat (kJ/(kg·°C))
F_R^*	Heat removal factor with characteristic temperature T* in reduced temperature for solar thermal collectors
$\overline{F_R^*}$	Heat removal factor with characteristic temperature T* in reduced temperature for PV-T collectors
F_R	Heat removal factor with the fluid inlet temperature used as the characteristic temperature in the calculation of the reduced temperature for solar thermal collectors
F_{AV}	Heat removal factor with the average fluid temperature used as the characteristic temperature in the calculation of the reduced temperature for solar thermal collectors
G	In-plane irradiance (kJ/(h·m^2))
m	Flowrate (kg/h)
Ns	Number of cells in series
P	Power (W)
T	Temperature (°C)
T_a	Ambient temperature (°C)
T_{rise}	Air temperature rise (°C)
T^*	Characteristic temperature (°C)
$(T^* - T_a)/G$	Reduced temperature (°C·h·m^2/kJ)
U_L^*	Collector heat loss coefficient with characteristic temperature T* in reduced temperature for solar thermal collectors (kJ/(h·m^2·°C))
$\overline{U_L^*}$	Collector heat loss coefficient with characteristic temperature T* in reduced temperature for PV-T collectors (kJ/(hm^2·°C))
V_{oc}	Open-circuit voltage (V)

Greek Symbols

β_{Voc}	Open-circuit voltage temperature coefficient (V/°C)
η	Efficiency
γ_{mpp}	Maximum power point temperature coefficient (W/°C)

$\gamma_{mpp,rel}$	Maximum power point relative temperature coefficient (1/°C)
$(\tau\alpha)_e$	Effective transmittance-absorptance product for solar thermal collectors
$\overline{(\tau\alpha)_e}$	Effective transmittance-absorptance product for PV-T collectors

Subscripts

a	Aperture
fm	Mean fluid
g	Gross
i	Inlet
L	Leakage
o	Outlet
PV	PV
PV,ref	Reference PV
PV,back_AVG	PV back surface average (°C)
th	Thermal
mpp	Maximum power point

Abbreviation

ECT	Equivalent cell temperature
MLR	Multiple linear regression
NOCT	Normal operating cell temperature
STC	Standard testing conditions

4.11 Apendices

4.11.1 Appendix A

The coefficient of correlation, R^2, is expressed as:

$$R^2 = 1 - \frac{\sum_{i=1}^{n}\left(y_{observed,i} - y_{predicted,i}\right)^2}{\sum_{i=1}^{n}\left(y_{observed,i} - \bar{y}\right)^2} \tag{4-10}$$

In Equation (4-10), *n* is the total number of observations, $y_{observed,i}$ is the i^{th} observed value, $y_{predicted,i}$ is the i^{th} value predicted by the model and $\bar{y}$ is the average of the *n* observed values. The mean bias error, MBE, and root mean square error, RMSE, are given as:

$$MBE = \frac{1}{n}\sum_{i=1}^{n}\left(y_{observed,i} - y_{predicted,i}\right) \tag{4-11}$$

$$RMSE = \sqrt{\frac{1}{n}\sum_{i=1}^{n}\left(y_{observed,i} - y_{predicted,i}\right)^2} \quad (4\text{-}12)$$

These errors can also be expressed as a percentage of the mean:

$$MBE\ \% = \frac{MBE}{\bar{y}} * 100 \quad (4\text{-}13)$$

$$RMSE\ \% = \frac{RMSE}{\bar{y}} * 100 \quad (4\text{-}14)$$

4.11.2 Appendix B

Uncertainties can be divided into Type A and Type B uncertainties. Type A uncertainties are obtained from statistical methods and Type B are evaluated by using other information such as manufacturer's specifications or calibration certificates. Type A standard uncertainty, u_A, is obtained from the same measurement taken several times. For bias-free measurement, it is given as:

$$u_A = \frac{s}{\sqrt{n}} \quad (4\text{-}15)$$

In Equation (4-15), s is the standard deviation expressed as:

$$s = \sqrt{\frac{\sum_{i=1}^{n}\left(y_{observed,i} - \bar{y}\right)^2}{n-1}} \quad (4\text{-}16)$$

The evaluation of a standard uncertainty of Type B, u_B, will vary with the type of estimate. A detailed explanation of the calculation of Type B uncertainties can be found in the International Organization for Standarization *Guide to the Expression of Uncertainty in Measurement* (ISO, 1995). The combined standard uncertainty, u_c, combines both Type A and Type B estimates. For a value calculated using a function *f*, the combined uncertainty u_c can usually be simplified to Equation (4-17) if the nonlinearity of *f* can be neglected.

$$u_c = \sqrt{\sum_{i=1}^{n} \left(\frac{\partial f}{\partial y_i}\right)^2 u(y_i)^2} \tag{4-17}$$

In Equation (4-17), the standard uncertainty u can be a Type A or a Type B uncertainty. The combined standard uncertainty is equivalent to one standard deviation or to the uncertainty for a confidence level of 68%. In order to express this uncertainty for other confidence levels, it can be multiplied by a coverage factor k. The result of this multiplication gives the expanded uncertainty, U:

$$U = ku_c \tag{4-18}$$

For a confidence level of 95%, k=2 and for a confidence level of 99%, k=2.58.

This method was used in this study to compute the expanded uncertainty which is what is represented with the bars on the graphs. For all measurements or computed values, a confidence level of 95% was used.

4.12 References

American Society of Heating, Refrigerating and Air-Conditioning (ASHRAE). (2010). *Methods of Testing to Determine the Thermal Performance of Solar Collectors* (ANSI/ASHRAE 93-2010).

Athienitis, A. K., Bambara, J., O'Neill, B., & Faille, J. (2011). A prototype photovoltaic/thermal system integrated with transpired collector. *Solar Energy*, *85*, 139-153.

Buchinger, J. (2006). *Recommendations on Testing of Solar Air Collectors* (Report WP 4.1 D2).

Collins, M. (2008). *Recommended Standard for Characterization and Monitoring of PV/Thermal Systems* (Report DB2). Cedar, MI, USA: IEA SHC. Retrieved from http://archive.iea-shc.org/publications/downloads/DB2_Recommended_Standard_for_the_ Characterization _and_Monitoring_of_PVThermal_Systems.pdf

European Committee for Standardization (ECS). (2005). *EN 12975-2 Thermal Solar Systems and Components - Solar Collectors - Part 2: Test methods* (EN 12975-2).

Florschuetz, L. (1979). Extension of the Hottel-Whillier Model to the Analysis of Combined Photovoltaic/Thermal Flat Plate Collectors. *Solar Energy*, *22*, 361-366.

Hottel, H., & Whillier, A. (1958). Evaluation of Flat-Plate Solar Collector Performance. *Transactions of the Conference on the Use of Solar Energy 2, Part I,* (pp. 74-104). Tucson: University of Arizona Press.

International Energy Agency (IEA). (2010). Energy Technology Perspectives 2010 - Scenarios & Strategies to 2015. Paris, France: IEA. Retrieved from http://www.iea.org/publications/freepublications/publication/etp2010.pdf

International Energy Agency Solar Heating and Cooling (IEA SHC) Programme Task 35. (2016). *PV/Thermal Solar Systems*. Cedar, MI, USA: IEA SHC. Retrieved from IEA SHC: http://www.iea-shc.org/task35

International Electrotechnical Commission (IEC). (1998). *Thin-Film Terrestrial Photovoltaic (PV) Modules - Design Qualification and Type Approval* (IEC 61646).

International Electrotechnical Commission (IEC). (2005). *Crystalline silicium terrestrial photovoltaic (PV) Modules - Design qualification and type approval* (IEC 61215).

International Electrotechnical Commission. (2011). *Determination of the equivalent cell temperature (ECT) for photovoltaic (PV) devices by the open-circuit voltage method* (IEC 60904-5).

International Organization for Standardization (ISO). (1995). *Guide to the Expression of Uncertainty in Measurement*.

Noguchi, M., Athienitis, A., Delisle, V., Ayoub, J., & Berneche, B. (2008). Net Zero Energy Homes of the Future: A Case Study of the EcoTerra Home in Canada. *Presented at the Renewable Energy Congress, Glasgow, Scotland, July 19-25, 2008.* http://www.annex32.net/pdf/articles/Net_Zero_Energy_Homes_of_the_Future.pdf

Othman, M., Yatim, B., Sopian, K., & Abu Bakar, M. (2007). Performance Studies on a Finned Double-Pass Photovoltaic-Thermal (PV/T) Solar Collector. *Desalination*, *209*, 43-49.

Pogharian, S., Ayoub, J., Candanedo, J., & Athienitis, A. (2008). Getting to a Net Zero Energy Lifestyle in Canada: The Alstonvale Net Zero House. *Presented at the 23rd European PV*

Solar Energy Conference, Valencia, Spain, September 2008. http://montrealzero.com/wp-content/uploads/2014/06/Getting-to-a-Net-Zero-Energy-Lifestyle-in-Canada.pdf

PV Catapult. (2005). *PVT Performance Measurements Guidelines- Guidelines for Performance Measurements of Liquid-Cooled Non-Concentrating PVT Collectors using c-Si cells* (Report PV Catapult D8-6).

PV Catapult. (2006). *PVT Roadmap A European Guide for the Development and Market Introduction for PV-Thermal Technology*.

Sandnes, B., & Rekstad, J. (2002). A Photovoltaic/Thermal (PV/T) Collector with a Polymer Absorber Plate. Experimental Study and Analytical Model. *Solar Energy, 72*(1), 63-73.

Tonui, J., & Tripanagnostopoulos, Y. (2007). Improved PV/T Solar Collectors with Heat Extraction by Forced ad Natural Air Circulation. *Renewable Energy, 32*, 623-637.

Zondag, H. (2008). *Main R&D Issues for PVT - A manufacturer's perspective* (Report DC2 IEA SHC Task 35). Cedar, MI, USA: IEA SHC.

Zondag, H., De Vries, D., Van Helden, W., & Van Zolingen, R. (2002). The Thermal and Electrical Yield of a PV-Thermal Collector. *Solar Energy, 72*(2), 113-128.

CHAPTER 5 ARTICLE 2: A NOVEL APPROACH TO COMPARE BUILDING-INTEGRATED PHOTOVOLTAICS/THERMAL AIR COLLECTORS TO SIDE-BY-SIDE PV MODULES AND SOLAR THERMAL COLLECTORS

Delisle, V., Kummert, M., (2014). *Solar Energy*, *100*, 50-65.

Note: The article in its original version used the abbreviations BIPV/T for building-integrated combined photovoltaics with thermal energy recovery. It was modified to BIPV-T in this chapter to provide consistency throughout the document. The word "encapsulation" was also changed to "encapsulant".

5.1 Abstract

Building-Integrated photovoltaics with thermal energy recovery (BIPV-T) shows great potential for integration into net-zero energy buildings. This technology is still not widely used, however. One of the reasons is that its advantages compared to traditional PV modules and solar thermal collectors are unclear. This study addresses the lack of a methodology on how to perform such comparison. It also presents a case study on how this novel approach can be used to demonstrate the actual energy and economic benefits of BIPV-T air systems compared to side-by-side PV modules and solar thermal collectors for residential applications. In this methodology, the thermal energy produced by both systems is transferred into water using a heat exchanger and the concept of annual equivalent useful thermal energy production is used to combine thermal and electrical energy. To perform the analysis, a detailed model of a BIPV-T system was developed and validated against experimental data. Then, the following systems were modeled in TRNSYS: a BIPV-T air system and side-by-side PV modules and liquid solar thermal collectors (PV+T). A case study was performed by simulating the performance of both systems on a 40 m^2 south-facing roof located in Montreal, Canada. The total energy produced by both systems was assessed by converting electricity into heat with various conversion factors. For a factor of 2, the BIPV-T system was found to produce 5% to 29% more equivalent useful thermal energy than the PV+T system for a water temperature at the heat exchanger inlet corresponding to 10 °C. Under similar operating conditions and for systems operating all year long, the acceptable cost to

recover the heat from the BIPV system in order to break even with the cost of the PV+T system was found to be 7,000 CAD.

5.2 Keywords

Building-Integrated Photovoltaics; Heat recovery; Hybrid Collector; Conversion

5.3 Introduction

In the next 5 years, building-integrated photovoltaics (BIPV) is set to become one of the fastest growing segments of the solar industry worldwide with a predicted capacity growth in the range of 50% or more from 2011 to 2017 (PikeResearch, 2012). This growing interest in BIPV is due, in part, to the fact that many countries are now establishing specific targets related to net-zero energy buildings (NZEBs). In order to achieve this goal, building designs must incorporate three essential concepts: energy conservation, energy efficiency and the optimal integration of renewable energy technologies. For this last aspect, BIPV offers significant advantages compared to standard rack-mounted PV modules because it does not only generate electricity, but also acts as an active component of the building envelope.

In recent years, building-integrated photovoltaics with thermal energy recovery (BIPV-T) has shown great potential to be integrated into NZEBs. In such systems, the heat generated by the PV module is recovered by a heat transfer fluid that can be either air or a liquid, producing both thermal and electrical energy simultaneously. BIPV-T offers the same advantages as BIPV, but in addition, it provides a more aesthetically pleasing look than side-by-side PV modules and solar thermal collectors and generally produces more energy for the same surface area. Although valuable for NZEBs, these benefits are often considered insufficient when the building's architectural aspect is not a primary design criterion or when a large amount of building surface area is available for mounting solar energy technologies. Thus, many building designers still prefer to implement traditional solar energy technologies such as side-by-side rack-mounted PV modules and liquid solar thermal collectors. For this reason, this article aims at identifying the actual energy and cost benefits of BIPV-T residential systems using air as the heat transfer fluid compared to more traditional solar energy technologies, i.e., side-by-side rack-mounted PV modules and liquid solar thermal collectors. In particular, the objectives are:

- To develop a methodology allowing the energy and cost benefit comparison of a BIPV-T air system with side-by-side PV modules and liquid solar thermal collectors,
- To use this methodology in a case study to compare the amount of energy produced by a BIPV-T air system to that generated by a system consisting of side-by-side PV modules and liquid solar thermal collectors, and;
- To identify the required cost to convert a BIPV system into a BIPV-T system so that the cost of the BIPV-T system breaks-even with the cost of side-by-side PV modules and solar thermal collectors.

5.4 Literature Review

Quantifying the performance of combined photovoltaic-thermal collectors (PV-T) or BIPV-T is a challenge because these systems produce two types of energy: thermal and electrical. In most applications, thermal and electrical energy do not have the same value. Thus, it is not straightforward to compare the performance of two PV-T or BIPV-T systems that have different electrical and thermal yields. When comparing a BIPV-T air system to a more traditional system such as side-by-side PV modules and liquid solar thermal collectors, an additional challenge occurs because thermal energy stored in air must be compared to thermal energy stored in a liquid. This section presents a review of studies that have looked at comparing PV-T or BIPV-T with PV modules, solar thermal collectors or other PV-T collector designs. It focuses on the performance indicators that have been used to encapsulate the performance of PV-T or BIPV-T collectors and on the main results obtained with these performance indicators.

5.4.1 Combined Energy or Exergy Efficiency

Some studies have used a combined efficiency, η_T, as a performance indicator for PV-T collectors defining it as the sum of the electrical and thermal efficiencies (Garg & Adhikari, 2000; Huang et al., 2001; Othman et al., 2007, Sopian et al., 2000):

$$\eta_T = \eta_{th} + \eta_{el} \tag{5-1}$$

Using this definition, Garg and Adhikari (2000) compared single glazed and double glazed PV-T air collectors. They concluded that the reduced heat losses of the double glazed system were not

worth the transmission losses, and thus, that a single glazed system was more appropriate. Chow et al. (2009) compared the performance of glazed and unglazed thermosyphon PV-T collectors. They found that the thermal efficiency of the glazed collector was greater than that of the unglazed collector (50.4% vs 40.8%), but that the electrical efficiency was lower for the glazed than for the unglazed collector (9.3% compared to 12.1%). When considering the combined efficiency as defined in Equation (5-1), they concluded that the glazed collector generally had a better performance. Using the combined exergetic efficiency of the collector as a performance indicator, however, they found that the unglazed configuration usually performed better except at high levels of radiation and ambient temperature.

Hegazy (2000) used the net combined efficiency, $\eta_{T,net}$, as a performance indicator to compare different PV-T collector designs:

$$\eta_{T,net} = \eta_{th} + \eta_{el,net} \tag{5-2}$$

In Equation (5-2), $\eta_{el,net}$ is the net electrical efficiency defined as:

$$\eta_{el,net} = \frac{\eta_{PV,system} P_{PV,DC} - P_{flow}/\eta_{fan}\eta_{motor}}{A_g G} \tag{5-3}$$

In Equation (5-3), A_g is the collector gross area, G is in the in-plane irradiance, $P_{PV,DC}$ is the DC PV system power, P_{flow} is the flow pumping power and η_{fan} and η_{motor} are the fan and electrical motor efficiencies, respectively. The PV system efficiency, $\eta_{PV,system}$, accounts for Balance Of System (BOS) losses (batteries, cables, inverter, etc.) and was estimated at 56% by Hegazy. This performance indicator was used to compare 4 designs of glazed PV-T air collectors using monocrystalline solar cells on a daily basis: with the air flowing over the absorber, the air flowing below the absorber, the air flowing on both sides of the absorber in a single pass configuration and the air flowing on both sides of the absorber in a double pass configuration. The best net combined efficiency was obtained with the air flowing on both sides of the absorber in a single pass configuration regardless of flowrate. Daily combined efficiencies for the Egyptian climate ranging from 32% to 54% were obtained for flowrates between 18 kg/(h·m^2) and 144 kg/(h·m^2).

5.4.2 Combined Primary Energy Saving Efficiency

Other researchers (Huang et al., 2001; Jian et al., 2008; Tiwari & Sodha, 2007) have used a combined primary energy saving efficiency, $\eta_{T,P}$, as a performance indicator for PV-T collectors. In this case, the electrical efficiency was converted into primary energy by dividing it by the grid efficiency at generating electricity, $\eta_{gen,grid}$, as shown in Equation (5-4):

$$\eta_{T,P} = \eta_{th} + \frac{\eta_{el}}{\eta_{gen,grid}} \tag{5-4}$$

Huang et al. (2001) used this definition to study the performance of an unglazed sheet-and-tube PV-T water collector using polycrystalline silicone cells (pc-Si). Using a grid efficiency of 38% corresponding to a typical thermal power plant, they obtained a daily combined primary energy saving efficiency of 38%. Jiang et al. (2008) evaluated the influence of PV coverage on the performance of a PV-T trombe wall also using the combined primary energy saving efficiency and a grid efficiency of 38%. They obtained that the combined primary energy saving efficiency of a PV-T trombe wall increased from 15% to 37.5% when increasing the PV coverage ratio from 0.2 to 0.9 even though the thermal efficiency decreased from 7.5% to 2.5%. Tiwari & Sodha (2007) also used this performance indicator to study the effect of glazing and Tedlar films on PV-T air collector designs. As expected, they found that glazed collectors had a greater thermal efficiency, but lower electrical efficiency than unglazed collectors. Using a grid efficiency of 40%, the benefit of a Tedlar film was established as being a function of flowrate and collector length.

This concept of primary energy was also used by Santbergen & van Zolingen (2008) to compare a PV-T system used for domestic hot water to side-by-side PV modules and solar thermal systems. In this case, however, the primary energy savings were defined as:

$$Q_{T,P} = \frac{Q_{th}}{\eta_{p\rightarrow th}} + \frac{Q_{el}}{\eta_{gen,grid}} \tag{5-5}$$

In Equation (5-5), $\eta_{p\rightarrow th}$ is the efficiency for converting primary energy to thermal energy. Using $\eta_{gen,grid} = 40\%$ and $\eta_{p\rightarrow th} = 65\%$ for the thermal efficiency of a conventional gas fired domestic hot water system, the primary energy savings of the PV-T system were estimated at

around 700 kWh/(m^2·y) compared to 300 kWh/(m^2·y) for a PV system and 500 kWh/(m^2·y) for a solar thermal system.

5.4.3 Equivalent Thermal or Electrical Energy Efficiency

In Athienitis et al. (2011), which presents the study of a BIPV-T transpired air collector, an equivalent thermal efficiency, $\eta_{th,eq}$, is introduced. In this case, the electrical energy is converted into thermal energy assuming it is being used to run a heat pump. Thus, the electrical energy is converted into thermal energy by multiplying it by the heat pump coefficient of performance (COP_{HP}) and $\eta_{th,eq}$ is given by:

$$\eta_{th,eq} = \eta_{th} + COP_{HP} * \eta_{el} \tag{5-6}$$

Coventry and Lovegrove (2003) looked at different methodologies to convert the thermal energy of a liquid PV-T collector used for domestic water heating into electricity. They considered several approaches based on exergy, greenhouse gas emissions, life cycle emissions and a market analysis. For this last approach, they considered both a free market energy cost and a renewable energy market energy cost where incentives and subsidies are available for renewable energy technologies. They obtained relative values of electrical energy over thermal energy varying between 1.33 (open market energy cost) and 16.8 (exergy analysis). A critical review of the different methods considered led the authors to conclude that the best approach was a market analysis based on renewable energy technologies. With this methodology, a relative value of electricity compared to thermal energy of 4.24 was obtained. A comparison of PV-T liquid systems using either c-Si modules or amorphous-silicon (a-Si) modules as the absorber showed that a-Si cells would be better only up to a relative value of 4.5.

5.4.4 Equivalent Area

In order to avoid mixing thermal and electrical energy, Bakker et al. (2005) compared a PV-T water heating system combined with a geothermal heat pump to side-by-side PV modules and solar thermal collectors producing the same amount of thermal and electrical energy. They found that the initial cost of the PV-T system was similar to that of the PV module and solar thermal collector side-by-side, but that the side-by-side system required 32% additional roof surface area. Da Silva & Fernandes (2010) used the same methodology to compare a glazed sheet-and-tube

PV-T liquid collector with pc-Si modules to side-by-side PV and solar thermal collectors producing the same amount of energy. They obtained annual thermal and electrical efficiencies of 15% and 9%, respectively for a four person household in Lisbon. Side-by-side PV and thermal systems producing the same amount of thermal and electrical energy would have required an additional area of 60% compared to the PV-T collector.

5.4.5 Combined Useful Energy

This concern related to dealing with two types of energy is a reality for all combined heating and power (CHP) technologies. For CHP technologies using a fuel as an energy source (Onovwiona & Ugursal, 2006), the performance is generally rated in terms of both electrical efficiency, $\eta_{el,CHP}$, and total combined efficiency, $\eta_{T,CHP}$, defined as:

$$\eta_{T,CHP} = \frac{P_{th,useful} + W_{el}}{F_{in}} \tag{5-7}$$

In Equation (5-7), F_{in} is the fuel input, W_{el}, is the electrical output and $P_{th,useful}$, is the useful thermal output.

5.4.6 Economic Indicators

In order to compare simple PV modules to PV-T water collectors, Erdil et al. (2008) used the incremental simple payback defined as the incremental cost of the PV-T collector compared to a PV module divided by the incremental annual energy savings. They found that the incremental simple payback period of a PV-T collector compared to a PV module was 1.7 year using the thermal energy for domestic hot water heating. Garg and Adhikari (2000) used the annual unit cost of useful energy delivered to study the cost-effectiveness of a PV-T air collector defined as the total annual cost of the system divided by the useful energy gain. This economic indicator was used to optimize the channel height of the collector. For a collector operating 300 days per year and 8 hours per day, they found that a height of 0.01 m was optimal up to a collector length of 4 m. For greater collector lengths, a value of 0.02 m was found to minimize this annual unit cost of useful energy delivered.

5.4.7 Conclusion

This review shows that several indicators can be used to assess the performance of PV-T systems or to compare their performance to that of other solar energy technologies. These performance indicators can be based on instantaneous, daily, monthly or annual calculations and can be developed from either economic, energy or exergy analysis. The results obtained strongly depend on both the performance indicator chosen and the relative value between the electricity and the thermal energy produced.

This review also demonstrates that when selecting the boundaries and control volumes of the study, several approaches can be taken. One of these approaches is to take only the collectors as a control volume and to compare the area required by the PV-T system and the side-by-side PV modules and solar thermal collectors to produce the same amount of thermal and electrical energy (da Silva & Fernandes, 2010). Another approach consists of expanding the control volume to the overall building space heating, ventilating or domestic hot water heating system (Bakker et al., 2005).

When comparing the performance of a BIPV-T air system with side-by-side PV modules and liquid solar thermal collectors, the first approach is interesting because it eliminates the need to choose a relative value to convert the electrical into thermal energy or vice-versa. On the other hand, it implies that thermal energy stored in air is directly compared to thermal energy stored in water. The second approach indirectly takes care of this issue because the actual usefulness of the thermal energy produced is taken into account. It has the main disadvantage, however, that the results obtained are very specific to the space heating, ventilating or domestic hot water heating technologies that are coupled with the solar energy technologies under study. Considering the value in each one of these approaches, a new methodology was developed. This methodology is described in Section 5.5.

5.5 Methodology

A new method was developed to take advantage of the different approaches discussed in Section 5.4.7 while eliminating the majority of their disadvantages. In this new method, a BIPV-T system and a system consisting of side-by-side PV modules and solar thermal collectors are mounted on roofs of identical surface areas. For the side-by-side system, the size of the liquid solar thermal

collector is set to that of a typical solar domestic hot water system. In both systems, the thermal energy collected is recovered by water circulating through a heat exchanger, but only if the thermal energy recovered is considered useful for the building according to various criteria for thermal energy usefulness. It is this useful thermal energy recovered by the heat exchanger that is considered as the system thermal energy production. This approach has the advantage of taking the actual usefulness of the thermal energy recovered into account. In addition, it keeps the results of the study general, because the solar energy technologies are not coupled with specific space heating, ventilating and domestic hot water heating systems.

Several steps were followed in order to develop a case study to compare the energy and economic performance of a BIPV-T air system to that of side-by-side PV modules and solar thermal liquid collectors. The first step consisted of determining the characteristics of the two systems required for comparison: the first one involving a BIPV-T air system and the second one including side-by-side PV modules and liquid solar thermal collectors. This step is presented in Section 5.5.1. For the BIPV-T air collector, a custom model was developed and validated to suit the purpose of the study as described in Section 5.5.2. Both systems were then modeled using TRNSYS version 17 (Klein et al., 2009). In order to fulfill the two main objectives of the study, i.e., to provide energy and economic comparisons between BIPV-T air systems and side-by-side PV modules and liquid solar thermal collectors, performance and economic indicators were developed. For the performance indicator, the concept of equivalent thermal energy production was used considering several relative values to convert electricity into thermal energy. As for the economic indicator, while the cost of PV modules and liquid solar thermal collectors are well-known, the cost of a BIPV-T air system is difficult to estimate because this technology is new and varies a lot from one project to another. Considering that it is the thermal part of the BIPV-T air system that is difficult to estimate, a new economic indicator was developed. This indicator corresponds to the required cost of the thermal part of the BIPV-T air system so that the total cost of the BIPV-T system breaks-even with that of side-by-side PV modules and solar thermal collectors. Section 5.5.3 provides information on the other components of the simulation and Sections 5.5.4 to 5.5.6 provide the details of the cost estimate for the different components of the system as well as the definition of the performance and economic indicators.

5.5.1 Description of the Systems

The two systems chosen for comparison are shown in Figure 5-1. Both systems are mounted on identical south-facing roofs having a 45° slope and an area of 40 m^2.

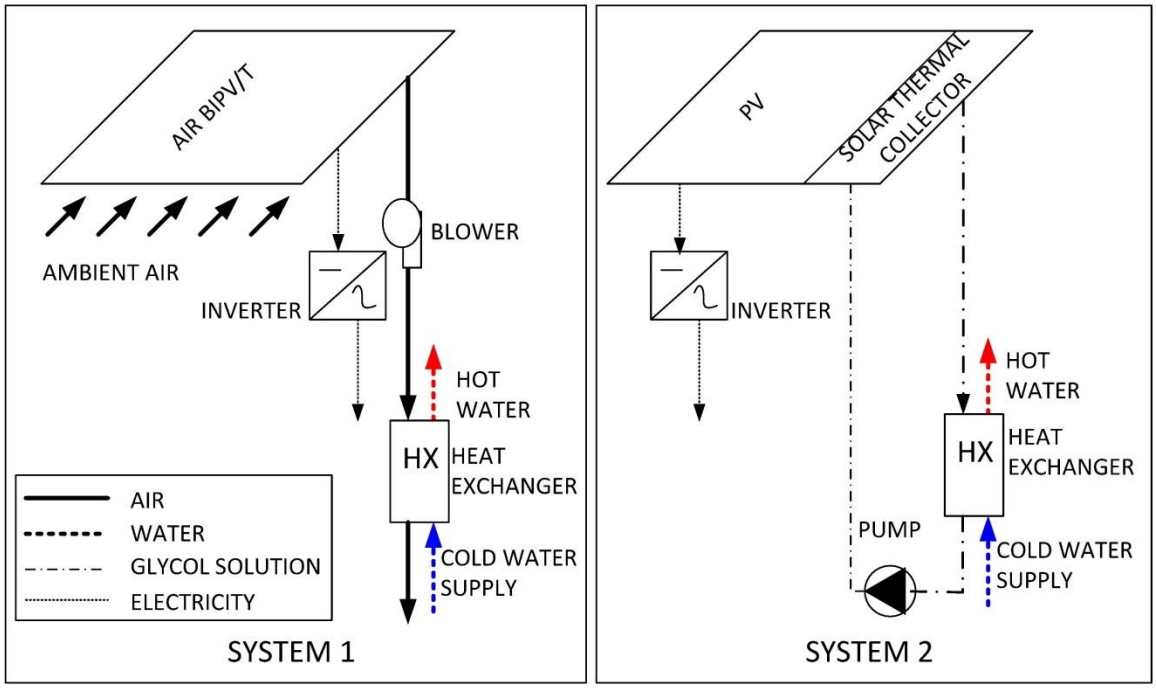

Figure 5-1: Schematic of systems

In System 1, the BIPV-T option, the roof of the house consists of a BIPV-T using air as the heat transfer fluid. The air is drawn directly from outdoor with a blower and brought to the house basement where the thermal energy recovered from the PV modules is transferred to cold water using a heat exchanger. In System 2, the PV+T option, PV modules and a liquid solar thermal system are mounted side-by-side. The solar thermal system operates in a closed-loop with a pump. It uses a solution consisting of 50% water and 50% propylene glycol as its heat transfer fluid. Similar to System 1, a heat exchanger (HX) is used to transfer the thermal energy stored in the hot fluid to cold water. The purpose of this heat exchanger is to convert the thermal energy produced by both systems into the same medium, i.e., water. In both systems a constant effectiveness heat exchanger is used with $\varepsilon_{HX} = 0.8$.

In System 2, the solar thermal collector system consists of 2 collectors mounted in series each having a gross area of 2.6 m^2. The total gross area of this system corresponds to 5.2 m^2, the average solar thermal collector system area installed in Canada in 2011 (ClearSky Advisors Inc., 2011). The solar thermal collector fluid is assumed to circulate at a constant flowrate of 54 kg/(h·m^2). The section of the roof area not covered by solar thermal collectors, 34.8 m^2, is used for rack-mounted PV modules. These modules have an efficiency of 15.2% and use mono-crystalline cells. The inverter is assumed to have a constant efficiency corresponding to $\eta_{inv} = 0.95$. Three different temperatures are used for the cold water supply: $T_{w,in} = T_{mains}$, $T_{w,in} = 10$ °C and $T_{w,in} = 20$ °C, where T_{mains} is the temperature of the city water. The water flowrate entering the heat exchanger was selected so that the product of the flowrate, m, and thermal capacity, c_p, of the water and glycol sides of the heat exchanger would be equal. Using $c_{p,w} = 4.19$ kJ/(kg · K) and $c_{p,g} = 3.56$ kJ/(kg · K), the water flowrate, m_w, was set at 239 kg/h. The pump power required to circulate the fluid was estimated at 2% of the solar thermal collector system maximum power, i.e., 72 W.

In System 1, the whole roof is the BIPV-T system. The air gap thickness (channel height) is 2.5 cm. The BIPV modules and inverter have the same characteristics than those used in System 2. Similar to System 2, the air flowrate in System 1 was selected so that the product of the flowrate and thermal capacity of the water corresponds to that of the air. Taking 1 kJ/(kg·K) as the air thermal capacity, the air flow rate was set at 25 kg/(h·m^2) which corresponds to 1000 kg/h. The blower power required to circulate the air in the BIPV-T system was set constant at 425 W.

The systems were modeled in the TRNSYS V17 simulation environment using the Canadian Weather for Energy Calculations (CWEC) weather file for Montreal. According to this weather file, the total annual irradiance on a 45° south-facing surface for Montreal is 1,506 kWh/m^2.

5.5.2 BIPV-T Model and Validation

The BIPV-T model developed for this study is a 2-D steady-state model inspired by the TRNSYS TESS library Type 569, but modified to include a number of features such as air infiltration/leakage and a PV model based on experimental data. A steady-state model was assumed to be sufficient for this analysis because the model was planned to be used for performing annual simulations. The model was developed under the assumptions that the

temperature is uniform along the system width and that the system edge heat losses can be neglected.

The BIPV-T system thermal resistance network is shown in Figure 5-2. Symbols are defined in the text below.

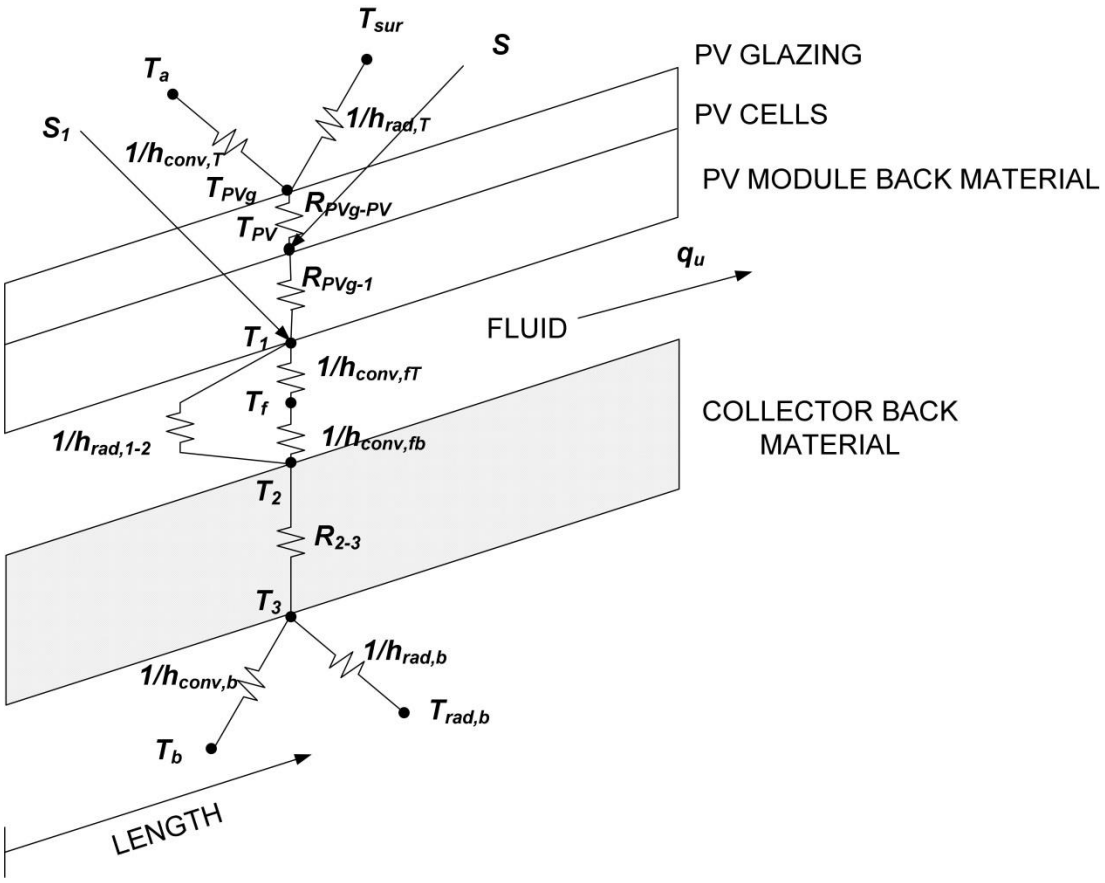

Figure 5-2: BIPV-T system thermal resistance network

The collector is divided into *n* elements in the length direction where each element has a length dy and a width, W, corresponding to the system width. Energy balances on the PV glazing layer, PV cells layer, PV module back material layer, air channel and top and bottom surfaces of the system back material, in this case the roof, are given in Equations (5-8) to (5-13) for the k^{th} element. The subscript *k* is not included in the equations for simplicity.

$$0 = h_{conv,T}\left(T_{PVg} - T_a\right) + h_{rad,T}\left(T_{PVg} - T_{sur}\right) + \left(\frac{T_{PVg} - T_{PV}}{R_{PVg-PV}}\right) \quad (5\text{-}8)$$

$$S + \left(\frac{T_{PVg} - T_{PV}}{R_{PVg-PV}}\right) = \left(\frac{T_{PV} - T_1}{R_{PVg-1}}\right) \quad (5\text{-}9)$$

$$\left(\frac{T_{PV} - T_1}{R_{PVg-1}}\right) + S_1 = h_{conv,fT}\left(T_1 - T_f\right) + h_{rad,1-2}(T_1 - T_2) \quad (5\text{-}10)$$

$$q_u = h_{conv,fT}\left(T_1 - T_f\right) - h_{conv,fb}\left(T_f - T_2\right) \quad (5\text{-}11)$$

$$h_{conv,fb}\left(T_f - T_2\right) + h_{rad,1-2}(T_1 - T_2) = \frac{(T_2 - T_3)}{R_{2-3}} \quad (5\text{-}12)$$

$$\frac{(T_2 - T_3)}{R_{2-3}} - h_{conv,b}(T_3 - T_b) - h_{rad,b}\left(T_3 - T_{rad,b}\right) = 0 \quad (5\text{-}13)$$

In Equations (5-8) to (5-13), $h_{conv,T}$ and $h_{rad,T}$ are the top convective and radiative heat transfer coefficients, $h_{rad,1-2}$ is the radiative heat transfer coefficient between the channel top and bottom surfaces, $h_{conv,b}$ and $h_{rad,b}$ are the system back surface convective and radiative heat transfer coefficients and $h_{conv,fT}$ and $h_{conv,fb}$ are the top and bottom air channel heat transfer coefficients, respectively. T_a is the ambient temperature, T_{sur} is the temperature of the surroundings, T_{PVg} is the top of the glass encapsulant temperature, T_{PV} is the PV cells' temperature, T_1 and T_2 are the temperatures of the top and bottom surfaces of the air channel, respectively, T_f is the fluid temperature in the channel, T_3 is the temperature at the back surface of the collector back material, T_b is the temperature in the zone at the back of the collector and $T_{rad,b}$ is the mean radiant temperature in that zone. S_1 is the radiation absorbed by the PV back material and q_u is the thermal energy collected. R_{PVg-PV} is the thermal resistance between the top of the glass encapsulant and the top of the PV cells, R_{PVg-1} is the thermal resistance between the top of the PV cells and the back surface of the PV cells back material and R_{2-3} is the thermal resistance between the top and back surfaces of the collector back material.

The thermal energy collected in the k^{th} element can be calculated with the following relation:

$$q_u W dy = m_o c_{p,o} T_{f,o} - m_i c_{p,i} T_{f,i} + m_L c_{p,a} T_a \tag{5-14}$$

In Equation (5-14), the subscripts *i* and *o* refer to the inlet and outlet of the k^{th} element, respectively. m is the fluid flowrate, m_L is the air leakage taken as a positive number when infiltration occurs and c_p is the air specific heat. By neglecting the variation of fluid properties with temperature, Equation (5-14) can be re-written as:

$$q_u W dy = c_p\left(m_o T_{f,o} - m_i T_{f,i}\right) - (m_o - m_i) c_p T_a \tag{5-15}$$

When there is no air leakage or infiltration in the collector, Equation (5-15) can be reduced to:

$$q_u W dy = m c_p\left(T_{f,o} - T_{f,i}\right) \tag{5-16}$$

The net absorbed solar radiation per unit of gross collector area in the cell layer, S, is given as:

$$S = IAM_{PV} (\tau\alpha)_{PV,N} G F_{cell} - \eta_{PV} G \tag{5-17}$$

In Equation (5-17), F_{cell} is the fraction of the collector gross area covered by PV cells, IAM_{PV} is the PV and encapsulant incidence angle modifier taking into account the sky diffuse, ground reflected and beam components of the solar radiation, $(\tau\alpha)_{PV,N}$ is the PV cell transmittance-absorptance product accounting for glass encapsulant at normal incidence angle, η_{PV} is the PV cell efficiency and *G* is the in-plane incident radiation.

The net absorbed solar radiation per unit aperture area in the PV module back material is given as:

$$S_1 = IAM_{bs} (\tau\alpha)_{bs,N} G (1 - F_{cell}) \tag{5-18}$$

In Equation (5-18), $(\tau\alpha)_{bs,N}$ is the PV module backsheet material transmittance-absorptance product and IAM_{bs} is the backsheet and encapsulant incidence angle modifier.

Neglecting framing radiative heat losses, the top radiative heat transfer coefficient, $h_{rad,T}$, is given as:

$$h_{rad,T} = \sigma \varepsilon_{PVg} \left(T_{PVg}^2 + T_{sur}^2\right)\left(T_{PVg} + T_{sur}\right) \tag{5-19}$$

In Equation (5-19), σ is the Stefan-Boltzmann constant and ε_{PVg} is the PV glazing emissivity. T_{sur} is the surroundings temperature in Kelvin given as:

$$T_{sur} = \left(F_{gnd}T_{gnd}^4 + F_{sky}T_{sky}^4\right)^{1/4} \tag{5-20}$$

In Equation (5-20), T_{gnd} and T_{sky} are the ground and sky temperatures in Kelvin and F_{gnd} and F_{sky} are the ground and sky view factors. In this case, it is assumed that the ground temperature corresponds to the ambient temperature. The back of the collector radiative heat loss coefficient, $h_{rad,b}$, is given as

$$h_{rad,b} = \sigma\varepsilon_{col,b}\left(T_3^2 + T_{rad,b}^2\right)\left(T_3 + T_{rad,b}\right) \tag{5-21}$$

where $\varepsilon_{col,b}$ is the emissivity of the zone interior surface behind which the BIPV-T is mounted. The radiative heat loss coefficient between surfaces 1 and 2 assuming a view factor of 1 between the two surfaces can be expressed as follows:

$$h_{rad,1-2} = \frac{\sigma(T_1^2 + T_2^2)(T_1 + T_2)}{\frac{1}{\varepsilon_1} + \frac{1}{\varepsilon_2} - 1} \tag{5-22}$$

In Equation (5-22), ε_1 and ε_2 are the emissivities of the top and bottom surfaces of the air channel, respectively.

In the standard IEC 61853-1 (IEC, 2011), it is recommended to characterize the performance of a PV module with a matrix containing the PV module maximum power point as a function of irradiance and PV temperature. The BIPV-T model developed uses this matrix to compute the PV module maximum power point at any irradiance level and PV cell temperature by using a linear interpolation for T_{PV} and a polynomial interpolation for G. The PV efficiency of the BIPV-T module or array, η_{PV}, is then estimated by dividing the maximum power point by the product of the collector sample area and irradiance.

The collector back surface heat transfer coefficient depends on the system mounting configuration. For a building-integrated system, $h_{conv,b}$ is the heat transfer coefficient at the interior surface of the zone on which the collector is mounted. According to ASHRAE (1997), the inner film heat transfer coefficient of surfaces at a 45° slope varies from 2.56 to

9.09 W/(m^2·K) depending on the surface emittance and direction of the flow. In this case, a value of 5 W/(m^2·K) is used.

In order to solve the equations above, four additional equations are introduced to calculate the following coefficients: the top natural and wind convective heat loss coefficients, h_{nat} and h_w, and the top and bottom air channel heat transfer coefficients, $h_{conv,fT}$ and $h_{conv,fb}$.

Notton et al. (2005) used more than 20 different combinations of convective heat loss coefficients for their double glazed PV module. They considered the following three scenarios to compute the top convective heat loss coefficient:

$$h_{conv,T} = h_w \tag{5-23}$$

$$h_{conv,T} = \mathrm{MAX}(h_w, h_{nat}) \tag{5-24}$$

$$h_{conv,T} = \sqrt[1/3]{h_{nat}^3 + h_w^3} \tag{5-25}$$

The results closest to their experimental data were obtained using only the forced convective heat transfer coefficient and the model of Cole & Sturrock (1977). Several models have been developed to estimate convective heat losses from PV modules, solar thermal collectors of PV-T collectors. Some of these models are summarized in where all heat transfer coefficients are given in W/(m^2·K) and the wind velocity V_w corresponds to the local wind speed.

For the heat transfer inside the air channel, in solar thermal air collectors, the air channel bottom ($h_{conv,fb}$) and top ($h_{conv,fT}$) heat transfer coefficients are typically assumed to be identical. The fluid heat transfer coefficient in the channel is a function of the Nusselt number, Nu, fluid thermal conductivity, k, and hydraulic diameter D:

$$h_{conv,f} = \frac{\mathrm{Nu}k}{D} \tag{5-26}$$

For air solar collectors, the Nusselt number of a laminar flow in a smooth channel is given as:

$$\mathrm{Nu} = 3.66 \tag{5-27}$$

In turbulent conditions, the following model of Dittus & Boelter (1985) is often used:

$$\mathrm{Nu} = 0.023\mathrm{Re}^{0.8}\mathrm{Pr}^{n} \tag{5-28}$$

In Equation (5-28), Pr is the Prandtl number, n=0.4 when the plate is warmer than the fluid and n=0.3 when the plate is cooler than the fluid. When there is no flow in the channel and the collector is under stagnation conditions, the Nusselt number is calculated as a function of the Rayleigh number, Ra, and the collector tilt, β, with the following relation from Hollands et al. (1976):

$$Nu = 1 + 1.44\left[1 - \frac{1708\left(\sin(1.8\beta)\right)^{1.6}}{\mathrm{Ra}\cos\beta}\right] * \max\left[0, \left(1 - \frac{1708}{\mathrm{Ra}\cos\beta}\right)\right] + \max\left[0, \left(\left(\frac{\mathrm{Ra}\cos\beta}{5830}\right)^{1/3} - 1\right)\right] \tag{5-29}$$

Table 5-1: Summary of models used to compute natural and forced convective heat transfer coefficients

Author	Model
Eicker (2003)	$h_{nat} = 1.78(T_c - T_a)^{1/3}$
McAdams (1954)	$h_{nat} = 5$
Pavylos (2008)	$h_w = 7.4 + 4V_w$ for windward surfaces $h_w = 4.2 + 3.5V_w$ for leeward surfaces
McAdams (1954)	$h_w = 5.7 + 3.8V_w$
Watmuff et al. (1977)	$h_w = 2.8 + 3V_w$
Cole & Sturrock (1977)	$h_w = 11.4 + 5.7V_w$ for windward surfaces $h_w = 5.7V_w$ for leeward surfaces
Sparrow et al. (1979)	$h_w = 0.86\mathrm{Re}_{L*}^{-1/2}\rho c_p V_w/\mathrm{Pr}^{1/3}$
Incropera & DeWitt (1996)	$\mathrm{Nu}_L = 0.664\mathrm{Re}_L^{1/2}\mathrm{Pr}^{1/3}$ for laminar flow $\mathrm{Nu}_L = 0.037\mathrm{Re}_L^{4/5}\mathrm{Pr}^{1/3}$ for turbulent flow
Test et al. (1981)	$h_w = 8.55 + 2.56V_w$
Sharples & Charlesworth (1998)	$h_w = 8.3 + 1.3V_w$ at 180° $h_w = 8.3 + 2.2V_w$ at 0° $h_w = 6.5 + 3.3V_w$ at 90°
Kumar & Mullick (2010)	$h_w = 6.90 + 3.87V_w$ for $V_w \leq 1.12$ m/s

Candanedo et al. (2011) developed the following heat transfer coefficient models for the top and bottom channel surfaces of a BIPV-T collector:

$\mathrm{Nu} = 0.052\mathrm{Re}^{0.78}\mathrm{Pr}^{0.4}$ for the top surface with $250 \leq \mathrm{Re} \leq 7.500$ (5-30)

$\mathrm{Nu} = 1.017\mathrm{Re}^{0.471}\mathrm{Pr}^{0.4}$ for the bottom surface with $250 \leq \mathrm{Re} \leq 7.500$ (5-31)

They compared the Nusselt number calculated with their model to that obtained with five other models including that of Dittus & Boelter. For Reynolds number up to 10,000, the predictions of their model was found to be generally among the highest whereas the predictions obtained with the model of Dittus & Boelter were among the lowest. In order to determine the models to be used to compute h_{nat}, h_w, $h_{conv,fT}$ and $h_{conv,fb}$ in the BIPV-T model, simulations were performed using various combinations of the different models. The results were then compared to experimental data collected on two unglazed c-Si air PV-T modules mounted in series in a building-integrated configuration having a total gross area of 3.51 m^2. The measurements used consist of 25 observations obtained under quasi-stationary conditions. The details of the experimental setup and uncertainties calculation can be found in Delisle & Kummert (2012). The measured and estimated parameters for the PV-T collector tested are summarized in Table 5-2.

Table 5-2: Parameters used for the model validation

Parameter	Measured/estimated	Value
A_g	Measured	3.513 ± 0.001 m^2
L	Measured	3.47 ± 0.0005 m
W	Measured	0.96 ± 0.001 m
th	Measured	0.105 ± 0.002 m
F_{cell}	Measured	0.865 ± 0.004
R_{PVg-PV}	Estimated	0.0036 ± 0.0018 (m^2·°C)/W
R_{PVg-1}	Estimated	0.023 ± 0.001 (m^2·°C)/W
R_{2-3}	Estimated	2.0 ± 0.1 (m^2·°C)/W
ε_1	Estimated	0.85 ± 0.04
ε_2	Estimated	0.87 ± 0.04
ε_{PV}	Estimated	0.85 ± 0.04
ε_b	Estimated	0.79 ± 0.04
$(\tau\alpha)_{bs,N}$	Estimated	0.36 ± 0.01
$(\tau\alpha)_{PV,N}$	Estimated	0.85 ± 0.01

The PV maximum power point matrix for the two modules in series is presented in Table 5-3.

Table 5-3: Matrix of the maximum power point as a function of T_{PV} and G

	T_{PV} (°C)				
G (W/m^2)	20	25	35	55	60
1100	506.5	495.3	484.2	461.9	417.3
1000	462.6	452.6	442.7	422.7	382.9
900	417.3	408.7	400.0	382.6	347.8
700	328.3	321.7	315.1	301.9	275.4
400	194.0	189.3	184.5	175.0	156.0
200	95.8	93.0	87.3	75.9	73.0

In order to consider the uncertainties related to the collector parameters and operating conditions, a Monte-Carlo simulation was performed. For each experimental observation, a normal distribution containing more than 4,500 points was created for the parameters, inputs and outputs using the estimated expanded uncertainties. Then, Monte-Carlo simulations were performed using various models for computing $h_{conv,T}$ and the models of Dittus & Boelter and Candanedo et al. to estimate h_f. The 8 scenarios providing results that were the closest to the experimental data are identified in Table 5-4.

Table 5-4: Scenarios for computing h_{nat}, h_w, $h_{conv,T}$ and h_f that showed the most potential

Scenario	h_{nat}	h_w	$h_{conv,T}$	h_f
DB-4	McAdams	Watmuff et al.	$\left({h_w}^3 + {h_{nat}}^3\right)^{1/3}$	Dittus & Boelter
DB-6	McAdams	Cole & Sturrock-Leeward	$\left({h_w}^3 + {h_{nat}}^3\right)^{1/3}$	Dittus & Boelter
DB-8	-	Incropera & DeWitt	$\max(h_w, h_{nat})$	Dittus & Boelter
DB-9	-	Incropera & DeWitt	$\left({h_w}^3 + {h_{nat}}^3\right)^{1/3}$	Dittus & Boelter
CAND-1	-	Pavylos-leeward	h_w	Candanedo et al.
CAND-2	-	McAdams	h_w	Candanedo et al.
CAND-4	McAdams	Watmuff et al.	$\left({h_w}^3 + {h_{nat}}^3\right)^{1/3}$	Candanedo et al.
CAND-9	-	Incropera & DeWitt	$\left({h_w}^3 + {h_{nat}}^3\right)^{1/3}$	Candanedo et al.

The comparison between the measured and predicted electrical and thermal efficiencies for the 8 scenarios presenting the most potential is presented in Figure 5-3. The overall mean bias error (MBE) and root mean squared error (RMSE) for the 25 observations are summarized in Figure 5-4. As it can be observed, the model of Candanedo et al. for h_f combined to that of Pavylos for leeward surfaces to compute h_w using $h_{conv,T} = h_w$ provides the best results (Cand-1). With this combination, the percentages of RMSE of the mean were found to be 3.75%, 7.5%, 12.5% and 3.5% for T_o, T_{PV}, η_{th} and η_{el}, respectively. The model of Candanedo et al. to compute h_f is only valid for Reynolds number lower than or equal to 7,500 which was the case for the 25 observations used for the validation. Considering the possibility of using higher Reynolds numbers, the scenario using the model of Dittus-Boelter for h_f and that of Incropera & DeWitt for h_w was implemented in the model for Reynolds numbers higher than 7,500.

The PV model developed for System 2 is very similar to the BIPV-T model described above. The only difference is that for System 2, the PV modules were assumed to be mounted close to the roof, so that there is no natural convection at the back of the modules.

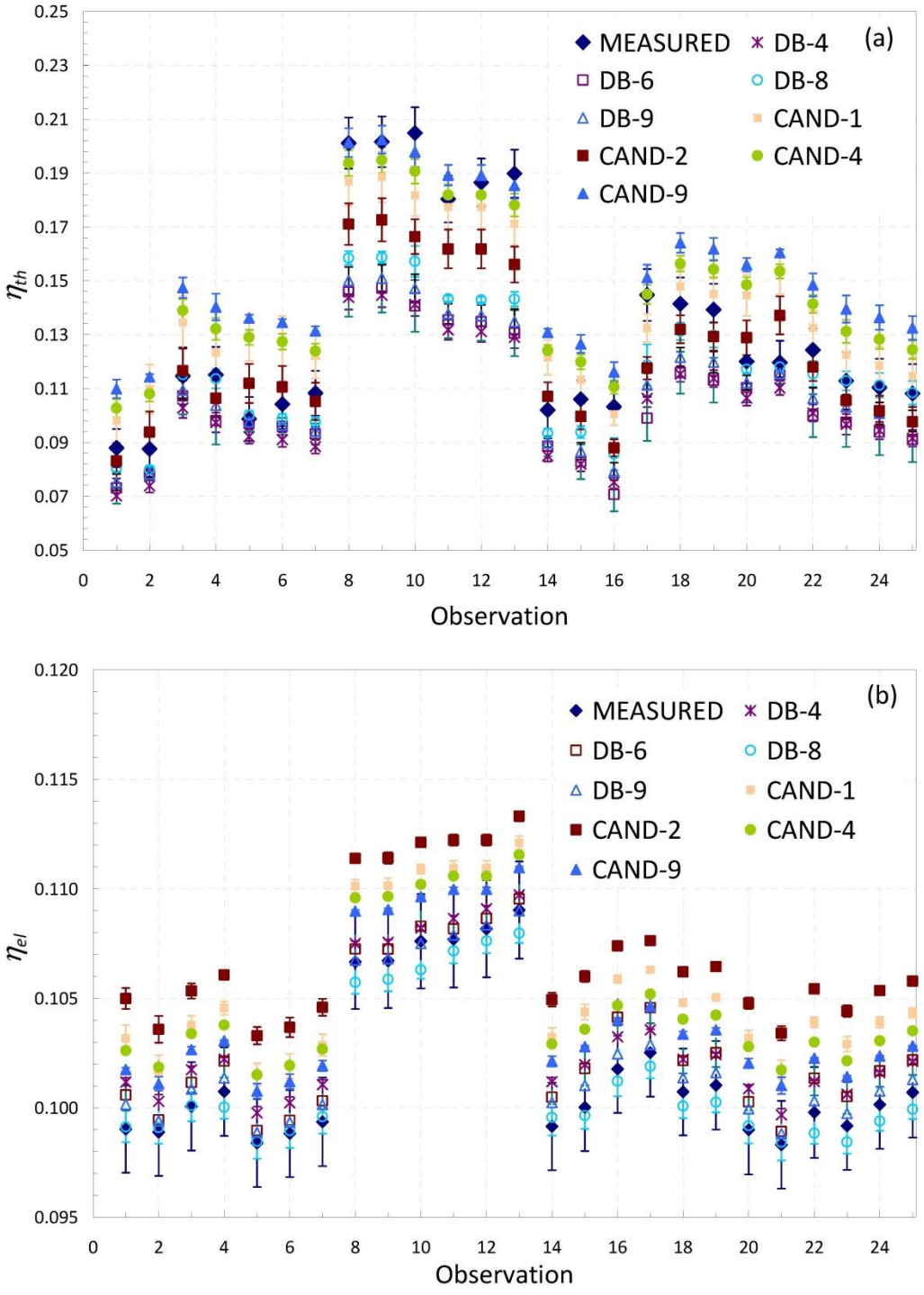

Figure 5-3: Comparison of the predicted and measured (a) thermal and (b) electrical efficiency, η_{th} and η_{el}, using the best scenarios for computing the fluid top convective heat transfer coefficient, $h_{conv,T}$ and the fluid heat transfer coefficient, h_f

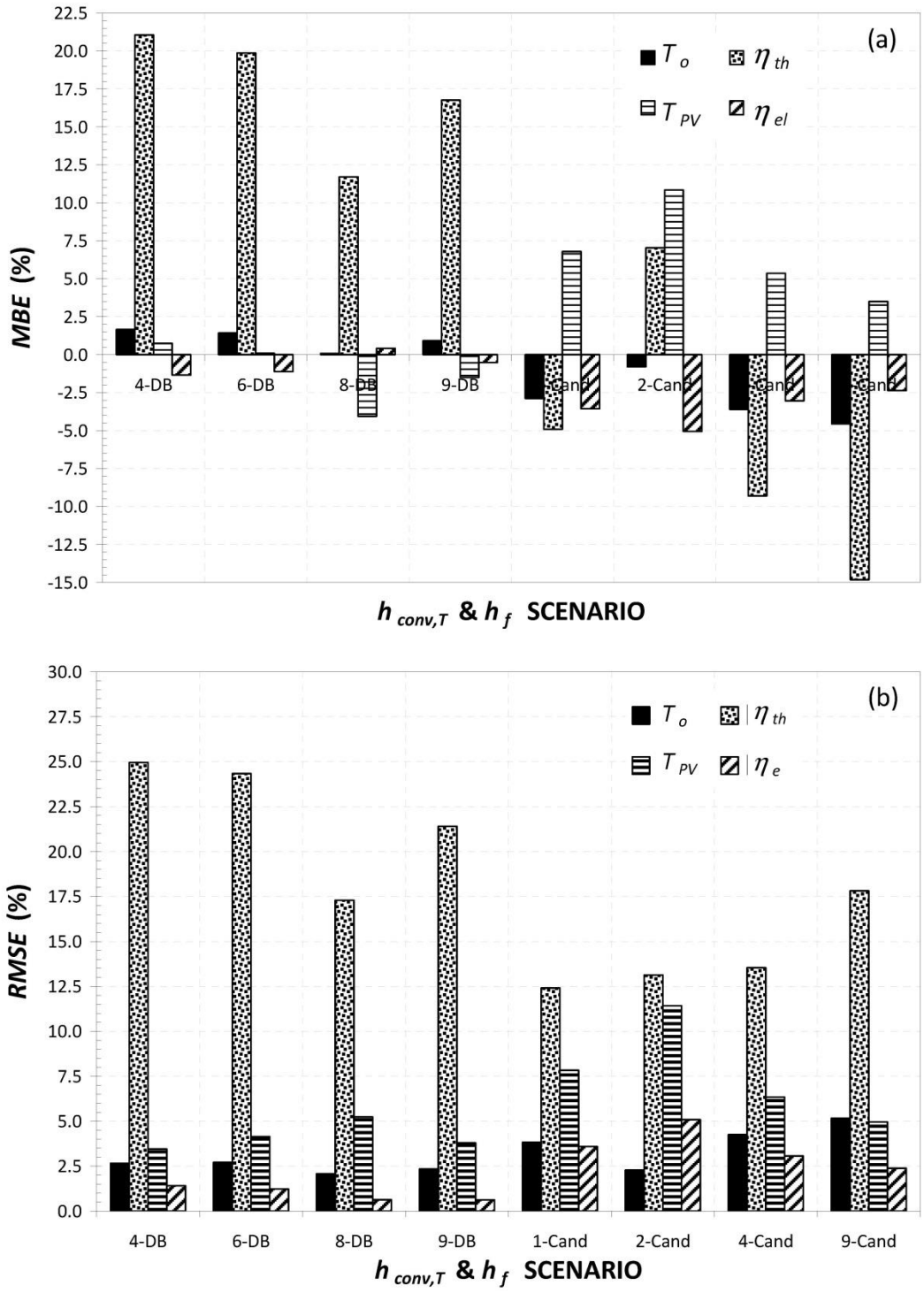

Figure 5-4: (a) Mean bias error and (b) root mean square error in predicting the fluid outlet temperature, T_o, the PV cells' temperature, T_{PV}, the thermal efficiency, η_{th}, and the electrical efficiency, η_{el}, for the 8 best scenarios for computing the fluid heat transfer coefficient, h_f and the fluid top convective heat transfer coefficient, $h_{conv,T}$

5.5.3 Other Components of the System

The TRNSYS standard component Type 1b was used for the solar thermal collector model. This model is based on performance curves obtained experimentally. It uses the coefficients of the 2nd order efficiency curve (a_0, a_1 and a_2) as well as the coefficients of the incidence angle modifier (IAM) curve (b_0 and b_1) as parameters. The thermal efficiency and IAM curves are given as:

$$\eta_{th} = a_0 - a_1 \frac{(T_{f,i} - T_a)}{G} - a_2 \frac{(T_{f,i} - T_a)^2}{G} \tag{5-32}$$

$$IAM = 1 - b_0 \left(\frac{1}{\cos\theta} - 1\right) - b_1 \left(\frac{1}{\cos\theta} - 1\right)^2 \tag{5-33}$$

In Equations (5-32) and (5-33), θ is the sun incidence angle on the collector, a_0 is the collector thermal efficiency at $T_{f,i} = T_a$, a_1 is the efficiency curve slope, a_2 is the efficiency curve curvature and b_0 and b_1 are the 1st and 2nd order IAM coefficients. In this study, typical glazed flat-plate collectors are used. The efficiency and IAM parameters used are summarized in Table 5-5.

Table 5-5: Parameters used for the solar thermal collector

Parameter	Value
a_0	0.69
a_1	3.40 W/(m^2·K)
a_2	0.02 W/(m^2·K^2)
b_0	0.19
b_1	0.0006

5.5.4 System Component Costs

The cost of the PV part of the BIPV-T system (System 1) and the total cost of the PV+T system (System 2) were estimated in 2011 Canadian dollars (CAD).

According to Natural Resources Canada (2012), the turnkey price for grid-connected PV systems of less than 10 kW in distributed applications was 6.79 CAD/W in 2011. This price was used as the PV system price for both Systems 1 and 2. In System 1, however, the BIPV-T system is

assumed to replace the actual roof since it consists of standard PV panels mounted on a roof with waterproofing material but with no roof covering. Therefore, the price of the roof covering material can be deducted from the PV system price. The roof covering material was assumed to be roof shingles since this is the most widely used material in Canada for roof covering of residential buildings. Using the RS Means Building Construction Cost Data Handbook (2013a), the cost of asphalt shingles was estimated at 1,800 CAD for a 40 m^2 roof including material and installation. Thus, in system 1, the cost of the BIPV part of the BIPV-T system was estimated at 39,485 CAD.

In 2011, the average selling price for the sale of residential domestic hot water systems in Canada having an average collector area of 5.2 m^2 was 3,848 CAD/system (ClearSky Advisors, 2011). This price, however, does not include installation. A second estimate was performed using the RS Means Green Building Cost Data handbook (2013b) including the equipment and installation of all the different components of System 2 (circulating pump, expansion tank, valves, high temperature cut-off and sensors, piping insulation, circulating fluid, collectors, etc.). A cost of 4,525 CAD was obtained. This cost was used for the solar thermal collector system of System 2. Note that this cost estimate excludes the cost of a tank that could be located downstream of the exchanger. The total cost of System 2 was estimated at 40,441 CAD including the PV modules, the balance of system and all the components of the solar thermal collector system excluding tanks.

5.5.5 Performance Indicators

As shown in Section 5.4, different methods can be followed to compute and present the performance of BIPV-T systems. In this study, an approach similar to that used for Combined Heat and Power (CHP) technologies is adopted because it is considered that roofs producing both thermal and electrical energy are CHP systems. The only difference from standard CHP technologies is that the sun is the energy source. An interesting aspect in the CHP technology performance assessment approach is that only the useful part of the thermal energy produced is considered in the calculation of the overall system performance. Accounting only for the useful thermal energy produced is necessary for BIPV-T systems because of the low temperature levels usually achieved. Thus, in this study, the following performance indicators are used:

- The annual useful thermal energy production, $Q_{th,u}$

- The net annual electricity production, $Q_{el,net}$
- The net annual combined useful equivalent thermal energy production, $Q_{th,eq,u}$

These performance indicators are calculated on an annual basis using the following relations:

$$Q_{th,u} = \int_{t=0}^{t=8760} P_{th,u} dt \tag{5-34}$$

$$Q_{el,net} = \int_{t=0}^{t=8760} \left(P_{PV}\eta_{inv} - P_{pumping}\right) dt \tag{5-35}$$

$$Q_{th,eq,u} = Q_{th,u} + C_{el-th} Q_{el,net} \tag{5-36}$$

In Equations (5-34) to (5-36), dt is the simulation timestep, $P_{th,u}$ is the rate of energy gain on the water side of the heat exchanger, P_{PV} is the electrical power production of the PV modules, η_{inv} is the inverter efficiency at converting current from DC to AC, $P_{pumping}$ is the pumping power required to circulate the air or liquid and C_{el-th} is the conversion coefficient used to convert electrical energy into equivalent thermal energy. Note that the PV system losses due to mismatch, wiring, dirt, snow and other factors are neglected. Considering that the relative value of electrical energy compared to thermal energy can vary significantly depending on the house HVAC system and fuel used, three conversion coefficients are used: $C_{el-th} = 1$, $C_{el-th} = 2$ and $C_{el-th} = 3$.

Determining the usefulness of the thermal energy produced on the water side of the heat exchanger requires that the thermal energy end-usage be known. In order to avoid implementing any heating, cooling or storage systems to keep the study as general as possible, criteria for determining thermal energy usefulness were developed. These criteria were elaborated based on the minimum and maximum outdoor ambient temperature, $T_{a,min}$ and $T_{a,max}$ and the minimum temperature rise on the water side of the heat exchanger, $T_{rise,w,min}$. $T_{a,min}$ and $T_{a,max}$ are used to indicate under which ambient temperature conditions the system runs. For example, a system that functions only in the winter, early spring and late fall would operate when the ambient temperature ranges from -20 °C to 10 °C ($T_{a,min} = -20$ °C and $T_{a,max} = 10$ °C). As for $T_{rise,w,min}$, it is used to set the minimum temperature rise required on the water side of the heat

exchanger in order for the system to be worth running. For instance, if the processes downstream of the heat exchanger bring important heat losses to the water, $T_{rise,w,min}$ might be set to 5 °C or even 10 °C so that there is still a net heat gain at the end of all the processes. The criteria used are summarized in Table 5-6. With this criterion, the thermal energy usefulness is related to the achieved temperature rise above the inlet temperature (as explained above, $T_{w,min}$ is set to 10 °C, 20 °C or T_{mains} depending on the scenario). For some applications, it could be more appropriate to assess the usefulness of thermal energy based on a minimum outlet temperature level (e.g., minimum acceptable temperature for domestic hot water, or minimum temperature level to drive a sorption machine for cooling). In that case, a criterion related to the absolute outlet temperature on the water side of the heat exchanger should be included.

Table 5-6: Criteria for determining thermal energy usefulness

CRITERIA	$T_{a,min}$ (°C)	$T_{a,max}$ (°C)	$T_{rise,w,min}$ (°C)
0	-30	35	0
1	-20	10	0
2	-20	10	2
3	-20	10	5
4	-20	10	10
5	-20	30	0
6	-20	30	2
7	-20	30	5
8	-20	30	10
9	-10	10	0
10	-10	10	2
11	-10	10	5
12	-10	10	10
13	-10	30	0
14	-10	30	2
15	-10	30	5
16	-10	30	10

When running a simulation, the heat transfer fluid is only allowed to circulate if the criterion of thermal energy usefulness is respected. If the criterion is not respected, $P_{th,u}$is set to 0, but P_{PV} is still computed. For System 1, the PV cells' temperature is calculated as if the collector was under stagnation conditions.

5.5.6 Economic Indicators

In addition to the performance indicators discussed above, economic indicators are also computed. One of these economic indicators is the cost of the system per unit of useful equivalent thermal energy produced over a year, $C_{QTH,eq,u}$. It is given as:

$$C_{QTH,eq,u} = \frac{C_{System}}{Q_{th,eq,u}} \tag{5-37}$$

In Equation (5-37), C_{System} is the system initial cost in CAD. Another economic indicator calculated is the required cost to recover the heat from the BIPV system (basically the cost to convert the BIPV to a BIPV-T system) to break-even with the cost of the side-by-side system, $C_{T,B-E(BIPV-T)}$. This cost is obtained by isolating $C_{T,B-E(BIPV-T)}$in the following relation:

$$\frac{C_{T,B-E(BIPV-T)} + C_{BIPV(BIPV-T)}}{Q_{th,eq,u(BIPV-T)}} = \frac{C_{PV+T}}{Q_{th,eq,u(PV+T)}} \tag{5-38}$$

5.6 Results and Discussion

5.6.1 Thermal and Electrical Energy Production

The comparison of the useful thermal and net electrical production for Systems 1 and 2 is shown in Figure 5-5 to Figure 5-7 for $T_{w,in} = T_{mains}$, 10 °C and 20 °C. From these figures, it can be observed that the BIPV-T system always produces more electrical energy than the PV+T system. This is due to the fact that the area covered by PV modules is 40 m^2 in the BIPV-T system compared to only 34.8 m^2 in the PV+T system. For the BIPV-T system, the net electrical energy production is much more affected by the end-use criteria than the useful thermal energy production. This is due to the blower power being more important than the pump power and the fact that contrary to the PV+T system, the PV cells' efficiency in the BIPV-T system is affected when the BIPV-T systems goes from operation mode to stagnation mode.

Regarding thermal energy production, for $T_{w,in} = T_{mains}$ and $T_{w,in} = 10$ °C, the BIPV-T system produces more useful thermal energy only for the criteria 0, 5-8 and 13-16, i.e., in the cases where the system is operational when the ambient temperature is above 10 °C. For $T_{w,in} = 20$ °C,

the PV+T system produces more useful thermal energy than the BIPV-T system for all criteria except 8 and 16. This shows that the benefit in terms of thermal energy production of the BIPV-T system compared to the PV+T system is strongly affected when the thermal energy recovered is transferred to a higher temperature medium.

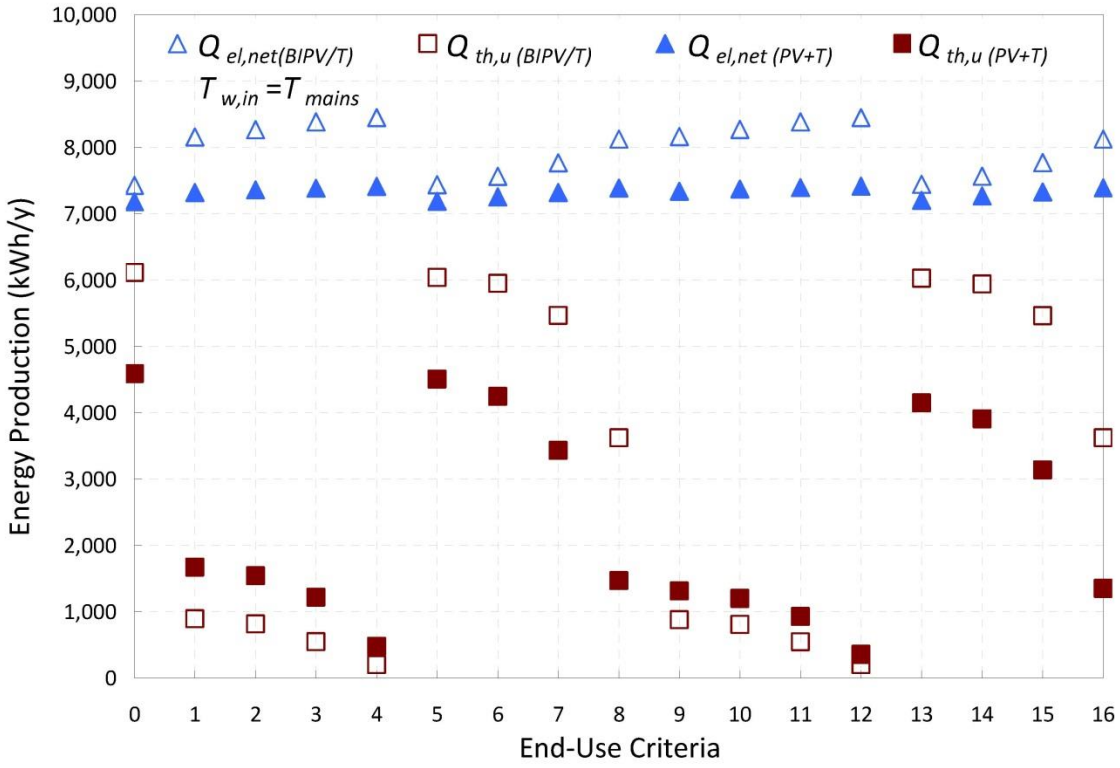

Figure 5-5: Comparison of the energy produced by the BIPV-T and the PV+T systems for a 40 m^2 roof in Montreal and $T_{w,in}$=T_{mains}

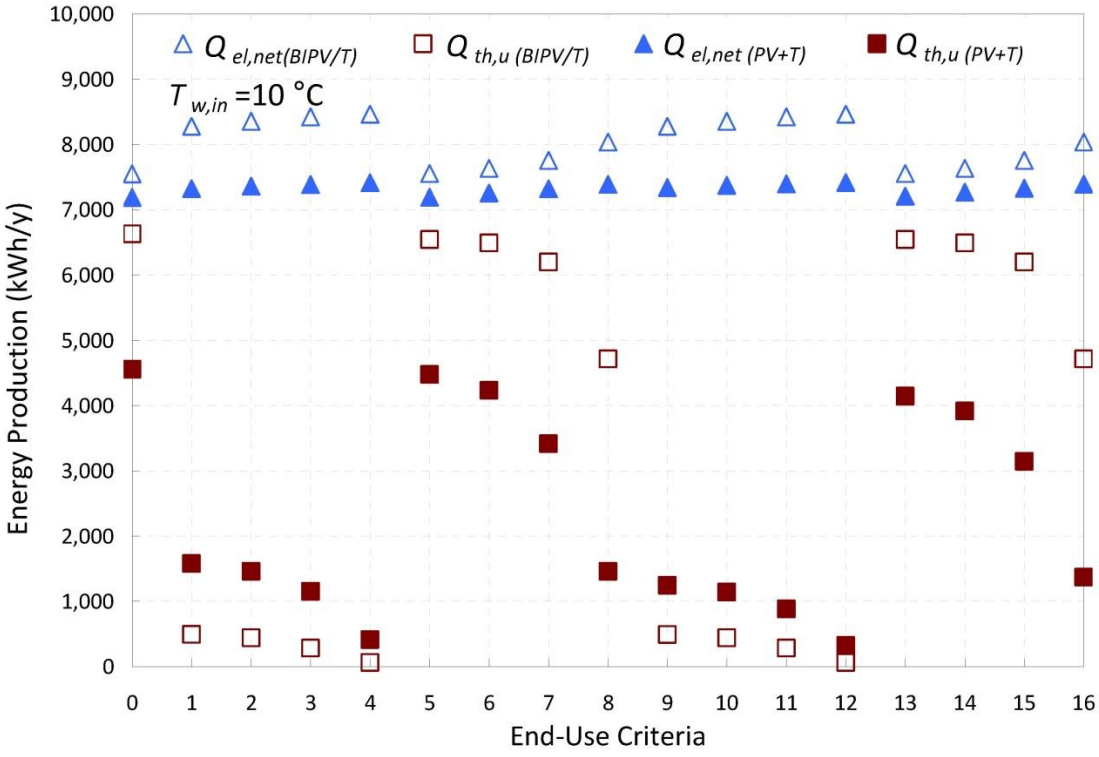

Figure 5-6: Comparison of the energy produced by the BIPV-T and the PV+T systems for a 40 m^2 roof in Montreal and $T_{w,in}$=10 °C

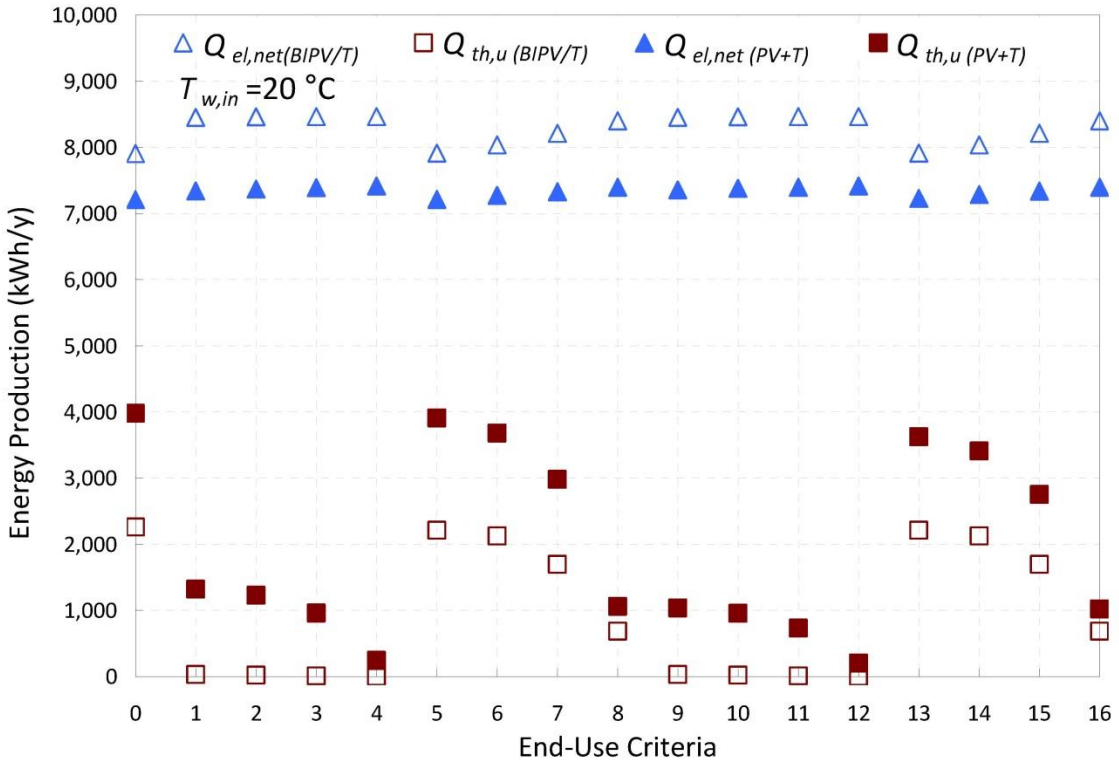

Figure 5-7: Comparison of the energy produced by the BIPV-T and the PV+T systems for a 40 m^2 roof in Montreal and $T_{w,in}$=20 °C

5.6.2 Equivalent Thermal Energy Production

Figure 5-8 to Figure 5-10 present the ratio of equivalent thermal energy production between the BIPV-T and PV+T systems for three different conversion factors C_{el-th}. As it can be observed, the criterion, conversion factor and water temperature at the heat exchanger inlet all have an impact on the benefit of the BIPV-T system compared to the PV+T system from an equivalent thermal energy production point of view.

Using $C_{el-th} = 1$, the BIPV-T thermal equivalent energy production exceeds that of the PV+T system by 0.6 to 34.4% for $T_{w,in} = T_{mains}$, -1.5% to 45.6% for $T_{w,in} = 10$ °C and -9.1% to 11.1% for $T_{w,in} = 20$ °C. Using $C_{el-th} = 2$, the BIPV-T thermal equivalent energy production exceeds that of the PV+T system by 5.5 to 23.2% for $T_{w,in} = T_{mains}$, 5.0% to 28.7% for $T_{w,in} =$

10 °C and -1.8% to 13.1% for $T_{w,in} = 20$ °C. Using $C_{el-th} = 3$, the BIPV-T thermal equivalent energy production exceeds that of the PV+T system by 7.3 to 19.0% for $T_{w,in} = T_{mains}$, 7.5% to 22.5% for $T_{w,in} = 10$ °C and 1.5% to 13.1% for $T_{w,in} = 20$ °C.

For $T_{w,in} = T_{mains}$ and $T_{w,in} = 10$ °C, the BIPV-T system generally produces more useful equivalent thermal energy regardless of the end-use criteria and conversion factor. For $T_{w,in} = 20$ °C, however, it is often not the case.

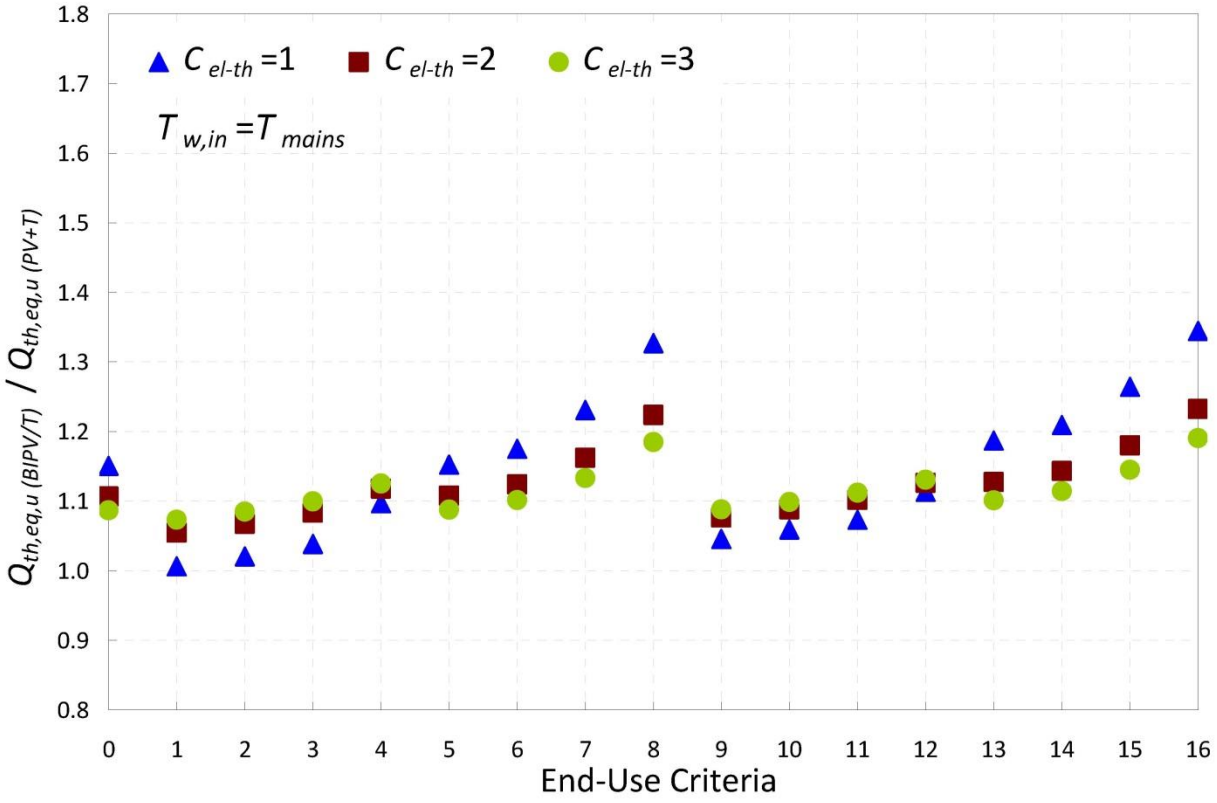

Figure 5-8: Ratio of equivalent useful thermal energy between the BIPV-T and PV+T systems for a 40 m^2 roof in Montreal and $T_{w,in}$=T_{mains}

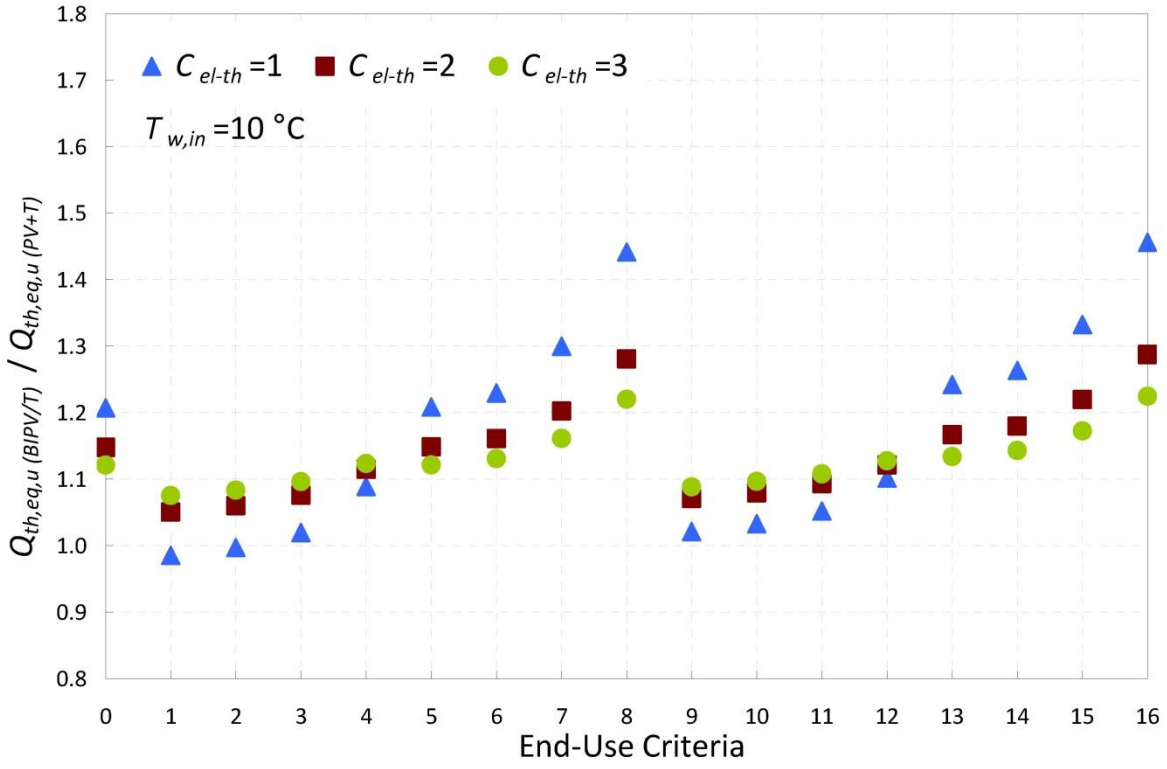

Figure 5-9: Ratio of equivalent useful thermal energy between the BIPV-T and PV+T systems for a 40 m^2 roof in Montreal and $T_{w,in}$=10 °C

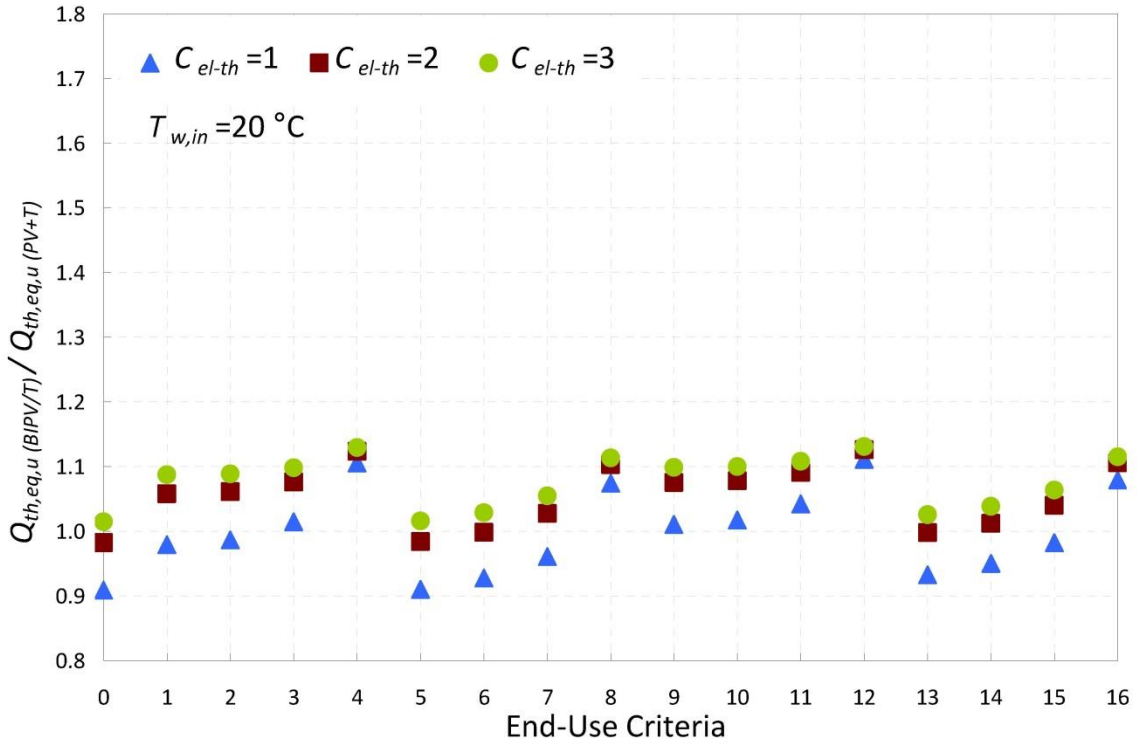

Figure 5-10: Ratio of equivalent useful thermal energy between the BIPV-T and PV+T systems for a 40 m^2 roof in Montreal and $T_{w,in}$=20 °C

The BIPV-T system always produces at least the same amount of useful equivalent thermal energy as the PV+T system using $C_{el-th} = 3$. Because the useful thermal energy production varies much more from one criterion to another, the variation of the equivalent thermal energy ratio is mainly driven by the useful thermal energy production. Thus, when the BIPV-T system produces more useful thermal energy than the PV+T system, the benefit of the BIPV-T in terms of equivalent thermal energy production is greater with $C_{el-th} = 1$ than with $C_{el-th} = 3$ because the value of the thermal energy is not reduced compared to the electrical thermal energy. Conversely, when the BIPV-T system produces less useful thermal energy than the PV+T system, the benefit of the BIPV-T is greater with $C_{el-th} = 3$ than with $C_{el-th} = 1$.

5.6.3 BIPV-T Break-Even Cost

Figure 5-11 to Figure 5-13 present the cost required to recover the heat from the BIPV system (the cost to convert the BIPV to a BIPV-T system) to break-even with the cost of the side-by-side

system (System 1). Break-even occurs when both the BIPV-T system and the PV+T system have the same cost in dollars (CAD) per unit of equivalent annual thermal energy production (kWh/y). As it can be observed, the trends are similar to that obtained in Figure 5-8 to Figure 5-10 and the break-even cost is extremely dependent on the end-use criteria, conversion factor and water temperature at the heat exchanger inlet. According to these graphs, the break-even cost of the thermal part of the BIPV-T system can vary between -2,700 CAD and 19,400 CAD. As mentioned before, the cost of recovering the heat in a BIPV-T system varies a lot with the type and size of system and its application. This cost is significantly affected by the type and length of ducting required to bring the thermal energy produced to its end-use point. For example, when there is a long distance between the roof and the location where the thermal energy is being used or converted, prices of BIPV-T systems tend to be higher. Also, implementing BIPV-T systems in existing homes can be more costly than in newly-built homes since design modifications might be required to make space for the ductwork. In fact, estimates using the RSMeans handbook and past experience with BIPV-T systems show that this cost could be anywhere from a few thousand dollars to as much as 20,000 dollars. For this case study, this means that in order for the BIPV-T system to have the same cost in $/(kWh/y) as the PV+T system, the acceptable cost of recovering the heat in the BIPV-T (i.e., the cost of blower, ducts, dampers, etc.) varies from (-2,700 CAD) to (19,400 CAD) depending on the selected criteria for thermal energy output usefulness. The low-end of the range is impossible to achieve, while the high-end of the range should be fairly easy to achieve.

Additional conclusions can be drawn from Figure 5-11 to Figure 5-13 . One of these conclusions is that there is little benefit in using a BIPV-T system with $T_{w,in} = 20$ °C. The reason is that under this condition, the BIPV-T only increases the equivalent useful thermal energy by about 10% or less and the cost of removing the heat must remain under 6,000 CAD in order to break-even with the cost of System 2. Another conclusion is that the benefit of a BIPV-T system compared to side-by-side PV modules and solar thermal collectors is much more important if it can operate at ambient temperatures above 10 °C, i.e., during the summer. For criteria where $T_{a,max} = 30$ °C (criteria 5 to 8 and 12 to 16), the BIPV-T produces in general over 10% more equivalent thermal useful energy than the PV+T system for $T_{w,in} = 10$ °C and $T_{w,in} = T_{mains}$. This is translated into a break-even cost for the heat recovery portion of the system that is greater than 5,000 CAD. The effect of the minimum ambient temperature required to operate the systems

is very little, however, even though it is usually slightly more beneficial to avoid operating the BIPV-T at ambient temperatures lower than -10 °C. Finally, considering that $Q_{th,eq,u(BIPV-T)}/Q_{th,eq,u(PV+T)}$ and $C_{T,BE(BIPV-T)}$both increase with $T_{rise,w,min}$ it can be concluded that the benefit of using a BIPV-T system compared to a PV+T system is better with a higher minimum temperature rise on the water side of the heat exchanger. This means that the negative impact on the annual energy production of increasing $T_{rise,w,min}$ is greater on the PV+T system than on the BIPV-T system.

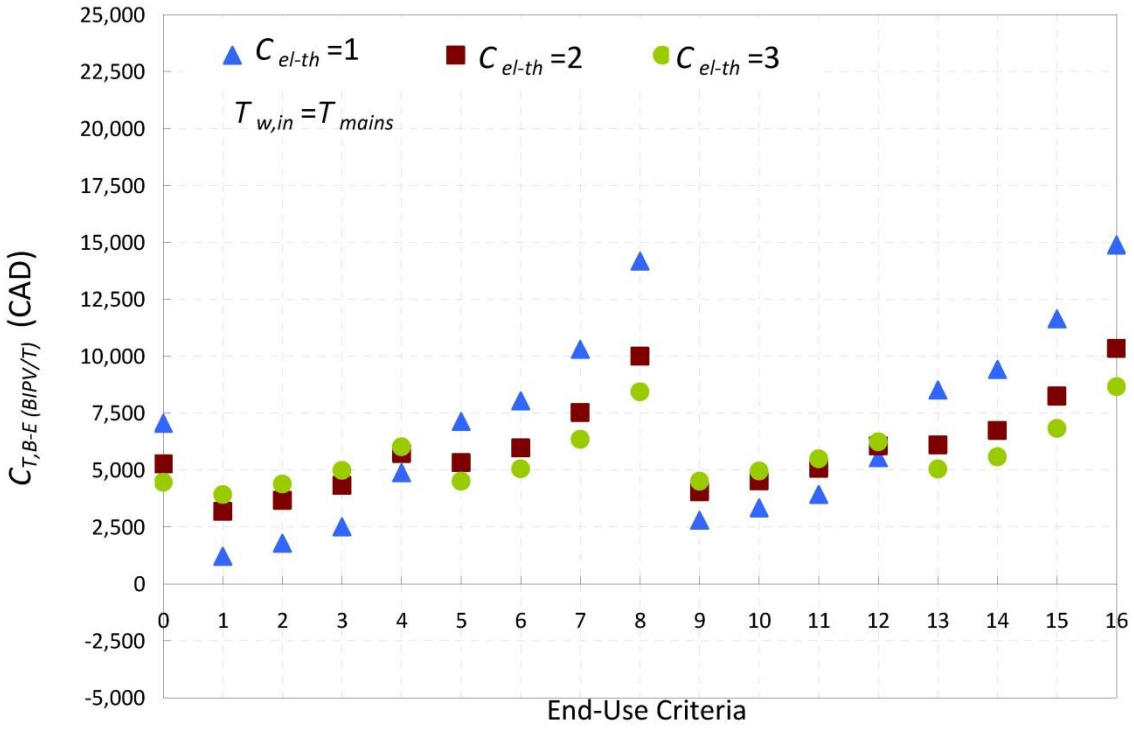

Figure 5-11: Cost required to recover the heat from the BIPV-T system to break-even with the cost of the PV+T system for a 40 m^2 roof in Montreal and $T_{w,in}$=T_{mains}

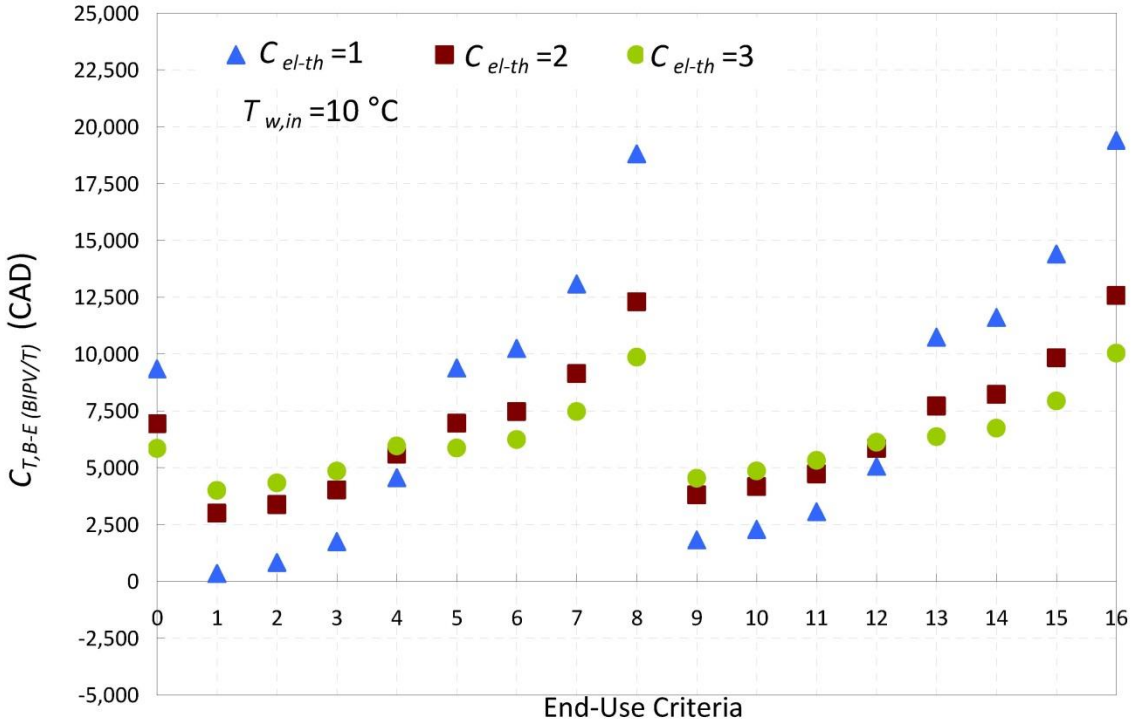

Figure 5-12: Cost required to recover the heat from the BIPV-T system to break-even with the cost of the PV+T system for a 40 m^2 roof in Montreal and $T_{w,in}$=10 °C

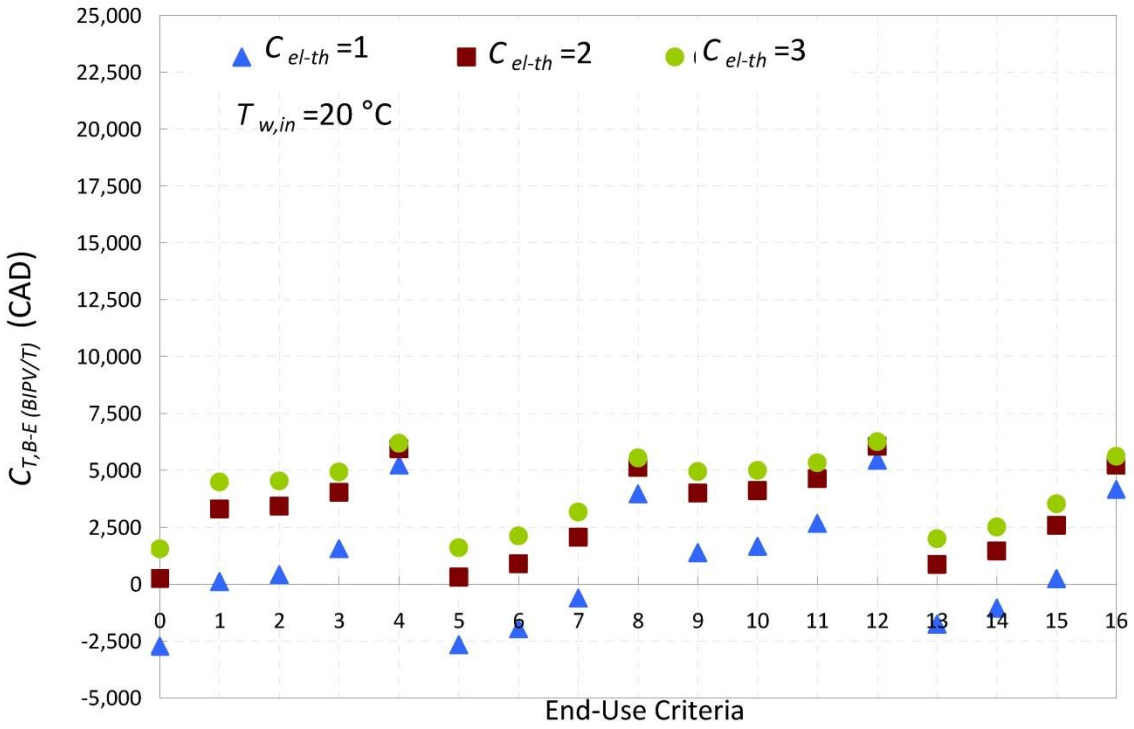

Figure 5-13: Cost required to recover the heat from the BIPV-T system to break-even with the cost of the PV+T system for a 40 m^2 roof in Montreal and $T_{w,in}$=20 °C

Figure 5-14 and Figure 5-15 provide a different representation of the ratio of equivalent useful thermal energy produced by the two systems and the cost required to recover the heat from the BIPV-T system to break-even with the cost of the PV+T system for $T_{w,in} = T_{mains}$ and $T_{w,in} =$ 10 °C, respectively. In these graphs, the points obtained with the various end-use criteria are grouped into four seasonal operating conditions based on $T_{a,min}$and $T_{a,max}$. Thus, criteria 1 to 4 ($T_{a,min} = -20$ °C and $T_{a,max} = 10$ °C) correspond to systems operating during winter, spring and fall, criteria 5 to 8 ($T_{a,min} = -20$ °C and $T_{a,max} = 30$ °C) correspond to systems operating all year long, criteria 9 to 12 ($T_{a,min} = -10$ °C and $T_{a,max} = 10$ °C) correspond to systems operating during spring and fall and finally, criteria 13 to 16 ($T_{a,min} = -10$ °C and $T_{a,max} =$ 30 °C) correspond to systems operating during spring, summer and fall. From these graphs, it can clearly be observed that both $Q_{th,eq,u(BIPV-T)}/Q_{th,eq,u(PV+T)}$and $C_{T,BE(BIPV-T)}$ are much greater when the BIPV-T system can operate in the summer.

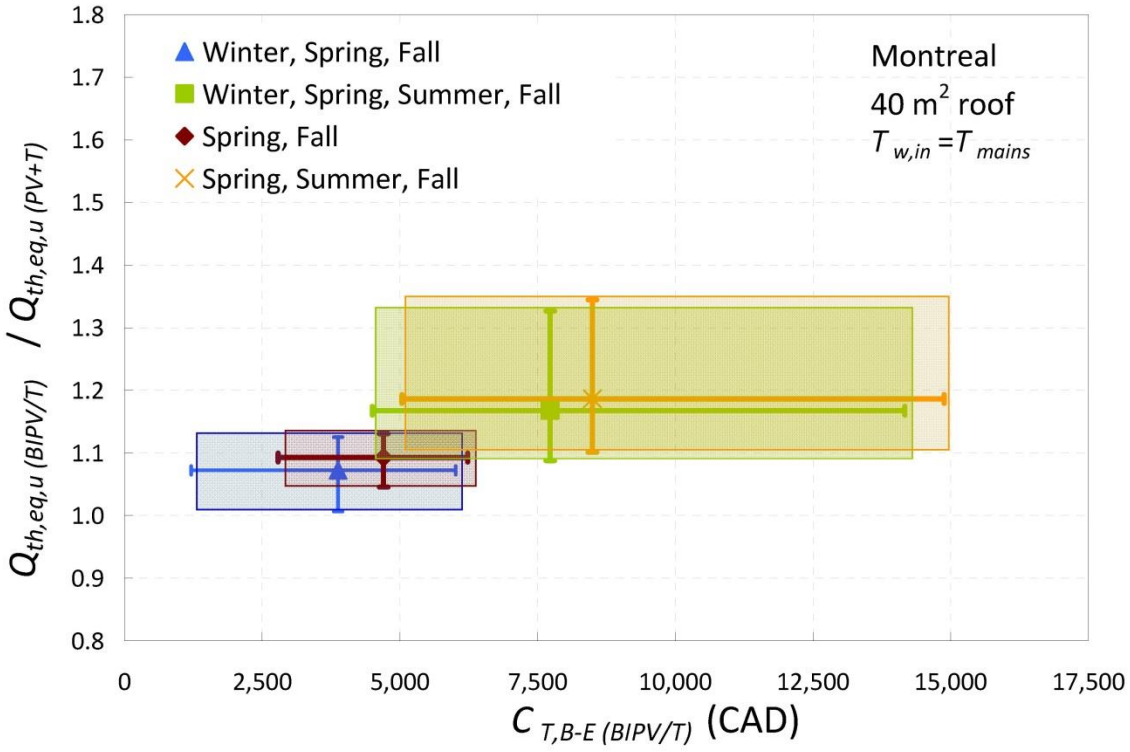

Figure 5-14: Ratio of equivalent useful thermal energy between the BIPV-T and PV+T systems as a function of the cost required to recover the heat from the BIPV-T system to break-even with the cost of the PV+T system for a 40 m^2 roof in Montreal and $T_{w,in}$=T_{mains}

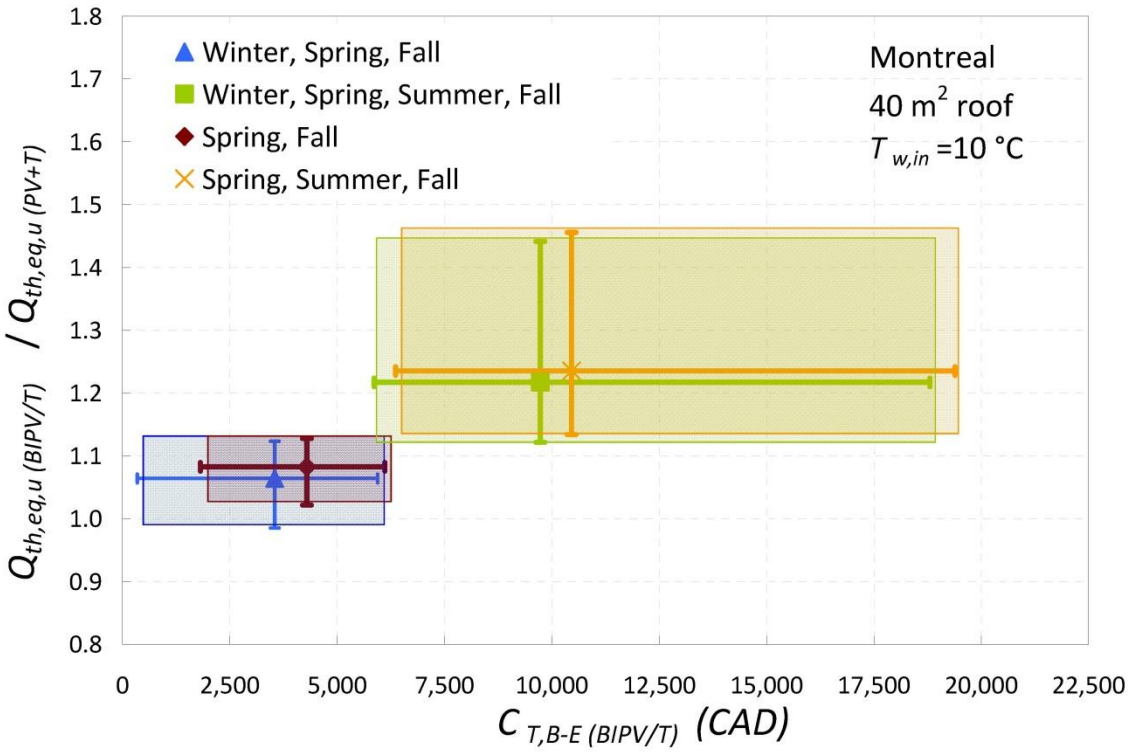

Figure 5-15: Ratio of equivalent useful thermal energy between the BIPV-T and PV+T systems as a function of the cost required to recover the heat from the BIPV-T system to break-even with the cost of the PV+T system for a 40 m^2 roof in Montreal and $T_{w,in}$=10 °C

These results were obtained considering that an ideal roof with no irregular design features was available. In reality, it might be more difficult to install a BIPV-T system on a roof with an unusual shape and design than side-by-side PV modules and solar thermal collectors. On that note, the potential for BIPV-T systems might be greater for new homes as opposed to existing homes where the architect can design the roof to facilitate the implementation of specific solar systems. Also, even if the results presented take the usefulness of the thermal energy produced into account, this study did not consider the possibility of installing the PV modules and the solar thermal collectors in the side-by-side system with different orientations (azimuth and slope). If the solar thermal energy produced is only useful for the house in the winter, one might prefer to install the solar thermal collectors at a greater slope than the PV modules to increase the thermal energy production during the colder months of the year. This aspect would probably have a small effect on the actual conclusions, however, because the competitiveness of the BIPV-T system

compared to the side-by-side system was found to be much more difficult to achieve if operated only during colder months.

5.7 Conclusions

This study presented an energy and economic comparison between a building-integrated combined photovoltaic-thermal (BIPV-T) air system and a traditional solar system consisting of side-by-side PV modules and liquid solar thermal collectors (PV+T) for residential applications. In order to perform this comparison, an analytical model of a BIPV-T system was developed and validated against experimental data. Then, the following systems were modeled in TRNSYS: a BIPV-T air system and side-by-side PV modules and liquid solar thermal collectors (PV+T). An innovative methodology was developed to deal with the challenge of comparing different types of energy. In this novel approach, the two systems are operated according to criteria for thermal energy usefulness and the thermal energy collected is transferred into water using a heat exchanger. The concept of equivalent useful thermal energy production is used to combine the electrical and thermal energy produced.

To demonstrate the usefulness of this approach, a case study for a residence was performed. The results are reported for a 40 m^2 south-facing roof located in Montreal, Canada. For a water temperature at the heat exchanger inlet corresponding to 10 °C, the BIPV-T thermal equivalent energy production was found to exceed that of the PV+T system in the range of -2% to 46%, 5% to 29% and 8% to 23% for electrical to thermal energy conversion factors of 1, 2 and 3, respectively. For a water temperature at the heat exchanger inlet corresponding to 10 °C, a thermal energy conversion factor of 2 and a system operating all year long, the acceptable cost to recover the heat from the BIPV system in order to break even with the cost of the PV+T system was estimated at approximately 7,000 CAD. It was found that there is little benefit in using a BIPV-T system when the thermal energy recovered is transferred to a higher temperature medium. For a water temperature at the heat exchanger inlet corresponding to 20 °C, the BIPV-T system only increased the equivalent thermal energy compared to a PV+T system by a maximum of 10%. In addition, the cost of recovering the heat from the BIPV system so that the cost of the BIPV-T breaks-even with that of the PV+T system was found to be around 6,000 CAD. Another main conclusion is that the benefit of a BIPV-T system compared to a PV+T system is more important if the BIPV-T system can provide useful thermal energy to the residence during the

summer. In fact, the BIPV-T system produced generally at least 10% more equivalent thermal useful energy than the traditional side-by-side PV+T system for the thermal energy usefulness criteria allowing the systems to operate in the summer for a required break-even cost greater than 5,000 CAD.

The results obtained with this case study are specific to the roof size and location chosen as well as the selected BIPV-T design. Nevertheless, this study shows that the benefit of a residential BIPV-T system compared to a standard system consisting of side-by-side PV modules and solar thermal collectors strongly depends on the usefulness of the thermal energy produced and on the relative value between the electrical and thermal energy. In other words, the thermal energy and electrical energy end-usage as well as the type of equipment they are replacing are essential to determine whether or not it is worth implementing a BIPV-T system from both energy and economic points of view. To increase this benefit, two approaches can be taken: reducing the actual cost of recovering the heat from a BIPV system or improving the system design to increase the amount of energy produced.

5.8 Acknowledgements

Funding for this work was provided by Natural Resources Canada through the ecoENERGY Innovation Initiative.

5.9 References

American Society of Heating, Ventilating and Air-Conditioning (ASHRAE). (1997). *ASHRAE Handbook Fundamentals.* Atlanta, GA, USA: ASHRAE.

Athienitis, A. K. (2007). Design of a Solar Home with BIPV-Thermal System and Heat Pump. *Proceedings of 2nd Canadian Solar Buildings Conference, Calgary*, June 10-14, 2007. http://citeseerx.ist.psu.edu/viewdoc/download?doi=10.1.1.667.5530&rep=rep1&type=pdf

Bakker, M., Zondag, H., Elswijk, M. S., & Jong., M. (2005). Performance and Costs of a Roof-Sized PV/Thermal Array Combined with a Ground Coupled Heat Pump. *Solar Energy, 78*, 331-339.

Candanedo, L., Athienitis, A., & Park, K. (2011). Convective heat transfer coefficients in a building-integrated photovoltaic/thermal system. *ASME Journal of Solar Energy Engineering, 133*(2).

Chow, T., Pei, G., Fong, K., Lin, Z., Chan, A., & Ji, J. (2009). Energy and Exergy Analysis of Photovoltaic/Thermal Collector with and without Glass Cover. *Applied Energy, 86*(3), 310-316.

ClearSky Advisors Inc. (2011). *Survey of Active Solar Thermal Collectors, Industry and Markets in Canada.* Ottawa, Canada: Natural Resources Canada. Retrieved from http://solarthermalworld.org/sites/gstec/files/survey_of_active_solar_thermal_collectors_2012_-_august.pdf

Cole, R., & Sturrock, N. (1977). The convective heat exchange at the external surface of buildings. *Building and Environment, 12*, 207-214.

Coventry, J., & Lovegrove, K. (2003). Development of an Approach to Compare the Value of Electrical and Thermal Output from a Domestic PV/Thermal System. *Solar Energy, 75*, 63-72.

da Silva, R., & Fernandes, J. (2010). Hybrid Photovoltaic/Thermal (PV/T) Solar Systems Simulation with Simulink/Matlab. *Solar Energy, 84*, 1985-1996.

Delisle, V., & Kummert, M. (2012). Experimental Study to Characterize the Performance of Combined Photovoltaic/Thermal Air Collectors. *Journal of Solar Energy Engineering, 134*.

Dittus, F., & Boelter, L. (1985). Heat transfer in automobile radiators of the tubular type. *International Community Heat Mass Transfer, 12*(1), 3-22.

Eicker, U. (2003). *Solar Technologies for buildings.* Chichester: John Wiley & Sons.

Erdil, E., Ilkan, M., & Egelioglu, F. (2008). An experimental study on energy generation with a photovoltaic (PV) - solar thermal hybrid system. *Energy, 33*, 1241-1245.

Garg, H., & Adhikari, R. (1997). Conventional hybrid photovoltaic/thermal (PV/T) air heating collectors: steady-state simulation. *Renewable Energy, 11*(3), 363-385.

Garg, H., & Adhikari, R. (2000). Studies on Cost Effectiveness of Hybrid Photovoltaic/Thermal (PV/T) Air Heating Collector. *World Renewable Energy Congress-VI, Brighton, United Kingdom, July 1-7 2000*, pp. 1098-1101.

Hegazy, A. (2000). Comparative study of the performance of four photovotlaic/thermal solar air collectors. *Energy Conversion and Management, 41*, 861-881.

Hollands, K.G.T., Unny, T.E., Raithby, G.D., & Konicek, L. (1976). Free Convection Heat Transfer Across Inclined Air Layers. *Heat Transfer, 98*, 189-193.

Huang, B., Lin, T., Hung, W., & Sun, F. (2001). Performance Evaluation of Solar Photovoltaic/Thermal Systems. *Solar Energy, 70*(5), 443-448.

Incropera, F., & DeWitt, D. (1996). *Fundamentals of Heat and Mass Transfer.* New York: John Wiley & Sons.

International Electrotechnical Commission (IEC). (2011). *Photovoltaic (PV) Module Performance Testing and Energy Rating – Part 1: Irradiance and Temperature Performance Measurements and Power rating* (IEC 61853-1).

Jiang, B., Ji, J., & Yi, H. (2008). The influence of PV coverage Ratio on Thermal and Electrical Performance of Photovoltaic-Trombe Wall. *Renewable Energy, 33*, 2491-2498.

Klein et al. (2009). *A TRaNsient SYstem Simulation Program - User Manual Version 17.* Madison, WI, USA: University of Wisconsin.

Kumar, S., & Mullick, S. (2010). Wind Heat Transfer Coefficient in Solar Collectors in Outdoor Conditions. *Solar Energy, 84*, 956-963.

McAdams, W. (1954). *Heat Transmission.* New York: McGraw-Hill.

Notton, G., Cristofari, C., Mattei, M., & Poggi, P. (2005). Modelling of a double-glass photovoltaic module using finite differences. *Applied Thermal Engineering, 25*, 2854-2877.

Natural Resources Canada (NRCan). (2012). *National Survey Report of PV Power Applications in Canada 2011.* Retrieved from iea-pvps.org/index.php?id=93&eID=dam_frontend_push&docID=1260

Onovwiona, H., & Ugursal, V. (2006). Residential Cogeneration Systems: Review of the Current Technology. *Renewable and Sustainable Energy Reviews, 10*, 389-431.

Othman, M., Yatim, B., Sopian, K., & Abu Bakar, M. (2007). Performance Studies on a Finned Double-Pass Photovoltaic-Thermal (PV/T) Solar Collector. *Desalination, 209*, 43-49.

Pavylos, J. (2008). A survey of wind convection coefficient correlations for building envelope energy systems' modeling. *Applied Thermal Engineering, 28*, 801-808.

PikeResearch. (2012). *Building Integrated Photovoltaics – BIPV and BAPV: Market Drivers and Challenges, Technology Issues, Competitive Landscape, and Global Market ForecastsNavigant biPV report.* Boulder: Navigant Consulting.

RS Means. (2013a). *RS Means Building Construction Cost Data.* Rockland, MA, USA: Reed Construction Data, Inc. .

RS Means. (2013b). *RS Means Green Building Cost Data.* Rockland, MA, USA: Reed Construction Data, Inc.

Santbergen, R., & van Zolingen, R. (2008). The aborption factor of crystalline silicon PV cells: a numerical and experimental study. *Solar Energy Materials and Solar Cells, 92*(4), 432-444.

Sharples, S., & Charlesworth, P. (1998). Full-Scale Measurements of Wind-Induced Convective Heat Transfer from a Roof-Mounted Flat Plate Solar Collector. *Solar Energy, 62*(2), 69-77.

Sopian, K., Liu, H., Kakac, S., & Veziroglu, T. (2000). Performance of a Double Pass Photovoltaic Thermal Solar Collector Suitable for Solar Drying Systems. *Energy Conversion & Management, 41*, 353-365.

Sparrow, E., Ramsey, J., & Mass, E. (1979). Effect of Finite Width on the Heat Transfer and Fluid Flow about an Inclined Rectangular Plate. *ASME Journal of Heat Transfer, 101*, 199-204.

Test, F., Lessman, R., & Johary, A. (1981). Heat Transfer during Wind Flow over Rectangular Bodies in the Natural Environment. *ASME Journal of Heat Transfer, 103*, 262-267.

CHAPTER 6 ARTICLE 3: COST-BENEFIT ANALYSIS OF INTEGRATING BIPV-T AIR SYSTEMS INTO ENERGY-EFFICIENT HOMES

Delisle, V., Kummert, M., (2016). *Solar Energy, 136,* 385-400.

Note: The article in its original version did not contain Appendix C. Section 6.11.3 was added to this chapter to provide additional information on the energy-efficient housing archetypes.

6.1 Abstract

The market share of building-integrated photovoltaics (BIPV) remains limited. One of the main barriers to its larger adoption is its initial capital cost, as BIPV is generally more expensive than traditional roof or façade mounted photovoltaic modules (PV). Converting BIPV systems into BIPV with thermal energy recovery (BIPV-T) can improve its benefit and competitiveness compared to other solar energy technologies. This benefit is difficult to estimate, however, as it strongly depends on the usefulness of the thermal energy produced and the incremental cost of the technology to recover the heat. This study aims at evaluating the cost-benefit of BIPV-T focusing on systems that use air as the heat recovery fluid and are integrated into all-electric energy-efficient homes located in heating dominated climates. This cost-benefit is evaluated using the concept of break-even cost defined as the maximum incremental cost to convert a BIPV system into a BIPV-T system to break-even with the cost of (a) a BIPV system and (b) side-by-side PV modules and solar thermal collectors (PV+T). To obtain this cost, the useful equivalent energy production of BIPV, BIPV-T and PV+T systems was first obtained for six energy-efficient housing archetypes located in various cities across Canada. Four different heat management scenarios were considered for the BIPV-T system: (1) fresh air preheating, (2) domestic hot water preheating through an air-to-water heat exchanger, (3) domestic hot water and space heating with an air-to-water heat pump and (4) domestic hot water heating (DHW) with a heat pump water heater. Compared to BIPV, BIPV-T systems always produce more useful energy and as a result, the break-even cost compared to a BIPV system was found to be always positive and up to 2,700 CAD for a medium 2-storey home located in Montreal. For that same house and considering the price of BIPV equal to that of standard roof-mounted PV modules, the break-even cost of a BIPV-T system compared to a PV+T system was estimated at 4,200 CAD. If

the price of BIPV were to get 10% lower than PV, however, this break-even cost could increase to 6,400 CAD.

6.2 Keywords

Building-integrated photovoltaics; Cost-benefit; Hybrid Collector; Integration

6.3 Introduction

Building-integrated photovoltaics (BIPV) is the "integration of solar photovoltaic power as a multifunctional building component" (Prasad & Snow, 2005). In addition to producing electricity, it protects the building from exterior elements by acting as a standard building envelope material. Compared to traditional roof or façade mounted photovoltaics (PV), BIPV shows great potential for both its dual functionalities and greater aesthetics. Nevertheless, its adoption remains limited since its market share in all PV installations is in the order of 1% to 3% worldwide (IEA PVPS, 2015). The first cost is one of the main barriers to its larger adoption since it is generally more expensive than standard PV modules. This situation could change with economy of scale, however, as the price of BIPV could be less than PV with a potentially lower installation cost and its offset of traditional building envelope material (James et al., 2011).

Two different pathways can be taken to improve the competitiveness or cost-benefit ratio of building-integrated photovoltaics compared to other solar technologies such as roof or façade mounted PV modules or solar thermal collectors: reducing its cost or increasing its benefit. BIPV with thermal energy recovery (BIPV-T) produces more energy than BIPV by converting the absorbed solar energy into both thermal and electrical energy simultaneously using the same roof or façade area. Thus, BIPV-T can increase the cost-benefit of BIPV as long as converting the thermal energy into useful energy remains affordable.

- This study looks at this particular aspect of BIPV-T focusing on systems that use air as the heat recovery fluid and are integrated into all-electric energy-efficient homes located in heating dominated climates. It aims at quantifying the amount of useful energy that can be produced by different residential systems and at estimating their targeted or break-even cost to remain competitive with other stand-alone solar energy technologies. In this study,

BIPV-T collectors are simulated with different heat management strategies to quantify the amount of energy that can be considered useful. The objectives are:

- To develop energy-efficient housing archetypes of different sizes and locations with solar energy technology integration potential.
- To quantify the energy savings of integrating BIPV-T systems into these homes.
- To compare these energy savings with other residential solar energy technologies such as BIPV and side-by-side PV modules and solar thermal collectors.
- To determine the break-even cost of a BIPV-T system to remain competitive with other solar energy technologies.

6.4 Literature Review

Integrating BIPV-T air collectors into buildings is a challenge. One of the reasons is that solar energy availability does not always coincide with energy demand. This is not really an issue for electricity, at least from the building's point of view, as the excess production can be sent back to the grid (for grid-connected buildings) or temporarily stored on-site (for off-grid or autonomous buildings). On the thermal side, however, hot air might be useful in heating dominated climates during winter and shoulder seasons for space heating purposes, but is not as desirable during summer months. Another reason why its integration is difficult is that the fluid outlet temperature obtained is not as high as in standard solar thermal collectors. Thus, BIPV-T products are more difficult to pair with storage solutions or to transfer the energy produced into another medium.

The following sections describe several strategies that have been investigated for utilizing the heat produced by BIPV-T or PV-T collectors focusing on air-based systems. BIPV-T collectors are defined as products that are integrated into the building and thus, that replace traditional façade cladding or roofing materials. PV-T collectors are mounted on top of the existing roof or building façade. Therefore, they are not integrated, but added to the building.

6.4.1 Fresh Air Preheating

Ventilation air preheating is by far the simplest application for BIPV-T air collectors. This is also a common application of solar air heaters especially in commercial or industrial buildings where fresh air requirements are important.

This type of coupling was used for the 288 m^2 unglazed transpired BIPV-T air collector of the John Molson Building School of Business in Montreal, Canada (Athienitis et al., 2011). This system is operated at a flowrate up to 7.5 m^3/s (~100 $kg/(h \cdot m^2)$) and produces 20 MWh/y of electricity and 55 MWh/y of useful thermal energy (Bambara, 2012). In the Mataro library near Barcelona, Spain, outdoor air is preheated by a BIPV-T façade and used for direct space heating. Compared to a brick façade, this system reduces the heating load by nearly 12% (Mei et al., 2003).

6.4.2 Air-Source Heat Pump Coupling

Another integration strategy for BIPV-T air collectors consists of using the thermal energy produced to increase the temperature of the fluid on the evaporator side of a heat pump to improve its coefficient of performance (COP).

Kamel and Fung (2014) completed simulations to evaluate the performance of a 46 m^2 BIPV-T air collector combined with an air source heat pump (ASHP) in different Canadian locations for a semi-detached prototype home. The solar assisted ASHP system was operated at 0.4 kg/s (~30 $kg/(h \cdot m^2)$). Compared to a stand-alone ASHP, this system reduced the energy consumption (compressor and outdoor fan) by 1,111 kWh/y (or 10.8%) for Edmonton and 1,188 kWh/y (or 18%) for Toronto.

Filliard et al. (2009) simulated the effect of coupling a 4 kW ASHP with a 30 m^2 PV-T air collector in a 135 m^2 single family house in Trappes, France. They investigated flowrates varying from 0 to 2,000 m^3/h (~75 $kg/(h \cdot m^2)$) and obtained that with the highest flowrate, the collector increased the heat pump COP from 3.06 to 3.67. It reduced the building heating energy consumption by only 2%, however, because of the additional fan required to recover the heat from the PV modules.

6.4.3 Water-Source Heat Pump Coupling

Coupling BIPV-T air collectors with water-source heat pumps (WSHP) has also been investigated. In this case, an air-to-water heat exchanger (HX) is required upstream of the heat pump to transfer the thermal energy recovered into water.

This integration strategy was examined by Ben Nejma et al. (2013) who simulated and validated experimentally a 70 m^2 PV-T air collector operated at 1,500 m^3/h (~25 kg/(h·m^2)) in a net-zero energy house (NZEH) in Chambéry, France. In this case, the water-to-water heat pump was coupled with a 1000 L storage tank supplying fan coils for space heating purposes. This system was found to reduce the space heating electrical consumption by approximately 150 kWh/y (or 10%) compared to the same system without a PV-T collector.

In Candanedo and Athienitis (2009), the effect of predictive controls on a 7.35 kW (electric) BIPV-T air collector coupled with a WSHP in a NZEH near Montreal, Canada, is presented. In this case, the 4,000 L storage tank is used to fulfill space heating demand through a radiant floor system. Optimizing the control strategy was found to reduce the WSHP energy consumption by an additional 195 kWh/y (or 23.5%).

6.4.4 Other Systems

Other systems studied include strategies where the thermal energy recovered is used for both space and domestic hot water (DHW) heating. Cartmell et al. (2004) examined the solar system of the Brocks Hill Environment Centre in the UK. This building has a 37 m^2 PV-T air collector coupled with a 12.5 m^2 solar air collector booster. The thermal energy recovered was either used directly to supply an air-handling unit or indirectly, to preheat water entering the main storage tank through an air-to-water heat exchanger. Monitored data showed that this system was able to contribute to 64.4% and 35% of the annual hot water and thermal loads, respectively.

In addition to water, other storage mediums have been investigated. Pantic et al. (2010) considered a BIPV-T air collector for both space and water heating coupled with a rockbed storage unit. During winter, the preheated fresh air was directly fed to the house air handling unit whenever space heating was required. It was stored in a rockbed storage unit for later use otherwise. In the summer, the air was used to heat water through an air-to-water heat exchanger.

For a winter day, the heat load was found to be reduced by nearly 49% after supplying heat from the rockbed storage.

Chen et al. (2010a) considered using a BIPV-T collector for space heating through a ventilated concrete slab (VCS) located in the basement of a house by operating the collector at 250 L/s (~15 kg/(h·m^2)). Results showed that between 9 and 12 kWh of thermal energy could be stored in the ventilated concreted slab during a clear sunny day with an outdoor temperature of 0 °C.

Other applications of building-integrated photovoltaics with heat recovery using air as the heat recover fluid include coupling with desiccant cooling machines for high temperature systems (Mei et al., 2006).

6.4.5 Conclusion

Table 6-1 provides a summary of the thermal performance of the various BIPV-T and PV-T air systems discussed in Sections 6.4.1 to 6.4.4. This review shows that comparing different BIPV-T and PV-T air systems is not straightforward since various indicators can be used to assess their performance. In addition, systems that appear to be similar can perform very differently depending on the location, control system, mechanical equipment, collector size and design as well as operating flowrate. For that reason, this study looks at BIPV-T collectors coupled with different systems for a range of building locations and sizes.

Table 6-1: Review of the performance of BIPV-T and PV-T air systems

Strategy	City (Country)	Thermal Performance	Ref.
Fresh air preheating (commercial)	Montreal (Canada)	55 MWh/y of useful thermal energy production	Bambara, 2012
	Barcelona (Spain)	Heating load reduction of 11.6%	Mei et al., 2003
Assisting ASHP (residential)	Edmonton (Canada)	1,111 kWh/y (10.8%) ASHP energy consumption reduction	Kamel & Fung, 2014
	Toronto (Canada)	1,188 kWh/y (18%) ASHP energy consumption reduction	Kamel & Fung, 2014
	Trappes (France)	2% building heating energy consumption reduction	Filliard et al., 2009
Assisting WSHP for space heating with storage tank and fan coils (residential)	Chambéry (France)	150 kWh (10%) space heating electrical consumption reduction	Ben Nejma et al., 2013
Assisting WSHP for space heating with storage tank and radiant floor (residential)	Montreal (Canada)	WSHP electrical consumption reduction by an additional 195 kWh/y (23.5%) with control strategy optimization	Candanedo & Athienitis, 2009
Supply of air handling unit for space heating and DHW preheating with air-to-water HX (commercial)	Leicester (UK)	Contribution to 64.4% of DHW load and 35% of space heating load	Cartmell et al., 2004
Space heating through a VCS	Montreal (Canada)	Storage potential of 9-12 kWh during a sunny day at 0 °C	Chen et al., 2010a Chen et al., 2010b

6.5 Methodology

In order to evaluate the energy savings and break-even cost of various BIPV-T air systems, several steps were followed. First, six energy-efficient housing archetypes representative of typical houses found in Canada were developed and implemented in six Canadian cities. As renewable energy technologies are generally installed on buildings that are already energy-efficient, the archetypes developed consist of brand new houses that achieve a level of energy-efficiency near 86 according to Canada's EnerGuide Rating System (ERS-86)

(NRCan, 2014a). When a level of 86 is reached for a house, it is generally the point where it starts to make sense financially to integrate renewable energy technologies.

These houses were modeled with the multi-zone building model (Type 56) in TRNSYS version 17 (Klein et al., 2009) and simulated with various scenarios of solar energy technologies added to the south-facing roof. These scenarios include:

- A BIPV-T system coupled with four different heat management strategies (BIPV-T);
- A BIPV system (BIPV), and;
- 5.2 m^2 solar thermal collectors used for DHW heating and the rest of the roof surface area covered with roof-mounted PV modules (PV+T).

For every archetype and location combination, the useful part of the energy produced by the different solar energy technology scenarios was calculated. Ultimately, the BIPV-T systems break-even costs with respect to a BIPV system and side-by-side PV modules and solar thermal collectors (PV+T) were calculated. Section 6.5.1 provides a description of the different archetype homes and locations. In Section 0, details on the different solar energy technology scenarios are given. Finally, Section 6.5.3 and 6.5.4 define the performance and economic indicators used in this analysis.

6.5.1 Energy-Efficient Housing Archetypes

6.5.1.1 Design and Sizes

According to the Canadian Home Builders Association (CHBA) (2012), the average size of new single-detached houses in Canada in 2012 was 177 m^2, varying from 139 m^2 to 204 m^2 across provinces. According to Canada's 2007 Survey of Household Energy Use (NRCan, 2010), 54% of the homes built between 2000 and 2007 were two storeys while 36% were one storey, 77% had a basement for foundation and nearly 88% had an attached garage of which 29% were one-car garages and 59% were two-car garages. In addition, 78% of Canadian homes had an attic. With this information, the 6 housing archetype shown in Figure 6-1 were developed to cover different sizes and types of homes: small bungalow (SB), medium bungalow (MB), large bungalow (LB), small 2-storey (S2S), medium 2-storey (M2S) and large 2-storey (L2S).

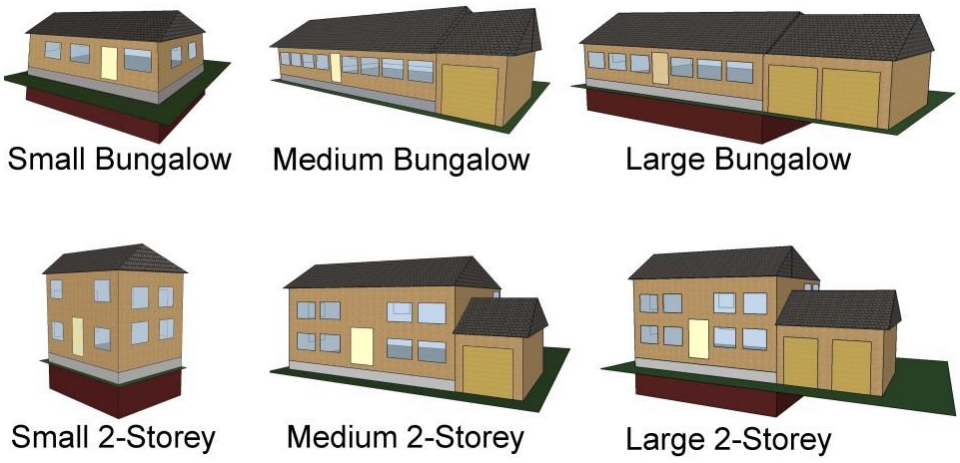

Figure 6-1: Energy-efficient housing archetypes (view of south-facing façade)

All homes have an attic type of roof with a gable pitch and a width-to-depth aspect ratio of 1.3. The latitudes of the locations selected vary between 45° and 60° as shown in Table 6-3. To ensure a good compromise between south-facing roof solar exposure, surface area and ease of roofing installation, the south-facing roof slope is set at 45° and the north-facing roof slope, at 25°. This roof design provides a south-facing roof to ground floor area ratio of 0.45 which is close to 0.4, a common ratio used to evaluate BIPV potential (Pelland & Poissant, 2006; IEA, 2002).

The window area on each façade was determined by targeting a fraction of south-facing window area over total floor area as close as possible to 7% (Charron & Athienitis, 2006) and a fraction of fenestration over wall area between 17% and 22% (NRC, 2010). The north, east and west façades have equal fenestration areas.

The mechanical ventilation requirements depend on the house volume as recommended in the R-2000 standard (NRCan, 2012). The heat recovery ventilator (HRV) fan power is set at 2.32 W/L/s with heat recovery efficiencies of 60% and 55% at 0 °C and -25 °C, respectively (NRC, 2010).

The daily lighting power and domestic hot water (DHW) load are both calculated based on the number of occupants according to the relations of Parekh et al. (2005) and the HOT2000 software (NRCan, 2014b), respectively. All homes have Energy Star appliances. The main appliances energy consumption corresponds to the average of the top 10 appliances available in Natural Resources Canada's list of Energy Star qualified products (NRCan, 2014c). In addition to the

main appliances, 1,450 kWh/y is added for small appliances (Charron, 2007). Table 6-2 provides a summary of the archetype homes' main characteristics.

Table 6-2: Main characteristics of housing archetypes

	Small Bungalow (SB)	Medium Bungalow (MB)	Large Bungalow (LB)	Small 2-Storey (S2S)	Medium 2-Storey (M2S)	Large 2-Storey (L2S)
Nb of occupants	2	4	4	2	4	4
Basement	Yes	No	Yes	Yes	No	Yes
Attached garage	No	1-car	1-car	No	1-car	2-car
Nb of floors (with basement)	2	1	2	3	2	3
Heated floor area (m^2)	139	177	242	139	177	242
South-facing roof area (m^2)	31.3	79.6	54.4	20.8	39.8	36.3
House volume (m^3)	340	443	592	342	443	596
Ventilation rate (L/s)	28.3	36.9	49.3	28.5	36.9	49.7
Lighting energy use (kWh/d)	1.85	2.34	2.34	1.85	2.34	2.34

6.5.1.2 Locations

The locations considered for the houses are summarized in Table 6-3. These were carefully selected to cover a wide range of both heating energy requirements and solar energy availability across Canada.

Table 6-3: Locations of housing archetypes

City	Province	Degree-days (°C)		Mean daily global insolation (MJ/m^2) (NRCan, 2013)	Latitude (°)
		Heating (below 18 °C)	Cooling (above 20 °C)		
Vancouver (VAN)	British-Columbia	3020	44	13.3	49.3
Halifax (HAL)	Nova Scotia	4199	104	14.1	44.6
Montreal (MTL)	Quebec	4614	235	15.6	45.5
Calgary (CAL)	Alberta	5147	41	17	51.0
Regina (REG)	Saskatchewan	5645	146	17.9	50.4
Whitehorse (WHI)	Yukon	6946	8	12.6	60.7

6.5.1.3 Envelope Properties

Table 6-4 provides a summary of the envelope properties at every location. These were selected based on the work of Ferguson & Carver (personal communication, 2014) who studied cost-optimal solution sets for various energy-efficiency target levels in Canadian homes. More information on the houses characteristics can be found in Delisle (2015).

Table 6-4: Envelope properties for selected locations

	VAN	HAL	MTL	CAL	REG	WHI
A-g[8] walls (RSI[9])	6.16	6.51	6.51	9.15	9.15	6.69
B-g[8] walls (RSI)	2.11	3.52	3.52	3.52	3.52	4.93
Ceilings (RSI)	10.56	10.56	10.56	14.1	17.6	19.36
Exposed floor (RSI)	5.46	5.46	5.46	5.46	5.46	6.34
Slab (RSI)	2.11 pc[10]	2.11 pc	2.11 pc	2.11 pc	2.11 pc	1.76 fc[10]
Windows U-Value	1.14	1.14	1.08	1.65	1.65	1.08
ACH[11] @ 50 Pa	0.6	1	0.6	0.6	0.6	0.5

[8] A-g: above-grade; B-g: below-grade

[9] RSI: thermal resistance (not including film coefficients) in SI units, i.e., $m^2 \cdot K/W$

[10] pc: perimeter coverage only for the insulation; fc: full coverage for the insulation

[11] Air change per hour

Additional information on the energy-efficient housing archetypes is available in Appendix C in Section 6.11.3.

6.5.2 Solar Energy Technology Scenarios

6.5.2.1 BIPV-T Air Systems

The BIPV-T air collector has an air gap thickness (channel height) of 3 cm. It has monocrystalline solar cells, an electrical efficiency of 15.2% at reference conditions and a temperature coefficient for efficiency of -0.46 %/°C. It is simulated using the unglazed 2-D steady-state BIPV-T model of Delisle & Kummert (2014). This model is based on the thermal resistance network shown in Figure 6-2. The variables used in this figure are defined in Section 6.9. The collector is divided into n elements in the direction of the flow (length) where each element has a length dy and a width W. Energy balances performed on the different layers (PV glazing, PV cells, PV module back material, air channel top surface, air channel, air channel bottom surface and roof back material) are given in Equations (6-1) to (6-6) for the k^{th} element. The subscript *k* is not included in the equations for simplicity.

$$0 = h_{conv,T}\left(T_{PVg} - T_a\right) + h_{rad,T}\left(T_{PVg} - T_{sur}\right) + \left(T_{PVg} - T_{PV}\right)/R_{PVg-PV} \tag{6-1}$$

$$S + \left(T_{PVg} - T_{PV}\right)/R_{PVg-PV} = \left(T_{PV} - T_1\right)/R_{PVg-1} \tag{6-2}$$

$$\left(T_{PV} - T_1\right)/R_{PVg-1} + S_1 = h_{conv,fT}\left(T_1 - T_f\right) + h_{rad,1-2}\left(T_1 - T_2\right) \tag{6-3}$$

$$q_u = h_{conv,fT}\left(T_1 - T_f\right) - h_{conv,fb}\left(T_f - T_2\right) \tag{6-4}$$

$$h_{conv,fb}\left(T_f - T_2\right) + h_{rad,1-2}\left(T_1 - T_2\right) = \left(T_2 - T_3\right)/R_{2-3} \tag{6-5}$$

$$\left(T_2 - T_3\right)/R_{2-3} - h_{conv,b}\left(T_3 - T_b\right) - h_{rad,b}\left(T_3 - T_{rad,b}\right) = 0 \tag{6-6}$$

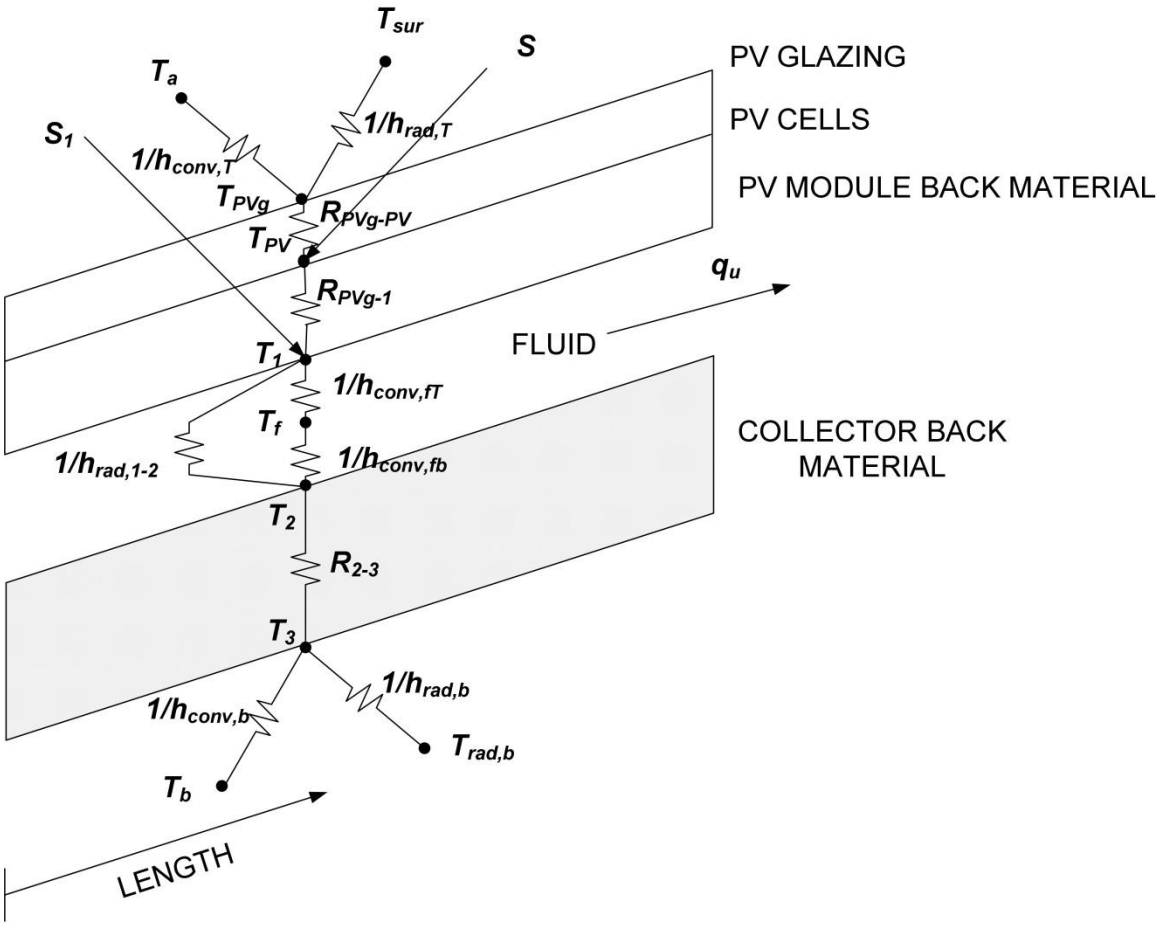

Figure 6-2: Thermal resistance network for the BIPV-T model

The net solar radiation per unit of gross collector area absorbed in the cell (S), and PV module back material layers (S_1) are given as:

$$S = IAM_{PV}(\tau\alpha)_{PV,N}GF_{cell} - \eta_{PV}G \tag{6-7}$$

$$S_1 = IAM_{bs}(\tau\alpha)_{bs,N}G(1 - F_{cell}) \tag{6-8}$$

By neglecting air leakage or infiltration, the thermal energy collected in the k^{th} element is given by:

$$q_u W dy = \dot{m}c_p\left(T_{f,o} - T_{f,i}\right) \tag{6-9}$$

In Equation (6-9), q_u is the thermal energy collected per unit of surface area, $\dot{m}$ is the air mass flow rate, c_p is the air specific heat and $T_{f,o}$ and $T_{f,i}$ are the fluid temperature at the outlet and inlet of the k^{th} element, respectively. The fluid top ($h_{conv,fT}$) and bottom ($h_{conv,fb}$) convective heat transfer coefficients are calculated using the model of Candanedo et al. (2011) up to Reynolds numbers of 7,500 and the model of Dittus & Boelter (1985) for higher Reynolds number. As for the top convective heat transfer coefficient, $h_{conv,T}$, it is estimated with the model of Pavylos (2008) for leeward surfaces for Reynolds numbers up to 7,500. The model of Incroprera & DeWitt (1996) is used for Reynolds numbers higher than 7,500. More details of the model are provided in Delisle & Kummert (2014).

Four different heat management strategies are considered. Depending on the strategy, active heat recovery is performed for the whole BIPV surface area or only for a fraction of it. When the system requires an additional fan to circulate air in the BIPV-T collector, its power consumption is estimated at 0.425 W/(kg/h). Based on the literature review presented in Section 6.4, these four heat management strategies are considered:

1. Preheating fresh air prior to entering the heat recovery ventilator
2. Coupling with an air-to-water heat exchanger to preheat DHW
3. Preheating the evaporator side of an air-to-water heat pump where the water is used for DHW and space heating purposes through coupling with a radiant floor system
4. Preheating the air entering a heat pump water heater for DHW heating purposes

These strategies are further described in Sections 6.5.2.1.1 to 6.5.2.1.4.

6.5.2.1.1 BIPV-T System 1 – Fresh Air Preheating

This first scenario is the simplest one and aims at reducing space heating requirements by using the BIPV-T collector to preheat fresh air. The houses ventilation rates vary between 28 and 50 L/s which would correspond to collector surface flowrates (i.e., flowrate per unit of collector surface area) in the range of 1 to 7 kg/(h·m^2) if the full roof area was used. Considering that the typical flowrate for air solar thermal collectors is between 20 and 120 kg/(h·m^2) (ASHRAE, 2014), heat recovery in this scenario is only applied to a fraction of the roof. The BIPV area with heat recovery (i.e., the BIPV-T area) is determined by targeting a surface

flowrate of 20 kg/(h·m^2) while matching the ventilation air requirements. As shown in Figure 6-3, this scenario requires an additional fan. This fan is turned on whenever the air temperature at the BIPV-T outlet is higher than outdoors by at least 5 °C (2 °C if the fan is already on). In other cases, the HRV draws fresh air directly from outdoors. The fan power is estimated at 1.5 times the power required by the HRV.

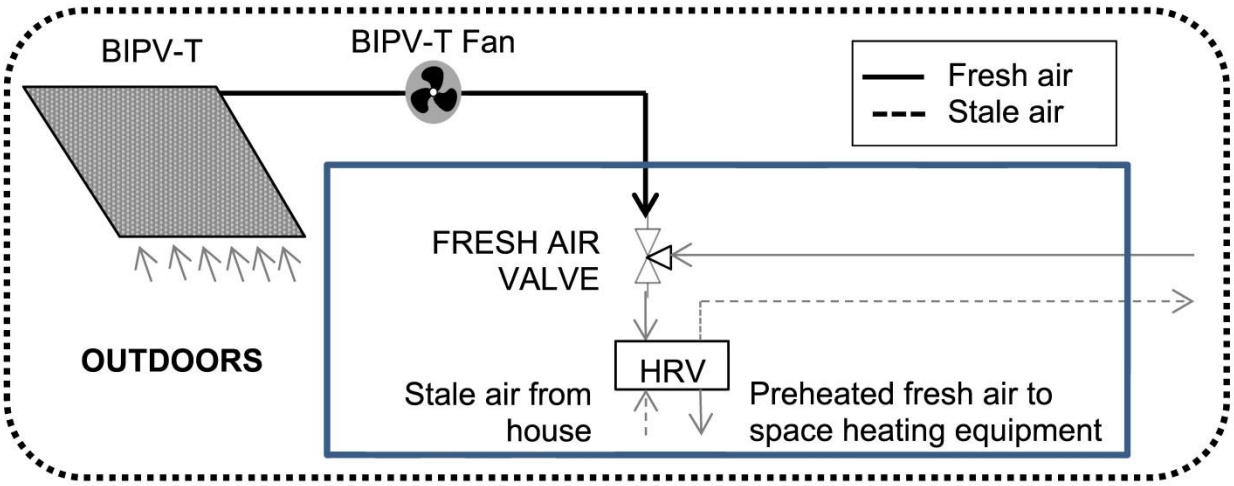

Figure 6-3: Schematic of roof scenario with BIPV-T System 1

6.5.2.1.2 BIPV-T System 2 – DHW Heating with an Air-to-Water Heat Exchanger

The second BIPV-T system scenario focuses on reducing domestic hot water heating requirements and is shown in Figure 6-4. In this case, the BIPV-T is coupled with a two tank DHW system similar to that described in Section 6.5.2.3. The fan is turned on when the temperature at the collector outlet is higher than outdoors by 5 °C (2 °C if the fan is already on) and higher than the preheat tank top temperature by 10 °C (4 °C if the fan is already on). The surface flowrate is set constant at 20 kg/(h·m^2).

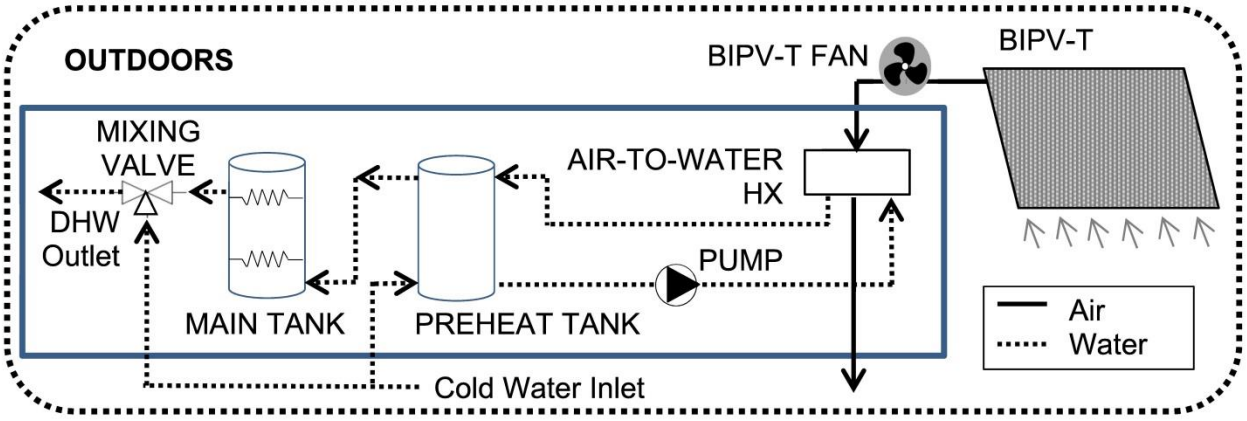

Figure 6-4: Schematic of roof scenario BIPV-T System 2

6.5.2.1.3 BIPV-T System 3 – DHW and Space Heating with an Air-to-Water Heat Pump

In this third and more complex system, the BIPV-T collector is coupled with the evaporator side of an air-to-water heat pump with the aim of reducing both space heating and domestic hot water heating demand. The preheated air is mixed with outdoor air prior to entering the heat pump to ensure that sufficient airflow is delivered to the evaporator. As shown in Figure 6-5, the heat pump produces hot water that can supply both a radiant floor system and a DHW tank. This tank has a coil internal heat exchanger and a single heating element of 3 kW.

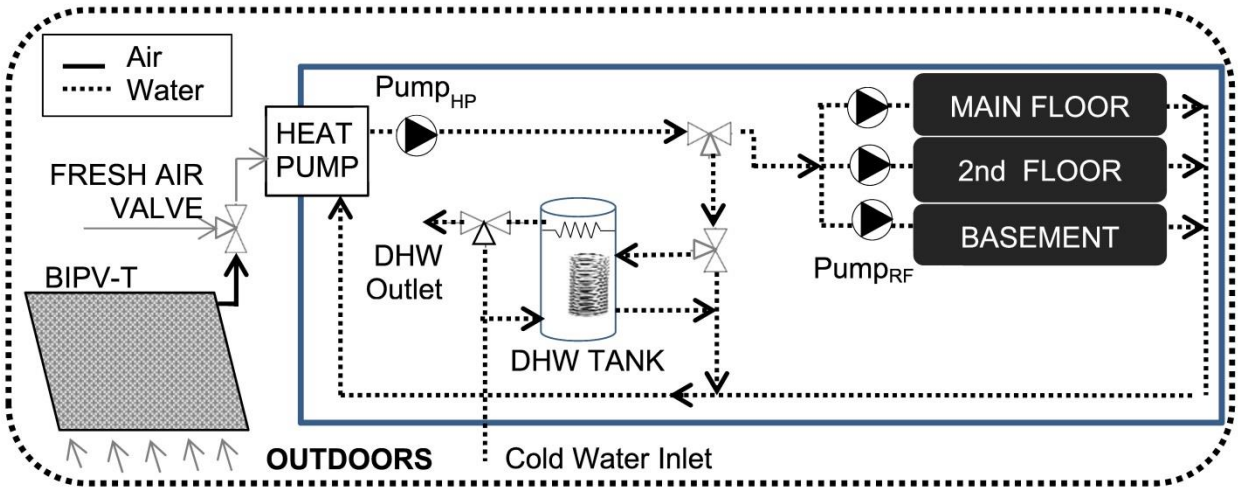

Figure 6-5: Schematic of roof scenario with BIPV-T System 3

The radiant floor system inlet temperature is regulated at 35 °C and the design temperature difference is fixed at 5.6 °C. Thus, in the model, when space heating is required, the water

flowrate on each floor is calculated based on the space heating demand for that particular floor and the design temperature difference.

The heat pump water and air flow rates are set constant at 0.27 L/s and 1.65 L/s, respectively. The heat pump maximum capacity and COP are a function of the water and air inlet temperatures and are estimated based on the manufacturer's information provided for the Daikin EQRL-018 heat pump. Information for that equipment is provided for air inlet temperatures between -15 °C and 7 °C and water outlet temperatures between 25 °C and 45 °C. Thus, when the heat pump air inlet temperature is higher than 7 °C, it is assumed that the heat pump performance corresponds to that at 7 °C. When the heat pump air inlet temperature is below -15 °C or the heat pump capacity is not sufficient to supply the space heating requirements, a 6 kW back-up electrical element is turned on.

The heat pump can operate under part load conditions through variation of the compressor inverter frequency. In the absence of heat pump performance data at part load conditions, however, it is assumed that under these conditions, the COP is not affected by the compressor frequency and that both air and water flowrates remain unchanged. The heat pump is not allowed to operate at less than 30% of its maximum capacity.

The other components of the BIPV-T air system shown in Figure 6-5 include a 90 W main circulation pump ($Pump_{HP}$) and 60 W pumps for every floor in the house ($Pump_{RF}$). A valve regulates the pressure drop on each floor to achieve the flowrate required.

The heat pump is turned on only when there is a space heating demand on one of the floors or when the temperature in the DHW tank at the location of the heat exchanger inlet is lower than the heat pump water outlet temperature (i.e., 35 °C). When the water temperature in the tank at the heat exchanger inlet is lower than at the heat pump outlet, the water that is not flowing into the radiant floor system enters the DHW tank heat exchanger. The DHW tank is bypassed otherwise.

The BIPV-T side of the fresh air valve is opened when the heat pump is on and when the air temperature at the collector outlet is higher than ambient by a minimum of 5 °C (2 °C if the valve is already opened). The BIPV-T flowrate is set at 60 kg/(h·m^2) and supplies between 21% (for the small 2-storey home) and 80% (for the medium bungalow home) of the total heat pump air flowrate requirements.

6.5.2.1.4 BIPV-T System 4 – DHW Heating with a Heat Pump Water Heater

In this scenario, the BIPV-T collector is used to preheat the air entering a heat pump water heater. It can have full or partial heat recovery depending on the roof size. The hot water produced is used strictly for DHW purposes. The heat pump water heater (HPWH) temperature is set at 55 °C and its performance is based on the specifications from a HPWH manufacturer (COP and heating time) (Noirot, 2015). Performance data is available for inlet air temperatures between -5 °C and 35 °C. Outside this range, the water heater operates strictly on its 1.5 kW auxiliary heating element. The heating element and the heat pump cannot be simultaneously turned on.

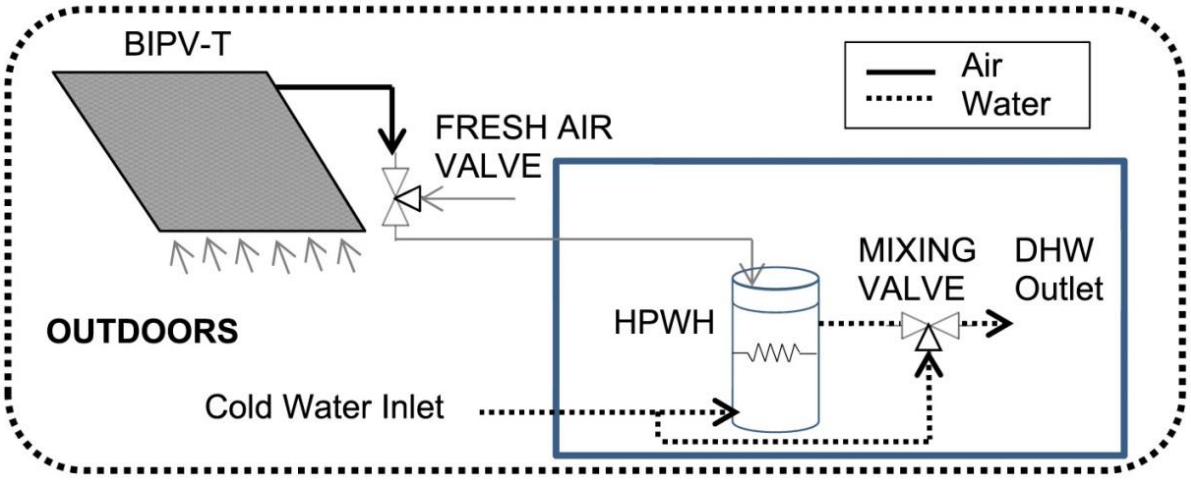

Figure 6-6: Schematic of roof scenario with BIPV-T System 4

The system uses a very simple control. The HPWH operates in heat pump mode as long as the tank temperature remains below 65 °C. As for the auxiliary heating element, it will only turn on if the tank temperature falls below 55 °C. The BIPV-T side of the fresh air valve is opened when the air temperature at the collector outlet is higher than ambient by a minimum of 5 °C (2 °C if the valve is already opened) and remains closed otherwise.

6.5.2.2 BIPV Roof

The BIPV roof scenario consists of monocrystalline BIPV modules covering the whole south-facing roof area. These modules have the same electrical characteristics than the BIPV-T roof described in Section 6.5.2.1. The DC electricity production is calculated with the BIPV-T model described in that same section, but operated under stagnation conditions.

6.5.2.3 Side-by-Side PV and Solar Thermal Collectors (PV+T)

In the side-by-side roof-mounted PV and solar thermal collectors scenario (PV+T), the south-facing roof area is fully covered with PV modules except for a surface of 5.2 m^2 that has two solar thermal collectors in series. The PV modules have the same electrical characteristics and losses than the BIPV-T roof in Section 6.5.2.1. In this scenario, however, the modules are not integrated into the roof, but mounted on a rack, on top of the roof covering material. The modules performance is assessed with the BIPV-T model described in Section 6.5.2.1 operated under natural ventilation conditions. As shown in Figure 6-7, the solar thermal collectors are coupled with a DHW heating system consisting of a heat exchanger, a preheat tank, a main tank and two circulation pumps.

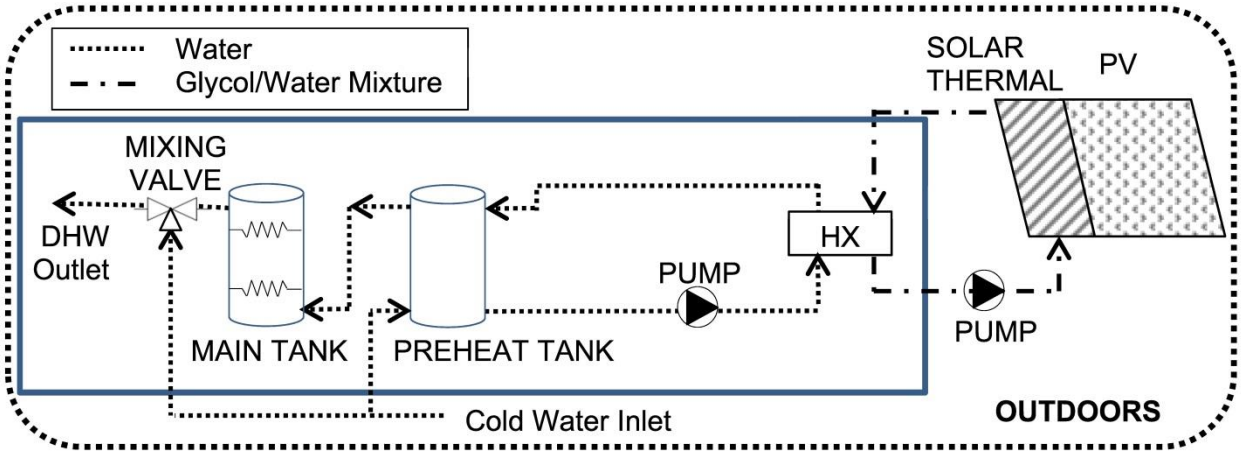

Figure 6-7: Schematic of PV+T roof scenario

Each tank has a volume of 0.227 m^3 and a diameter/height aspect ratio of 0.3086. The main tank has 4.5 kW bottom and top heating elements controlled in a master-slave operation with a setpoint of 55 °C. The TRNSYS standard component Type 1b is used to simulate the solar thermal collector. This model uses the following 2nd order efficiency curve:

$$\eta_{th} = a_0 - a_1 \frac{\left(T_{f,i} - T_a\right)}{G} - a_2 \frac{\left(T_{f,i} - T_a\right)^2}{G} \tag{6-10}$$

In Equation (6-10), a_0 is the collector thermal efficiency at $T_{f,i} = T_a$ and a_1 and a_2 are the efficiency curve slope and curvature, respectively. The solar thermal collector simulated has the following efficiency curve parameters: $a_0 = 0.69$, $a_1 = 3.40\ \mathrm{W/(m^2 \cdot K)}$ and $a_2 = 0.02\ \mathrm{W/(m^2 \cdot K^2)}$. The fluid circulates in the solar thermal collector at a rate of 54 kg/(h·m^2) and is a mixture composed of equal parts of water and glycol. It transfers heat to water circulating between the bottom and top of the preheat tank through a heat exchanger that has a constant effectiveness of 80%. The flowrate on the water side of the heat exchanger is such that the product of the flowrate and thermal capacity on both sides of the heat exchanger are equal. The power of each pump is estimated at 2% of the solar thermal collector maximum power, i.e., 72 W. These pumps are turned on only when the glycol mixture temperature at the collector outlet is higher than the water temperature at the top of the preheat tank by at least 10 °C (2 °C if it is already on).

6.5.3 Performance Indicator

The concept of useful equivalent *electrical* energy is used to combine the electrical and thermal energy produced by a BIPV-T system. The useful equivalent electrical energy produced by a system (S), $Q_{el,eq,u(\mathrm{S})}$, is defined as:

$$Q_{el,eq,u(\mathrm{S})} = Q_{el,u,SH(\mathrm{S})} + Q_{el,u,DHW(\mathrm{S})} + Q_{el,u,SC(\mathrm{S})} + Q_{el,net,prod(\mathrm{S})} \tag{6-11}$$

In Equation (6-11), $Q_{el,net,prod(\mathrm{S})}$ is the system net electrical energy production and $Q_{el,u,SH(\mathrm{S})}$, $Q_{el,u,SC(\mathrm{S})}$ and $Q_{el,u,DHW(\mathrm{S})}$ are the useful equivalent electrical energy production for space heating (*SH*), space cooling (*SC*) and domestic hot water heating (*DHW*). These terms are calculated with respect to a reference system (REF) using the following relations:

$$Q_{el,u,SH(\mathrm{S})} = Q_{el,SH(\mathrm{REF})} - Q_{el,SH(\mathrm{S})} \tag{6-12}$$

$$Q_{el,u,SC(\mathrm{S})} = Q_{el,SC(\mathrm{REF})} - Q_{el,SC(\mathrm{S})} \tag{6-13}$$

$$Q_{el,u,DHW(\mathrm{S})} = Q_{el,DHW(\mathrm{REF})} - Q_{el,DHW(\mathrm{S})} \tag{6-14}$$

$$Q_{el,net,prod(\mathrm{S})} = \left(Q_{el,prod(\mathrm{S})} - Q_{el,cons(\mathrm{S})}\right) - \left(Q_{el,prod(\mathrm{REF})} - Q_{el,cons(\mathrm{REF})}\right) \tag{6-15}$$

In order for these equations to be valid, the space heating, space cooling and domestic hot water heating systems of both the reference and actual systems have to be electric.

Each one of the 6 roof scenarios (BIPV, PV+T, BIPV-T System 1, BIPV-T System 2, BIPV-T System 3 and BIPV-T System 4) described in Section 6.5.2.1 is compared with its own reference case. All reference cases have a standard roof that does not produce any electrical or thermal energy. Except for the PV+T scenario, the mechanical system (for SH, SC and DHW heating) of the reference case is the same as in the solar energy technology scenario that it is being compared with. It is simply not solar assisted. For BIPV-T System 1 (fresh air preheating), space heating is supplied by an ASHP for both the reference system and the BIPV-T scenario. For the PV+T reference scenario, DHW is provided by a standard dual element electric DHW tank.

6.5.4 Economic Indicator

6.5.4.1 Break-Even Cost Definition

The cost of BIPV-T systems remains difficult to evaluate since these installations are not very common yet. For this reason, the concept of break-even cost is used. It is defined as the maximum cost to recover the heat from a BIPV system (i.e., the cost to convert the BIPV into a BIPV-T system) to break-even with the cost of another solar energy technology (Delisle & Kummert, 2014) in dollars per unit of useful energy produced. The higher the break-even cost of a system, the easier it is to be competitive with other technologies.

By setting the cost of BIPV-T and BIPV systems to be equal per unit of useful energy produced, the following relation is obtained:

$$\frac{C_{T,B-E(\text{BIPV-T vs BIPV})} + C_{\text{BIPV}}}{Q_{el,eq,u(\text{BIPV-T})}} = \frac{C_{\text{BIPV}}}{Q_{el,eq,u(\text{BIPV})}} \tag{6-16}$$

In Equation (6-16), C_{BIPV} is the cost of the BIPV system and $C_{T,B-E(\text{BIPV-T vs BIPV})}$ is the break-even cost of a BIPV-T system relative to a BIPV system. Similarly, setting the cost of a BIPV-T system equal to that of side-by-side PV and solar thermal systems gives:

$$\frac{C_{T,B-E(\text{BIPV-T vs PV+T})} + C_{\text{BIPV}}}{Q_{el,eq,u(\text{BIPV-T})}} = \frac{C_{\text{PV+T}}}{Q_{el,eq,u(\text{PV+T})}} \tag{6-17}$$

In Equation (6-17), $C_{\text{PV+T}}$ is the cost of the PV+T system and $C_{T,B-E(\text{BIPV-T vs PV+T})}$ is the break-even cost of a BIPV-T system relative to a PV+T system. The BIPV-T break-even cost with respect to BIPV and PV+T systems is obtained by isolating $C_{T,B-E}$ in Equations (6-16) and (6-17):

$$C_{T,B-E(\text{BIPV-T vs BIPV})} = \frac{C_{\text{BIPV}}}{Q_{el,eq,u(\text{BIPV})}} Q_{el,eq,u(\text{BIPV-T})} - C_{\text{BIPV}} \tag{6-18}$$

$$C_{T,B-E(\text{BIPV-T vs PV+T})} = \frac{C_{\text{PV+T}}}{Q_{el,eq,u(\text{PV+T})}} Q_{el,eq,u(\text{BIPV-T})} - C_{\text{BIPV}} \tag{6-19}$$

Break-even costs can also be expressed in terms of roof surface area, A_{roof}, as specific break-even costs defined as:

$$C''_{T,B-E(\text{BIPV-T vs BIPV})} = \frac{C_{T,B-E(\text{BIPV-T vs BIPV})}}{A_{roof}} \tag{6-20}$$

$$C''_{T,B-E(\text{BIPV-T vs PV+T})} = \frac{C_{T,B-E(\text{BIPV-T vs PV+T})}}{A_{roof}} \tag{6-21}$$

The concept of break-even cost can be further explained with a fictitious example. Assuming a generic roof for which a 2.2 kWp BIPV system costs 10,000 CAD (C_{BIPV}) and produces 2,500 kWh/y of electricity ($Q_{el,eq,u(\text{BIPV})}$). Further assuming that if a BIPV-T system were to be used as the roof instead of a BIPV system, the equivalent useful electrical energy production would be 3,000 kWh/y ($Q_{el,eq,u(\text{BIPV-T})}$). By substituting these numbers in Equation (6-18), the break-even cost is estimated at 2,000 CAD. This means that if the cost of upgrading from a BIPV to a BIPV-T system is 2,000 CAD, the cost-benefit of both systems is equivalent. If it is less than 2,000 CAD, the BIPV-T system is more beneficial and if it is higher, it is simply not worth it adding thermal recovery to the BIPV system from an economic point of view.

6.5.4.2 Cost of Side-by-Side PV and Solar Thermal Collectors (PV+T)

The cost of roof-mounted PV is fairly well-documented. According to the 2014 National Survey Report of PV Power Applications in Canada (Poissant & Bateman, 2014), the average installed residential PV system price was 3.65 CAD/W for systems smaller than 10 kW.

As for the cost of solar thermal collectors for DHW preheating, recent quotes obtained from various distributors show that the cost of package systems varies between 4,000 CAD to as much as 8,000 CAD. The median installed cost is close to 7,500 CAD. For that reason, this study uses an installed cost of 7,500 CAD for solar domestic hot water heating systems.

6.5.4.3 BIPV Cost

The cost of BIPV systems is not as well-known as the cost of standard PV modules because of the small market penetration. In 2011, the US National Renewable Energy Laboratory (NREL) completed a study on the potential cost of BIPV residential applications (James et al., 2011) if this technology was to become more widely adopted. Using the 2010 US PV system price as a benchmark, the potential installed cost of c-Si BIPV was estimated at 5.02 USD/W compared to 5.71 USD/W for a standard c-Si PV module corresponding to a reduction in the order of 12%. This reduced cost could be mainly explained by the elimination of hardware racking and its associated labor costs even though the capital cost is higher than for standard PV products. In 2012, the same methodology lead to a potential installed cost for c-Si BIPV of 3.33 USD/W compared to 4.31 USD/W for standard PV modules, corresponding to a reduction of nearly 23% (James et al., 2012). In 2014, the Solar Energy Application Centre (SEAC) completed a survey on BIPV pricing in the Netherlands (Verbene & van den Donker, 2015) by asking BIPV systems' suppliers to quote on two virtual Dutch homes with a pitched roof to make the house net electricity zero. For a newly built home, BIPV in-roof mounting systems were found to be 7% to 10% more expensive than standard PV systems.

Considering the different potential costs of BIPV, three cost scenarios are considered to estimate the break-even cost of BIPV-T air systems. One of the scenarios considers that BIPV is 10% more expensive than PV ($C_{\mathrm{BIPV}} = 1.1\ C_{\mathrm{PV}}$). Moderately optimistic scenarios are explored where BIPV cost as much as PV ($C_{\mathrm{BIPV}} = C_{\mathrm{PV}}$) or even 10% less ($C_{\mathrm{BIPV}} = 0.9\ C_{\mathrm{PV}}$) if economy of scale could be achieved resulting from a wider adoption.

6.6 Results and Discussion

6.6.1 House Energy Consumption

The housing archetypes annual energy requirements by end-use (excluding equipment efficiency) are shown in Figure 6-8 for every location in ascending order of heating degree days. The energy requirements vary from 10,735 kWh/y for the small bungalow in Vancouver up to 22,335 kWh/y for the medium bungalow in Whitehorse. Except for Vancouver, the main load is space heating. For the medium 2-storey home, space heating represents between 25% (Vancouver) and 47% (Whitehorse) of the total energy requirements.

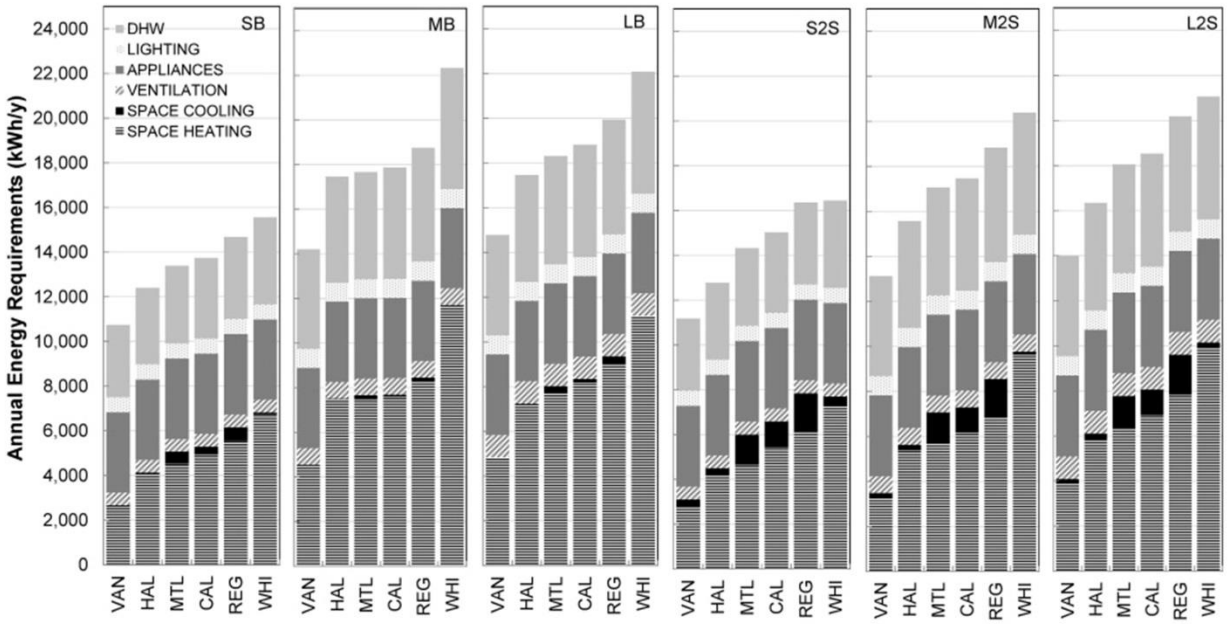

Figure 6-8: Energy requirements of housing archetypes by end-use

6.6.2 Useful Equivalent Energy Production

Figure 6-9 and Figure 6-10 show the amount of useful equivalent energy produced by the different solar energy scenarios for the city of Montreal grouped by housing archetype and for the medium 2-storey house grouped by location, respectively.

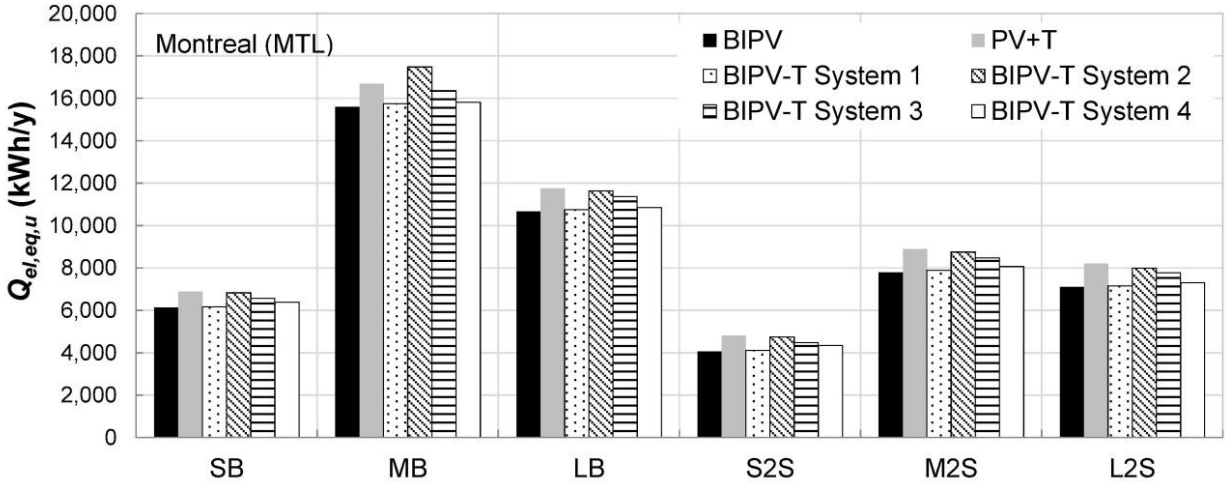

Figure 6-9: Useful equivalent electrical energy for Montreal grouped by housing archetype

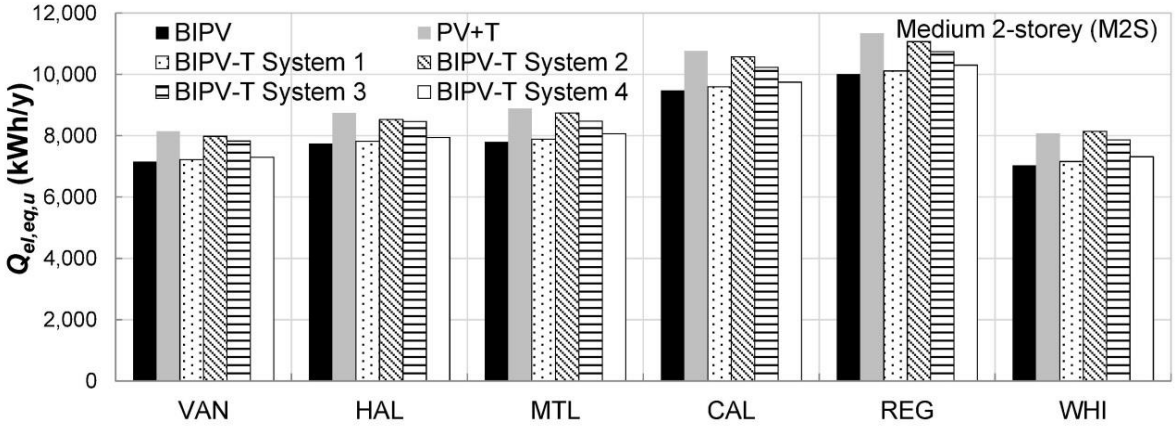

Figure 6-10: Useful equivalent electrical energy for the medium 2-storey house grouped by location

As expected, all BIPV-T scenarios produce more useful equivalent electrical energy than the BIPV scenario regardless of location and housing archetype. For example, BIPV-T System 2 in the medium 2-storey house in Montreal produces nearly 16% (or 850 kWh/y) more useful equivalent electrical energy than the BIPV system. This is not necessarily the case when comparing with the PV+T scenario, however, as it depends on the heat management strategy used, the housing archetype and the location. Among all BIPV-T systems, System 2 (DHW preheating) always produces the most useful equivalent electrical energy regardless of location and housing archetype. It is generally similar to the PV+T system (within 1% for the medium 2-storey house in Montreal) and slightly higher for the medium bungalow. BIPV-T System 1 (fresh

air preheating) always produces the least amount of useful energy followed closely by System 4 (heat pump water heater). This is because the HRV in System 1 already does very well at preheating fresh air. Similarly, the heat pump water heater in System 4 significantly reduces the DHW load as is, without being solar-assisted. As a result, the BIPV-T contribution in these systems is somewhat diluted. System 3 (air-to-water heat pump) produces generally less than the PV+T scenario, but more than Systems 1 and 4.

6.6.3 Break-Even Cost

6.6.3.1 BIPV-T vs BIPV

The break-even and specific break-even costs of the BIPV-T systems compared to a BIPV system are shown in Figure 6-11 and Figure 6-12 for Montreal grouped by housing archetype and for the medium 2-storey house grouped by location, respectively. In these figures, the columns represent the case where $C_{\mathrm{BIPV}} = C_{\mathrm{PV}}$. The upper bound of the error bars is for $C_{\mathrm{BIPV}} = 1.1\, C_{\mathrm{PV}}$ and the lower bound, for $C_{\mathrm{BIPV}} = 0.9\, C_{\mathrm{PV}}$. The results for all locations and housing archetypes are provided in Appendix A (Section 6.11.1).

As expected, the break-even cost for a particular BIPV-T system varies with both housing archetype and location. Also, it is positive for all cases since BIPV-T systems always produce more useful energy than BIPV systems. The highest break-even cost is obtained with System 2 (DHW preheating) since it produces the most useful equivalent electrical energy. For that particular scenario and considering $C_{\mathrm{BIPV}} = C_{\mathrm{PV}}$, the maximum allowed cost to upgrade from a BIPV to a BIPV-T system ranges from 1,900 to 5,300 CAD (50 to 90 CAD/m^2) for Montreal. The system with the second highest break-even cost is System 3 (air-to-water heat pump for DHW and space heating). In that case, the break-even cost varies from 1,200 to 2,100 CAD (30 to 60 CAD/m^2) for Montreal. Systems 1 and 4 both have break-even costs that are less than 1,000 CAD. For the medium 2-storey home, the maximum break-even cost is always obtained for Whitehorse, the city with the highest number of heating degree-days and lowest mean daily global insolation, regardless of the heat management strategy.

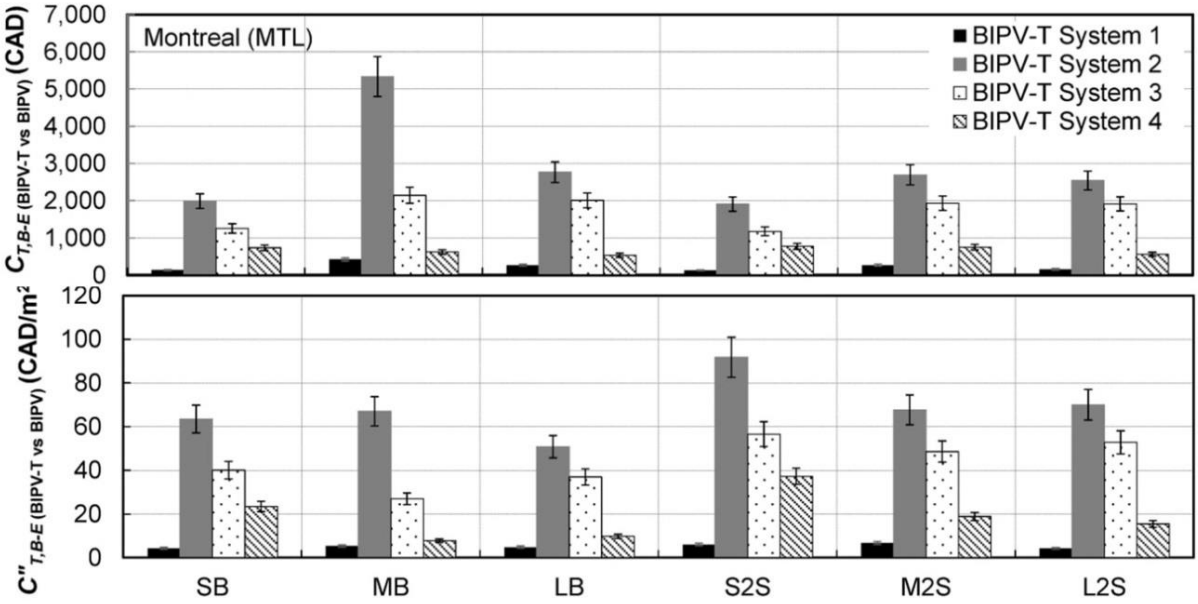

Figure 6-11: Break-even and specific break-even costs compared to a BIPV system for Montreal

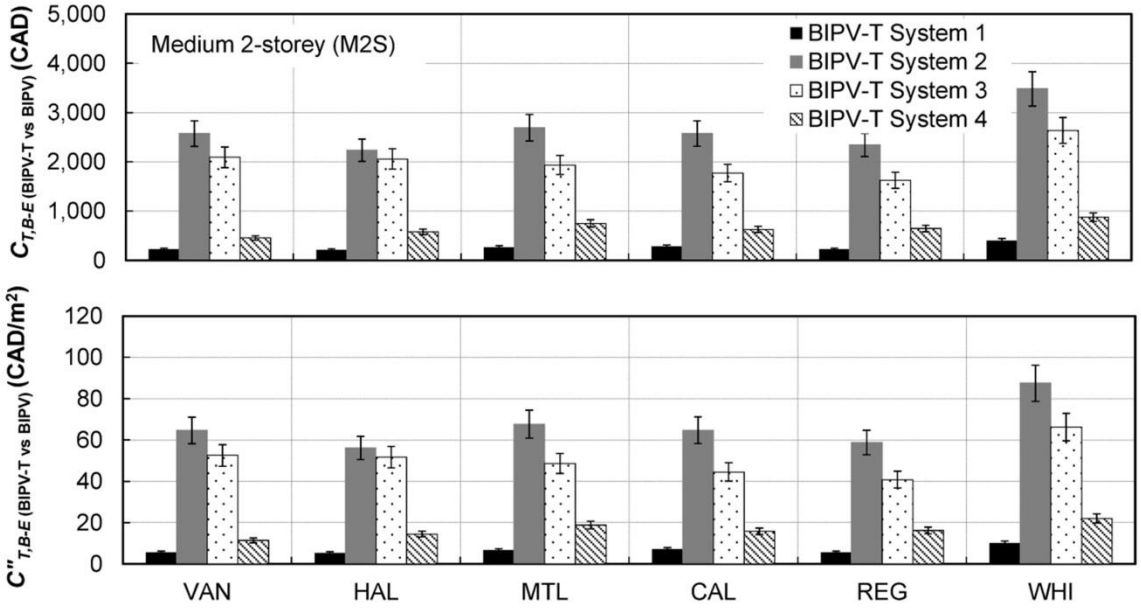

Figure 6-12: Break-even and specific break-even costs compared to a BIPV system for the medium 2-storey home

6.6.3.2 BIPV-T vs PV+T

Figure 6-13 and Figure 6-14 present the break-even and specific break-even costs compared to a PV+T system for Montreal grouped by housing archetype and for the medium 2-storey house grouped by location, respectively. On these graphs, the columns represent the case where $C_{\mathrm{BIPV}} = C_{\mathrm{PV}}$ and the error bars upper and lower bounds show the scenarios where $C_{\mathrm{BIPV}} = 0.9\ C_{\mathrm{PV}}$ and $C_{\mathrm{BIPV}} = 1.1\ C_{\mathrm{PV}}$, respectively. The results for all locations and housing archetypes are provided in Appendix B (Section 6.11.2).

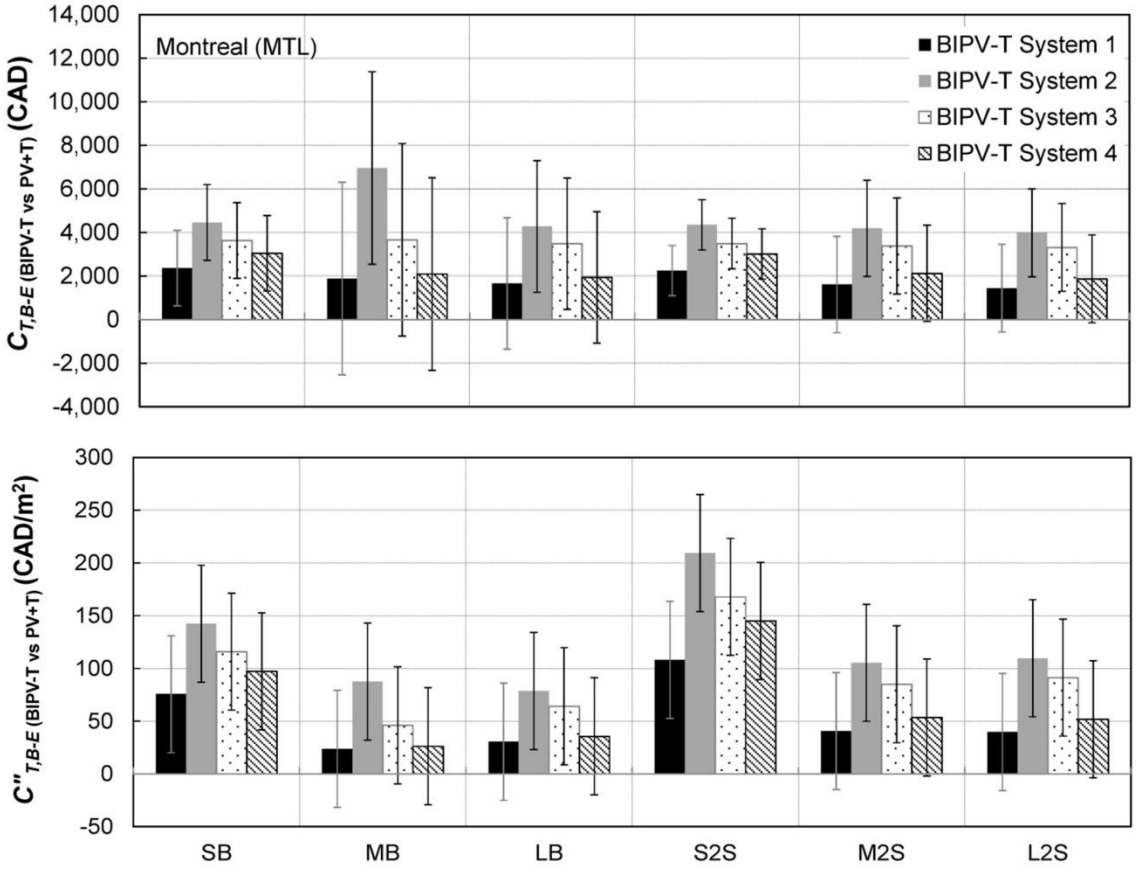

Figure 6-13: Break-even and specific break-even costs compared to a PV+T system for Montreal grouped by housing archetype

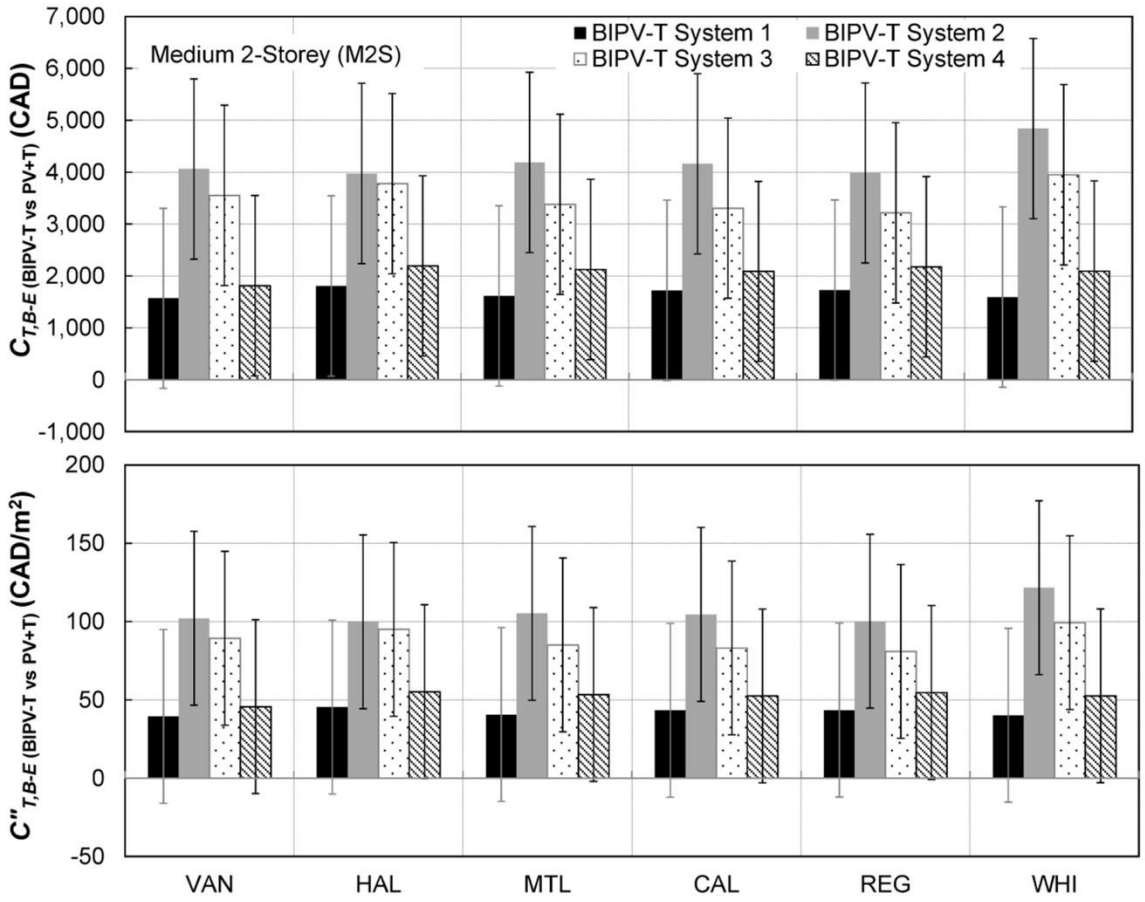

Figure 6-14: Break-even and specific break-even costs compared to a PV+T system for the medium 2-storey home grouped by location

From these figures, it can be observed that the break-even cost is always positive when the cost of BIPV is less than or equal to standard PV, but not systematically when $C_{\mathrm{BIPV}} = 1.1\, C_{\mathrm{PV}}$. Thus, the cost of BIPV has a greater influence on the break-even cost of BIPV-T relative to a PV+T system than to a BIPV system.

Considering the housing archetypes located in Montreal (Figure 6-13), the smallest break-even cost is always obtained for systems 1 and 4 (fresh air preheating and heat pump water heater). For System 1, the break-even cost ranges from 1,400 to 2,400 CAD (20 to 110 CAD/m^2) for $C_{\mathrm{BIPV}} = C_{\mathrm{PV}}$ and 3,400 to 6,300 CAD (80 to 160 CAD/m^2) for $C_{\mathrm{BIPV}} = 0.9\, C_{\mathrm{PV}}$. Similar ranges are obtained for System 4 with break-even costs varying between 1,900 and 3,000 CAD (25 and 150 CAD/m^2) for $C_{\mathrm{BIPV}} = C_{\mathrm{PV}}$ and 3,900 and 6,500 CAD (80 and 200 CAD/m^2) for $C_{\mathrm{BIPV}} = 0.9\, C_{\mathrm{PV}}$. The highest break-even cost is obtained with System 2 (DHW preheating). For that case, it varies

from 4,000 to 7,000 CAD (90 to 210 CAD/m^2) for $C_{\mathrm{BIPV}} = C_{\mathrm{PV}}$ and from 5,500 to 11,400 CAD (130 to 270 CAD/m^2) for $C_{\mathrm{BIPV}} = 0.9\ C_{\mathrm{PV}}$.

As shown in Figure 6-14, the effect of location on the break-even cost is not as important as the housing archetype. For the medium 2-storey house, the highest break-even cost is obtained for Whitehorse and that, for all BIPV-T systems. For System 2, the break-even cost varies between 4,000 and 4,900 CAD (100 and 120 CAD/m^2) for $C_{\mathrm{BIPV}} = C_{\mathrm{PV}}$ and 6,200 and 7,000 CAD (160 and 180 CAD/m^2) for $C_{\mathrm{BIPV}} = 0.9\ C_{\mathrm{PV}}$. For System 3, it varies between 3,200 and 4,000 CAD (90 and 100 CAD/m^2) for $C_{\mathrm{BIPV}} = C_{\mathrm{PV}}$ and 5,400 and 6,200 CAD (140 and 160 CAD/m^2) for $C_{\mathrm{BIPV}} = 0.9\ C_{\mathrm{PV}}$.

6.6.3.3 Discussion

BIPV-T systems always produce more useful equivalent electrical energy than BIPV systems. Thus, it is always possible for BIPV-T to be cost-competitive with BIPV regardless of the cost of BIPV relative to standard PV modules. When comparing with a roof consisting of side-by-side PV modules and solar thermal collectors (PV+T), it is almost always the case as well. This is shown in Figure 6-15 where the break-even cost of the different systems compared to both BIPV and PV+T systems is presented for all housing archetypes and locations combined. On this figure, the marker represents the average break-even cost for all housing archetypes and locations for a specific BIPV cost relative to standard roof-mounted PV. The lower and upper bounds of the boxes show the minimum and maximum costs among all housing archetypes and locations combinations.

According to this figure, BIPV-T systems are most of the time competitive with PV+T systems. A maximum break-even cost of 4,000 CAD is still achieved with BIPV costing 10% more than PV for System 2. This number increases to 12,000 CAD with BIPV costing 10% less than PV. Systems 2 and 3 have higher break-even costs than Systems 1 and 4, but these are not necessarily the best options since they require a greater investment. Considering the HRV and heat pump water heater to already be in the reference house, the upgrade cost from a BIPV system to a BIPV-T system only includes the cost difference between the modules and the required ducting. System 2 has to include the cost of an air-to-water heat exchanger. These types of heat exchangers are generally very bulky and can be costly. Tripanagnostopoulos et al. (2006)

estimated the cost of an air-to-water heat exchanger in BIPV-T applications at 1,200 Euros (~1,800 CAD) in 2005.

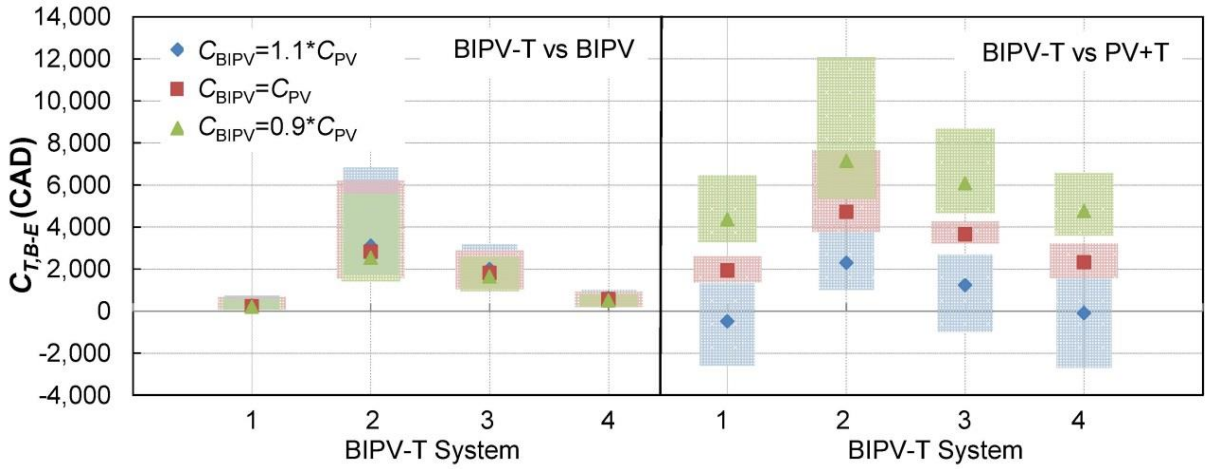

Figure 6-15: BIPV-T system break-even cost compared to BIPV and PV+T systems

The cost of standard roof-mounted PV systems is expected to continue to decrease in the future. Assuming that the cost of BIPV systems can still be expressed in terms of relative cost to that of PV, such cost decrease will reduce the BIPV-T break-even cost relative to a BIPV system. This additional cost will increase, however, when comparing with a PV+T system.

6.7 Conclusions

This study aimed at providing an estimate of the maximum allowed cost to upgrade from a BIPV to a BIPV-T air system in order for that BIPV-T system to remain cost competitive with (a) a BIPV roof or (b) side-by-side roof-mounted PV modules and solar thermal collectors. This cost, defined as the break-even cost is based on the useful equivalent electrical energy produced and was obtained for different high performance Canadian housing archetypes and four BIPV-T air collector coupling scenarios: (1) fresh air preheating, (2) DHW preheating through and air-to-water heat exchanger, (3) DHW and space heating with an air-to-water heat pump and (4) DHW heating with a heat pump water heater.

The results show that compared to a BIPV system, a BIPV-T system always produces more useful energy. For example, a System used for DHW preheating (System 2) in a medium 2-storey house in Montreal was found to produce nearly 16% more useful equivalent electrical energy than a BIPV roof of the same size. Compared to a PV+T system, however, the type of house and heat management strategy greatly influenced the amount of useful energy produced. Among all BIPV-T systems, System 2 (DHW preheating) was found to produce the most useful equivalent electrical energy. This production is generally similar to the PV+T system (within 1% for the medium 2-storey home in Montreal) and slightly higher for the medium bungalow.

Assuming the cost of BIPV equal to that of standard PV modules, the break-even cost of a BIPV-T system compared to a BIPV system for a medium 2-storey home in Montreal was estimated at 300 CAD for System 1, 2,700CAD for System 2, 1,900 CAD for System 3 and 800 CAD for System 4. If a designer was to consider installing BIPV on a building, it would make sense to select a BIPV-T system if the incremental cost does not exceed this break-even cost. It could also provide a greater cost-benefit if the incremental cost is actually lower than the break-even cost.

The break-even cost compared to a PV+T system was found to strongly depend on the cost of BIPV relative to PV. For a medium 2-storey home in Montreal, the break-even cost of a BIPV-T system compared to a PV+T system considering the cost of BIPV equal to that of PV was estimated at 1,600 CAD for System 1, 4,200 CAD for System 2, 3,400 CAD for System 3 and 2,100 CAD for System 3. For a BIPV cost 10% lower than PV, however, this break-even cost could be increased to 3,800 CAD for System 1, 6,400 CAD for System 2, 5,600 CAD for System 3 and 4,300 CAD for System 4. Lower break-even costs were obtained for Systems 1 (fresh air preheating) and 4 (heat pump water heater), but this is because the reference systems for these scenarios are already performing very well without being solar-assisted. These options are nevertheless interesting because they are simple to integrate and their added cost consists only of the upgrade from a BIPV to a BIPV-T collector and its associated ducting. System 2, on the other hand, requires an additional air-to-water heat exchanger which can represent a significant extra cost by itself.

The break-even costs presented in this study can be considered conservative. Higher acceptable upgrade costs could be achieved by performing more in-depth optimization of controls and

mechanical components sizing to increase the amount of thermal energy converted into useful energy. A similar analysis could also be done for multi-unit residential or commercial buildings. These types of buildings have more potential for façade-integrated photovoltaic systems with thermal energy recovery than roof-integrated systems. In addition, the fresh air requirements are more important. As a result, the performance of System 1 where the BIPV-T is used for fresh air preheating would certainly be more interesting than in a single-family house scenario.

6.8 Acknowledgements

Funding for this work was provided by Natural Resources Canada through the ecoENERGY Innovation Initiative.

6.9 Nomenclature

Symbols

A_{roof}	Roof area (m^2)
C_{BIPV}	Cost of a BIPV system (CAD)
C_{PV+T}	Cost of side-by-side PV and solar thermal systems
$C_{T,B-E}$	Break-even cost (CAD)
$C''_{T,B-E}$	Break-even cost per unit of roof surface area or specific break-even cost (CAD/m^2)
dy	Length of control volume (m)
F_{cell}	Fraction of the collector gross area covered by PV cells (-)
G	Total incident solar radiation (kJ/(h·m^2))
$h_{conv,b}$	Collector back surface convective heat transfer coefficient (kJ/(h·m^2·K))
$h_{conv,fb}$	Bottom air channel heat transfer coefficient (kJ/(h·m^2·K))
$h_{conv,fT}$	Top air channel heat transfer coefficient (kJ/(h·m^2·K))
$h_{conv,T}$	Top convective heat transfer coefficient (kJ/(h·m^2·K))
$h_{rad,b}$	Collector back surface radiative heat transfer coefficient (kJ/(h·m^2·K))
IAM_{bs}	Backsheet and encapsulant incidence angle modifier (-)
IAM_{PV}	PV cells and encapsulant material incidence angle modifier (-)
$\dot{m}$	Mass flow rate (kg/h)
q_u	Thermal energy collected (kJ/(h·m^2))
$Q_{el,cons}$	Annual electricity consumption (kWh/y)
$Q_{el,DHW}$	Annual electricity consumption for domestic hot water heating (kWh/y)
$Q_{el,eq,u}$	Useful equivalent electricity production (kWh/y)
$Q_{el,net,prod}$	Net electricity production (kWh/y)
$Q_{el,prod}$	Electricity production (kWh/y)

$Q_{el,SC}$	Space cooling electricity consumption (kWh/y)
$Q_{el,SH}$	Space heating electricity consumption (kWh/y)
$Q_{el,u,SH}$	Useful equivalent electricity production for space heating (kWh/y)
$Q_{el,u,DHW}$	Useful equivalent electricity production for domestic hot water heating (kWh/y)
$Q_{el,u,SC}$	Useful equivalent electricity production for space cooling (kWh/y)
R_{2-3}	Thermal resistance between the top and back surfaces of the collector back material (h·m^2·K/kJ)
R_{PVg-1}	Thermal resistance between the top of the PV cells and the back surface of the PV cells back material (h·m^2·K/kJ)
R_{PVg-PV}	Thermal resistance between the glass encapsulant and the PV cells (h·m^2·K/kJ)
S	Net solar radiation absorbed in the cell per unit of gross collector area (kJ/(h·m^2))
S_1	Net solar radiation absorbed in the PV module back layer per unit of gross collector area (kJ/(h·m^2))
T_1	Air channel top surface temperature (K)
T_2	Air channel bottom surface temperature (K)
T_3	Temperature at the back surface of the collector back material (K)
T_a	Ambient temperature (K)
T_b	Zone temperature at the back of the collector (K)
T_f	Fluid temperature (K)
$T_{f,i}$	Fluid inlet temperature (K)
$T_{f,o}$	Fluid outlet temperature (K)
T_{PV}	PV cells temperature (K)
T_{PVg}	Top of the glass encapsulant temperature (K)
$T_{rad,b}$	Mean radiant temperature of the zone at the back of the collector (K)
T_{sur}	Temperature of the surroundings (K)
W	Collector width (m)
η_{PV}	PV cells efficiency (-)
η_{th}	Thermal efficiency (-)
$(\tau\alpha)_{bs,N}$	PV module backsheet material transmittance-absorptance product (-)
$(\tau\alpha)_{PV,N}$	PV cell transmittance-absorptance product accounting for glass encapsulant at normal incidence angle (-)

Subscripts

BIPV	Building-integrated photovoltaics
BIPV-T	Building-integrated photovoltaics with thermal energy recovery
PV+T	Side-by-side PV modules and solar thermal collectors
REF	Reference
s	System

6.10 References

American Society of Heating, Refrigerating and Air-Conditioning (ASHRAE). (2010). *Methods of Testing to Determine the Thermal Performance of Solar Collectors* (ANSI/ASHRAE 93-2010).

Athienitis, A. K., Bambara, J., O'Neill, B., & Faille, J. (2011). A prototype photovoltaic/thermal system integrated with transpired collector. *Solar Energy, 85*, 139-153.

Bambara, J. (2012). *Experimental Study of a Façade-integrated Phovoltaic/thermal System with Unglazed Transpired Collector* (Masters Thesis, Concordia University, Montreal, Quebec). Retrieved from http://spectrum.library.concordia.ca/ 974610/6/ Bambara_MASc_F2012.pdf

Ben Nejma, H., Guiavarch, A., Lokhat, I., Auzenet, E., Claudon, F., & Peuportier, B. (2013). In-Situ Performance Evaluation by Simulation of a Coupled Air Source Heat Pump/PV-T Collector System. *Proceeding of BS2013:* 13th *Conference of International Building Performance Simulation Association, Chambéry, France, August 26-28, 2013.* http://www.ibpsa.org/proceedings/BS2013/p_1006.pdf

Canadian Home Builder's Association (CHBA). (2012). *45th Pulse Survey of new home builders and renovators*. Retrieved from http://www.chba.ca/uploads/pulse%20survey%20results/ main%20report2012.pdf

Candanedo, J. A., & Athienitis, A. K. (2009). Application of Predictive Control Strategies in a Net Zero Energy Solar House. *PLEA2009 - 26th Conference on Passive and Low Energy Architecture, Quebec City, Canada, June 22-24, 2009.* http://www.plea2009.arc. ulaval.ca/Papers/2.STRATEGIES/2.2%20Heating%20and%20Cooling/ORAL/2-2-03-PLEA2009Quebec.pdf

Candanedo, L., Athienitis, A., & Park, K. (2011). Convective heat transfer coefficients in a building-integrated photovoltaic/thermal system. *ASME Journal of Solar Energy Engineering, 133*(2).

Cartmell, B., Shankland, N., Fiala, D., & Hanby, V. (2004). A multi-operational ventilated photovoltaic and solar air collector: application, simulation and initial monitoring feedback. *Solar Energy, 76*, 45-53.

Charron, R. (2007). *Development of a Generic Algorithm Optimisation Tool for the Early Stage Design of Low and Net-Zero Energy Solar Homes* (PhD Thesis, Concordia University, Montreal, Canada). Retrieved from http://spectrum.library.concordia.ca/975818/

Charron, R., & Athienitis, A. (2006). Design and Optimization of Net Zero Energy Solar Homes. *ASHRAE Transactions*, 112, 285-295.

Chen, Y., Athienitis, A., & Galal, K. (2010a). Modeling, design and thermal performance of a BIPV/T ssytem thermally coupled with a ventilated concrete slab in a low energy solar house: Part 1, BIPV/T system and house energy concept. *Solar Energy, 84*, 1892-1907.

Chen, Y., Galal, K., & Athienitis, A. (2010b). Modeling, design and thermal performance of a BIPV/T system thermally coupled with a ventilated concrete slab in a low energy solar house: Part 2, ventilated concrete slab. *Solar Energy, 84*, 1908-1919.

Delisle, V. (2015). *Models of Energy-Efficient Canadian Home Archetypes* (Internal Report RP-TEC 2015-047). Varennes, Canada: CanmetENERGY.

Delisle, V., & Kummert, M. (2014). A novel approach to compare building-integrated photovoltaics/thermal air collectors to side-by-side PV modules and solar thermal collectors. *Solar Energy, 100*, 50-65.

Dittus, F., & Boelter, L. (1985). Heat transfer in automobile radiators of the tubular type. *International Community Heat Mass Transfer, 12*(1), 3-22.

Filliard, B., Guiavarch, A., & Jabbour, M. (2009). Simulation of the thermal interaction between a building integrated photovoltaic collector and an airsource heat pump. *CISBAT 2009 - Renewables in a changing climate: from nano to urban scale, Sep 2009, Lausanne, Switzerland*, pp. 555-560. https://hal.archives-ouvertes.fr/hal-00574652/document

Incropera, F., & DeWitt, D. (1996). *Fundamentals of Heat and Mass Transfer.* New York: John Wiley & Sons.

International Energy Agency (IEA). (2002). *Potential for Building Integrated Photovoltaics* (Report IEA-PVPS T7-4: 2002). Paris, France: IEA. Retrieved from http://www.iea-pvps.org/index.php?id=9&eID=dam_frontend_push&docID=394

International Energy Agency Photovoltaic Power Systems Programme (IEA PVPS) Task 15. (2015). St-Ursen, Switzerland: IEA PVPS. *Enabling Framework for the Acceleration of BIPV*. Retrieved from http://iea-pvps.org/index.php?id=task15

James, T., Goodrich, A., Woddhouse, M., Margolis, R., & Ong, S. (2011). *Building-Integrated Photovoltaics (BIPV) in the Residential Sector: An Analysis of Installed Rooftop Prices* (Technical Report NREL/TP-6A20-53103). Golden, CO, USA: NREL. Retrieved from http://www.nrel.gov/docs/ fy12osti/53103.pdf

James, T., Goodrich, A., Woddhouse, M., Margolis, R., & Ong, S. (2012). *Building-Integrated Photovoltaics (BIPV) in the Residential Section: An Analysi*s of Installed Rooftop Prices, (Presentation NREL/PR-6A20-55027). Golden, CO, USA: NREL. Retrieved from http://www.nrel.gov/docs/ fy12osti/55027.pdf

Kamel, R. S., & Fung, A. S. (2014). Modeling, simulation and feasibility analysis of residential BIPV/T+ASHP system in cold climate-Canada. *Energy and Buildings, 82*, 758-770.

Klein et al. (2009). *A TRaNsient SYstem Simulation Program - User Manual Version 17.* Madison, WI, USA: University of Wisconsin.

Mei, L., Infield, D., Eicker, U., Loveday, D., & Fux, V. (2006). Cooling potential of ventilated PV façade and solar air heaters combined with a desiccant cooling machine. *Renewable Energy, 31*, 1265-1278.

Mei, L., Infield, D., Eicker, U., & Fux, V. (2003). Thermal modelling of a building with an integrated ventilated PV façade. *Energy and Buildings, 35*, 605-617.

National Research Council Canada (NRC). (2010). *National Building Code of Canada 2010* (NBC 2010).

Natural Resources Canada (NRCan). (2010). *2007 Survey of Household Energy Use (SHEU-2007).* Ottawa, Canada: NRCan. Retrieved from http://oee.nrcan.gc.ca/ publications/statistics/ sheu07/pdf/sheu07.pdf

Natural Resources Canada (NRCan). (2012). *2012 R-2000 Standard*. Ottawa, Canada: NRCan. Retrieved from https://www.nrcan.gc.ca/sites/www.nrcan.gc.ca/files/oee/files/pdf/2012%20R2000%20Standard%20EN.pdf

Natural Resources Canada (NRCan). (2013). *Photovoltaic potential and solar resource maps of Canada*. Ottawa, Canada: NRCan. Retrieved from http://pv.nrcan.gc.ca

Natural Resources Canada (NRCan). (2014a). *EnerGuide Home Evaluations*. Ottawa, Canada: NRCan. Retrieved from http:// www.nrcan.gc.ca/energy/efficiency/housing/home-improvements/5005

Natural Resources Canada (NRCan). (2014b). HOT2000 software (Version 10.51). Ottawa, Canada: NRCan. Retrieved from http://www.nrcan.gc.ca/energy/efficiency/housing/home-improvements/17725

Natural Resources Canada (NRCan). (2014c). *List of ENERGY STAR qualified products*. Ottawa, Canada: NRCan. Ottawa, Canada: NRCan Retrieved from http://www.nrcan.gc.ca/energy/products/ energystar/why-buy/13631

Noirot. (2015). *Cylia 2 chauffe-eau thermodynamique*. Retrieved from http://www.noirot.fr/media/ notices/Notice_cylia_2.pdf

Pantic, S., Candanedo, L., & Athienitis, A. (2010). Modeling of energy performance of a house with three configurations of building-integrated photovoltaic/thermal systems. *Energy and Buildings, 42*, 1779-1789.

Parekh, A., Swinton, M., Szadkowski, F., & Manning, M. (2005). *Benchmarking of energy savings associated with energy efficient lighting in houses* (NRCC-50874). Ottawa, Canada: NRCC. Retrieved from http://aceee.org/files/proceedings/2006/data/papers/SS06_Panel9_Paper23.pdf

Pavylos, J. (2008). A survey of wind convection coefficient correlations for building envelope energy systems' modeling. *Applied Thermal Engineering, 28*, 801-808.

Pelland, S., & Poissant, P. (2006). An Evaluation of the Potential of Building Integrated Photovoltaic in Canada. *31st Annual Conference of Solar Energy Society of Canada (SESCI), August 20-24, 2006, Montreal, Canada*. https://www.nrcan.gc.ca/sites/

www.nrcan.gc.ca/files/canmetenergy/files/pubs/2006-047_OP-J_411-SOLRES_BIPV_new.pdf

Poissant, Y., & Bateman, P. (2014). *National Survey Report of PV Power Applications in Canada 2014*. Ottawa, Canada: NRCan. Retrieved from http://www.cansia.ca/uploads/7/2/5/1/72513707/national_survey_report_of_pv_power_applications_in_canada_2014.pdf

Prasad, D., & Snow, M. (2005). *Designing with Solar Power - A Source Book for Building Integrated Photovoltaics (BiPV)*. London, UK: The Images Publishing Group Pty Ltd and Earthscan.

Thevenard, D., & Pelland, S. (2013). Estimating the uncertainty in long-term photovoltaic yield predictions. *Solar Energy, 91*, 432-445.

Tripanagnostopoulos, Y., Souliotis, M., Battisti, R., & Corrado, A. (2006). Performance, Cost and Life-cycle Assessment Study of Hybrid PVT/AIR Solar Systems. *Progress in Photovoltaics: Research and Applications, 14*, 65-76.

Verberne, G., & van den Donker, M. (2015). *BIPV Pricing in The Netherlands - 2014 Price Benchmark Report*. Retrieved from http://www.seac.cc/fileadmin/seac/user/doc/SEAC_-_BIPV_Pricing_in_The_Netherlands_2014.pdf

6.11 Appendices

6.11.1 Appendix A

Figure 6-16 provides additional information to Figure 6-11 and Figure 6-12. It shows the break-even and specific break-even costs of the BIPV-T systems compared to a BIPV system. It is split into 4 sections for each BIPV-T system heat management scenario. The locations are represented on the x-axis and each marker is for a specific housing archetype. The upper bound of the error bars is for $C_{BIPV}=1.1*C_{PV}$ and the lower bound, for $C_{BIPV}=0.9*C_{PV}$.

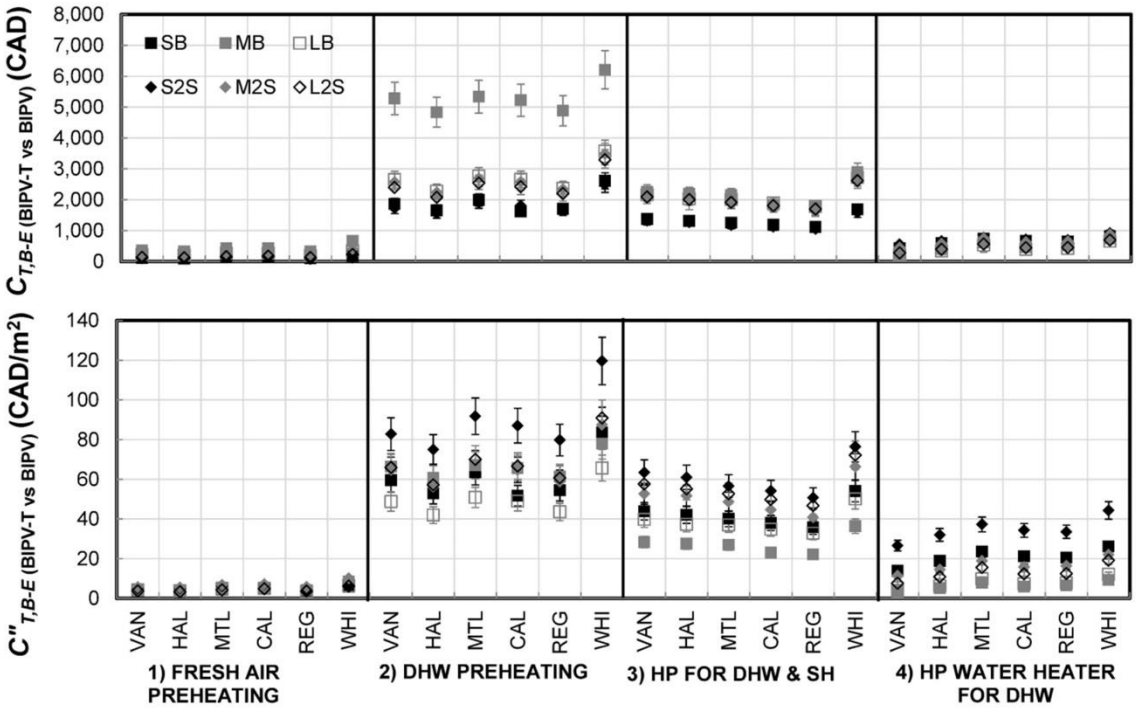

Figure 6-16: Break-even and specific break-even costs of the BIPV-T systems compared to a BIPV system

6.11.2 Appendix B

Figure 6-17 to Figure 6-20 are complementary to Figure 6-13 and Figure 6-14 and present the break-even cost of BIPV-T compared to PV+T for the four heat management scenarios. They are split into 3 sections where each section represents a specific cost of BIPV relative to standard roof-mounted PV systems. The locations are shown on the x-axis and each marker represents a specific housing archetype.

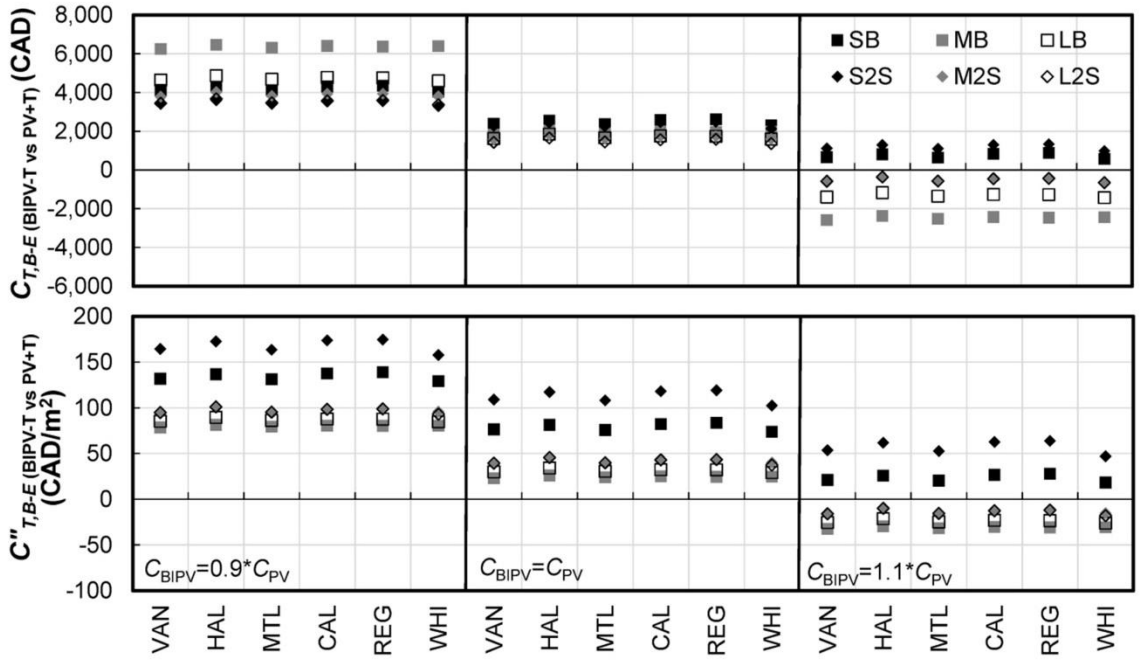

Figure 6-17: Break-even and specific break-even costs for BIPV-T System 1 compared to a PV+T system

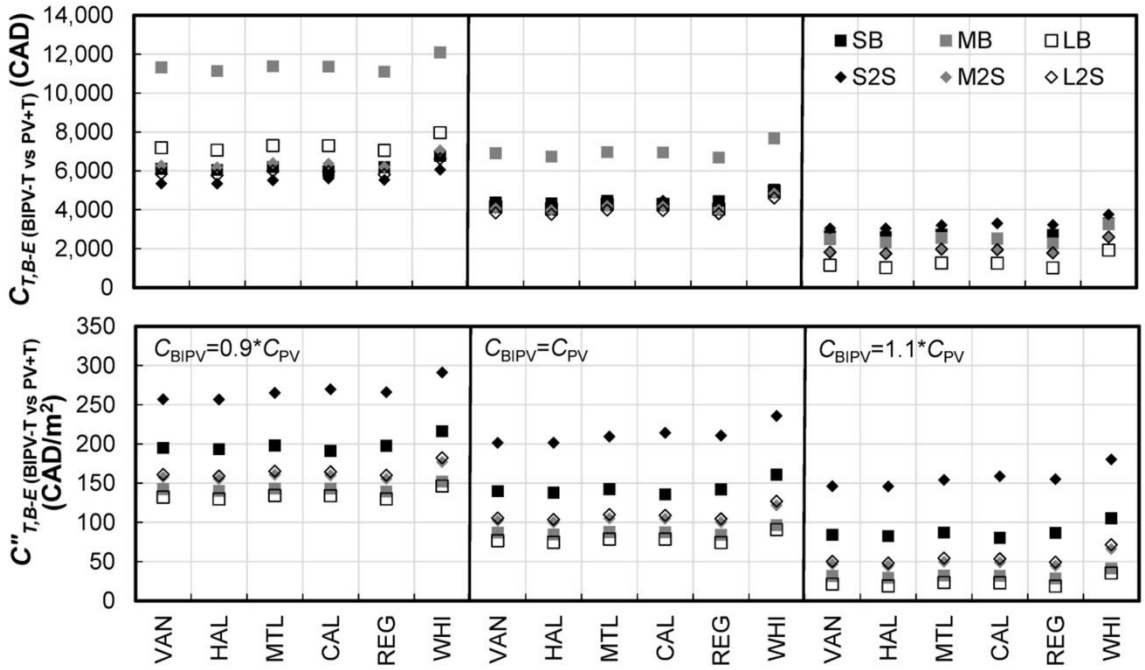

Figure 6-18: Break-even and specific break-even costs for BIPV-T System 2 compared to a PV+T system

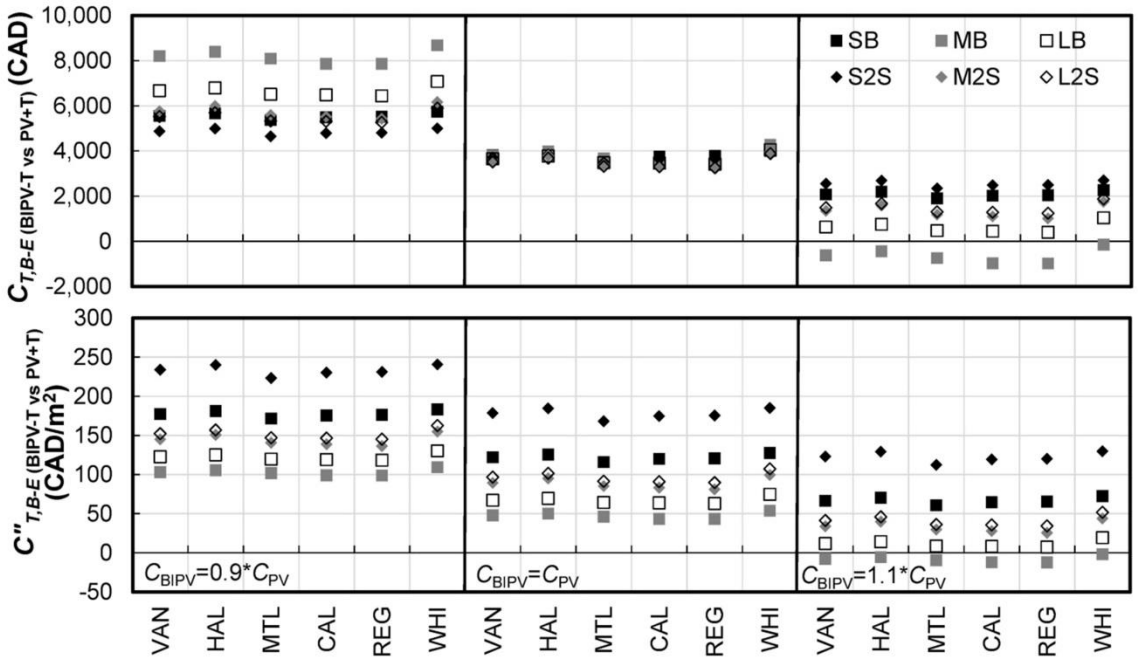

Figure 6-19: Break-even and specific break-even costs for BIPV-T System 3 compared to a PV+T system

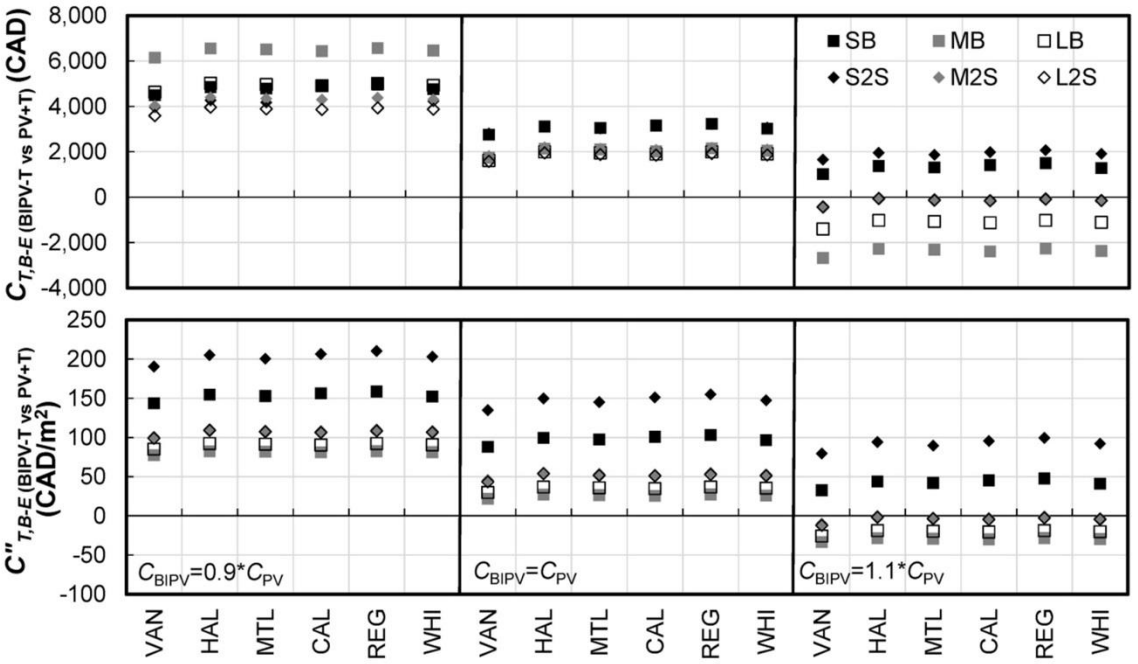

Figure 6-20: Break-even and specific break-even costs for BIPV-T System 4 compared to a PV+T system

6.11.3 Appendix C

6.11.3.1 Roof Slope

In order to determine the roof slope on the north-side of the house, different combinations were considered and compared with the following rule of thumb stating that there is approximately 0.4 m^2 of rooftop area with good BIPV potential (in this case the south-facing roof area) for every m^2 of building ground floor area (Pelland & Poissant, 2006; IEA, 2002). The comparison of the different south-facing roof areas for various north-facing slopes is shown in Table 6-5. From this table, the most realistic south-facing roof area is obtained with a north-facing roof slope of 25°. This slope was selected for all homes.

Table 6-5: Comparison of south-facing roof area for different gable pitch roof designs

	South-facing roof area (m²)			Ratio of south-facing roof area over ground floor area		
North-facing roof slope	25°	35°	45°	25°	35°	45°
Small Bungalow	31.3	40.5	49.1	0.45	0.58	0.71
Medium Bungalow	79.6	103.1	125.2	0.45	0.58	0.71
Large Bungalow	54.4	70.5	85.6	0.45	0.58	0.71
Small 2-storey	20.8	27.0	32.8	0.45	0.58	0.71
Medium 2-storey	39.8	51.5	62.6	0.45	0.58	0.71
Large 2-storey	36.3	47.0	57.0	0.45	0.58	0.71

6.11.3.2 Domestic Hot Water Load

The daily domestic hot water (DHW) load is calculated based on the number of occupants according to the following relation given in the HOT2000 software (NRCan, 2014b):

$$\text{Hot water load} = 85 + 35 * \text{Nb of occupants} \tag{6-22}$$

Using Equation (6-22), daily hot water loads of 225 L/d and 155 L/d are obtained for the houses with 4 and 2 occupants, respectively.

CHAPTER 7 GENERAL DISCUSSION

The main objectives of this thesis are to develop and validate experimentally a model applicable to BIPV-T and PV-T air collectors, to implement this model in an energy simulation tool, to address the main issues with the performance characterization of the technology and finally, to use the validated model to inform on the cost-benefit of integrating BIPV-T air collectors in high performance homes. Ultimately, the goal is to make a significant scientific contribution to improve the level of understanding of this technology and develop awareness on its potential and limitations. This could lead to an increased interest from solar and building components manufacturers in developing products and packaged systems that are cost competitive with other solar technologies. This Chapter discusses how the different methodologies developed and results obtained in Chapter 4 to Chapter 6 provide an added value to the current state of scientific knowledge on PV-T technology.

The literature review presented in Chapter 2 showed that the performance characterization of PV modules with heat recovery was not as straightforward as combining testing procedures for PV modules and solar thermal collectors. In a PV-T collector, the PV cells act as the thermal absorber so the electrical performance affects the thermal performance and vice-versa. When it comes to characterization, it is not clear how this interaction can be captured because the performance of stand-alone PV modules and solar thermal collectors is affected by different variables. The electrical efficiency of PV modules depends mainly on the temperature of the cells and the irradiance level. As for the thermal efficiency of solar thermal collectors, it is affected by the ratio of the temperature difference between the collector inlet and the ambient air over the irradiance, the flowrate and for unglazed collectors, by the wind speed. Previous work (PV Catapult, 2005) had suggested that the cell temperature could be used to encapsulate the interaction between the thermal and electrical performance, but this link had not been demonstrated. One of the challenges with using the cell temperature is that this measurement is not necessarily easy to obtain in a PV-T collector. This is not only due to the temperature gradient across the collector, but also to the fact that the back of the cells is not always accessible for sensor mounting. Chapter 4 offers a substantial contribution with respect to performance characterization of PV-T air collectors. It shows that under heat recovery conditions, the PV cells' temperature can be predicted with the irradiance level and the inlet and outlet fluid

temperatures. Since these variables are intrinsically part of the thermal performance characterization, the temperature of the solar cells can be used to link the electrical and thermal yield. This relation was further demonstrated by presenting a graphical method that fully encapsulates the collector performance. The system of plots that was developed can be used to estimate the collector thermal and electrical yield from the environmental and operating conditions. Furthermore, the work presented in Chapter 4 shows that the equivalent cell temperature method can be used as a valid alternative to estimate the PV cells' temperature in a PV-T collector. It gives a good representation of the actual temperature of the solar cells and solves both the issues of temperature gradient and PV cells accessibility for sensor mounting.

In Chapter 5, the development of a model of an air-based PV-T collector is proposed. This model is also applicable for building-integrated products and is meant for collectors having a single inlet and outlet operating in either a closed-loop or an open-loop configuration. It was validated using experimental data collected following a unique procedure specifically developed for air PV-T collectors. It was also calibrated by comparing the experimental data against the model prediction using a wide variety of convective heat transfer correlations to minimize the discrepancies between the model prediction and the experimental results. An important contribution to PV-T and BIPV-T system modeling capacity was done by implementing this model in an energy simulation tool. This is necessary to study how the thermal energy produced by a PV-T or BIPV-T air collector can be converted into useful energy for a building.

The literature review also showed that there were several challenges when trying to quantify and compare the cost-benefit of BIPV-T technology because both the cost and benefit are not straightforward to estimate. The benefit is difficult to evaluate because two types of energy with different values are being produced. As for the cost, it can considerably vary from one project to another because the technology is relatively new on the market and often consists of a custom product developed for a specific building and application. Chapter 5 and Chapter 6 present a significant advancement to cost-benefit analysis methodologies by proposing a new approach to compare BIPV-T technologies to other solar energy technologies. This method uses the concept of break-even cost defined as the maximum incremental cost to recover the heat from a BIPV system to break-even with the cost (in dollars per unit of useful energy produced) of the solar energy technology that it is being compared with. The useful energy captures both the thermal and electrical yield into one single metric accounting only for the useful part of the thermal

energy produced by the system. The break-even cost includes the ducts, fan and HVAC equipment that have been added to the building to recover the heat from the BIPV system and translate it into useful energy. To remain competitive, the actual incremental cost must be lower than the break-even cost. Thus, the higher the break-even cost, the easier it is for a BIPV-T system to be competitive with other technologies.

In Chapter 5, this new approach for cost-benefit analysis is used to compare a BIPV-T air system with an identical roof having side-by-side PV modules and solar thermal collectors (PV+T). The useful part of the thermal energy produced is determined using fictitious criteria for thermal energy end-usage. Compared to the PV+T system, the BIPV-T system was found to produce anywhere between -2% and 46% more useful equivalent energy on an annual basis. As for the break-even cost, it varied from a few hundred dollars to 7,000 CAD for a 3-season usage (excluding summer) to as much as 20,000 CAD for a 4-season system. The use of criteria based on ambient temperature and temperature rise for determining the useful part of the thermal energy produced provided a wide range of results.

To narrow the range of break-even cost obtained in Chapter 5, the BIPV-T and solar thermal systems were coupled with real heat management strategies to quantify the true amount of useful thermal energy produced. These results are presented in Chapter 6 where BIPV-T systems are integrated in energy-efficient homes in different locations across Canada. To perform this analysis, six housing archetypes were developed to cover different sizes and types of homes typically found in Canada: small bungalow, medium bungalow, large bungalow, small 2-storey, medium 2-storey and large 2-storey. As renewable energy systems are generally installed on buildings that are already energy-efficient, these archetypes have the particularity of achieving a level of energy-efficiency near 86 according to Canada's EnerGuide Rating System (ERS-86). This level of performance is generally considered as a pivot point where it becomes financially interesting to integrate renewable energy technologies rather than further improve the envelope and HVAC systems. These energy-efficient homes were modeled in an energy simulation tool to allow coupling with the BIPV-T model developed in Chapter 5. These models present a significant contribution to modeling capabilities of integrated energy systems for high performance homes.

BIPV-T systems were integrated in these energy-efficient homes using four different heat management strategies: (1) fresh air preheating, (2) DHW preheating through and air-to-water heat exchanger, (3) DHW and space heating with an air-to-water heat pump and (4) DHW heating with a heat pump water heater. The useful equivalent energy was compared to that produced by the same house with a BIPV roof or with a roof where side-by-side PV modules and solar thermal collectors are mounted. Compared to a BIPV system, a BIPV-T system was found to always produce more useful energy. Compared to a PV+T system, however, the type of house and heat management strategy greatly influenced the amount of useful energy produced. Assuming the cost of BIPV equal to that of standard PV modules, the break-even cost of a BIPV-T system compared to BIPV for a medium 2-storey home in Montreal was found to vary between 300 CAD and 2,700 CAD. Compared to a PV+T system, this break-even cost ranged from 1,600 CAD to 4,200 CAD. For a BIPV cost 10% lower than PV, however, this break-even cost could be anywhere from 3,800 CAD to 6,400 CAD. This information represents a substantial contribution to guidelines on BIPV-T system design. It indicates the maximum incremental cost that should be associated with converting a BIPV roof into a BIPV-T system to remain cost-competitive with other solar technology options.

CHAPTER 8 CONCLUSION AND RECOMMENDATIONS

This thesis presented a novel method to characterize the performance of PV-T or BIPV-T air collectors. It showed that the equivalent cell temperature could be used as an alternative method to obtain the PV cells' temperature in a PV-T collector. This temperature can be predicted using some of the variables that characterize the thermal performance. Thus, it can be used as a link between the electrical and thermal yield. The performance characterization method presented requires further research, however. For example, it is not clear if the relation obtained to predict the equivalent cell temperature is applicable to systems of different sizes or series/parallel connections. Further testing would also be required to determine if the parameters obtained for the equivalent cell temperature correlation are site-specific. Another important aspect of PV-T collectors is that these often operate under stagnation or natural ventilation conditions since the production of thermal energy is not always necessary. Models to predict the PV temperature under such operating conditions would need to be established.

The model developed for air-based PV-T and BIPV-T collectors presented in Chapter 5 was validated with experimental data and implemented in the energy simulation tool TRNSYS. This allowed coupling the thermal part of the collector with a building and its HVAC components to study the performance of not only the collector, but also the full system. This model was validated with experimental data collected on a specific PV-T product. To confirm that it can also be used with collectors of different designs and solar cell technologies, further validation of the model with additional PV-T products would be required. Also, since this model is based on steady-state conditions, it would be useful to identify the limits of its applicability in transient simulations when it is being coupled with other systems.

This thesis also presented a novel approach to compare the cost-benefit of air-based BIPV-T technology with other solar energy technologies. To quantify the benefit, the concept of equivalent annual useful energy was proposed to deal with the fact that thermal and electrical energy have a different value. In this method, only the useful part of the thermal energy is considered in the calculation of the overall performance. As for the cost, since it is not straightforward to estimate because BIPV-T is still a niche product, the concept of break-even cost was used. It is defined as the maximum incremental cost that should be associated with converting a BIPV roof into a BIPV-T system. To remain cost-competitive with other solar

technology options, the actual incremental cost must be lower than the break-even cost. This thesis has mainly focused on finding the break-even cost for different types of systems. This was done under the assumption that the actual incremental cost of a BIPV-T system as a mainstream product is unknown even though its equivalent annual useful energy can be estimated. Further case studies could be performed using this approach reversely. For example, if the incremental cost of a BIPV-T system for a specific building and project is known, it would be interesting to calculate the amount of energy that should be converted into useful energy in order to be competitive with other solar energy technologies. The gap between actual and required useful energy could be filled by either improving the conversion of thermal energy into useful energy or improving the performance of the collector itself. The latter could be done by investigating collector heat enhancement strategies.

The break-even cost of BIPV-T systems integrated in energy-efficient homes of different sizes and various locations was evaluated for the four following heat management strategies:

1. Fresh air preheating prior to entering a heat recovery ventilator (HRV)
2. DHW preheating through and air-to-water heat exchanger
3. DHW and space heating with an air-to-water heat pump
4. DHW heating with a heat pump water heater

The lowest break-even costs were obtained with BIPV-T systems used for fresh air preheating (strategy 1) prior to entering a HRV and DHW heating with a heat pump water heater (strategy 4). This is because these systems already perform very well as stand-alone technologies, without being solar-assisted. These options are nevertheless interesting because they are simple to integrate and their added cost is less than in the two other strategies. Recommendations for future work would include performing more in-depth optimization of controls and mechanical components sizing to increase the amount of thermal energy converted into useful energy. Other heat management strategies than those considered in this study could also be investigated. It would also be important to evaluate the break-even cost of BIPV-T technology for commercial and multi-residential buildings. Fresh air preheating is not a very promising heat management strategy in single-family homes, but it will be different in buildings with higher fresh air ventilation requirements.

Assuming the cost of BIPV equal to that of standard PV modules, the break-even cost of a BIPV-T system compared to BIPV for a medium 2-storey home in Montreal was found to vary between 300 CAD and 2,700 CAD. Compared to a PV+T system, this break-even cost ranged from 1,600 CAD to 4,200 CAD. For a BIPV cost 10% lower than PV, however, this break-even cost could be anywhere from 3,800 CAD to 6,400 CAD. As new products are being introduced on the market and more BIPV-T projects experimenting different heat management strategies are being realized, it will become easier to estimate the actual cost of such systems. Further work comparing the break-even cost to the actual incremental cost would be important to identify how close BIPV-T is from being economically viable.

BIBLIOGRAPHY

Chapters included (1, 2 4, 5)

American Society of Heating, Ventilating and Air-Conditioning (ASHRAE). (1997). *ASHRAE Handbook Fundamentals.* Atlanta, GA, USA: ASHRAE.

American Society of Heating, Refrigerating and Air-Conditioning (ASHRAE). (2010). *Methods of Testing to Determine the Thermal Performance of Solar Collectors* (ANSI/ASHRAE 93-2010).

Athienitis, A. K. (2007). Design of a Solar Home with BIPV-Thermal System and Heat Pump. *Proceedings of 2nd Canadian Solar Buildings Conference, Calgary*, June 10-14, 2007. http://citeseerx.ist.psu.edu/viewdoc/download?doi=10.1.1.667.5530&rep=rep1&type=pdf

Athienitis, A. K., Bambara, J., O'Neill, B., & Faille, J. (2011). A prototype photovoltaic/thermal system integrated with transpired collector. *Solar Energy, 85*, 139-153.

Bakker, M., Zondag, H., Elswijk, M. S., & Jong., M. (2005). Performance and Costs of a Roof-Sized PV/Thermal Array Combined with a Ground Coupled Heat Pump. *Solar Energy, 78*, 331-339.

Bambara, J. (2012). *Experimental Study of a Façade-integrated Phovoltaic/thermal System with Unglazed Transpired Collector* (Masters Thesis, Concordia University, Montreal, Quebec). Retrieved from http://spectrum.library.concordia.ca/ 974610/6/ Bambara_MASc_F2012.pdf

Ben Nejma, H., Guiavarch, A., Lokhat, I., Auzenet, E., Claudon, F., & Peuportier, B. (2013). In-Situ Performance Evaluation by Simulation of a Coupled Air Source Heat Pump/PV-T Collector System. *Proceeding of BS2013:* 13th *Conference of International Building Performance Simulation Association, Chambéry, France, August 26-28, 2013.* http://www.ibpsa.org/proceedings/BS2013/p_1006.pdf

Bernier, M., & Plett, E. (1988). Thermal Performance Representation and Testing of Air Solar Collectors. *Journal of Solar Energy Engineering, 110*(2), 74-81.

Buchinger, J. (2006). *Recommendations on Testing of Solar Air Collectors* (Report WP 4.1 D2).

Canadian Home Builder's Association (CHBA). (2012). *45th Pulse Survey of new home builders and renovators*. Retrieved from http://www.chba.ca/uploads/pulse%20survey%20results/main%20report2012.pdf

Canadian Standards Association. (2012). *CAN/CSA-F378 Series-11 - Solar Collectors* (CAN/CSA-F378).

Candanedo, J. A., & Athienitis, A. K. (2009). Application of Predictive Control Strategies in a Net Zero Energy Solar House. *PLEA2009 - 26th Conference on Passive and Low Energy Architecture, Quebec City, Canada, June 22-24, 2009.* http://www.plea2009.arc.ulaval.ca/Papers/2.STRATEGIES/2.2%20Heating%20and%20Cooling/ORAL/2-2-03-PLEA2009Quebec.pdf

Candanedo, L., Athienitis, A., & Park, K. (2011). Convective heat transfer coefficients in a building-integrated photovoltaic/thermal system. *ASME Journal of Solar Energy Engineering, 133*(2).

Cartmell, B., Shankland, N., Fiala, D., & Hanby, V. (2004). A multi-operational ventilated photovoltaic and solar air collector: application, simulation and initial monitoring feedback. *Solar Energy, 76*, 45-53.

Charron, R. (2007). *Development of a Generic Algorithm Optimisation Tool for the Early Stage Design of Low and Net-Zero Energy Solar Homes* (PhD Thesis, Concordia University, Montreal, Canada). Retrieved from http://spectrum.library.concordia.ca/975818/

Charron, R., & Athienitis, A. (2006). Design and Optimization of Net Zero Energy Solar Homes. *ASHRAE Transactions*, 112, 285-295.

Chen, Y., Athienitis, A., & Galal, K. (2010a). Modeling, design and thermal performance of a BIPV/T sytem thermally coupled with a ventilated concrete slab in a low energy solar house: Part 1, BIPV/T system and house energy concept. *Solar Energy, 84*, 1892-1907.

Chen, Y., Galal, K., & Athienitis, A. (2010b). Modeling, design and thermal performance of a BIPV/T system thermally coupled with a ventilated concrete slab in a low energy solar house: Part 2, ventilated concrete slab. *Solar Energy, 84*, 1908-1919.

Chow, T., Hand, J., & Strachan, P. (2003). Building-integrated photovoltaic and thermal applications in a subtropical hotel building. *Applied Thermal Engineering, 23*, 2035-2049.

Chow, T., Pei, G., Fong, K., Lin, Z., Chan, A., & Ji, J. (2009). Energy and Exergy Analysis of Photovoltaic/Thermal Collector with and without Glass Cover. *Applied Energy, 86*(3), 310-316.

ClearSky Advisors Inc. (2011). *Survey of Active Solar Thermal Collectors, Industry and Markets in Canada.* Ottawa, Canada: Natural Resources Canada. Retrieved from http://solarthermalworld.org/sites/gstec/files/survey_of_active_solar_thermal_collectors _2012_-_august.pdf

Cole, R., & Sturrock, N. (1977). The convective heat exchange at the external surface of buildings. *Building and Environment, 12*, 207-214.

Collins, M. (2008). *Recommended Standard for Characterization and Monitoring of PV/Thermal Systems* (Report DB2). Cedar, MI, USA: IEA SHC. Retrieved from http://archive.iea-shc.org/publications/downloads/ DB2_Recommended_Standard for_the _Characterization _and_Monitoring_of_PVThermal_Systems.pdf

Coventry, J., & Lovegrove, K. (2003). Development of an Approach to Compare the Value of Electrical and Thermal Output from a Domestic PV/Thermal System. *Solar Energy, 75*, 63-72.

da Silva, R., & Fernandes, J. (2010). Hybrid Photovoltaic/Thermal (PV/T) Solar Systems Simulation with Simulink/Matlab. *Solar Energy, 84*, 1985-1996.

Delisle, V. (2015). *Models of Energy-Efficient Canadian Home Archetypes* (Internal Report RP-TEC 2015-047). Varennes, Canada: CanmetENERGY.

Delisle, V., & Kummert, M. (2012). Experimental Study to Characterize the Performance of Combined Photovoltaic/Thermal Air Collectors. *Journal of Solar Energy Engineering, 134*.

Delisle, V., & Kummert, M. (2014). A novel approach to compare building-integrated photovoltaics/thermal air collectors to side-by-side PV modules and solar thermal collectors. *Solar Energy, 100*, 50-65.

Dittus, F., & Boelter, L. (1985). Heat transfer in automobile radiators of the tubular type. *International Community Heat Mass Transfer, 12*(1), 3-22.

Eicker, U. (2003). *Solar Technologies for buildings.* Chichester: John Wiley & Sons.

Erdil, E., Ilkan, M., & Egelioglu, F. (2008). An experimental study on energy generation with a photovoltaic (PV) - solar thermal hybrid system. *Energy*, *33*, 1241-1245.

European Committee for Standardization (ECS). (2005). *EN 12975-2 Thermal Solar Systems and Components - Solar Collectors - Part 2: Test methods* (EN 12975-2).

Filliard, B., Guiavarch, A., & Jabbour, M. (2009). Simulation of the thermal interaction between a building integrated photovoltaic collector and an airsource heat pump. *CISBAT 2009 - Renewables in a changing climate: from nano to urban scale, Sep 2009, Lausanne, Switzerland*, pp. 555-560. https://hal.archives-ouvertes.fr/hal-00574652/document

Florschuetz, L. (1979). Extension of the Hottel-Whillier Model to the Analysis of Combined Photovoltaic/Thermal Flat Plate Collectors. *Solar Energy*, *22*, 361-366.

Garg, H., & Adhikari, R. (1997). Conventional hybrid photovoltaic/thermal (PV/T) air heating collectors: steady-state simulation. *Renewable Energy*, *11*(3), 363-385.

Garg, H., & Adhikari, R. (2000). Studies on Cost Effectiveness of Hybrid Photovoltaic/Thermal (PV/T) Air Heating Collector. *World Renewable Energy Congress-VI, Brighton, United Kingdom, July 1-7 2000*, pp. 1098-1101.

Goetzler, W., Guernsey, M., & Droesch, M. (2014). *Research & Development Needs for Building-Integrated Solar Technologies.* Retrieved from http://energy.gov/sites/ prod/files/2014/02/f7/ BIST_TechnicalReport_January2014_0.pdf

Gordon, J. (1981). On non-linear effects in flat-plate collector efficiency curves. *Solar Energy, 26*(3), 265-266.

Harrison, S., McClenahan, D., & Nielsen, V. (1989). The Performance of Unglazed Solar Collectors. *Proceedings of the 15th Annual Conference of the Solar Energy Society of Canada, Penticton, British-Columbia, June 19-21, 1989*.

Hegazy, A. (2000). Comparative study of the performance of four photovotlaic/thermal solar air collectors. *Energy Conversion and Management, 41*, 861-881.

Hollands, K.G.T., Unny, T.E., Raithby, G.D., & Konicek, L. (1976). Free Convection Heat Transfer Across Inclined Air Layers. *Heat Transfer, 98*, 189-193.

Hottel, H., & Whillier, A. (1958). Evaluation of Flat-Plate Solar Collector Performance. *Transactions of the Conference on the Use of Solar Energy 2, Part I,* (pp. 74-104). Tucson: University of Arizona Press.

Huang, B., Lin, T., Hung, W., & Sun, F. (2001). Performance Evaluation of Solar Photovoltaic/Thermal Systems. *Solar Energy, 70*(5), 443-448.

Incropera, F., & DeWitt, D. (1996). *Fundamentals of Heat and Mass Transfer.* New York: John Wiley & Sons.

International Energy Agency (IEA). (2002). *Potential for Building Integrated Photovoltaics* (Report IEA-PVPS T7-4: 2002). Paris, France: IEA. Retrieved from http://www.iea-pvps.org/index.php?id=9&eID=dam_frontend_push&docID=394

International Energy Agency (IEA). (2010). Energy Technology Perspectives 2010 - Scenarios & Strategies to 2015. Paris, France: IEA. Retrieved from http://www.iea.org/publications/freepublications/publication/etp2010.pdf

International Energy Agency Solar Heating and Cooling (IEA SHC) Programme Task 35. (2016). *PV/Thermal Solar Systems*. Cedar, Michigan, USA: IEA SHC. Retrieved from IEA SHC: http://www.iea-shc.org/task35

International Energy Agency Photovoltaic Power Systems Programme (IEA PVPS). (2015). *Trends 2015 in Photovoltaic Applications.* St-Ursen, Switzerland: IEA PVPS. Retrieved from http://www.iea-pvps.org/fileadmin/dam/public/report/national/IEA-PVPS- Trends_ 2015 _- _MedRes.pdf

International Energy Agency Photovoltaic Power Systems Programme (IEA PVPS) Task 15. (2015). *Enabling Framework for the Acceleration of BIPV.* St-Ursen, Switzerland: IEA PVPS. Retrieved from http://iea-pvps.org/index.php?id=task15

International Electrotechnical Commission (IEC). (1995). *Photovoltaic devices - Part 9: Solar simulator performance requirements* (IEC 60904-9).

International Electrotechnical Commission (IEC). (1998). *Thin-Film Terrestrial Photovoltaic (PV) Modules - Design Qualification and Type Approval* (IEC 61646).

International Electrotechnical Commission (IEC). (2005). *Crystalline silicium terrestrial photovoltaic (PV) Modules - Design qualification and type approval* (IEC 61215).

International Electrotechnical Commission. (2011). *Determination of the equivalent cell temperature (ECT) for photovoltaic (PV) devices by the open-circuit voltage method* (IEC 60904-5).

International Electrotechnical Commission (IEC). (2011). *Photovoltaic (PV) Module Performance Testing and Energy Rating – Part 1: Irradiance and Temperature Performance Measurements and Power rating* (IEC 61853-1).

International Organization for Standardization (ISO). (1995). *Guide to the Expression of Uncertainty in Measurement*.

International Organization for Standardization. (2013). *Solar Energy - Solar thermal collectors - Test methods* (ISO 9806).

James, T., Goodrich, A., Woddhouse, M., Margolis, R., & Ong, S. (2011). *Building-Integrated Photovoltaics (BIPV) in the Residential Sector: An Analysis of Installed Rooftop Prices* (Technical Report NREL/TP-6A20-53103). Washington, DC, USA: US Department of Energy. Retrieved from http://www.nrel.gov/docs/ fy12osti/53103.pdf

James, T., Goodrich, A., Woddhouse, M., Margolis, R., & Ong, S. (2012). *Building-Integrated Photovoltaics (BIPV) in the Residential Sector: An Analysi*s of Installed Rooftop Prices, (Presentation NREL/PR-6A20-55027). Washington, DC, USA: US Department of Energy. Retrieved from http://www.nrel.gov/docs/ fy12osti/55027.pdf

Jiang, B., Ji, J., & Yi, H. (2008). The influence of PV coverage Ratio on Thermal and Electrical Performance of Photovoltaic-Trombe Wall. *Renewable Energy, 33*, 2491-2498.

Kalogirou, S. (2001). Usef of TRNSYS for Modelling and Simulation of a Hybrid PV-Thermal Solar Systems for Cyprus. *Renewable Energy, 23*, 247-260.

Kamel, R. S., & Fung, A. S. (2014). Modeling, simulation and feasibility analysis of residential BIPV/T+ASHP system in cold climate-Canada. *Energy and Buildings, 82*, 758-770.

King, D., Boyson, W., & Kratochvill, J. (2004). *Photovoltaic Array Performance Model* (Sandia Report SAND2004-3535). Washington, DC, USA: US Department of Energy. Retrieved from http://prod.sandia.gov/techlib/access-control.cgi/ 2004/043535.pdf

Klein et al. (2009). *A TRaNsient SYstem Simulation Program - User Manual Version 17.* Madison: University of Wisconsin.

Kramer, K. S. (2013). *IEA-SHC Task 43: Solar Rating and Certification Procedures - White Paper on Solar Air Heating Collectors.* Cedar, MI, USA: IEA SHC. Retrieved from https://www.iea-shc.org/data/sites/1/publications/ Final% 20White%20Paper%20Air% 205-31-13.pdf

Kumar, S., & Mullick, S. (2010). Wind Heat Transfer Coefficient in Solar Collectors in Outdoor Conditions. *Solar Energy, 84*, 956-963.

Lomanowski, B. (2010). *BIPV/T Solar Assisted Heat Pump Systems for Residential Heating Applications: ESP-r Model Development*. Ottawa, Canada: Natural Resources Canada.

Magare, D., Sastry, O., Gupta, R., Betts, T., Gottschalg, R., Kumar, A., Bora, B., & Singh, Y.K. (2016). Effect of seasonal spectral variations on performance of three different photovoltaic technologies in India. *International Journal of Energy and Environmental Engineering, 7*(1), 93-103.

Marion, B. (2012). Influence of Atmospheric Variations on Photovoltaic Performance and Modeling their Effects for Days with Clear Skies. *Proceedings of 38th IEEE Photovoltaic Specialists Conference, Austin, June 2012.*

Mei, L., Infield, D., Eicker, U., & Fux, V. (2003). Thermal modelling of a building with an integrated ventilated PV façade. *Energy and Buildings, 35*, 605-617.

Menicucci, D., & Fernandez, J. (1988). *User's Manual for PVFORM: A Photovoltaic System Simulation Program for Stand-Alone and Grid Interactive Applications.* Washington, DC, USA: US Department of Energy. Retrieved from prod.sandia.gov/techlib/access-control.cgi/1985/850376.pdf.

McAdams, W. (1954). *Heat Transmission.* New York: McGraw-Hill.

National Research Council Canada (NRC). (2010). *National Building Code of Canada 2010* (NBC 2010).

National Renewable Energy Laboratory (NREL). (2015). *EnergyPlus Documentation - Engineering Reference - The Reference to EnergyPlus Calculations.* Washington, DC, USA: US Department of Energy. Retrieved from https://energyplus.net/sites/default/files/pdfs_v8.3.0/EngineeringReference.pdf

Natural Resources Canada (NRCan). (2010). *2007 Survey of Household Energy Use (SHEU-2007).* Ottawa, Canada: NRCan. Retrieved from http://oee.nrcan.gc.ca/publications/statistics/ sheu07/pdf/sheu07.pdf

Natural Resources Canada (NRCan). (2012a). *2012 R-2000 Standard*. Ottawa, Canada: NRCan. Retrieved from https://www.nrcan.gc.ca/sites/www.nrcan.gc.ca/files/oee/files/pdf/2012%20R2000%20Standard%20EN.pdf

Natural Resources Canada (NRCan). (2012b). *National Survey Report of PV Power Applications in Canada 2011*. Ottawa, Canada: NRCan. Retrieved from iea-pvps.org/index.php?id=93&eID= dam_frontend_push&docID=1260

Natural Resources Canada (NRCan). (2013). *Photovoltaic potential and solar resource maps of Canada*. Ottawa, Canada: NRCan. Retrieved from http://pv.nrcan.gc.ca

Natural Resources Canada (NRCan). (2014a). *EnerGuide Home Evaluations*. Ottawa, Canada: NRCan. Retrieved from http:// www.nrcan.gc.ca/energy/efficiency/housing/home-improvements/5005

Natural Resources Canada (NRCan). (2014b). HOT2000 software (Version 10.51). Ottawa, Canada: NRCan. Retrieved from http://www.nrcan.gc.ca/energy/ efficiency/housing/home-improvements/17725

Natural Resources Canada (NRCan). (2014c). *List of ENERGY STAR qualified products*. Ottawa, Canada: NRCan. Retrieved from http://www.nrcan.gc.ca/energy/products/energystar/why-buy/13631

Noguchi, M., Athienitis, A., Delisle, V., Ayoub, J., & Berneche, B. (2008). Net Zero Energy Homes of the Future: A Case Study of the EcoTerra Home in Canada. *Presented at the*

Renewable Energy Congress, Glasgow, Scotland, July 19-25, 2008. http://www.annex32.net/pdf/articles/Net_Zero_Energy_Homes_of_the_Future.pdf

Noirot. (2015). *Cylia 2 chauffe-eau thermodynamique*. Retrieved from http://www.noirot.fr/media/ notices/Notice_cylia_2.pdf

Notton, G., Cristofari, C., Mattei, M., & Poggi, P. (2005). Modelling of a double-glass photovoltaic module using finite differences. *Applied Thermal Engineering, 25*, 2854-2877.

Othman, M., Yatim, B., Sopian, K., & Abu Bakar, M. (2007). Performance Studies on a Finned Double-Pass Photovoltaic-Thermal (PV/T) Solar Collector. *Desalination, 209*, 43-49.

Onovwiona, H., & Ugursal, V. (2006). Residential Cogeneration Systems: Review of the Current Technology. *Renewable and Sustainable Energy Reviews, 10*, 389-431.

Pantic, S., Candanedo, L., & Athienitis, A. (2010). Modeling of energy performance of a house with three configurations of building-integrated photovoltaic/thermal systems. *Energy and Buildings, 42*, 1779-1789.

Parekh, A., Swinton, M., Szadkowski, F., & Manning, M. (2005). *Benchmarking of energy savings associated with energy efficient lighting in houses* (NRCC-50874). Ottawa, Canada: NRC. Retrieved from http://aceee.org/files/proceedings/2006/data/papers/ SS06_Panel9_Paper23.pdf

Pavylos, J. (2008). A survey of wind convection coefficient correlations for building envelope energy systems' modeling. *Applied Thermal Engineering, 28*, 801-808.

Pelland, S., & Poissant, P. (2006). An Evaluation of the Potential of Building Integrated Photovoltaic in Canada. *31st Annual Conference of Solar Energy Society of Canada (SESCI), August 20-24, 2006, Montreal, Canada*. https://www.nrcan.gc.ca/sites/ www.nrcan.gc.ca/files/canmetenergy/files/pubs/2006-047_OP-J_411-SOLRES_BIPV_new.pdf

PikeResearch. (2012). *Building Integrated Photovoltaics – BIPV and BAPV: Market Drivers and Challenges, Technology Issues, Competitive Landscape, and Global Market ForecastsNavigant biPV report.* Boulder, CO, USA: Navigant Consulting.

Pogharian, S., Ayoub, J., Candanedo, J., & Athienitis, A. (2008). Getting to a Net Zero Energy Lifestyle in Canada: The Alstonvale Net Zero House. *Presented at the 23rd European PV Solar Energy Conference, Valencia, Spain, September 2008.* http://montrealzero.com/wp-content/uploads/2014/06/Getting-to-a-Net-Zero-Energy-Lifestyle-in-Canada.pdf

Poissant, Y., & Bateman, P. (2014). *National Survey Report of PV Power Applications in Canada 2014.* Ottawa, Canada: NRCan. Retrieved from http://www.cansia.ca/uploads/7/2/5/1/72513707/national_survey_report_of_pv_power_applications_in_canada_2014.pdf

Prasad, D., & Snow, M. (2005). *Designing with Solar Power - A Source Book for Building Integrated Photovoltaics (BiPV)*. London, UK: The Images Publishing Group Pty Ltd and Earthscan.

PV Catapult. (2005). *PVT Performance Measurements Guidelines- Guidelines for Performance Measurements of Liquid-Cooled Non-Concentrating PVT Collectors using c-Si cells* (Report PV Catapult D8-6).

PV Catapult. (2006). *PVT Roadmap A European Guide for the Development and Market Introduction for PV-Thermal Technology*.

Ross, R. (1976). Interface design considerations for terrestrial solar cell modules. *Proceedings of the 12th IEEE Photovoltaic Specialists Conference, Baton Rouge*. http://www2.jpl.nasa.gov/adv_tech/photovol/ppr_75-80/Interface%20Des%20Consid_PVSC76.pdf

Sandnes, B., & Rekstad, J. (2002). A Photovoltaic/Thermal (PV/T) Collector with a Polymer Absorber Plate. Experimental Study and Analytical Model. *Solar Energy, 72*(1), 63-73.

Santbergen, R., & van Zolingen, R. (2008). The aborption factor of crystalline silicon PV cells: a numerical and experimental study. *Solar Energy Materials and Solar Cells, 92*(4), 432-444.

Sharples, S., & Charlesworth, P. (1998). Full-Scale Measurements of Wind-Induced Convective Heat Transfer from a Roof-Mounted Flat Plate Solar Collector. *Solar Energy, 62*(2), 69-77.

Sopian, K., Liu, H., Kakac, S., & Veziroglu, T. (2000). Performance of a Double Pass Photovoltaic Thermal Solar Collector Suitable for Solar Drying Systems. *Energy Conversion & Management, 41,* 353-365.

Sparrow, E., Ramsey, J., & Mass, E. (1979). Effect of Finite Width on the Heat Transfer and Fluid Flow about an Inclined Rectangular Plate. *ASME Journal of Heat Transfer, 101*, 199-204.

RS Means. (2013a). *RS Means Building Construction Cost Data.* Rockland, MA, USA: Reed Construction Data, Inc.

RS Means. (2013b). *RS Means Green Building Cost Data.* Rockland, MA, USA: Reed Construction Data, Inc.

Santbergen, R., & van Zolingen, R. (2008). The aborption factor of crystalline silicon PV cells: a numerical and experimental study. *Solar Energy Materials and Solar Cells, 92*(4), 432-444.

Skoplaki, E., Boudouvis, A., & Pavylos, J. (2008). A simple correlation for the operating temperature of photovoltaic mdules of arbitrary mounting. *Solar Energy Materials & Solar Cells, 92*, 1393-1402.

Sopian, K., Liu, H., Kakac, S., & Veziroglu, T. (2000). Performance of a Double Pass Photovoltaic Thermal Solar Collector Suitable for Solar Drying Systems. *Energy Conversion & Management, 41,* 353-365.

Test, F., Lessman, R., & Johary, A. (1981). Heat Transfer during Wind Flow over Rectangular Bodies in the Natural Environment. *ASME Journal of Heat Transfer, 103*, 262-267.

Thevenard, D., & Pelland, S. (2013). Estimating the uncertainty in long-term photovoltaic yield predictions. *Solar Energy, 91*, 432-445.

Thornton, J., Bradley, D. M., Blair, N., Duffy, M., LaHam, N., & Naik, A. (2012). *TessLibs 17 - Electrical Library Mathematical Reference.* Madison, WI, USA: Thermal Energy System Specialists.

Tiwari, A., & Sodha, M. (2007). Parametric Study of Various Configurations of Hybrid PV/Thermal Air collector: Experimental Validation of Theoretical Model. *Solar Energy Materials & Solar Cells, 91*, 17-28.

Tiwari, A., Barnwal, P., Sandhu, G., & Sodha, M. (2009). Energy Metrics Analysis of Hybrid-Photovoltaic (PV) Modules. *Applied Energy, 86*, 2615-2625.

Tonui, J., & Tripanagnostopoulos, Y. (2007). Improved PV/T Solar Collectors with Heat Extraction by Forced ad Natural Air Circulation. *Renewable Energy, 32*, 623-637.

Tripanagnostopoulos, Y., Nousia, T., Souliotis, M., & Yianoulis, P. (2002). Hybrid Photovoltaic/Thermal Solar Systems. *Solar Energy, 72*, 217-234.

Tripanagnostopoulos, Y., Souliotis, M., Battisti, R., & Corrado, A. (2006). Performance, Cost and Life-cycle Assessment Study of Hybrid PVT/AIR Solar Systems. *Progress in Photovoltaics: Research and Applications, 14*, 65-76.

University of Strathclyde - Energy Systems Research Unit. (2002). *The ESP-r System for Building Energy Simulation - User Guide Version 10 Series.* Retrieved from http://www.esru.strath.ac.uk/Documents/ESP-r_userguide.pdf

US Department of ENERGY (US DOE). (2013). *EnergyPlus engineering reference - The reference to EnergyPlus calculations (v 8.1)*. Washington, DC, USA: US Department of Energy.

Verberne, G., & van den Donker, M. (2015). *BIPV Pricing in The Netherlands - 2014 Price Benchmark Report*. Retrieved from http://www.seac.cc/fileadmin/seac/user/doc/SEAC_-_BIPV_Pricing_in_The_Netherlands_2014.pdf

Zondag, H. (2008). *Main R&D Issues for PVT - A manufacturer's perspective* (Report DC2 IEA SHC Task 35). Cedar, MI, USA: IEA SHC.

Zondag, H., De Vries, D., Van Helden, W., & Van Zolingen, R. (2002). The Thermal and Electrical Yield of a PV-Thermal Collector. *Solar Energy, 72*(2), 113-128.